Winter 2010

Concentrations, Distributions and Chemical Speciation of Zinc and Cadmium in the Equatorial and South Atlantic Ocean

Gonzalo G. Carrasco
Old Dominion University

CONCENTRATIONS, DISTRIBUTIONS AND CHEMICAL SPECIATION OF ZINC AND CADMIUM IN THE EQUATORIAL AND SOUTH ATLANTIC OCEAN

by

Gonzalo G. Carrasco
M.Sc., 2007, Old Dominion University

A Dissertation Submitted to the Faculty of
Old Dominion University in Partial Fulfillment of the
Requirement for the Degree of

DOCTOR OF PHILOSOPHY

OCEANOGRAPHY

OLD DOMINION UNIVERSITY
December, 2010

Approved by:

John R. Donat (Director)

Patricia Pleban (Member)

Gregory Cutter (Member)

ABSTRACT

CONCENTRATION, DISTRIBUTION AND CHEMICAL SPECIATION OF ZINC AND CADMIUM IN THE EQUATORIAL AND SOUTH ATLANTIC OCEAN

Gonzalo G. Carrasco
Old Dominion University, 2010
Director: Dr. John R. Donat

Certain trace metals are important cofactors in enzymatic systems and are thus, essential for life in the world's oceans. Two of these metals, Zn and Cd, are required by phytoplankton for enzymes that facilitate carbon uptake (Morel and Price, 2003). In seawater the total dissolved concentration of a metal (M_{TD}) is distributed among different chemical species and this chemical speciation dictates a metal's bioavailability. Strong organic metal-binding ligands greatly affect the metal's chemical speciation in the ocean, potentially limiting phytoplankton growth by reducing the concentrations of Zn^{2+} and Cd^{2+}, the bioavailable forms of these two metals to levels below those required for optimal, or even minimal, growth (Ellwood, 2004).

In this study, Zn and Cd concentrations, distributions and chemical speciation in the Equatorial and Western South Atlantic Ocean are discussed. The focus, initially on Zn and Cd and their complexing ligands, shifts from depth profiles to sources to processes to analysis of specific hot spots. Zn_{TD} and Cd_{TD} profiles mimic silicate and phosphate. Three separate, metal-specific, complexing ligands for Zn and Cd are reported, thanks to the use of a novel mathematical tool (TDI). Notable features include potential regional influences on the Zn_{TD}, Cd_{TD} and ligand distribution exerted on surface waters near the Amazon River plume and on subsurface waters by a hypoxic region in the Equatorial Atlantic.

As of water masses of more widespread distribution, the influence of factors like the Amazon River particles / Equatorial area high productivity on intermediate water masses and the Congo River shelf matter on deep water masses show high Zn_{TD} and Cd_{TD}

and very high ligand concentrations (L), in contrast to the Zn_{TD} and silicate rich water masses originated near the Southern Ocean. The Zn_{TD} / silicate ratios show the widespread presence of a Zn_{TD} subsurface local maximum, suggesting Zn regeneration linked to grazing. A study of the ligand suggests some of them are related to primary productivity and some are related to grazing. Some ligands are very refractory and others are transported in intermediate and deep water masses as both their concentrations and binding strengths (logK) decrease as they age (estimated residence time ~ 130 years), suggesting potential global distributions of a consortium of decaying ligands.

The chemical speciation and bioavailability of Zn and Cd are compared with some inferred Co speciation data. This region of the Atlantic Ocean is not prone to limitation due to the sufficient concentration of free Zn^{2+} in surface waters, in contrast to regions where intermediate and deep waters are to upwell, which could show limitation due to low Zn^{2+} and Cd^{2+}.

This thesis is dedicated to Sara, Giulliana, Susana and Gonzalo;
my future, present and past.

"*... el mar se derrama, ahogándome ...*"

Héroes del Silencio

ACKNOWLEDGMENTS

I would like to acknowledge all the persons who participated, inspired, helped or in some way or another were part of this. I might end up forgetting some, for which I start by expressing my sincere apologies. Though I am who will obtain the diploma, a lot of the merit goes to people who made it possible for me to be able to focus on work for the years I spent at grad school.

First and foremost, I thank Dr John Donat for his enthusiastic mentoring. Since the day I arrived to the Lab, his open-door policy and his eagerness to discuss topics science- and life-related alike (sometimes over beer and cigars at Taps) were crucial. He supported me as a research assistant for many years. And he encouraged me to follow my guts and my genes with being a teaching assistant, which I enjoyed a lot (maybe too much). He is a fantastic teacher, which is very inspirational. He let me work it out over many loops, and sometimes pursuit directions which weren't precisely his first choice. He believed in me when it was needed, and he didn't in some other instances, and that was part of the challenge of becoming a scientist. And it was all good. I will be forever in debt with you, Dr D.

Dr Cutter was a very important figure too. The attention to detail in classes I took with him is great. His criticism for this dissertation was very thoughtful. I have to say it, after a learning-curve, I like his humor and persona. And, for sure, I enjoyed and will enjoy time spent in ships with him.

Having not only had Dr Pleban in my dissertation committee, but having also worked for her as a teaching assistant, I can say how fine of a teacher and lady she is. She provided interesting questions and comments on this dissertation, for which I am thankful.

I also thank other professors related with the work I present in this dissertation and who had the diligence to read some chapters of this dissertation, including: Dr. Peter Croot at IFM-GEOMAR, Germany and now at the University of Plymouth, UK, whose Zn data from the Southern Ocean was essential for comparisons with this study. Dr. Loes Gerringa at NIOZ, the Netherlands, read the math chapter and provided helpful comments.

Other professors, not directly related to this work but to whom I express gratitude for all the help and good times together, include: Dr Johnson, with whom teaching an Oceanography lab for 550 plus students was a pleasure; Dr Dobbs, who as GPD helped as much as he could; Dr Zimmerman, who as chair of OEAS helped me very much too, and whose reading course I enjoyed so much; Dr Burdige, whose reading courses I enjoyed too, as much as his humor.

In the Lab, I couldn't have done without: John Consolvo, whose epic patience, endurance and attention to detail inspired me; Duncan "the Hammer" Byers, whose constant provocations and good-intentioned criticism helped me focus; Christina Dryden, whose enjoyable company was very much appreciated; Matt "Mustafa" Brown,

who in the time spent in the Lab together kept the good-karma level high. Cynthia Wickstrom and Dr. Rodney T. Powell performed the total dissolved metal analyses and I thank them for this.

Separate mention to Pete "Iu Baba" Morton, my labmate and buddy , with whom surmounting the insurmountable and exploring the non-explored direction for fixing things, interpreting data and being good human beings and fathers was in every day's to-do-list. We still have a lot to do, Pete, but we've gotten this far together!

In the same category fits Hussain "el Baharaini" Abdulla, with whom lunching (yes, this word exists!) some good Chinese food and talking life and science was such a pleasure. Dude, where are you? Where were you? Thanks for all the guidance and help, brother!

It's worth to mention also that having had daughters born to our respective wives (one *per capita*) in the same couple of weeks in the late summer 2004 with Pete and Hussain has made us not only more aware of many things, but also real "*compadres*". I love their families as if they were mine!

Luis and Jose Luis are in a separate category as well, for they were not Labmates, but they helped me out immensely with work. Luis helped substantially with the math problem over a whole summer, and that was also a crucial part, a turning point in the development of my data for this dissertation; for that I am extremely thankful, buddy.

Jose Luis, with his "drop-in anytime" policy for both his office and his house was something out of this world, a truly inspiring oceanographer and friend, *gracias amigo* for all the help with physical oceanography and big-picture oceanography and science. And, your house was the closest to having a big family in Norfolk.

Talking about family, I am profoundly and sincerely thankful to my father Gonzalo and my mother Susana, not only for making things possible, but more importantly for being such inspirational characters both of you in your own way, for contaminating with the curiosity bug from a very early age, and for allowing me to follow my own path. My brothers Roberto and Ricardo were fantastic companions when a kid and are very good friends as an adult, and I thank them for their support, too.

A generation back, my two grandmothers Imelda and Teresa were and still are incredibly supportive and inspirational, being one a pioneer teacher in my home country and the other an *émigrée extraordinaire* and the sweetest singing voice in my memories. My grandfather Gaston, an adventurer who I didn't have the luck to meet in person but whose *nom de guerre* I use, and my grandfather Rodolfo, whose collection of old books was a fascinating world to dive into, are also thanked.

Thanks be given to my in-laws Oswaldo and Ana Maria for helping us out in times of uncertainty and illness. I will be forever in debt to you.

My several academic generations of friends in Norfolk made life a pleasure, and

they include Luis and Lee at the YMCA; Roberto and the pinpon gang; Jose Luis, Ivonne, Diego (thanks a lot for help with printing), Andrea, Stacy, Heber, Toskolina "Jodorowska"; in the last months Roberto, Fenha, Hernaldo "el Maestro", Frank; and from previous times Ruslan, Tariq, Stuart, Nicolas, Nolwenn and Mathew. My dear landlady team includes, over the years: Mackie, Liz, Peggy and also Tosca.

Talking about old friends, Alberto "Enanon", thanks for showing me the wonders of the ocean and how to keep an open-minded attitude to so many things. Alejandro "Capi" and Jorge "Baraba", you are the best friends I could have ever wished for!

I should mention also Professors from college and school that are part of this madness: Dr. Briceno at UCSM; Dr. Salinas at UCMS, for teaching me the basics of analytical chemistry; Q.F. Jessica Paredes, for working together in a thesis that opened the environmental curiosity in me to get into the water chemistry field; and Prof. Luis Chara for showing the beauty of chemistry in high school, your course rocks *profe*!

Lastly, I would like to express my infinite gratitude and admiration to my wife Giulliana and my daughter Sara. Thanks for all the inspiration, listening ears and comforting attitude. But, most of all, for all the patience and faith in me. Learning from you about the other side of existence (in many ways) is always fascinating and comforting. You are my sun, my moon, my sky and my stars, and the ultimate reason for my being. I love you two with all my heart, monkeys!

TABLE OF CONTENTS

Page

LIST OF TABLES

LIST OF FIGURES

CHAPTER 1

INTRODUCTION

Certain metals are important cofactors in enzymatic systems and are thus, essential for life in the world's oceans. Two of these metals, Zn and Cd, are used by phytoplankton for enzymes that facilitate carbon uptake (Morel and Price, 2003). In seawater, the total dissolved concentration of a metal (M_{TD}) is distributed among different chemical species, and this chemical speciation dictates a metal's bioavailability. Strong organic metal-complexing ligands, produced by phytoplankton (Moffett and Brand, 1996), by bacterial, viral or zooplankton activity, or simply produced by organic matter conglomeration, can greatly affect the metal's chemical speciation in the ocean, potentially limiting phytoplankton growth by reducing the concentrations of Zn^{2+} and Cd^{2+} and their inorganic complexes, the bioavailable forms of these two metals according to the free-ion model (Sunda and Guillard, 1976), to levels below those required for optimal, or even minimal, growth (Ellwood, 2004). Understanding Zn and Cd chemical speciation in seawater is important to evaluate the effect of these metals' bioavailable chemical species on photosynthesis and carbon uptake, ultimately related to global climate (Hong et al., 2005).

Zn and Cd speciation has been studied in the North Pacific, North Atlantic and Southern Oceans (Bruland, 1989, 1992; Ellwood and van den Berg, 2000; Ellwood, 2004), and results show the presence of strong organic ligands which complex more than 95 % and 70 % of dissolved Zn and Cd, respectively. In this dissertation, I report the results of my studies of Zn and Cd speciation in the Equatorial and South Atlantic Ocean, a very diverse region. My overall objective is to determine the influences of organic matter coming from the Amazon River, the presence of an hypoxic zone in the Equatorial East Atlantic off Africa, the layering of water masses typical of the Atlantic Ocean and other factors on these metals' chemical speciation.

Samples were taken during the Intergovernmental Oceanographic Commission's (IOC), 1996 Contaminant Baseline Survey cruise (Montevideo, Uruguay to Bridgetown, Barbados), an international effort sponsored by UNESCO. This cruise was one of a series whose goal is to determine baseline concentrations of metals and organic contaminants in the major oceans, in order to allow future identification of anthropogenic effects. The stations sampled during the IOC 1996 cruise in the Western South and Equatorial Atlantic Ocean are shown in Fig. 1 (Cutter and Measures, 1999). Water samples collected at various depths at vertical profile stations along the cruise track were analyzed for their Zn and Cd chemical speciation using anodic stripping voltammetry at a thin mercury film deposited on a rotating glassy carbon disk electrode (TMF-RGCDE-ASV; Bruland, 1989, 1992). Trace metals in the samples were preconcentrated by complexation with the ligands APDC/DDDC followed by solvent extraction and analyzed by graphite furnace atomic absorption spectrophotometry (GF-AAS; Bruland et al., 1979; Ellwood, 2004).

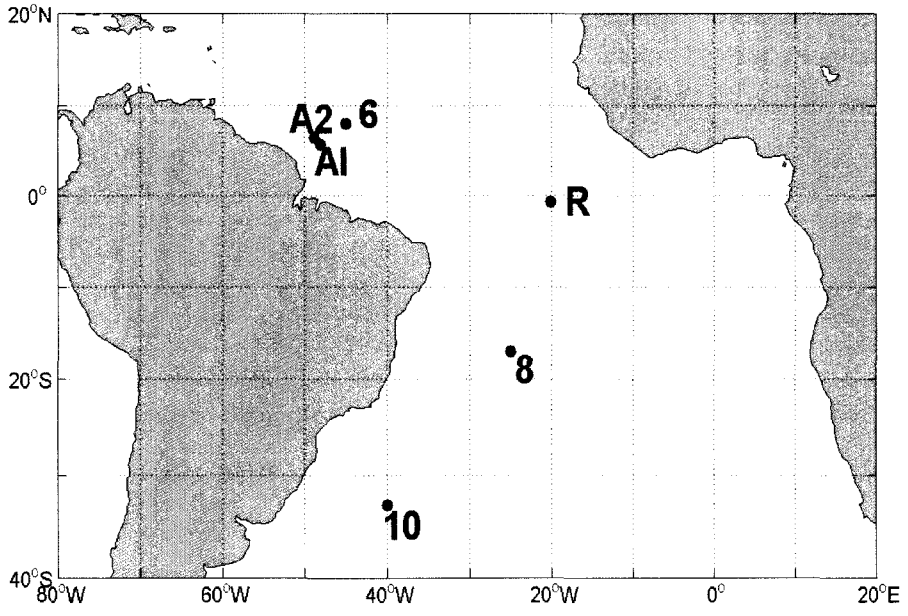

Fig. 1. Location of 1996 IOC Contaminant Baseline Survey cruise vertical profile sampling Stations Amazon 1 and 2 (A1 and A2), 6, Romanche (R), 8 and 10.

1.1. BACKGROUND

Nearly all of the chemical elements are present in the ocean (Nozaki, 1997), but only in the last few decades have the concentrations of trace metals in the world's oceans been determined without systematic contamination, due to improvements in trace metal clean laboratory procedures (Bruland, 1980) and in analytical methods. The concentrations of bioactive metals like Fe, Zn, Co, Cd, Cu have subsequently been reported at nM (10^{-9} M) or lower concentrations (Lohan et al., 2005; Ellwood, 2004; Saito and Moffett, 2001; Morel et al., 2003; Donat and Bruland, 1995).

The importance of some bioactive trace metals in the ocean is based on the effect that their bioavailable concentrations have on photosynthesis occurring in oceanic surface waters. Global photosynthesis in turn affects atmospheric CO_2 concentrations and the ramifications of photosynthetic carbon sequestration may extend to global climate change (Hong et al., 2005). The macronutrients phosphate, nitrate and silicate are required by phytoplankton to perform photosynthesis. These nutrients have characteristic depth profiles in the ocean with very low concentrations at surface, where photosynthetic uptake is at its maximum, increasing concentrations with depth as respiration increases and having absolute maximum values where maximum cumulative respiration occurs along the oceanic conveyor belt. The average ratio of these nutrients' concentrations is expressed by the Redfield ratio ($C_{106}N_{16}P_1$; Redfield et al., 1963). Fe, Zn, Cd, Co and other metals have been recently determined in several phytoplankton species' cellular content, and the inclusion of the ratios of these metals to the macronutrients and to each other ($(C_{124}N_{16}P_1S_{1.3}K_{1.7}Mg_{0.56}Ca_{0.5})_{1000}\,Sr_{5.0}Fe_{7.5}Zn_{0.80}Cu_{0.38}Co_{0.19}Cd_{0.21}Mo_{0.03}$) has been proposed (Ho et al., 2003). Since the macronutrients' depth profiles are inherently defined by biological activity, a comparison of the macronutrients' depth profiles with those of metals provides hints about which elements might have a biological role as micronutrients.

Of all the bioactive trace metals, Fe has been the most extensively studied (e.g. Martin and Fitzwater, 1988; Bruland et al., 2005; Sarthou et al., 2007). It has a macro-

nutrient-like depth profile and is known to enhance primary productivity, whether in natural dust deposition events (Jickells et al., 2005) or in artificial fertilizations (e.g. Boyd et al., 2007). According to the Fe hypothesis of the late John Martin (Martin and Fitzwater, 1988), carbon sequestration is enhanced after Fe addition.

The relationship and interaction between various metals' bioavailable fractions has been studied in phytoplankton laboratory cultures (Sunda and Huntsman, 2000), and the results indicate that synergism and antagonism can exist between different bioactive metals. For example, Cu appears to interfere with the uptake of other trace metals such as Zn or Mn (Sunda and Huntsman, 1998). Zn, Cd and Co can replace each other, with varying degree of efficiency, in enzymatic functions related to carbon acquisition (Price and Morel, 1990). Crawford et al. (2003) provided some field evidence suggesting that Fe fertilizations can be optimized by adding Zn, leading to increased primary production.

1.1.1. Zinc

Zn is a trace metal known to be part of many enzymatic systems (Coleman, 1998). In the ocean, Zn is the enzymatic cofactor in two important systems: phosphatases, the enzymes that break non-bioavailable organic phosphate into bioavailable inorganic phosphate (Lipscomb and Strater, 1996; Dyhrman and Palenik, 2003; Shaked, 2006; Jakuba et al., 2008), and carbonic anhydrases (CA), the enzymes for the extra and/or intracellular conversion of HCO_3^- into CO_2, the preferred chemical form of carbon for biological uptake (Badger and Price, 1994; Buitenhuis et al., 2003). In surface waters, Zn concentrations are low as it is taken up and used for these enzymatic functions, where phytoplankton photosynthetic activity creates a demand for it, or adsorbed onto particles. As depth increases, the concentration of Zn increases as particles undergo two processes: microbial decomposition of the organic phases and dissolution of the inorganic phases. Thus, Zn has a nutrient-type depth profile. Sufficiently low Zn concentrations could potentially limit primary productivity in surface waters (Ellwood, 2004). Further, given its requirements, an equivalent to the Fe hypothesis has been concocted for Zn (Morel et al., 1994).

Zn's depth profiles mimic the macronutrient silicate in the oceans (Bruland, 1980, 1989; Ellwood and van den Berg, 2000; Ellwood, 2004), with subnanomolar surface concentrations that increase gradually with depth to concentrations of ~ 2 - 3 nM, along with silicate dissolution. The influence of Zn on the silicate uptake has been studied recently, with some pointing to increased uptake and some showing the opposite (Reuter and Morel, 1981; de la Rocha et al., 2000; Franck et al., 2003). Diatoms, the phytoplankton group responsible for most of carbon sequestration (Smetacek, 2000), sink due to their heavy silica frustules. Thus, Zn and silicification are intimately related, especially in regions close to the Southern Ocean, where very high Zn and silicate concentrations and diatomaceous carbon export occur.

1.1.2. Cadmium

In contrast to Zn, Cd was known as a toxic metal until recently. The fact that it had a nutrient-like depth profile was a paradox (Hunter et al., 1997). Cd uptake has been reported in the English Channel (Dixon et al., 2006) and empirical evidence suggested a relationship between Zn, Cd and Co (Price and Morel, 1990; Sunda and Huntsman, 1995, 1996) that suggested a biological role for Cd, yet a reason for this was elusive for years.

Recently Cd and Co were found to play central roles as enzymatic cofactors of CA (Lane and Morel, 2000a and b), enzymes traditionally known to have Zn as a cofactor. Inter-replacement of the three metals in CA is possible (Xu et al., 2007) and logical, given the similarity of the outer shell electronic distribution and the expected similarity in biochemical functions, despite Cd's reputation as a toxic element. It has been hypothesized that when concentrations of Zn are limiting, Cd and/or Co, whose dissolved concentrations are usually lower than Zn's, can replace Zn in some of its biochemical functions (Price and Morel, 1990). Furthermore, inter-replacement of Zn, Cd and Co is hypothesized to have occurred in autotrophic phytoplankton for C uptake, depending on each of the three metals' availability throughout the ~ 4 billion years of history of the atmosphere/ocean system (Saito et al., 2003). Later, another CA was found to work only with Cd in the first exclusive biochemical role for Cd (Lane et al., 2005).

Cd's depth profiles mimic the macronutrient phosphate (Bruland, 1992; de Baar et al., 1994; Yeats et al., 1995; Rutgers van der Loef et al., 1997; Ellwood, 2004), with picomolar or subpicomolar surface concentrations that increase to reach a subnanomolar maximum at the maximum respiration depth below the euphotic zone. The Cd/phosphate relationship has been extensively studied from a global ocean perspective (de Baar et al., 1994; Loscher et al., 1997), with mathematical models (Elderfield and Rickaby, 2000) and mechanistic studies (Cullen, 2003, 2006). Now that a biological role for Cd has been discovered, oceanic regimes with low Zn and Cd (and Co) concentrations should be studied for potential biological limitation, like the Southern Ocean (Ellwood, 2004) or the Subarctic North Pacific (Carrasco and Donat, in preparation).

1.1.3. Speciation and bioavailability of metals

A trace metal's dissolved concentration (operationally defined as what passes through a 0.22 μm filter) has more biological importance than a metal's total concentration, since the colloidal and particulate fractions have less potential for interaction with phytoplankton, simply because of their sizes. The total dissolved metal (M_{TD}) is composed of three fractions or species, namely, the free hydrated metal cation ($M(H_2O)_x^{n+}$) or M^{n+}, inorganic complexes (MX_i, where X is an inorganic anion like sulfate, chloride, carbonate, hydroxide) and organic complexes (ML, where L is a ligand that could be organic matter, humics, fulvics, phytoplankton exudates and/or phytoplankton metabolites).

The inorganic metal fraction (M', the sum of the concentrations of M^{n+} and MX), is generally considered to be bioavailable according to the free ion model (Sunda and Guillard, 1976). The phytoplankton growth limiting M' concentration of some metals has been studied for some relevant phytoplankton species (Brand et al., 1983; Brand et al., 1986; Sunda and Huntsman, 1992).

The inorganic speciation of metals has been well constrained for seawater (Turner et al., 1981; Morel, 1983; Byrne et al., 1988). Zn's inorganic species are mostly chlorides, hydroxides and carbonates, while Cd's is dominated by chlorides. Free Zn

(Zn^{2+}) accounts for ~ 50 % of Zn_{TD}, in clear contrast to the free Cd (Cd^{2+}), which accounts for less than 3 % of Cd_{TD}.

The organic speciation of metals has only been studied over the past, 20 years. Organic ligands have been reported to have extremely high affinities and relative specificities for certain metals, which causes their organic complexes to dominate metal speciation in oceanic waters. For example, more than 98 % and 70 % of of Zn_{TD} and Cd_{TD} species are reported to be organic complexes in surface ocean waters (Bruland, 1989, 1992). Thus, the presence of organic ligands is hypothesized to regulate the M' concentration to levels optimal for the growth of organisms excreting them (Morel and Price, 2003; Lohan et al., 2005). Organic complexation may in turn cause phytoplankton limitation by a certain metal if the M' concentration is lower than the biological requirement (Sunda and Huntsman, 2005; Lohan et al., 2005). By producing ligands and lowering the M', some phytoplankton species could outcompete other phytoplankton species with higher metal requirements (Whitfield, 2001), suggesting some ML complexes might be available to specific phytoplankton species only, possibly via receptor-site compatibility.

Specific cases have been reported where, despite very low M_{TD} concentrations and the presence of organic ligands bringing the M' down to very low ranges, there was no metal limitation. This implies the ML complex could be bioavailable for some phytoplankton species (Ellwood, 2004; Coale et al., 2005), thus questioning the validity of the free ion model's. Specifically, acquisition Fe ligands called siderophores, presumably produced by phytoplankton not only are bioavailable, but have been shown to help the solubilization and uptake process (Miethke and Marahiel, 2007; Maldonado and Price, 1999).

1.1.4. Identity and source of the organic ligands

Except for the Fe-complexing siderophores, the chemical identities, properties and structure of the strong metal-complexing ligands are still largely unknown, although important progress has been made (Bruland, 1989, 1992; Moffett and Brand, 1996; Wells

et al., 1998; Vasconcelos et al., 2002; Lohan et al., 2005). A significant portion of these ligands is thought to be of relatively low molecular weight, (less than 1 KDa; Wells et al., 1998; Ellwood, 2004), and sulfide, thiols or organic polymers of thiols (phytochelatins) are suspected to be either precursors, or a part or the whole ligand (al-Farawati and van den Berg, 1998; Dryden et al., 2007; Dupont and Ahner, 2005).

These metal-complexing ligands are believed to be organic molecules produced by phytoplankton to either keep the metals in solution and help uptake, or to detoxify deleterious metal concentrations (Bruland, 1989, 1992; Moffett and Brand, 1996; Lohan et al., 2005). I will refer to these two possible types as "acquisition" and "detox" ligands. Evidence of the former is production of a ligand by specific phytoplankton species when exposed to increased Zn concentrations (Vasconcelos et al., 2002; Lohan et al., 2005), and the latter when stressed with toxic Cu concentrations (Moffett and Brand, 1996; Croot et al., 2000). Lohan et al. (2005) showed that after the onset of certain conditions, Zn ligand production is rather fast (less than 1 day).

Another source of ligands in estuaries and coastal regions is suspected to be organic matter from the bottom part of the water column near the seabed, known as the benthic zone (Skrabal et al., 1997, 2000, 2006; Carrasco et al., 2002). These processes have been suggested to have global influence (Shank et al., 2004), but specific regions' effects need to be studied thoroughly to estimate their scope. Recently continental shelves have been suggested as a source of Fe and other trace metals (Lam et al., 2006, 2008; Morton et al., 2008) and ligands (Carrasco et al., 2008) to the world's oceans.

A ligand's strength is expressed in terms of its affinity for a specific metal through a stability constant K, usually expressed as a conditional stability constant (K'), depending on certain environmental parameters of the waters. In this study, all K's determined and compared are expressed as $K'_{ML'M'}$, conditional stability constants of the ML complex with respect to the inorganic metal fraction; a K' with respect to free metal is converted into a K's with respect to inorganic metal by dividing it by the inorganic side reaction coefficient (α_M). These K's are usually several orders of magnitude higher than

those of non-specific organic ligands (e.g. humics or fulvics) or inorganic ligands (Moffet et al., 1997; Xue and Sunda, 1997). Conversely, these organic ligands' concentrations ([L]) are usually orders of magnitude lower than those of nonspecific organic ligands or inorganic ligands (Byrne et al., 1988; al-Farawati and van den Berg, 1998; Kozelka and Bruland, 1998), given that a very small concentration of a very strong metal-specific organic ligand can affect the chemical speciation of a metal by binding to a higher amount of M_{TD} than higher concentrations of weaker non-specific organic or inorganic ligands. The product of the K' and the [L] is the organic side reaction coefficient (α_{MLi}), also referred to as the complexing index (CI) in this text, which defines the extent of complexation caused by a particular ligand (Bruland, 1989; Kozelka and Bruland, 1998).

Organic ligands have been reported to be metal specific for Zn, Cd and other metals in estuaries (Kozelka and Bruland, 1998) and somewhat-specific for Zn and Cd in oceanic regimes (Ellwood, 2004). Studies have shown the presence of one or two or even three different complexing ligands for each metal, each displaying a particular distribution, usually the stronger ligand (L1) at lower concentrations than the weaker (L2 or L3). For references of ligands determined in natural waters, see: Cu and Ni, Donat et al. (1994); Zn, Cd, Cu and Pb, Kozelka and Bruland (1998); Zn and Cu, Muller et al. (2001); Zn, Cu and Mn, Muller et al. (2003), Zn and Cd, Carrasco et al. (2002, 2008). Sometimes the term L_T is used to refer to the concentration of all ligands added together. The extent of Cu complexation effected by organic ligands L1, L2 and L3, for example, in the Narragansett Bay is larger for L1 than for L2 and for L3 mainly because the higher value for K'_{CuL1} with respect to K'_{CuL2} or K'_{CuL3} (log K' for L1, L2 and L3 are 12.0, 8.8 and 7.7, respectively, Kozelka and Bruland, 1998). In a mesocosm study in coastal waters, Muller (2003) found a similar situation: slightly higher concentrations of the weaker ligands overwhelmed by 4-order-of-magnitude-stronger strong ligands for Cu (log K' for L1, L2 and L3 are 13.7, 9.0 and 7.4, respectively).

1.1.5. Previous Zn and Cd speciation results in Coastal and Estuarine regions

Zn speciation has been studied in coastal and estuarine areas including the Chesapeake Bay (Henry and Donat, 1996; Carrasco et al., 2002); Narragansett Bay

(Kozelka and Bruland, 1998) and a fjord off Norway (Muller et al., 2003). Most studies reported one Zn ligand with logK' ~ 8.5 - 10.0 in concentrations (or activities, rather, given that their chemical identitites are unknown) ranging from tens to hundreds of nM, high Zn_{TD} ~ 4 - 70 nM, generally representing more than 95 % of the Zn_{TD}. Carrasco et al. (2002) observed two ligands simultaneously (logK1 ~ 10.1, logK2 ~ 8.6) in concentrations ~ 15 - 25 nM (L_T), Zn_{TD} ~ 5 - 15 nM in the Chesapeake Bay; at higher metal concentrations (20 - 90 nM) only L2 could be perceived, and in some of the highest concentration range (70 - 165 nM) no ligands could be perceived; these ligands complexed 40 - 99.9 % of the Zn_{TD}. Muller et al. (2003) reported the presence of a Zn-binding ligand following an *Emiliana huxleyii* bloom in a mesocosm study and they suggested that ligands can originate from dead or decaying phytoplankton.

Kozelka and Bruland (1998) studied the Cd speciation (along with Zn, Cu and Pb) in Narragansett Bay and found one Cd ligand with logK' ~ 8.9 was present in concentrations ~ 4 nM well in excess of the low Cd_{TD} ~ 0.3 - 0.9 nM, and complexing 73 - 83 % of the Cd_{TD}. These results are very similar to those of Muller et al. (1996) for Southampton Bay and Kozelka (unpublished) for San Francisco Bay, where a single Cd ligand with very similar strength (logK' ~ 8.5) was observed. Carrasco et al. (2002) observed in the Chesapeake Bay two Cd ligands (logK1 ~ 9.5, logK2 ~ 8.4) in concentrations ~ 1 nM (L_T), in excess of Cd_{TD} ~ 0.1 - 0.2 nM; at higher metal concentrations (0.4 - 0.6 nM) only L2 could be perceived; these ligands complexed 10 - 70 % of the Cd_{TD}.

Muller et al. (2001) reported the speciation of Zn and other metals in surface waters of the Black Sea. One Zn ligand of logK' ~ 9.8 is present in concentrations 8 - 23 nM, in excess of Zn_{TD} (1 - 6 nM) complexing 82 - 97 % of the Zn_{TD} (Muller et al., 2001).

1.1.6. Previous Zn and Cd speciation results in oceanic regimes

Until recently, very few studies of Zn and Cd speciation have been reported in open ocean regimes, and only for the few stations in the North Atlantic (Ellwood and van den Berg, 2000), the North Pacific (Bruland, 1989; Donat and Bruland, 1990; Bruland,

1992; Lohan et al., 2005), and the Subarctic Pacific (Ellwood, 2004). In the past two years, the Southern Ocean, including a transect along the Zero meridian and other across the Drake Passage (Baars and Croot, submitted) and a Western Subarctic North Pacific study (Carrasco et al., 2008) have been reported and are discussed, as well as a single upper 200m station in the North Atlantic (Jakuba et al., 2008).

Bruland (1989) determined Zn speciation in the upper 600m of the North Pacific and Ellwood and van den Berg (2000) studied the upper 2000m in the North Atlantic. Both of these sets of results show 0.4 - 2.2 nM of only one Zn ligand with logK' ~ 10.0 - 10.6 in low Zn_{TD} ~ 0.1 - 0.7 nM, complexing more than 95 % of the Zn_{TD}. In Southern Ocean surface waters, 1.6 - 2.2 nM of a Zn ligand with logK' ~ 10.0 decreased the very low Zn_{TD} (0.006 - 0.060 nM) to Zn^{2+} concentrations below the reported limiting concentrations, though no actual limitation was observed (Ellwood, 2004). A similarly strong, yet less concentrated ligand (logK' ~ 9.9, L ~ 1 nM), was observed in the upper, 200m of the North Atlantic (Jakuba et al., 2008) in higher Zn_{TD} of 0.2 - 0.7 nM. Lohan et al. (2005) reported a ligand with a logK' ~ 10.5 to be present at a concentration of 0.72 nM in waters with 0.07 nM Zn_{TD} and, after some metal additions they observed the production of up to 10 times more of what they hypothesize to be an "acquisition" ligand. Carrasco et al. (2008) reported an intricate intermediate and deep water mass situation in the upper 1000m of the Western North Pacific, with two Zn ligands (logK's 11.4 and 9.5) and suggested that some ligands were transported from continental shelves of marginal seas to the middle of the Pacific Ocean in decreasing concentrations, on top of others being mainly found in surface waters. Baars and Croot (submitted) recently report two Zn ligands in waters of the Southern Ocean (logK's 10.4 and 9.1), which are present in different water masses down to 3000m at concentrations below those of Zn_{TD}, as well as along the Zero meridian transect, where the ligand/metal ratio changes dramatically with latitude.

Cd speciation has been reported only by Bruland (1992) and Carrasco et al. (2008) in the North Pacific, and Ellwood (2004) in the Southern Ocean. Bruland (1992) and Ellwood (2004) reported a single Cd ligand of very similar strength (logK' 10.5) present

in the upper, 200m of both oceans. Bruland (1992) found this strong ligand only in the upper 200m of the 600m he analyzed, while Ellwood studied only the upper 100m. In general, the observed strong ligand existed at concentrations 2-3 orders of magnitude higher than the low Cd_{TD} present (~ 0.002 - 0.004 nM), complexing greater than 70 % of the Cd_{TD}. Carrasco et al. (2008) observed three Cd ligands (logK's 11.2, 9.9 and 9.2) in the upper 1000m of the Western North Pacific, related to transport of marginal seas organic matter along intermediate and deep water masses and also *in situ* surface water phytoplankton production, too.

In summary, in estuarine, coastal and oceanic regimes the presence of Zn and Cd ligands appears to control these metals' speciation. Recent oceanic studies suggest an apparent connection between estuarine and coastal regimes' ligands, evidenced by the distribution of rather strong metal complexing ligands. Though terrestrial organic matter is believed to have weak complexing ligands, phytoplankton communities in estuarine and coastal regions complex the high Zn_{TD} and Cd_{TD} concentrations, decreasing the Zn^{2+} and Cd^{2+} values to ranges slightly above those of oceanic regimes. Specific hot spots of ligand production in regions of water mass formation need to be studied more thoroughly, so that the potential transport and global distribution of ligands produced there can be estimated. While in estuarine and coastal regions the concentrations of Zn^{2+} and Cd^{2+} are below toxic levels, similar or stronger ligands in oceanic regimes could produce these required metals' bioavailable concentrations to decrease to or below limiting ranges.

1.2. MAIN GOAL AND SPECIFIC QUESTIONS

Understanding Zn and Cd chemical speciation resulting from organic complexation in seawaters is important to evaluate the effect of these metals' bioavailable chemical species on carbon uptake and then on primary productivity in the world's ocean. For my Ph.D. dissertation research, I have studied Zn and Cd speciation in the Equatorial and South Atlantic, a very diverse region of the Atlantic not studied before, characterized by unique oceanographic features including the potential source of metals and organic matter from the Amazon River, the presence of an oxygen minimum zone in the

Equatorial East Atlantic off Africa and the layering of water masses typical of the Atlantic Ocean, that could influence these metals' chemical speciation.

Samples taken during the IOC 1996 Contaminant Baseline Survey cruise (Montevideo, Uruguay to Bridgetown, Barbados) in the Western South and Equatorial Atlantic Ocean (Fig. 1) provided the opportunity to study the input of the Amazon River and organic matter originated presumably near the Congo River, the oxygen minimum zone off of Equatorial Africa and the intermediate and deep water masses present in the Atlantic Ocean as they travel away from their sources. An evaluation of the pointed sources and influences, compared with the continuum of metal and ligand concentrations to be found in the aging water masses will provide information needed to estimate each factor's relative importance.

1.2.1. Study site

The Equatorial and South Atlantic Ocean is characterized by the following salient features. The Amazon River, the largest input of freshwater into the world's oceans, is a source of metals (Zn, Schiller and Boyle, 1985; Cd, Boyle et al., 1982; Rutgers van der Loeff et al., 1997), organic matter and nutrients (Conkright et al., 2000; Mikkelsen, 1997; Hu et al., 2004; Rutgers van der Loeff et al., 1997), and may be a source of organic complexing ligands (Powell and Donat, 2001), not only on a regional scale, but possibly in a wider scale (Conkright et al., 2000; Lenes et al., 2005). Sampling of stations near the Amazon River mouth during the IOC 1996 cruise occurred around the maximum river discharge season (Ffield, 2005), so a noticeable riverine effect was expected and observed in stations nearer the river's mouth. The presence of low oxygen concentrations in the Equatorial East Atlantic off Africa (Cutter and Measures, 1999) means that hypoxic conditions or even an oxygen minimum zone (OMZ) were to be encountered and affect redox speciation of metals (Hopkinson et al., 2007) and also chemical speciation. The oxygen concentrations were low, and thus their effect on Zn and Cd's chemical speciation are discussed. Finally, the layering of water masses typical of the Atlantic Ocean has been determined long ago; the water mass structure of the IOC 1996 cruise stations is detailed in Cutter and Measures (1999), and certain metals have been reported to have

"signature" concentration from specific water masses formed at high latitudes (e.g. Cd, Yeats, 1995; Saager et al., 1997; Se, Cutter et al., 2001; Fe, Laes et al., 2003). Further, Ellwood and van den Berg (2000) and Baars and Croot (2010) reported Zn speciation in locations related to the formation location of some water masses studied here, which are discussed.

1.2.2. Specific Questions

My primary goal is to elucidate the influence of the processes that define the Equatorial and South Atlantic Ocean's Zn and Cd chemical speciation and the potential effect this might have on phytoplankton photosynthesis. In this regard, I set out to answer the following specific questions:

1. What is the chemical speciation of Zn and Cd in the Equatorial and South Atlantic Ocean? Is either Zn or Cd biolimiting in stations occupied in this region? Does the ancillary biological and chemical data match the expected limitation (or not)?

2. Does the Amazon River input of organic matter act as a source of organic complexing ligands? How does this riverine organic matter affect Zn and Cd chemical speciation? Is this effect localized near the mouth of the Amazon River or is the effect more in a regional scale, spread out throughout the South Atlantic Ocean, as some studies suggest? How do allochthonous riverine and authocthonous phytoplanktonic organic complexing ligands compare in their efficiency to complex Zn and Cd?

3. How does the low oxygen region off equatorial Africa affect the Zn and Cd speciation? What can this say about ligand production in this sort of environments?

4. What effect does the layering of water masses in the Atlantic Ocean have on depth profiles of Zn, Cd and, potentially, organic ligands that bind to either metal? Is there a "signature" concentration of metals and/or organic ligands from each water

mass? What can be inferred about residence times of organic ligands in these water masses?

5. Is there any other source of metals or ligands to the area? How localized or regional is its effect, compared with the abovementioned influencing factors?

6. What ramifications do these pointed sources and processes have on regional and global scales? How do they affect the chemical speciation of Zn and Cd in surface waters elsewhere in the global oceans?

CHAPTER 2

METHODS

Samples taken during the IOC 1996 expedition, collected at various depths at vertical profile stations, were analyzed for their Zn and Cd chemical speciation using anodic stripping voltammetry (Bruland, 1989, 1992). Preconcentration of samples for M_{TD} analyses are performed by complexation with the ligands APDC/DDDC and solvent extraction following Bruland et al.'s (1979) method and Ellwood's (2004) improvements. Ancillary data (e.g. salinity, temperature, pH, chlorophyll-*a*, etc.) are available in the hydrography paper (Cutter and Measures, 1999), or at Dr. Measures' website http://www.soest.hawA2.edu/oceanography/faculty/measuresIOCcruise.html. To compare Zn and Cd data with total dissolved Co, Bowie et al.'s (2002) data from nearby South Atlantic stations were used since some samples were taken within one or two months after the IOC 1996 samples were obtained.

2.1. SAMPLING CONSIDERATIONS

2.1.1. Sampling Site and Ancillary Data

During the 1996 IOC expedition, six vertical profile stations were occupied in the subtropical and tropical Atlantic between May and June from Montevideo, Uruguay to Georgetown, Barbados. Exact station locations are presented in Table 1 and shown in Fig. 1. More hydrographic data can be found in the Results and Discussion chapter and in Cutter and Measures (1999), as well as information on the methodology used for the unpublished ancillary data.

2.1.2. Sampling and Storage

Water samples for trace metal analyses were collected using trace metal clean techniques (Bruland et al., 1979). All sample manipulation and analyses were performed in a class-100 clean air work area, with the goal of maintaining the integrity of the

sample. Water samples were collected using Teflon-coated 30-L GO-Flo bottles (General Oceanics©), previously rinsed with weak optima-grade HNO_3 (hereafter "O-HNO_3"), MQ and seawater, and deployed on a Kevlar hydrographic line to obtain the depth profile samples. After capturing the seawater sample at the appropriate depth, the GO-Flo bottles were placed in a clean lab supplied with filtered air and pressurized using filtered suprapure N_2 gas and filtered through a 0.22 μm pore-size polypropylene cartridge filter (MSI Inc). All samples were kept double-bagged to prevent contamination.

Separate sub-samples obtained for M_{TD} and speciation analyses were collected in 1L acid-washed fluorinated high density polyethylene (FLPE) and 1L acid-washed high density polyethylene (HDPE) bottles (Fisher Scientific), respectively. M_{TD} samples were acidified to pH 2 with optima-grade HCl (hereafter "O-HCl") and then stored for 6-12 months prior to analysis. Speciation samples were frozen immediately after filtering and kept frozen and in the dark, and were thawed just before being analyzed.

Table 1

Vertical profile stations occupied during the 1996 IOC cruise. All stations depth profiles were analyzed completely except Amazon 1 and 2 (only upper 400m).

Station	Dates	Latitude	Longitude	Depth (m)
Amazon 1	15 June	5.72°N	48.09°W	3625
Amazon 2	16-17 June	6.49°N	48.80°W	4030
6	11-13 June	8.00°N	45.00°W	4610
Romanche	3-4 June	0.59°S	20.03°W	6560
8	28-30 May	17.0°S	25.00°W	5150
10	21-23 May	33.0°S	40.00°W	4650

2.2. ANALYSES AND CALCULATIONS

2.2.1. Total Dissolved Metal Analyses

For the M_{TD} analyses, graphite furnace atomic absorption spectroscopy (GFAAS) was used, preceeded by a a solvent extraction method (Bruland et al., 1979) in which the ligands ammonium pyrrolidine dithiocarbamate (APDC) and diethyl dithiocarbamate (DDC) are added to the seawater sample to complex the metals. These complexes are then extracted into chloroform. The chloroform extract is taken to dryness and the residue is digested in hot O-HNO_3, taken to dryness and the metals are reconstituted in 1M O-HNO_3 and analyzed by GFAAS.

The separation funnels and evaporation cups used are all made of acid-cleaned Teflon, except the final high-concentration (~ 200 times the natural concentration) vials, which are made of polypropylene. The analysis was performed using a Perkin Elmer 4100 ZL atomic absorption spectrophotometer with Zeeman background correction. The technique was tested by running standard reference materials (SRM), checking blanks continuously and determining recoveries of metals off of SRMs. The concentration of metals was determined by standard additions.

The total dissolved metal analyses were performed by a Donat Research Group Technician, Cynthia Wickstrom, and a Postdoctoral Research Associate, Dr. Rodney T. Powell.

2.2.2. Complexation Analyses

For the complexation and speciation analyses, differential pulse anodic stripping voltammetry (DPASV) at a thin mercury film deposited on a rotating glassy carbon disk electrode (TMF-RGCDE) was used, following the methodology described by Bruland (1989, 1992) and Donat and Bruland (1990). DPASV determines metal speciation directly by measuring the concentration of M' (the inorganic metal fraction) in equilibrium with organically-complexed metal in an aliquot of sample as the metal concentration is increased during a titration of the organic complexes.

The potential applied to the TMF-RGCDE is controlled using a potentiostat. When applied potentials are more negative than the oxidation potential of the metal of interest, M' is reduced to M^0 which then electrodeposits as an amalgam into the TMF on the RGCDE. The electrodeposition step is performed for a time period that concentrates M^0 to detectable levels. M^0 is then reoxidized out of the amalgam by ramping the potential in the positive direction, yielding a current that is proportional to the concentration of M' present in the aliquot of sample.

The electrochemical instrumentation used consisted of an EG&G 264A (Princeton Applied Research) voltammetric analyzers connected to an electrochemical cell consisting of a PAR Rotel2 RGCDE (carbon disk diameter is 6 mm, maximum rotation speed 4000 RPM) working electrode (WE), a platinum wire counter electrode (CE) and a Ag/AgCl reference electrode (RE). The electrochemical cell was set in a plexiglass cell stand which accommodates one additional position for sample purging. Both CE and RE are covered with acid-washable Teflon sleeves and porous Vycor glass frits, while the WE body is plexiglass. The three electrodes and the sample are inside a ~ 60 ml Teflon sample cup when in operation, and while on stand-by are stored in a plexiglass cup that isolates the WE and allows the RE and CE to soak in pH 2 O-HCl solution overnight.

The instruments were prepared for analysis by polishing the WE with 0.05 μm-size gamma alumina (Buehler) at 500 RPM for 30 seconds, followed by a quick pH 2 acid rinse and a final 2 minute rinse at 4000 RPM in two separate MQ aliquots. Then a TMF was platted on the WE by platting a de-aerated ~50 μM Hg solution prepared from triple-distilled Hg (Bethlehem Apparatus) for 10 minutes at -1.3 V. The fresh TMF was stripped for 2 minutes in two separate aliquots of MQ at 0.0 V to minimize any possible Zn or Cd contamination in the Hg film. A control deposition on the second MQ aliquot can gauge the levels of Zn or Cd present, which should be "zero" at this point. If they are observed to be significant, the WE should be polished again and a new TMF platted, until contamination levels are low enough for the sample to be processed. The goal here is to keep contamination at bay in the TMF, the only reagent in ASV besides the standard used for the standard additions.

Before analyzing a sample, an aliquot of ~ 40 ml seawater sample was run through the whole analytical procedure (electrodeposition, scan and stripping, see below) to condition the WE. The scan also gives an estimate of the natural Zn' and Cd' concentrations, so that the approximate addition scheme can be estimated.

Then a previously de-aerated zero-addition aliquot of ~ 40 ml of sample in a Teflon cup (cup A) was platted for 15 minutes at -1.3 V, in the electrodeposition step. Then a 30 second period of no potential being applied and no rotation on the RGCDE follows, in the quiescence time. After that, the current is measured as the potential was ramped in the positive direction starting at – 1.3 V and continuing until Zn and Cd peaks show up in a voltammogram. Zn usually shows around - 1.1 V and Cd around – 0.9 V. This scan step is carried at a rate of 10 mV per second, with differential pulses added onto the linear scan, 5 pulses of 100 mV per second, to increase the method's sensitivity. Finally a stripping step, consisting of a 2-minute deposition at - 0.15 V was performed, in order to strip all Zn and Cd ions from the TMF into the sample, in order to both have a clean film that can be used for the next sample's aliquot and to maintain the aliquot's Zn and Cd concentration intact.

Then a second de-aerated zero-addition aliquot in a second cup (cup B) was plated, starting another electrodeposition, scan and stripping cycle, while the sample in cup A equilibrated with some additions of Zn and Cd for ~ 20 minutes, the amount of time it took the other cup to go through the electrodeposition, scan and stripping cycle. This leap-frogging addition scheme continued between cup A and cup B for somewhere between 12 and 14 additions, which added to the two zero-addition points constitute enough points to mathematically be able to support data for more than one ligand, if there were any (Miller and Bruland, 1997). The additions were performed in incrementally higher additions, trying to maximize the level of detail where the ligand depletion curves off into the linear portion of the titration (Garnier et al., 2004).

In this study, simultaneous Zn and Cd titrations were performed at a deposition potential of -1.3 V after some testing with simultaneous and non-simultaneous Zn and Cd

titrations (Carrasco et al., in preparation). Briefly, simultaneous titrations have been discouraged because of the potential for Cd ligands to be over-reduced at potentials more negative than - 0.9 V (Bruland, 1992). To test for potential reduction of Cd ligands at – 1.3 V, separate Cd titrations were run at - 0.9 V and at - 1.3 V, showing significatively similar L and log K' results. Moreover, most of the Bruland's 1989 and 1992 studies were performed with simultaneous Zn and Cd titrations.

Additionally, two instrumental setups were run simultaneously, allowing for every sample to be run twice. The results reported here are the averages of these two runs.

2.2.3. Determination and Optimization of Ligand Concentration (L) and Stability Constant (logK)

The aforementioned titration provides data that can be mathematically manipulated to obtain the organic ligand(s) concentration(s), L, and the strength(s) of the complex(es) they form with the metal of interest, K. There are several mathematical solutions, involving linear and non-linear approaches (Garnier et al., 2004). Briefly, Miller and Bruland (1997) showed that the two linear models used (Ruzic and Scatchard plots) produce L and K data with method-inherent errors, more so if there is a mixture of two or more ligands. Gerringa et al. (1995) and Garnier et al. (2004) used non-linear approaches and showed that smaller errors are produced using them.

I designed and used a novel protocol which involves a series of linear approaches, the Langmiur-Ruzic-van den Berg (Ruzic, 1982) and the Scatchard plots (Scatchard, 1949; Mantoura and Riley, 1975; Miller and Bruland, 1997), which uses raw titration data, allows visualization of the Ruzic linearization, estimates L and K values using the Scatchard linearization and produces results that are then entered and optimized by a non-linear solution, the Gerringa plot (Gerringa et al., 1995), through a Levenberg-Marquadt minimum error estimation program in MatLab (Carrasco et al., in preparation). The next chapter is completely devoted to explaining this improvement of the existing mathematical tools.

2.2.4. Chemical Speciation Calculation

After Turner et al.'s (1981) and Byrne et al.'s (1988) seminal papers showed how to adequately calculate the inorganic speciation of elements, researchers began to develop software that can do all the mathematical calculations implied in adapting these calculations to specific oceanic environmental conditions. Thus, using salinity, pH and temperature of the sample, the free concentrations of the major inorganic anions forming complexes with the metals and the stability constants of their metal complexes were calculated using an ion pairing computer program (van den Berg, online unpublished computer program at http://www.liv.ac.uk/~sn35/Marine_Electrochemistry.html). Then the metal speciation was calculated using the chemical equilibrium modeling program MINEQL+ ©, with the salinity-pH-temperature corrected values of the inorganic complexes stability constants and the organic complexes [L]s and K's (obtained from the mathematical manipulation of the metal titration output data) as inputs.

CHAPTER 3

A NEW COMPREHENSIVE MATHEMATICAL SOLUTION TO INTERPRET METAL COMPLEXATION TITRATIONS

In seawater, the total dissolved concentration of a metal (M_{TD}) is distributed among different chemical species, and this chemical speciation dictates a metal's bioavailability. Strong organic metal chelating ligands can greatly affect the metal's chemical speciation in the ocean by reducing the concentrations of free metal (M^{n+}), the bioavailable form of these metals according to the free-ion model (Sunda and Guillard, 1976). The metal complexation can enhance growth by reducing concentrations of toxic forms or by enhancing the solubility of nutrient metal. Understanding these bioactive metals' chemical speciation in seawaters is important to evaluate their bioavailable chemical species effect on photosynthesis and carbon uptake, ultimately related to global climate (Hong et al., 2005).

The procedure to calculate trace metals' chemical speciation involves four steps. First, the M_{TD} is determined in an aliquot of acidified and UV-oxidized sample. Secondly, a metal titration of the organic ligands is performed in an aliquot of the natural sample. These titrations can be monitored using electroanalytical techniques by either anodic stripping voltammetry (ASV) or cathodic stripping voltammetry (CSV; ASV, Bruland, 1989, 1992; CSV, van den Berg, 1985). Using ASV to monitor a titration of a ligand by a metal, it is possible to determine the stability constant of the ML complex with respect to the inorganic metal $K'_{ML,M'}$, while CSV can be used to determines the stability constant of the ML complex with respect to the free metal $K'_{ML,M}{}^{n+}$. A simple conversion of $K'_{ML,M'}$ into $K'_{ML,M}{}^{n+}$ can be done by multiplying the former by the inorganic side reaction coefficient α_M to obtain the latter, as follows:

$$K'_{ML,M'} \times \alpha_M = K'_{ML,M}{}^{n+} \qquad (1)$$

The program described in this chapter can work with titration data produced by both techniques, since all the ratios of M'/ML and ML/M' for ASV, or M^{n+}/ML and ML/M^{n+} for CSV, is calculated and only a manual final conversion of K' is needed to be able to compare similar parameters.

The third step to calculate metal speciation is to interpret the titration and obtain the organic ligand(s) concentration(s), L, and the strength(s) of the complex(es) they form with the metal of interest, K', one can use any of the three mathematical approaches that have been historically used: a Ruzic or a Scatchard linearization or the Gerringa non-linear approach (Ruzic, 1982; van den Berg, 1982; Scatchard, 1949; Miller and Bruland, 1997; Gerringa et al., 1995). Finally, the metal's chemical speciation can be calculated using programs like MINEQL and some simple chemical and physical parameters of the natural sample (pH, salinity, temperature).

Few comparative studies have been written about the three mathematical approaches that can be used to interpret a titration (e.g. Miller and Bruland, 1997; Garnier et al., 2004), focusing on the level of uncertainty each method poses on the final parameters produced, L and K. Still, most scientists use only one of those mathematical methods, generally fixing it to a specific number of ligands, usually one. This may be the case because in order to produce statistically sound L and K values a titration needs to have certain features, mainly low noise and a certain minimum number of titration additions.

I developed Titration Data Interpreter (TDI), a MatLab program that uses sequential Ruzic & Scatchard linear approaches to obtain an initial set of L and K values, which are then optimized with the Gerringa non-linear approach into a final set of L and K values through a Levenberg-Marquadt minimum errors iteration step that fits them to the original titration data. The titration and all three mathematical approaches can be graphed, for a thorough visual examination by the researcher. The overall objective of this chapter is to describe TDI and to evaluate its performance at interpreting metal titrations.

To evaluate TDI, datasets of real and modeled titrations from relevant literature (Bruland, 1989; Bruland, 1992; Donat and Bruland, 1990; Ellwood, 2004; Kozelka and Bruland, 1998; Lohan et al., 2005; van den Berg et al., 2006; Tian et al., 2006; Garnier et al., 2004; Miller and Bruland, 1997; Carrasco and Donat, 2001 and Carrasco et al., 2008) were processed, and the robustness of their L and K results were examined and compared with the original results reported in each publication. Specifically the following points were examined:

- the level of uncertainty in each parameter produced.
- the level of correlation between published results and those obtained by TDI,
- the apparent dilemma that originates when having to decide for a 1-ligand model or a 2-ligand model and possible ramifications of either case,

Finally, the internal calibration, slope-iteration methodology of Hudson et al. (2003) and the hypothesis that humics as weak ligands can be mathematically difficult to evaluate with these mathematical approaches (Voelker and Kogut, 2001) are discussed in light of TDI's performance.

3.1. BACKGROUND

3.1.1. Metal titrations

The metal complexation parameters, L and K can be determined by a few different analytical methods. When the electroanalytical methods anodic stripping voltammetry (ASV) or cathodic stripping voltammetry (CSV) are used, the metal titration produces an electrical current for each addition of the metal. When using ASV, the electrical signal is proportional to the concentration of inorganic metal (M' for Zn, Cd, Cu, Pb) present in a sample aliquot:

$$i_p = S \times M' = S \times M^{n+} \times \alpha_M \qquad (2)$$

where i_p is the peak oxidation current of the metal, S is the instrumental analytical sensitivity, M' is the concentration of the inorganic metal, which is equal to the free metal M^{n+} multiplied by the inorganic side reaction coefficient α_M. Complexation of the metal by organic ligands reduces the signal by lowering the concentration of the inorganic metal.

An aliquot sample that has been acidified (pH2) for months and recently UV-oxidized sample, so that the organic ligands are degraded, is used for a M_{TD} determination. A short series of standard additions (3-5 additions) is made and a linear response is observed when plotting signal vs. metal additions, with a slope equal to S and a negative x-intercept which corresponds to the M_{TD} present in the sample. In the absence of organic ligands, a linear relationship should be observed in the concentration range between the limit of detection (LOD) and limit of linearity (LOL), i.e. the lowest and the highest concentrations reportable by the method in linear response.

ASV measures the inorganic metal fraction, and organic complexation decreases the fraction of metal that ASV detects, lowering the analytical signal. Once the organic ligands are saturated, the analytical response increases with increasing metal additions until the sensitivity is equal to that obtained in the absence of organic ligands. For a metal titration an aliquot of the natural sample is used, and a longer series of standard additions is made until several (at least 3 or 4) additions reflect a linear signal to M_{TD} response, indicating that the ligands are saturated.

Adding the sample's M_{TD} to the series of additions made in the titration yields the total M_{TD} in the sample during the titration at each titration point. In this unperturbed sample, as explained in the previous paragraph, organic ligands affect the linear relationship between signal and M_{TD} in a way that a signal-depletion is observed in the first points of the titration. A gradual tendency to merge with the last-points trend, where the ligand is presumed to be saturated if the last points are in a straight line whose slope should be close to the analytical sensitivity S observed in the M_{TD} determination, i.e. in the absence of organic ligands. An extrapolation of the slope of the last points of a

titration with organic ligand(s) and the correct addition scheme should yield a positive x-intercept roughly equal to the total ligand(s) concentration(s) (L_T) (see Fig. 2)

At concentrations below L_T, the signal depletion is evidenced as a curved signal to M_{TD} relationship, which can be rather abrupt if strong ligands are present (Bruland, 1989, for example) or more gradual if ligands with slightly lower binding strengths are present. But at concentrations higher than the L_T, once the ligand(s) are titrated by the metal added, a linear signal to M_{TD} response is observed (see Fig. 2).

At each titration point, the M_{TD} concentration is equal to the sum of its two fractions, the inorganically complexed M', and the organically complexed ML, according to the mass balance equation:

$$M_{TD} = M' + ML \qquad (3)$$

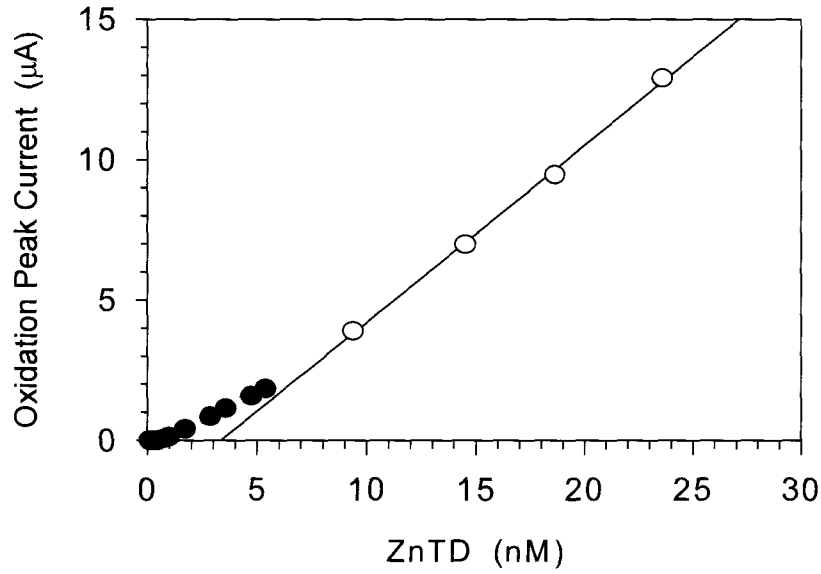

Fig. 2. Zinc titration of a complexing ligand or ligands. The slope of the last four additions in the titration curve (open circles) is used to calculate data for the plots.

Using the slope S of the linear portion of a titration curve M' can be calculated. From the metal mass balance, ML can be calculated and, finally, M' to ML and ML to M' ratios are determined. These four data are used in the linear and non-linear approaches to determine L and K.

3.1.2. Previously used mathematical approaches

Mathematical approaches used to evaluate and interpret metal titrations include Ruzic/van den Berg/Langmuir (hereafter referred to as Ruzic; Ruzic, 1982; van den Berg, 1982), Scatchard (Scatchard, 1949; Mantoura and Riley, 1975; Miller and Bruland, 1997), Gerringa (Gerringa et al., 1995) and, recently, PROSECE (Garnier et al., 2004). Ruzic obtains the L and K parameters from a M'/ML to M' plot, Scatchard from a ML/M' to ML, Gerringa from a ML to M' and PROSECE from a logM' to log M_{TD}.

Ruzic plots provide a graphical representation of the M'/ML to M' relationship. They yield, in the absence of much scatter, a linear section from which L and K for a single ligand can be calculated using the following equations:

$$L = 1 / \text{slope of straight line} \quad (4)$$

$$K = 1 / (\text{y-int} \times L) \quad (5)$$

In the presence of one ligand L, the Ruzic plot is a straight line with positive slope and positive y-intercept. In the presence of more than one ligand, these plots are curved near the plot origin and this curvature can be subtle and is often difficult to distinguish the curved section from the linear section, especially when the data are scattered, as can be seen in Fig. 3. A mathematical approach to divide the Ruzic plot into two sub-plots, to get L and K for both ligands was developed later (Pizeta and Branica, 1997).

While the Ruzic plots exhibit a subtle curvature that can be hard to distinguish in the presence of two or more ligands, Scatchard plots magnify the distinction between a weak and a strong ligand. A Scatchard plot provides a graphical representation of the ML/M'

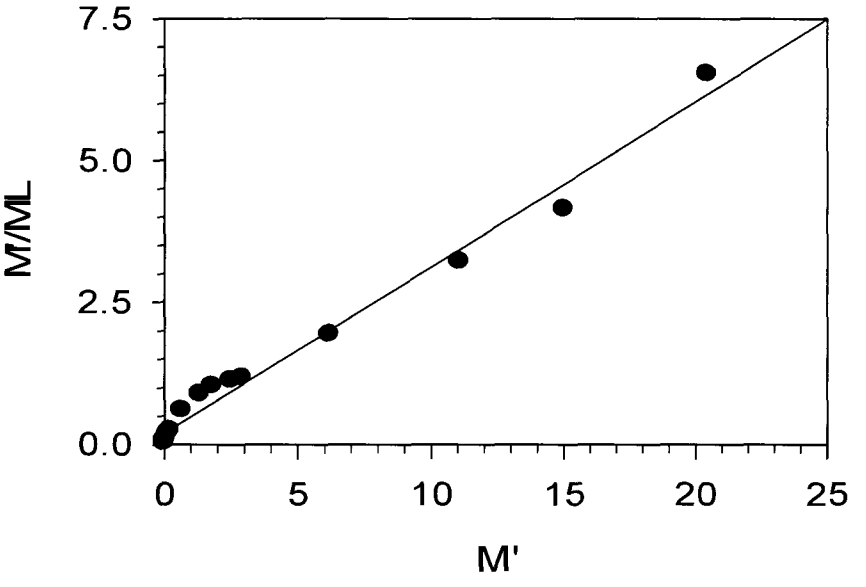

Fig. 3. Ruzic plot of the titration curve shown in Fig. 2. A curve near the origin indicates two ligands.

to ML relationship, and is broken, in the case of two organic ligands present, into two subsections. In the case of only one ligand present, the Scatchard plot looks linear, thus providing for a clear visual distinction between the two-ligand and the one-ligand cases. The L and K for the ligand or ligands can be easily calculated from the slope and x-intercept of each subsection or the complete plot.

$$L = \text{x-intercept of each subsection} \tag{6}$$

$$K = -\text{ slope of each subsection} \tag{7}$$

Standard procedure includes an iteration of the L obtained, assuming fixed K values, until a value close to the y-intercept is obtained satisfactorily for each subsection. This way that Scatchard plots minimize error in both L and K in comparison to Ruzic plots (Miller and Bruland, 1997). In order to obtain the best L and K possible, Miller and Bruland

(1997) used only the first two and the last two points of a Scatchard plot in a scatter-free, ideal titration dataset to obtain K values closer to the "true" values. This puts all the stress on two points in each end of the titration and assumes perfect instrumental response. In real titrations, with scatter and slightly imperfect instrumental response, the number of points to be included for each subset needs to be more than two points, for sure, and is studied for each specific case.

In all four plots (titration curve and Ruzic, Scatchard and Gerringa plots), the addition points, made using a leap-frogging scheme in two sub-samples in separate cups, were planned to have increasing metal concentrations and are, thus, ordered from the first two points, usually the zero additions, then the first to the last addition. Each titration point can then be followed in the graphs from the left to the right, as M_{TD}, M' and ML increase along the titration from point to point.

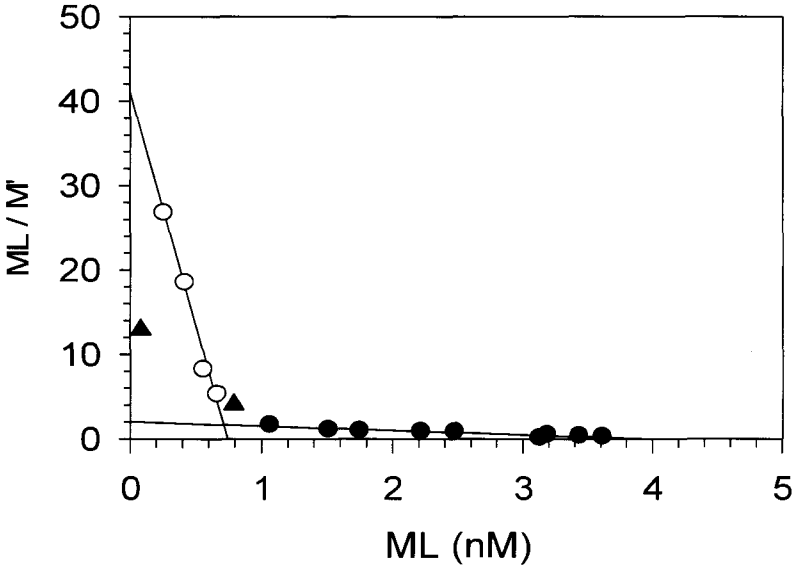

Fig. 4. Scatchard plot of the titration curve shown in Fig. 2. The dog-leg shape confirms the presence of two ligands. Each ligand data subset's points are indicated by circles (open and closed). From the best fit lines' slopes and x-intercepts, L and K values are calculated.

In Fig. 4, four points were used for the L1 subset (points 2 - 5, open circles) and nine points were used for the L2 subset (points 7 - 15, closed circles). Note that subjectivity arises when choosing which points to consider as belonging to each ligand subsection. In this specific case, points represented by the closed triangles (points 1 and 6) were arbitrarily not selected by the researcher because they do not represent the linear trend of each ligand data subset. In the end, datasets consisting of four and nine points, out of fifteen total titration points, were interpreted as defining the features of each respective ligand.

A more comprehensive view of the titration is needed, where all the points in the titration are considered for each parameter and, therefore, the weight of an individual outlier would not affect too dramatically a parameter defined by three or four points in a subset. Gerringa plots use all data points to calculate each of the L and K parameters, according to the following equation:

$$y = ((L1 \times K1 \times x) / (1 + (K1 \times x))) + ((L2 \times K2 \times x) / (1 + (K2 \times x))) \qquad (8)$$

Ruzic and Scatchard plots of titration curves obtained from samples containing only one ligand look different from those containing two ligands. While both Ruzic and Scatchard plots look linear for a one-ligand case, a two-ligand Ruzic plot shows a curvature near the origin and a Scatchard plot shows a dog-leg shape (Figs. 3 and 4). In contrast, a Gerringa plot (Fig. 5) looks always curved, whether having one or two or more ligands present, and the only possible visual estimation is the ~ L_T which is approximated by the y-intercept of the extended horizontal region of the plot once the curve plateaus at high metal concentrations. So, it is necessary to assume the number of ligands present in the sample before attempting to fit a titration dataset to a Gerringa plot. It is common practice to assume one ligand only, though there are cases where a preliminary evaluation is performed using either linearization, obtaining the number of ligands and initial L and K parameters, and then fitting the titration data to equation (8) using the observed number of ligands (e.g. Powell and Donat, 2001).

This mathematical approach was originally developed to interpret titration curves that were too scattered for Ruzic or Scatchard, usually those obtained from estuarine samples with very high concentrations of organic matter that could be a source of one or more several ligand classes (Gerringa et al., 1995). So, it is a common practice to run Gerringa plots by assuming a fixed number of ligands, usually one ligand only (e.g. Croot et al., 2002; Saito and Moffett, 2001; Jakuba et al., 2008b). This could be for statistical reasons (each parameter needs a minimum of four titration points in order to obtain statistically sound parameters), or because of the general tendency to adopt a conservative approach interpreting metal complexation titrations.

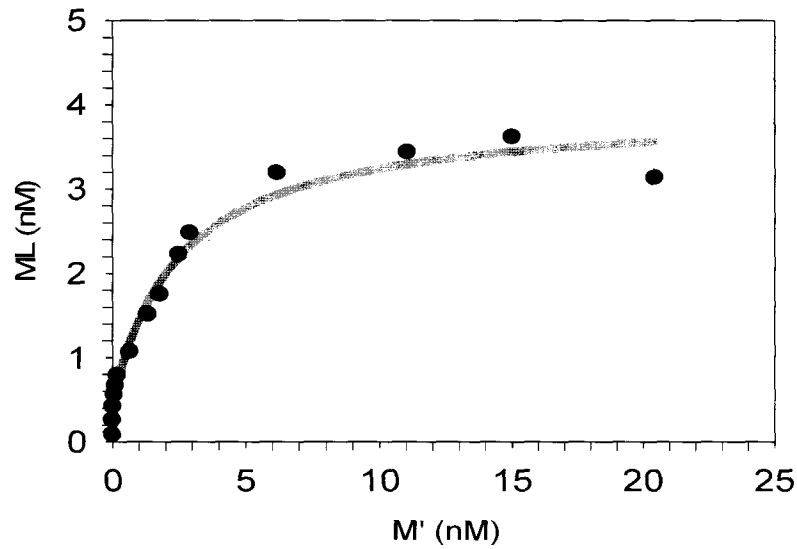

Fig. 5. Gerringa plot of the titration curve shown in Fig. 2. The line represents the iterated L and K values plugged into equation (8).

3.1.3. Introduction to TDI

Working with modeled data, Miller and Bruland (1997) showed that linear approaches like Ruzic and Scatchard produce L and K parameters with method-inherent errors, more so if there are a two or more ligands present. Garnier et al. (2004) compared linear and non-linear approaches on modeled data and showed that non-linear approaches produced smaller errors than linear approaches. Most recent papers use a conservative one-ligand one-mathematical approach (e.g. Croot et al., 2002; Saito and Moffett, 2001; Jakuba et al., 2008b).

With the aim of improving the statistical robustness and certainty of the parameters produced by a metal titration's mathematical interpretation, I have created a program in MatLab that uses raw titration data, allows visualization of all three mathematical approaches, estimates L and K values using the Scatchard linearization and optimizes those values by minimizing errors using a Levenberg-Marquadt minimum error iterative routine on the Gerringa non-linear approach. Not only does the program yield more robust parameters, but it also reduces dramatically the time involved and the chance to err when copying and pasting data from one step to the next and from one spreadsheet to another.

3.1.4. TDI's input and output

TDI's input is simply i_p and M_{TD}.

The output consists of four graphs and a set of thirteen numbers. The graphs are: titration curve, and Ruzic, Scatchard and Gerringa plots. The thirteen numbers produced are grouped in: titration data (S, x-intercept, r^2 of linear portion); Scatchard data (initial logK1, L1, logK2, L2) and Gerringa data (optimized logK1, L1, logK2, L2 plus logK0, L0 in case of zero signal points). Scatchard plot data represent initial L and K values, while Gerringa plot data represent the final optimized L and K values. The Gerringa plots show a curve obtained by fitting equation (8) to these final values, along with original titration data points.

As discussed earlier, Ruzic and Scatchard plots show if there is one or two ligands. There are three estimates of L_T that can be compared: the titration's and the Scatchard plot's x-intercepts and the Gerringa's y-intercept. Some titrations start with points that do not show any electric signal (zero-signal points). These titration points are assumed to be caused by the presence of a strong ligand that does not allow for any M^{n+} to be observed at the voltmamogram, whose concentration (L0) is estimated to be halfway between that of the last zero-signal point and that of the first point that produces an electric signal. This ligand's stability constant (logK0) can not be calculated, and is thus estimated as a minimum, which gets optimized into the Gerringa calculation. In such titrations, L0 needs to be added to the Scatchard and Gerringa's estimates of L_T (based on titration points that show electrical signal) to obtain a new L_T, and this new L_T can be compared with the titration's estimate. In titrations that start with zero-signal points whose Scatchard plots show the presence of two ligands, L and K parameters for three ligands are produced by TDI.

3.1.5. TDI's operating procedures step by step

In the titration curve step, TDI plots signal (i_p, in mA) vs. M_{TD} (nM); selects a number of points to be considered for the linear portion; obtains the robust slope of the linear portion, S; calculates its x-intercept and calculates M' and ML.

In the Ruzic linearization step, TDI plots M'/ML ratio vs. M' (nM)

In the Scatchard linearization step, TDI plots ML/M' ratio vs. ML (nM); looks up the robust r^2 of the whole dataset; decides if 1 or 2 ligands are present by comparing the r^2 of the whole dataset with a set value (the criterion is: if r^2 > a set value, then one ligand is present; if r^2 is < a set value, then two ligands are present). It then divides the whole dataset into 1 or 2 sub-sets, determines the robust slopes and x-intercepts of each subset, and then calculates K and L for each ligand at each subset.

In the Gerringa non-linear fit step, TDI plots ML (nM) vs. M' (nM) from original data; fits robustly the Scatchard L and K estimates to equation (8); iterates L and K until a

minimum error point is reached with respect to the original data, using a non-linear Levenberg-Marquadt (LM) least squares iterative fitting algorithm; and finally plots the curve obtained by fitting the final iterated and optimized L and K values to equation (8) on top of the original data points.

All linearizations and slopes in TDI's regression analyses are robust, i.e., a fit with weights for each point based on closeness of fit to linear regression and without outliers, including both the linear (linear section of the titration, Ruzic and Scatchard plots) and the non-linear (Gerringa plot) regressions.

If the titration curve does not achieve linear signal to M_{TD} response at reasonably high series of metal additions, either an S-iteration (as suggested by Hudson et al., 2003) or another longer, complete titration should be performed. I will discuss more about this later in a final note about Hudson et al.'s (2003) paper.

3.1.6. Levenberg-Marquardt vs. other iterative algorithms

Levenberg-Marquardt (LM) is a least-squares iterative fitting algorithm. LM uses a gradually changing damper that makes iterating steps bigger when far from the minimum like the Steep Descent (SD) algorithm and smaller when close to the minimum like the Gauss-Newton algorithm (GN) algorithm (Nielsen, 2006). LM can optimize bad initial values better than SD, or GN. LM is more robust than SD and GN, as it can find a solution even if it starts very far off the true minimum (Nielsen, 2006).

3.1.7. TDI's Tuning Constraints

TDI has a series of tuning constraints that the researcher can change. Some of these constraints, discussed in detail in the discussion section, are:

- Number of points in the linear portion of the titration.
- Threshold r^2 of whole Scatchard dataset to choose between one or two ligands.
- Number and range of points for each ligand subset approximation at Scatchard.

- Lowest logK' difference between L1 and L2.
- Outlier for L1 and/or L2 subsets to be considered or not.

Tuning these to the level of methodological scattter, TDI can be adapted to the technique and sensitivity used. Once properly tuned, the first question TDI answers is if there are one, two or three ligands present. This is accomplished by comparing the r^2 of the whole dataset with an researcher-set value at the Scatchard plot since this kind of plot highlights graphically the difference between ligands better than a Ruzic plot. A one-ligand Scatchard plot looks like a straight line; in contrast, a two-ligand plot looks like a dog-leg. Hence, the former very likely has a higher r^2 value than the latter and they can be discriminated from each other this way. Then TDI determines the ligand(s)'s L and K features.

3.1.8. TDI's typical graphical and data output

Fig. 6 shows a typical graphical output of a titration dataset run by TDI. This figure should be compared to Figs. 2, 3, 4 and 5, which are the same plots obtained manually using the same titration curve data. The Ruzic plot's curve near the plot's origin evidences the presence of two ligands, which is corroborated by the Scatchard plot dog-leg shape. The visual estimate of the L_T in the titration curve (~ 3.5 nM) is close to those at the Scatchard (~ 3.7 nM) and the Gerringa (~ 3.7 nM) plots, though the Scatchard plot shows this distributed in L1 and L2 approximate values of ~ 0.7 and ~ 3.0 nM. These concentrations are estimated by simple observation of the x-intercepts of the titration curve and the Scatchard plot, and the y-intercept of the Gerringa plot.

Table 2 compares results obtained with TDI and with typical manual separate Scatchard and Gerringa mathematical analyses. Manual analyses are obtained using an Excel© spreadsheet and SigmaPlot© regression analysis, respectively. Both TDI and the manual run produce a titration L_T estimate (~ 3.3 nM) significantly lower than the more accurate Scatchard (~ 4.0 nM) and the optimized Gerringa (~ 3.9 nM) L_T values. All the titration points showed an electrical signal, as there is no zero-signal ligand data. Though this titration data shows very little scatter (once the least fitting points are taken from each

Scatchard subset), there is some difference between the manual and the TDI's Scatchard L and K values, because of the use of robust linearizations in TDI's run. The logKs show less variability than the concentrations. In general, the TDI and the manual estimates are similar. In the next section, these similarities and differences are analysed and discussed.

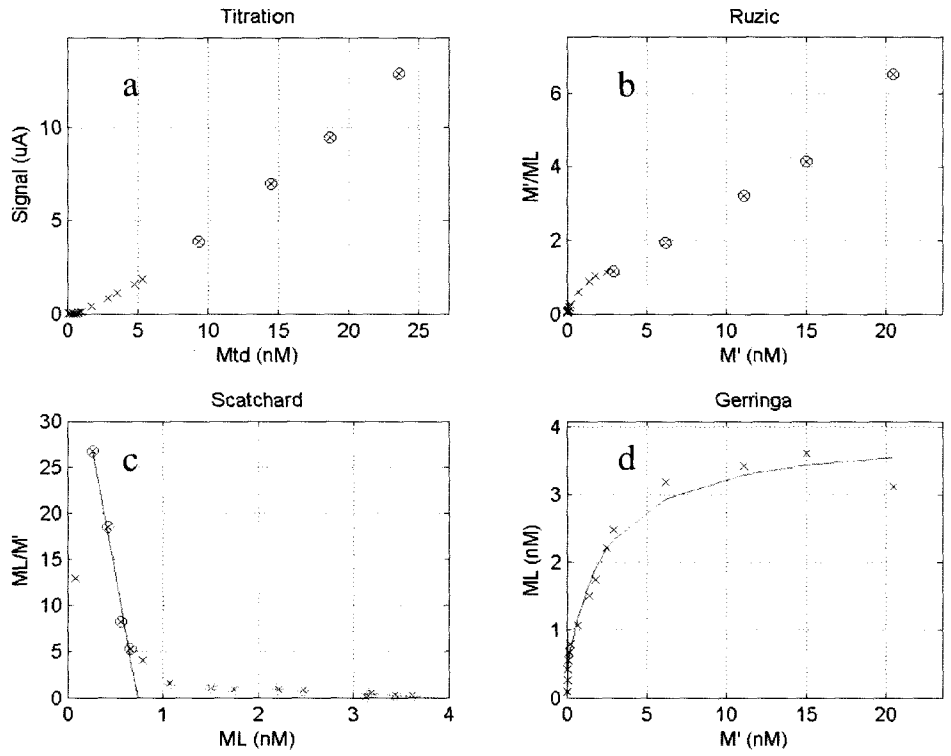

Fig. 6. TDI's graphic output of the titration curve shown in Fig. 2. They are the titration curve (a) and the Ruzic (b), Scatchard (c) and Gerringa (d) plots of the titration curve's data (compare to Figs. 2 - 5). In this specific case, the last four additions in the titration curve are selected (blue circles), and their slope (green line) used to calculate the data in the three plots. In the Ruzic plot, the last five points (blue circles) are selected, but a curve near the origin indicates two ligands. The Scatchard dog-leg shape confirms the presence of two ligands; each ligand data subset's points are indicated by circles (red and green) and their best fit lines graphed (red and green lines). From these lines' slopes and x-intercepts, initial L and K values are calculated. When optimized L and K values are plugged into equation (8), they produce the red line in the Gerringa plot.

Table 2

TDI and Manual Data output of the titration curve shown in Fig. 1.

	Titration			Scatchard				Gerringa				Zero signal	
	Slope	x-int	r^2	logK1	L1	logK2	L2	logK1	L1	logK2	L2	logK0	L0
TDI	0.631	3.342	0.999	10.74	0.742	8.70	3.247	10.97	0.490	8.60	3.441	ND	ND
Manual	0.631	3.345	0.999	10.74	0.742	8.71	3.215	10.86	0.504	8.59	3.436	ND	ND

3.2. RESULTS AND DISCUSSION

3.2.1. Evaluating the Scatchard-to-Gerringa parameter optimization

After deciding which points are considered as belonging to each ligand subset, the Scatchard plot results show an initial set of L and K values, which are fitted in the final Gerringa iteration and optimized into the final L and K values. This raises a question of apparent subjectivity during the selection of points in the Scatchard step, which depends on the tuning constraints' setup. The question is how effective the Gerringa L-and-K optimizing capacity is to turn initial L and K parameters into consistent and robust final parameters that represent a "true" minimum.

To answer these questions, different tuning constraints were used to select different combinations of points for each ligand data subset in the Scatchard plot of the titration curve data used in Fig. 6, in order to obtain Fig. 7 and Table 3. Thus, in Figs. 7a and 7b different points than those selected to obtain Figs. 4 and 6 are selected. In Fig. 7a's Scatchard plot, points 2 through 5 and 9 through 15 are initially selected, with the least weighing point (the outlier) being excluded from each data subset. That results in points 2 through 4 and 9, 10, 11, 13, 14 and 15 being selected for each ligand subset. These points, plotted in Fig. 7a as red and green circles, represent a more selective choice of data points than each subset before taking the outlier. Point 5 in the first data subset and point 12 in the second are the points with the least correlation with the rest of points in each subset. Thus, after these points are discarded, each subset has a higher r^2. This agrees with Miller and Bruland's (1997) criterion, which determines the L and K using a Scatchard plot with the first two and the last two points of a titration. The first-good-three and last-good-six points' Scatchard plot produces L and K parameters that are optimized in the Gerringa step of this TDI run into L and K that are very similar to those in Fig. 6 (see Table 3).

a

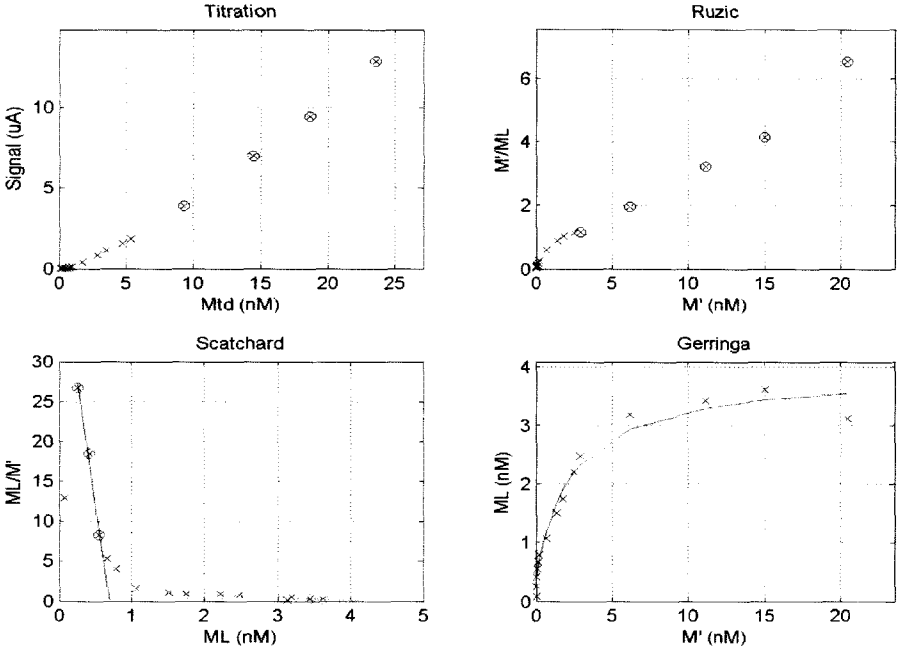

b

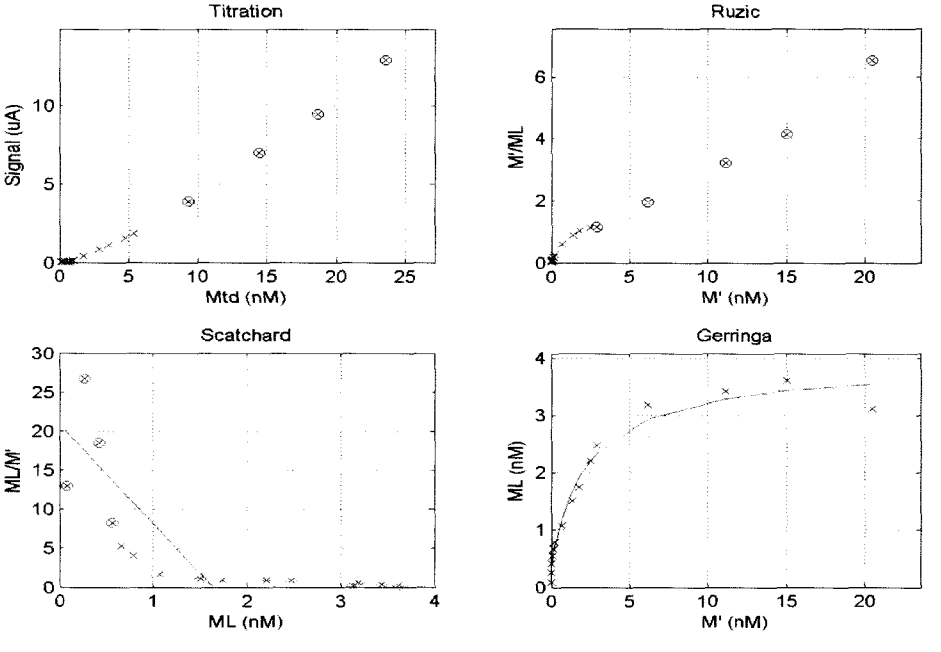

Fig. 7. Graphic outputs of the titration curve shown in Fig. 2, using different points for each ligand data subset at the Scatchard estimation step. One shows a good choice of points for each data subset (a) and other does not (b).

Table 3

TDI's data outputs of Figs. 7a and 7b, using the titration curve shown in Fig. 1.

	Titration			Scatchard				Gerringa				Zero signal	
	Slope	x-int	r^2	logK1	L1	logK2	L2	logK1	L1	logK2	L2	logK0	L0
Fig 7a	0.631	3.342	0.999	10.79	0.702	8.62	3.586	10.87	0.501	8.60	3.432	ND	ND
Fig 7b	0.631	3.345	0.999	10.10	1.651	8.70	2.338	10.87	0.501	8.60	3.432	ND	ND

In contrast, in Fig. 7b's Scatchard plot for both data subsets, a less logical choice of points is intentionally made by turning off the outlier exclusion step in the tuning constraints. The resulting L1 data subset includes points 1 through 4; since point 1 is not in good linear correlation with the rest of points of the L1 subset, the best fit line produced, though representing the average of the points in the subset, has a low r^2 value and a slope that gives too much weight to point 1. For the L2 data subset, points 7 through 15 are used, whose best fit line has also a lower r^2 value than the more selective subset used in Fig. 7a. As a result, the Scatchard plot L and K estimates for Figs. 7a and 7b are different (see Table 3). Regardless of the intentional "bad" initial parameters provided by these subsets, Gerringa optimizes these low- r^2 subsets into exactly the same L and K parameters than those produced with the better choice of points of Fig. 7a (see Table 3). This highlights the ample L and K optimizing capacity of the Gerringa step of TDI, even in the case of "bad" Gerringa inputs.

Using exactly the same titration curve data, different results were obtained by virtue of using different point-selection and outlier-exclusion constraints. Comparing these results, shown graphically in Figs. 6, 7a and 7b and numerically in L and K data shown in Tables 2 and 3, I can evaluate the Gerringa optimization capacity: the L and K parameters obtained using different initial L and K parameters produce consistent, robust, final parameters that represent a "true" minimum. The initial L and K values can be far from the minimum, but TDI iterates both values in such a way that a "true" minimum is reached, as can be evidenced by having almost the same final L and K values produced by three different data treatments.

Figs. 6, 7a and 7b show the TDI graphic output for the same titration curve data. Thus, in this specific case the titration curve and Ruzic plot for each run are the same. Still, they are shown in these and similar figures in the rest of this chapter for two reasons. First, it is essential to compare the four graphs at all times, focusing on the visual ligand estimates explained before. Secondly, some of the TDI runs where same titration data are compared have slight differences in the number of points on the linear section of the titration curve that are pointed out and discussed.

3.2.2. Comparing Ideal and Non-ideal outputs

Figs. 6, 7a and 7b and Tables 2 and 3 show three TDI outputs of a relatively easy-to-process titration. The Ruzic plot presents a clear curvature near the origin, suggesting the presence of two ligands; this is confirmed by the dog-leg shape of the Scatchard plot, whose L and K parameters for two ligands are fitted to the Gerringa plot to obtain very similar final, optimized L and K values. Clearly, the two-ligand model is appropriate for this titration curve's data. Working out this titration either manually or with TDI is easy, as there is no doubt that this titration curve's data indicate the presence of two ligands in this sample. More so, even a bad choice of points is buffered by the ample optimization capacity of the Gerringa step.

Frequently, Ruzic and Scatchard plots of titration data do not clearly show whether there are only one or more than one ligands. Data from a titration curve from Lohan et al. (2005) are used to illustrate this point; Figs. 8a and 8b show the TDI graphic outputs of the same titration data, whose Scatchard plots are interpreted with a one-ligand model and a two-ligand. TDI was forced to interpret this titration as having one and two ligands, respectively, by changing one tuning constraint: the threshold r^2 of the whole dataset used to evaluate the Scatchard plot. A close examination of the Ruzic plot suggests the presence of more than one ligand. The Scatchard plots in Fig. 8 suggest two ligands. The Gerringa plots show a better points-to-line fit for the two ligand fit (Fig. 8b) than for the one-ligand fit (Fig. 8a), which gives too much weight to the last point and seems to underweight the two titration points before the last.

Deciding if this particular titration has one or two ligands is not a simple decision, and using TDI these two possible cases can be compared and a decision can be made, evaluating the graphic and data outputs altogether. Clearly, a better decision can be made only when all the mathematical tools are used simultaneously. Using either Ruzic or Scatchard plots alone would have made it more difficult and subjective to decide about the number of ligands present in this not-easy-to-interpret titration (Fig. 8) than in the easy-to-interpret titration shown in Figs. 6 and 7. And that is why this program was developed: to avoid the researcher bias at the moment of making this decision, to let

mathematical criterion make the decision, instead, by using all four interpreting mathematical tools at once so that their graphical and numerical output can be compared.

Note that the Scatchard plot for the two-ligand interpretation (Fig. 8b) selects titration points 2 to 5, and that this choice yields a larger negative slope for the stronger ligand that produces logK1. Given that the data are quite scattered about this line, Gerringa iterates significantly the initial logK1 into the final logK1, with an increase of 0.80 log units. At the same time, L1 is brought down to almost half the initial value. In contrast, the weaker ligand changes to a lower extent (0.28 log units decrease and 30% increase for the logK2 and L2, respectively), because of a better fit of the initial parameters among themselves in the L2 subset.

These numerical changes in both parameters are possible because TDI iterates both L and K when optimizing parameters between Scatchard and Gerringa in order to find the "true" minimum point. Traditional manual Ruzic and Scatchard operating procedures, in contrast, iterate L only, assuming fixed K values (e.g. Kozelka and Bruland, 1998). A consequence of this double-parameter iteration is that the final L and K parameters resemble those that would be obtained by the Miller and Bruland (1997) first-two- and last-two-points titration interpretation. These optimized parameters would look as if in a Scatchard plot, the best fit lines constructed with initial ligand estimates were pushed towards the y- and x-axis, respectively for the strong and the weak ligand.

Lohan et al. (2005) used only a Ruzic plot to interpret this titration, and they produced a one-ligand L and K results set (L = 2.6 nM and logK' = 10.8). These results are similar to TDI's one-ligand interpretation results (L = 2.3 nM and logK' 10.3, see Table 4). In contrast, the results of TDI's two-ligand interpretation are L1 = 0.7 nM, logK1' = 11.8, L2 = 1.9 nM and logK2' = 9.7. These different L and K parameters are discussed later in this chapter. However, this two-ligand interpretation has some caveats, as the titration curve consists of nine points only, so the two ligand L and K parameters are not statistically strong. A longer titration would produce more solid parameters. An analysis of longer titrations (e.g. Fig. 13) is later in this chapter.

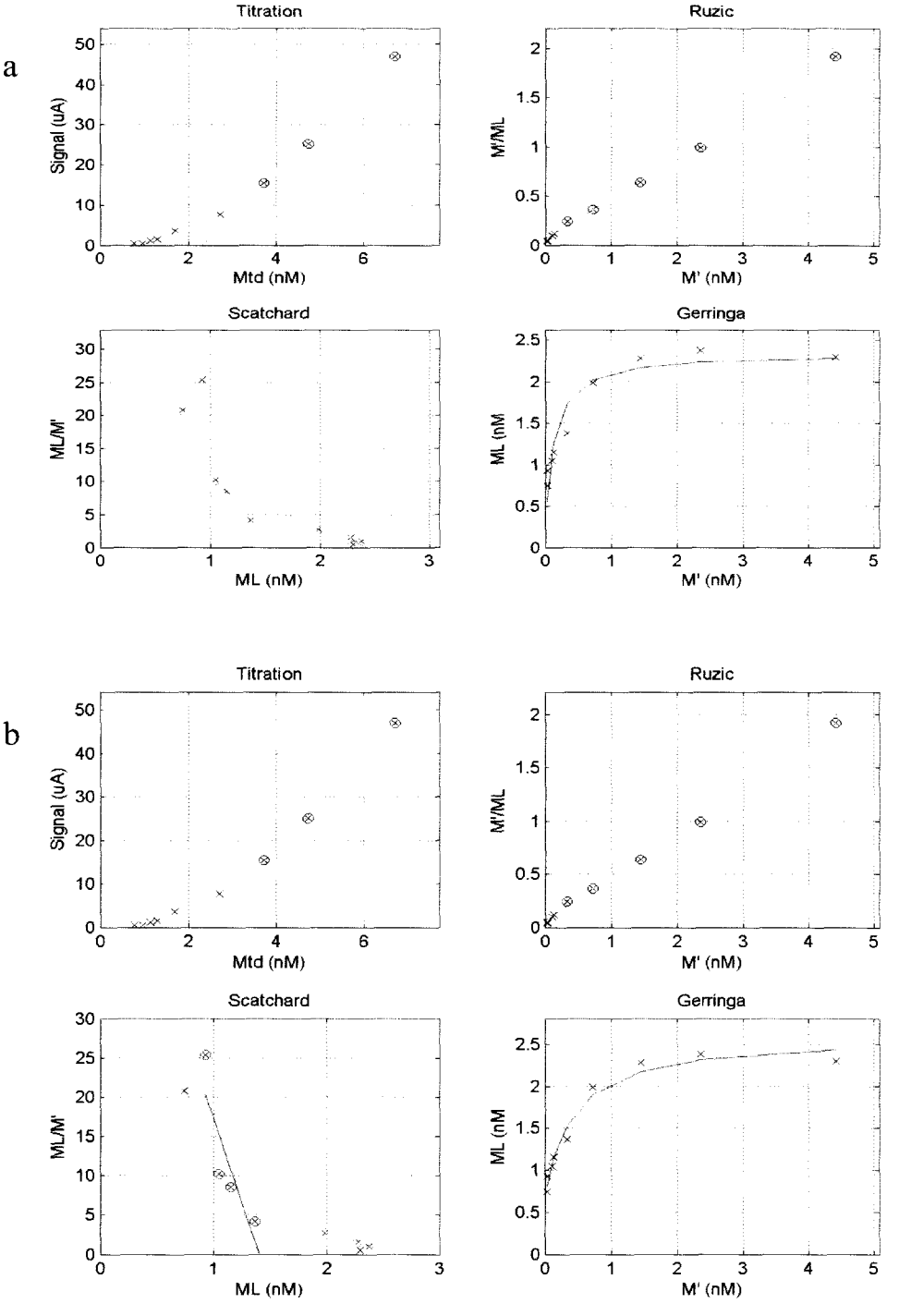

Fig. 8. TDI's graphic output of two possible interpretations of a metal titration for Zn using CSV (Lohan et al., 2005). The Scatchard plot of one interpretation shows the presence of only one ligand (a) and the other, two ligands (b).

Table 4

TDI's data output of two interpretations of Lohan et al. (2005) data.

	Titration			Scatchard				Gerringa				Zero signal	
	Slope	x-int	r^2	logK1	L1	logK2	L2	logK1	L1	logK2	L2	logK0	L0
Fig 8a	10.66	2.318	0.999	10.16	2.452	ND	ND	10.26	2.343	ND	ND	ND	ND
Fig 8b	10.66	2.318	0.999	10.63	1.405	9.64	1.218	11.75	0.736	9.67	1.873	ND	ND

3.2.3. Guidelines for setting up TDI's Tuning Constraints

Understanding the tuning constraints well is essential to setting up TDI well, so that it can interpret a titration correctly. When working titrations manually with either of the mathematical tools aforementioned, the decision about which points to consider for each data subset, and ultimately the decision about a titration being interpreted using a one-ligand or a two-ligand model are made by the researcher. Then, interpreting a whole station or a complete cruise's worth of titration curves is needed to keep a homogeneous criterion for all similar data. Trying to minimize researcher bias and potential heterogeneity, I developed TDI to have a program make those decisions with a consistent mathematical criterium. This criterion is defined by the researcher by determining and tuning the proper constraints. Finally, the results can be reviewed and evaluated.

All the parameters that can be tuned follow, with the common values used in this study in the last line of each sub-section:

- Number of points in the linear portion of the titration.
  Three points is safe when four large metal additions finalize a "complete" titration, that is, one that ends in a very linear section. Long linear titrations can use four or more, while incomplete still-curving titrations need to use two points or maybe use Hudson et al.'s (2003) S-iteration step.
  I used four points for most of the titration curves discussed in this study.

- Threshold r^2 of whole Scatchard dataset to choose between one or two ligands.
  The r^2 can be set up between 0.7 and 0.9, depending on analytical noise levels or scatter. A value of 1.0 can be used to force a two-ligand interpretation, and 0.0 to force a one-ligand.
  I used a variety of numbers around 0.8.

- Number and range of points for each ligand data subset at the Scatchard step.
  This normally should be the first four and the last four points, a conservative approach to Miller and Bruland (1997) using the first and last to points.

I generally used points 2 to 5 and three-before-last to last, depending on the scatter of the first and last titration point and the total number of additions.

- Number of iterations in Gerringa optimization.
  100 iterations usually find the minimum. A higher value can be used, but it makes the program slower.
  I used 100 iterations.

- Lowest L_T concentration to be reported.
  Depending on the element analysed, the method, the instrument used and the analytical sensitivity.
  I used 0.010 nM.

- Limit of detection (LOD) of the method.
  It depends on the element analysed, the method, the instrument used, the size of the RGCDE and the analytical sensitivity. The LOD should not vary much within a study, but maybe between elements and analytical systems. It is used to calculate logK0' when zero-signal points are present in the titration.
  I used 0.003 nM for Zn and Cd, a very consistent average for this study.

- Lowest difference between logK1 and logK2.
  A higher number merges not-so-different ligands while a lower number separates ligands.
  I used 0.7 log units because analytically is the lowest reasonable difference at the low noise and scatter levels that this study showed.

- Outlier for L1 and/or L2 subset to be considered or not.
  Depending on scatter levels and potential significance of the point mathematically furthest from the trend set by the rest of points, the outlier could be considered or not. If the titration curve is long, it is usually better to exclude the most outlying point of each subset. If the titration is short, ridding of points makes the resulting

parameters less statistically solid.

Depending on the size of the titration curve, I usually discarded the outlier from each data subset in the Scatchard plot.

3.2.4. Evaluating TDI's performance

After practicing with some titrations obtained in the instrument used in this study (so that real scatter and noise are included), the tuning constraints were properly set up by the researcher. Then, TDI's performance was evaluated. Real and modeled titration curves' data from relevant publications (Bruland, 1989; Bruland, 1992; Donat and Bruland, 1990; Ellwood, 2004; Kozelka and Bruland, 1998; Lohan et al., 2005; van den Berg et al., 2006; Tian et al., 2006; Garnier et al., 2004; Miller and Bruland, 1997; Carrasco and Donat, 2001 and Carrasco et al., 2008) were processed. Their results are compared with the original publication results in the following sections.

To extract data from figures in publications, G3data was used. This is a tool for extracting data from graphs developed at the University of Helsinki and available in the Linux community (Frantz, website). A comparison of raw titration data obtained directly from the authors and figure-obtained data from Donat et al.'s (1990) Zn titration curve shows that the electrical signal and concentration points are very similar. Comparing the L and K' produced after analyzing both datasets with TDI, the results produced are comparable: the direct-data results are: L = 1.95 nM and logK' = 10.6, and the picture-obtained-data results are L = 1.96 nM and logK' = 10.5.

To evaluate TDI's performance thoroughly, I examined specifically the following three points:

a) The level of uncertainty in each parameter produced.

The uncertainty of the parameters produced by TDI can be calculated in 2 possible ways. It can either be mathematically spread from the signal to M' to M'/ML and ML/M' to the Scatchard plot L and K approximations to the Gerringa plot L and K final values. Or it can be simply estimated by averaging the

Gerringa plot L and K final values for two titrations obtained using separate instruments run in tandem and calculating the standard deviation (SD). The last is a more conservative approach, since it should yield a higher uncertainty than that obtained calculating it for one titration, for it includes intra-instrument variability.

TDI's uncertainties for both the Scatchard plot L and K estimates and the Gerringa plot final, optimized L and K values are compared with those obtained using different mathematical methods in relevant recent literature references in Table 5. The uncertainties reported in this table come all from real data, as modeled data cannot have the same instrumental inherent uncertainties (papers dealing with modeled data add random noise to their datasets to make them realistic). The uncertainties are expressed as relative standard deviation in percent ligand concentration and log K' units (L% RSD and logK' RSD).

All the references in this table use Ruzic plot only as their titration curve interpretating tool. They produce variable values, with RSDs below, 20 % L and 0.6 logK'. Jakuba et al.'s (2008b) data were processed with both Ruzic and Gerringa, and their data shows a very high level of certainty for the L and a lower level for the logK' for the Ruzic plot interpretation (5 % L and 0.6 logK') and the inverse for the Gerringa plot interpretation (15 % L and 0.2 logK'). Since TDI works sequentially, it gets a higher level of uncertainty for the initial Scatchard plot L and K estimates (20 % L and 0.2 logK') that decreases as the Gerringa plot optimization produces the final, more certain parameters (10 % L and 0.1 logK'). These final uncertainties are comparable and better than the uncertainties of any other mathematical method used by itself for the L, and definitely better for the logK'. Thus, the logK's produced by TDI are of the best quality compared with the literature data.

Table 5

Uncertainties in the L and logK' produced by some mathematical methods compared with TDI.

L RSD (% L)	logK'RSD (logK' units)	Reference	Mathematical method
5	0.2	Donat and Bruland (1990)	Ruzic plot
17	0.3	Bruland (1989)	Ruzic plot
15	0.2	Bruland (1992)	Ruzic plot
5	0.2	Ellwood (2004)	Ruzic plot
5	0.6	Jakuba et al. (2008b)	Ruzic plot
15	0.2	Jakuba et al. (2008b)	Gerringa plot
20	0.2	This study	TDI's Scatchard plot
10	0.1	This study	TDI's Gerringa plot

b) The level of correlation between published results and those obtained by TDI.

The best way to gauge the level of correlation between published results and TDI-obtained results is to compare L and K parameters produced by some mathematical method in the publications with those produced by TDI on exactly the same dataset of real titration curve data.

Fig. 9 shows the TDI results of a titration curve reported by Ellwood (2004). The final L and K parameters reported in the paper are L = 2.2 nM and log K' = 9.8, which are in very good agreement with TDI's L = 2.1 nM and logK' = 9.8. Another example is in the titration used for testing G3data, where good correlation exists between Donat and Bruland's (1990) L = 2.00 nM and log K' = 10.2 results and TDI's results L = 1.96 nM and logK' = 10.5.

In contrast to real titration curve data, modeled datasets are unrealistically long (~ 30 points, which would take, in the conditions analysis were run in this study, ~ 12 hours). The tuning constraints need to be changed accordingly. Once properly tuned, the Land K parameters obtained by TDI match pretty well the literature values. I will not show any of these comparisons because I want to focus on real-data reproducing ability in this study.

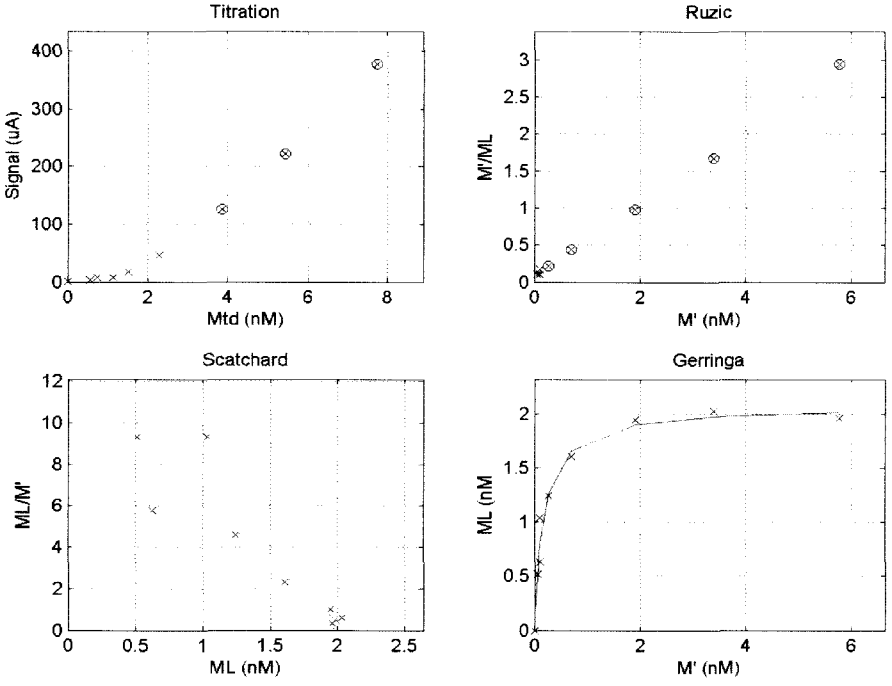

Fig. 9. TDI's graphic output of a Zn titration curve (Ellwood, 2004). Interpretation shows L = 2.2 nM and log K' = 9.8, in very good agreement with TDI's results L = 2.1 nM and logK' = 9.8.

c) The apparent dilemma that originates when having to decide to use a one-ligand model or a two-ligand model and possible ramifications.

Ideally, the complete-dataset Scatchard plots of samples with two ligands should have lower r^2 than those where one ligand only is present, with little variability between the r^2 of titrations obtained with the same instrument, element and analytical conditions. In reality, despite having TDI well tuned for the level of noise and scatter that my instruments impose on the titrations, the Scatchard plots of some two-ligand-containing titration curves paradoxically have a higher r^2 than those of some one-ligand titrations. This is because of scatter, as data subsets with low or high r^2 still produce L and K' parameter(s) from their x-intercept(s) and slope(s). This could end up being reflected in some graphic outputs that do not make sense, i.e. Ruzic and Scatchard plots with negative and positive slopes, respectively.

To test for the capacity of TDI to correct for nonsensical outputs, I forced some titrations that clearly have only one ligand to produce two-ligand L and K parameters in the Scatchard plot step. I forced this by using a 1.0 value for the threshold r^2 of whole Scatchard dataset to choose for all titration curves to be interpreted as having two ligands. All datasets are forced to be considered to have two ligands. TDI produces initial Scatchard plot L and K parameters for two ligands. Once these parameters are plugged into the Gerringa plot optimization step, the "correcting" logic steps discussed next start to work.

Bruland's (1989) Zn ASV data, interpreted in his original paper as having one ligand with L = 0.9 nM and logK' = 10.6, is used. Before forcing for two ligands, TDI is forced to do a one-ligand interpretation (using an r^2 value of 0.0 for the aforementioned tuning constraint) and the results obtained, L = 0.9 nM and logK' = 10.8, were found to be in very close agreement with Bruland's. The two-ligand Scatchard estimates should be fixed into one-ligand final results that resemble these parameters.

Fig. 10a shows the one-ligand interpretation, followed by three two-ligand initial Scatchard estimations corrected into one-ligand final Gerringa interpretations (Figs. 10b, 10c and 10d). Numerically, the four different approaches yield exactly the same final parameters: L = 0.9 nM and logK' = 10.8, demonstrating that this is a robust set of final L and K parameters, that represents a "true" minimum being reached. This is obtained by virtue of any of the three "correcting" mechanisms described next:

i. Eliminating one of the two ligands. In the Scatchard plot of Fig. 10b, one ligand subset with negative slope and other with positive slope are obtained. The positive slope line (green line) would yield a nonsensical negative K value. Thus, it is deleted, following a specific command in the program.

ii. Averaging similarly strong ligands. In the Scatchard plot of Fig. 10c, there are two ligands with a difference in logK' values smaller than that set up by the corresponding tuning constraint. Thus, these two ligands are merged into just one ligand of average binding strength and average concentration. Interestingly, even if this tuning constraint is set up to a very low value (0.01 logK' difference between ligands' binding strength), so that ligand parameters for two ligands are produced by Scatchard and optimized into the Gerringa plots, TDI still "quasi-merges" them by producing two separate concentrations of a ligand of almost the same strength (difference in logK' lower than 0.05 logK' units), that could finally be added.

iii. Fixing "crazy" Scatchard plot values. In Fig. 10d, there is one ligand subset with negative slope and another with positive slope. After the positive slope ligand is eliminated, the remaining ligand is defined by a set of points of low correlation such that an initial L and K set of values is

produced. In this specific case, these results are L = 1.6 nM and logK' = 10.3, and they clearly do not match neither L_T estimate (the titration curve or the Gerringa plot). These initial L and K parameters are iterated in the Gerringa step into exactly the same values that were obtained with the previous two two-ligand-into-one cases, i.e. L = 0.9 nM and logK' = 10.8.

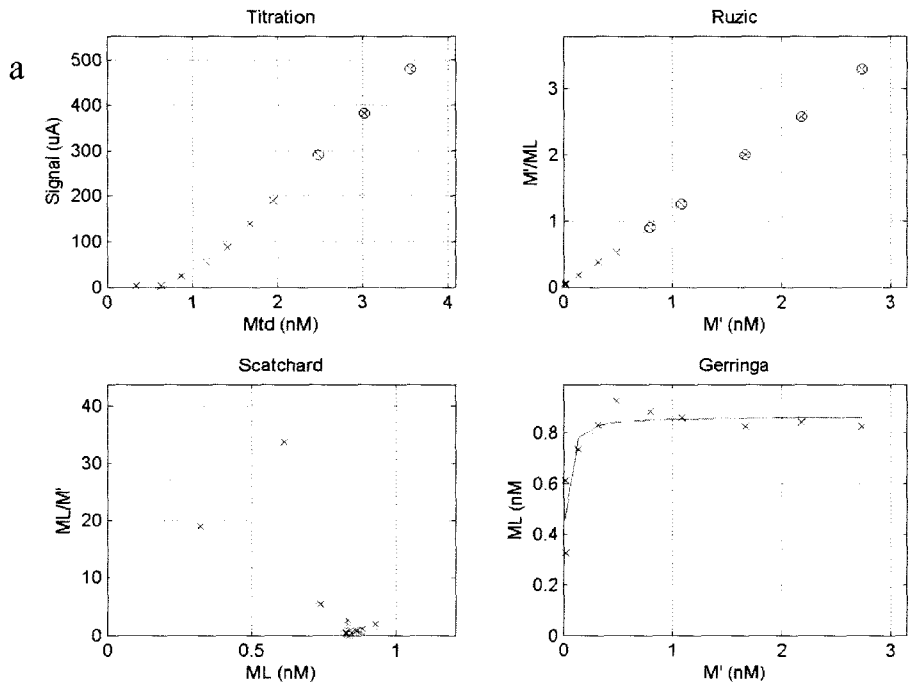

Fig. 10. TDI's graphic output of the one-ligand interpretation of Bruland's (1989) Zn ASV titration curve data (a) and three different two-ligand interpretations with Scatchard plot initial estimates corrected into one-ligand final Gerringa plot interpretations (b, c and d). After the two-ligand-into-one-ligand corrections, the four different approaches yield exactly the same final L and K parameters: L = 0.9 nM and logK' = 10.8.

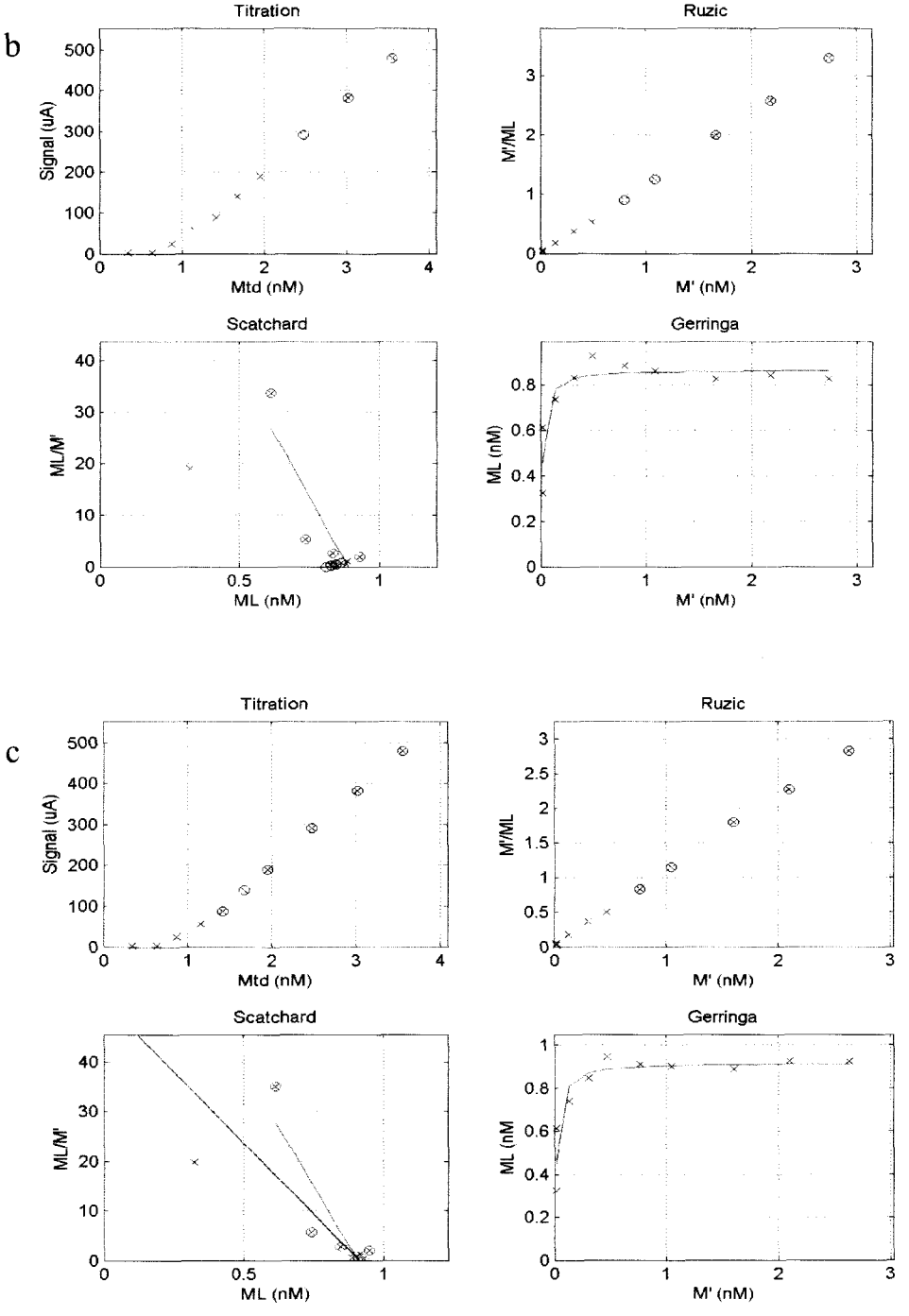

Fig. 10. Continued.

d

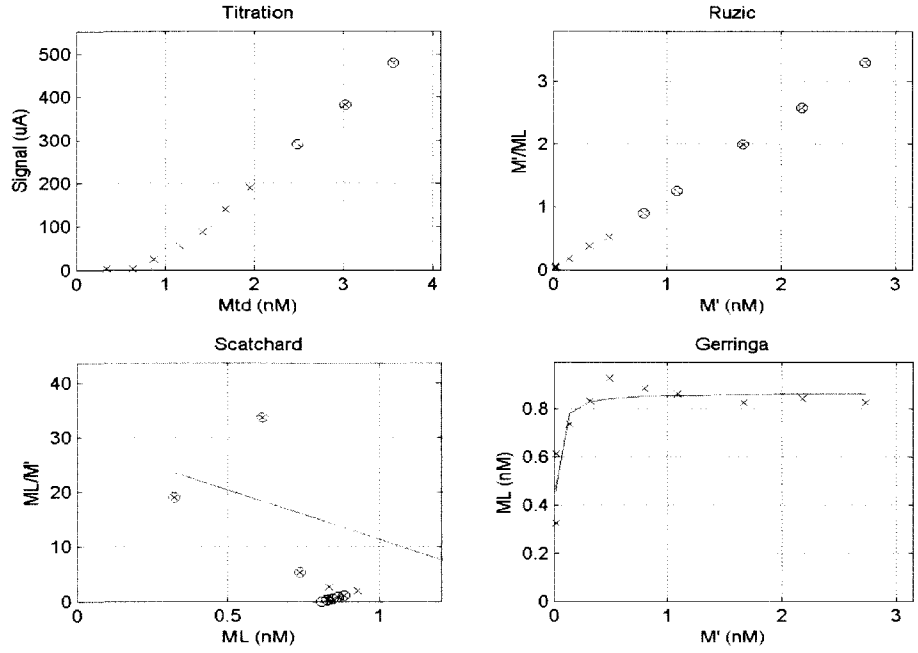

Fig. 10. Continued.

As stated earlier, properly setting the tuning constraints is important. In this case, it delineates a program that can "correct" non-sensical two-ligand initial L and K parameters into true-minimum one-ligand final L and K values. The Scatchard step is the decision-making part of the program, which works under the assumption that the tuning constraints have been properly set up. About the stress that is put on properly tuning these constraints, two mutually-exclusive possible approaches can be used, either:

i. A reasonable r^2 breakpoint between one and two ligands interpretations of the complete-dataset Scatchard plot should be set, so that TDI can decide the number of ligands present, or

ii. All titration curves should be forced-run as having two ligands, assuming that one-ligand cases that are incorrectly interpreted as two-ligand will be corrected into one-ligand cases.

In order to establish a reasonable r^2 breakpoint, the tuning constraints need to be personalized to the instrument, the method, the LOD, the noise and scatter level, the detection window, the number of points in each titration, etc. Despite all proper tuning, modeled and real data studied sometimes produced r^2 values that do not make sense (two-ligand data Scatchard plots should necessarily have a lower r^2 than one-ligand datasets). If this approach is chosen, proper tuning with one-ligand and two-ligand real titration curve data (using model ligands like EDTA or NTA) in a specific instrument should be performed before running natural organic ligand titrations. Yet, some groups of datasets simply can not get turned into logical r^2 sets of datasets with lower r^2 for two-ligand Scatchard plots.

To test the second approach, datasets with definitely one ligand only and with two ligands were forced to be interpreted as both one-ligand and two-ligand cases. Ultimately, the researcher should compare and review both of the TDI's forced results and decide the most appropriate number of ligands by comparing the fitting level of either case to either number of ligands in the Gerringa plot. That is, the researcher should visually gauge how close the points are to the line in the Gerringa plot, since the points represent a dataset that produces the Scatchard L and K estimates and the line represents the Gerringa-optimized L and K values fitted to equation (8). Rather than demanding super-tuning the constraints to find later nonsensical complete dataset r^2 values, this approach requires proper tuning of the point-selection step (which was conservatively set to points 2 to 5 for L1 subset and n-5 to n for L2 subset) and choosing to eliminate outliers in each data subset. This means selectively choosing few points in each end of the Scatchard plot, following Miller and Bruland (1997) first-two-and-last-two-points logic.

Fig. 11 shows the two possible interpretations (as a one-ligand and a two-ligand case) for the certainly one-ligand case. Fig. 12 shows the same two possible interpretations for a certainly two-ligand case. Fig. 13 shows the same for a case in which it is not clear if one or two ligands are present, which should be compared with Fig. 8, a similar case but with fewer titration points than all these titrations. For the three figures, a one-ligand interpretation (Figs. 11a, 12a and 13a) is presented before a two-ligand interpretation (Figs. 11b, 12b, 13b).

The r^2 values for the Scatchard plot complete dataset of the titrations corresponding to Figs. 11, 12 and 13 are, respectively, 0.75, 0.62 and 0.86. This means that the two-ligand dataset has a lower r^2 than the one-ligand dataset, which makes sense. But the dataset shown in Fig. 13, that ultimately is interpreted as a two-ligand dataset, has a higher r^2 than Fig. 11's one-ligand dataset, which does not make sense. Regardless of how well tuned the constraints are, and how logically the points for each subset are selected, if the r^2 of the whole dataset is to be the deciding criterion between one- and two-ligand datasets, it would not work for the titration curve dataset that produces Fig. 13.

By virtue of running all three datasets for the two interpretations, that is, for one- and two-ligands, the researcher can easily compare and evaluate the graphs and conclude that Fig. 11 is a one-ligand case with some noise, Fig. 12 is a two-ligand with very little noise, and that Fig. 13, which initially could have been interpreted as a case without a defined number of ligands, is a case with two ligands. This is evidenced by the subtle curvature in the Ruzic plot and the better fit of the Gerringa plot in Fig. 13a than in Fig. 13b. Note that if the r^2 of the Scatchard plot complete dataset were the deciding criterium, Fig. 13 would have been defined as a one-ligand case, contradicting the conclusions obtained by the researcher after carefully looking at TDI's graphic outputs for the two cases.

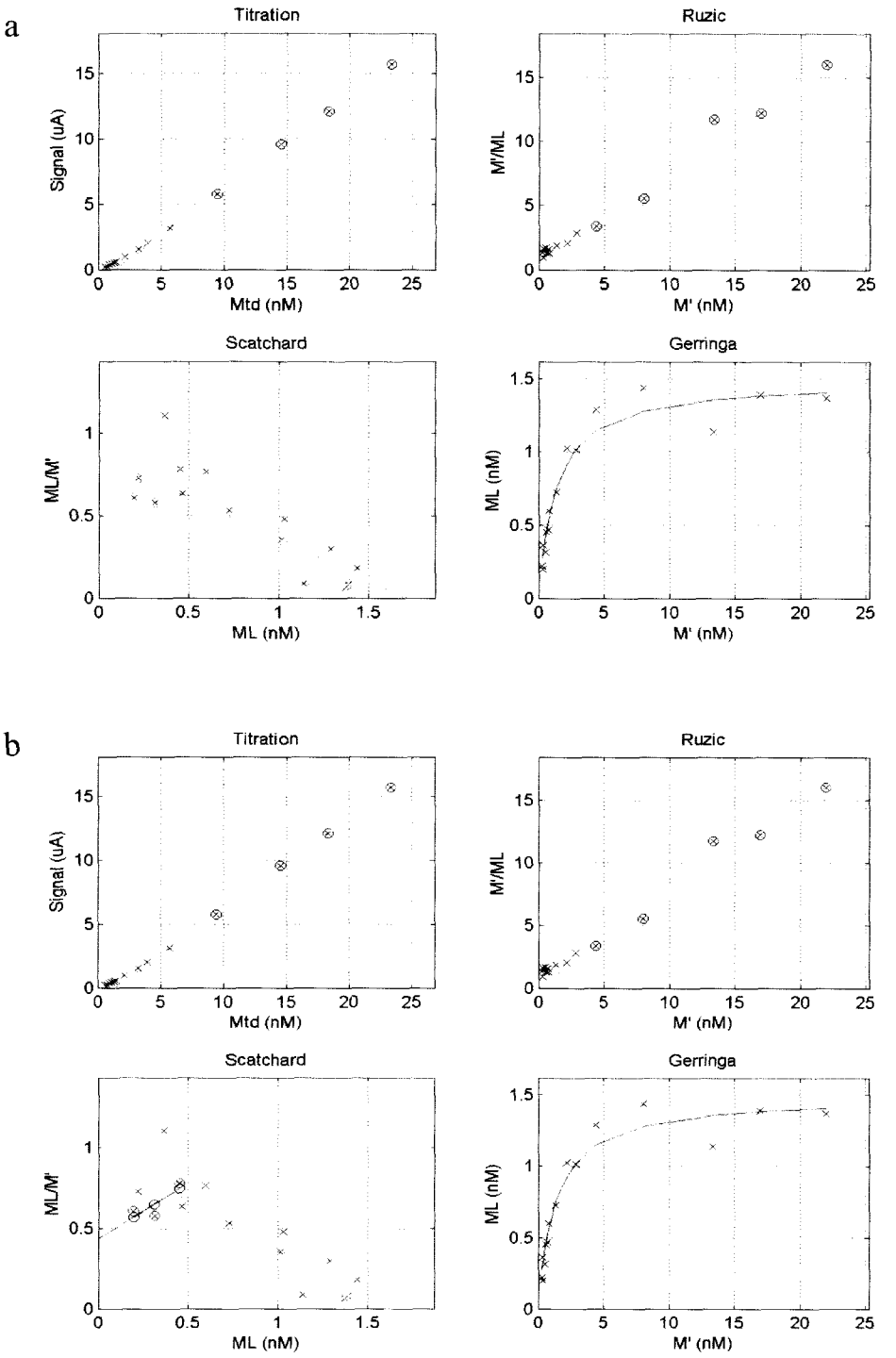

Fig. 11. TDI's graphic output of a titration with definitely one ligand forced for one and two ligands. Sample: IOC 1996 Stn 8, 110 m, red electrode.

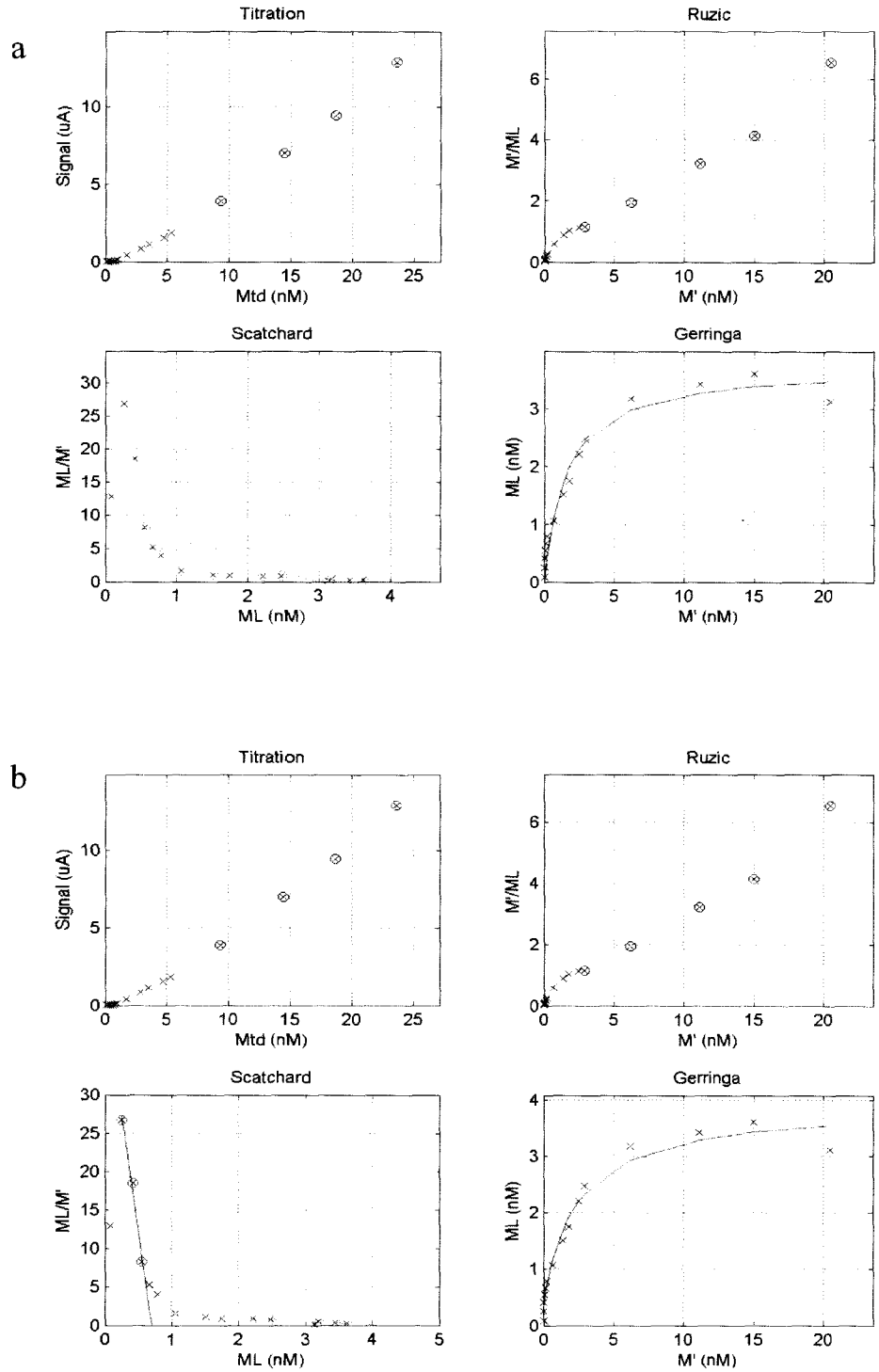

Fig. 12. TDI's graphic output of a titration with definitely two ligands forced for one and two ligands. Sample: IOC 1996 Stn 8, 170 m, red electrode.

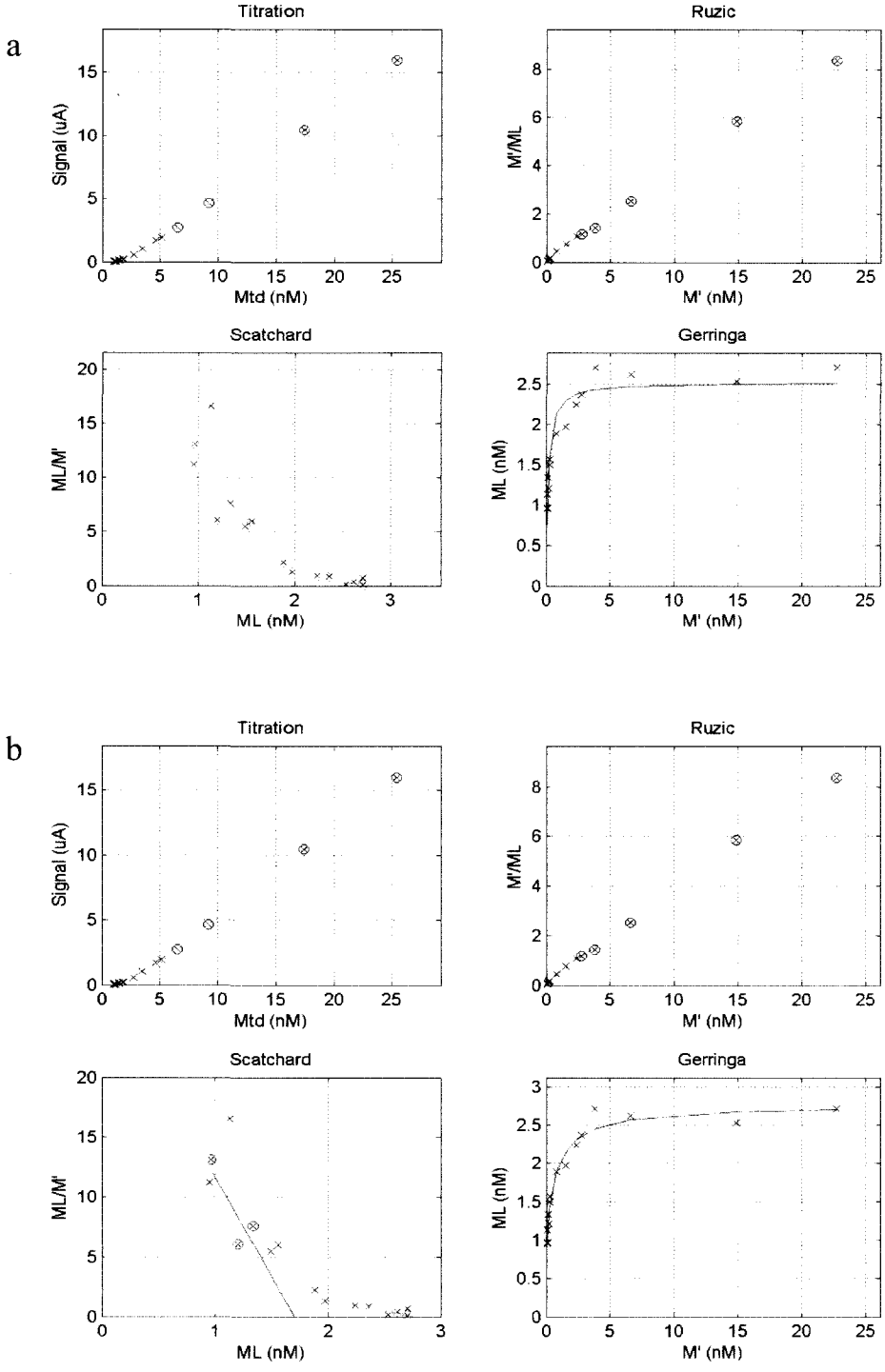

Fig. 13. TDI's graphic output of a titration without a clear number of ligands forced for one and two ligands. Sample: IOC1996. Stn 8, 500m, green electrode.

When looking at the numerical TDI output of the two cases of all three titration curves (shown in Table 6), it should be noticed how, regardless of the one- or two-ligand forcing, Fig. 11 yields exactly the same L and K results; Fig. 12 offers only one set of correct two-ligand results and Fig. 13 shows two possible answers. By looking at the graphic output, the numerical output and, in this case with the extra help of the oceanographic sense (all three titrations come from a single station, only depth differs, and a ligand with a logK' ranging between 8.60 and 9.00 is present in all three depths, while a stronger ligand with a logK' ranging between 10.67 and 10.87 is present in the two deeper samples, those analyzed in Figs. 12 and 13), the two-ligand case can be strongly suggested.

If Figs. 8 and 13, both of them cases in which it is not clear if one or two ligands are present, are compared, the first noticeable difference between them is the number of titration points. Fig. 7 has a total of nine points (zero addition and eight additions), while Fig. 12 has fifteen points (zero addition plus fourteen additions). Statistically, it is possible to talk about the four L and K parameters obtained from Fig. 13, with an average of almost four points supporting each. For Fig. 7, merely two points give information for each parameter. In Gerringa non-linear plots, all points give information for all parameters (whether they are two or four). However, a case like this, with an uncertain number of ligands present, is better resolved with longer, more detailed titrations.

All the titrations in this study are long titrations, with thirteen to fifteen additions, allowing statistically for two or three ligand interpretations (if there are two ligands on top of a zero-signal ligand). The only exceptions are when there is a high initial concentration of M_{TD}, where fewer additions are made because the ligand is already saturated with metal and, thus, no clear curvature can be seen in the titration curve, the Ruzic and Scatchard plots turn very noisy and sometimes unreadable and the Gerringa plot provides the optimized L and K parameters.

Table 6

TDI's Data output of two interpretations of three typical titration cases: definitely one ligand, definitely two ligands and not sure if one or two ligands, corresponding to Figs. 11, 12 and 13.

	Titration			Scatchard				Gerringa				Zero signal	
	Slope	x-int	r^2	logK1	L1	logK2	L2	logK1	L1	logK2	L2	logK0	L0
Fig. 11a	0.717	1.334	0.999	8.70	1.705	ND	ND	8.88	1.494	ND	ND	ND	ND
Fig. 11b	0.717	1.334	0.999	ND	ND	8.78	2.260	8.88	1.494	ND	ND	ND	ND
Fig. 12a	0.631	3.342	0.999	8.52	2.960	ND	ND	8.80	3.745	ND	ND	ND	ND
Fig. 12b	0.631	3.342	0.999	10.79	0.702	8.69	3.439	10.87	0.501	8.60	3.432	ND	ND
Fig. 13a	0.705	2.641	1.000	9.78	2.556	ND	ND	9.80	2.529	ND	ND	ND	ND
Fig. 13b	0.705	2.641	1.000	10.22	1.709	9.26	1.059	10.61	1.217	9.00	1.555	ND	ND

In conclusion, I recommend using TDI to interpret metal titrations by forcing a two-ligand fit, and then forcing a one-ligand fit. One-ligand cases forced to a two-ligand fit will fall into one-ligand by virtue of any of the three correcting mechanisms mentioned before. However, the opposite is not true; two-ligand cases forced to a one-ligand fit will not fall into a two-ligand case, and the researcher has to evaluate the case and make a decision.

One example of this is Fig. 12a, where the two-ligand case is forced to a one-ligand fit. TDI will produce results, but it is evident from the graphic output that Fig. 12b is correct and that Fig. 12a is not. Fig. 12a shows a Gerringa plot with good fit, but both the Ruzic and the Scatchard show the presence of two ligands. Once again, examining all four graphs is essential to making the best evaluation.

Fig. 12a is clearly wrong, but it was obtained by forcibly fitting a two-ligand case to a one-ligand fit. In some reported cases, when only short titrations are available and when simple mathematical approaches are used (like Lohan et al., 2005, Fig. 8; and Ellwood, 2004, for example), a conservative interpretation of the titration lead the authors to state that there is only one ligand. If the range of the titration shown in Fig. 13 had been shorter, or if only the Scatchard or Ruzic approach had been used, a conservative one-ligand interpretation would have been safe, too.

The most important ramification of conservatively defining a sample as having one ligand when two ligands are really present, is underestimating the complexing index (CI), which is explained in the next section along with a close examination of some relevant cases where conservative one-ligand interpretations are used.

3.2.5. Complexing Index (CI) underestimation

Consider the formation of a 1:1 complex between a metal cation and a ligand molecule:

$$M + L \rightarrow ML \quad (9)$$

This complex-formation reaction is governed by an equilibrium constant K, which is mathematically equal to the concentration of the product ML divided by the product of the concentrations of M and L:

$$K = [ML] / [M] \times [L] \quad (10)$$

Reorganizing (10), the complexing index (CI) can be mathematically defined as:

$$CI = K \times [L] = [ML] / [M] \quad (11)$$

where CI is equal to the product of the equilibrium constant K of the complex times the concentration of the ligand L, which is equal to the ratio of the complexed metal concentration ML to the concentration of uncomplexed metal M. In other words, CI represents the complexing capacity of a ligand, defined by its concentration and its binding strength, that is, how much of the metal the ligand can complex, which is to say the proportion of complexed metal to uncomplexed metal.

Examples of possible CI underestimation are found in Lohan et al. (2005), Ellwood (2004) and a couple of titrations presented before here (Figs. 12 and 13), which are evaluated in light of this topic.

Lohan et al. (2005; Fig. 8) reported having one ligand with L = 2.6 nM and logK' = 10.8 yielding a CI ~ 160, was found by TDI to have L = 2.343 nM and logK' = 10.26 (CI ~ 42.6; Fig. 8a) when interpreted as having one-ligand, and L1 = 0.736 nM, log K1 = 11.75 and L2 = 1.873 nM, logK2 = 9.67 (CI ~ 413.9 + 8.8 = 422.6), when interpreted as having two ligands (Fig. 8b). A visual comparison of the Gerringa plot points and the line shows a better fit for the two ligand interpretation. Likewise, Ellwood (2004; Fig. 14) reported having one Cd ligand with L = 1.31 nM and logK' = 10.2 (CI ~ 19.4), was found by TDI to have L = 1.179 nM and logK' = 11.30 (CI ~ 235.2; Fig. 14a) when interpreted as one-ligand, and L1 = 0.740 nM, log K1 = 11.66 and L2 = 0.707 nM, logK2 = 9.25 (CI ~ 338.2 + 1.3 = 339.5) when interpreted as two-ligand (Fig. 14b). There is better fit for the two-ligand Gerringa plot, too. Fig. 13 is an example of a case in which it is not clear if one or two ligands are present. It is interpreted by TDI to have L = 2.529 nM and logK' = 9.80 (CI ~ 16.0; Fig. 13a) when interpreted as one-ligand, and L1 = 1.217 nM, log K1 = 10.61 and L2 = 1.555 nM, logK2 = 9.00 (CI ~ 49.6 + 1.6 = 51.2) when interpreted as two-ligand (Fig. 13b). There is better fit for the two-ligand Gerringa plot, too. Fig. 12, an example of a case that clearly has two ligands, is interpreted by TDI to have L = 3.745 nM and logK' = 8.80 (CI ~ 2.4; Fig. 11a) when interpreted as one-ligand, and L1 = 0.501 nM, log K1 = 10.87 and L2 = 3.432 nM, logK2 = 8.60 (CI ~ 37.1 + 1.4 = 38.5) when interpreted as two-ligand (Fig. 11b). There is very little difference between the fit levels for the Gerringa plots for either interpretation for this case.

The ratio of the one-ligand CI to the two-ligand CI, expressed as a percentage, is a dimensionless number that illustrates to what percentage of the real, two-ligand fit is the CI being underestimated by using a conservative, one-ligand fit when there are two ligands. By using a conservative one-ligand Ruzic approach, Lohan et al. (2005) and Ellwood (2004) underestimated the CI by the following factors:

Lohan et al. (2005) (Fig. 8)	$CI_{(1L)} / CI_{(2L)} = 42.6 / 422.6 = 10\ \%$
Ellwood (2004) (Fig. 14)	$CI_{(1L)} / CI_{(2L)} = 235.2 / 339.5 = 69\ \%$

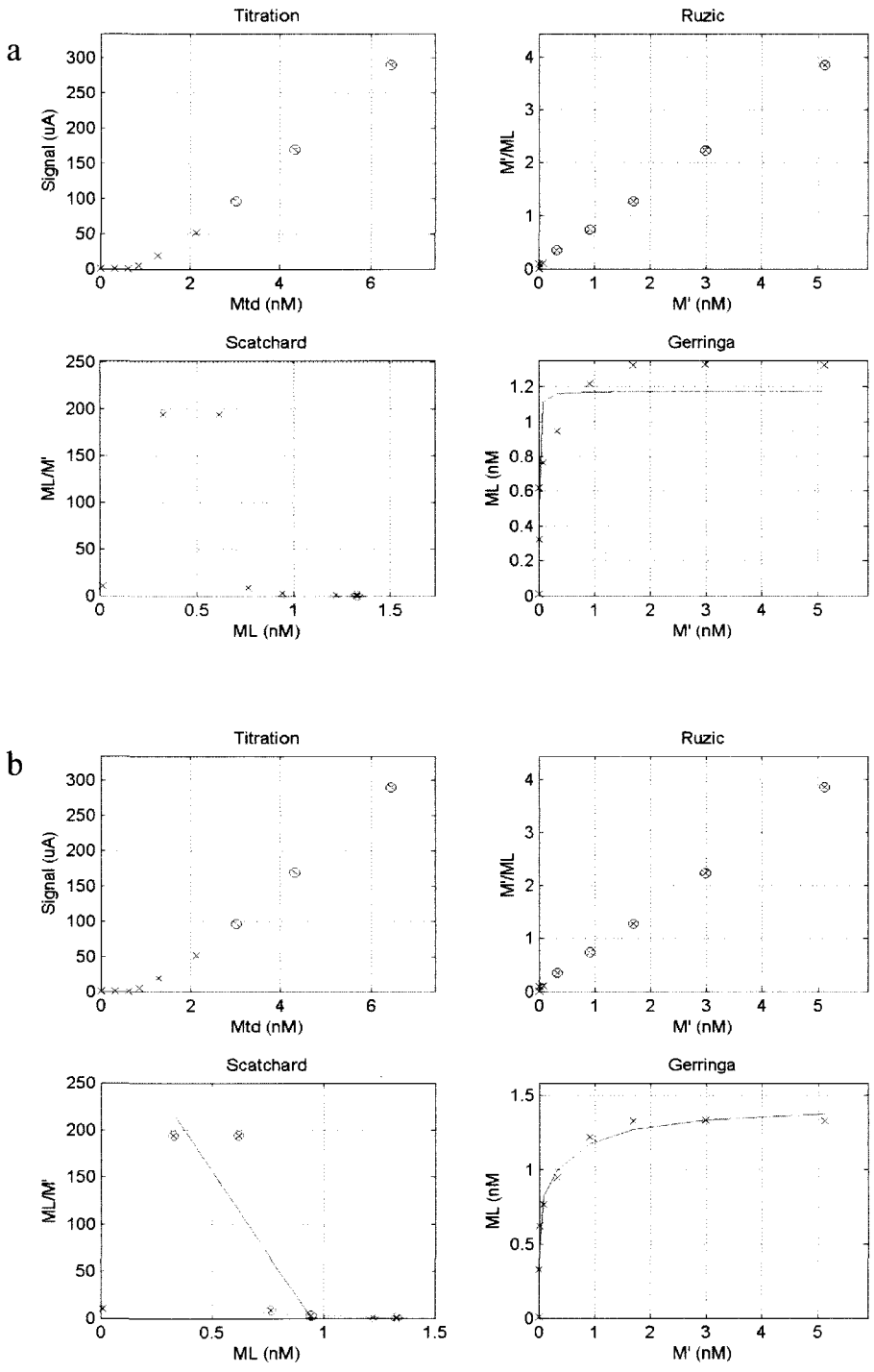

Fig. 14. TDI's graphic output of Ellwood's (2004) titration interpreted as having one (a) and two (b) ligands. His interpretations is L = 1.31 nM and logK' = 10.2.

Similarly, if the one-ligand interpretation of the titration shown in Fig. 13 was used instead of the two-ligand fit, the underestimation of CI would be:

Fig. 13 (one or two) $CI_{(1L)} / CI_{(2L)} = 16.0 / 51.2 \approx 31\ \%$

More so, the titrations shown in 12 is clearly a two-ligand case, and would show an even bigger CI underestimation if the one-ligand model were used (e.g. a shorter titration or researcher's error).

Fig. 12 (two-ligands) $CI_{(1L)} / CI_{(2L)} = 2.4 / 38.5 = 6\ \%$

In summary, the range of CI underestimation of three titrations that show the presence of two ligands when using TDI but that do not clearly indicate the presence of more than one ligand when using simpler mathematical approaches like Ruzic plots, is between 10 % and 69 % of the two-ligand CI. If a two-ligand titration were interpreted as one-ligand by mistake, the CI underestimation would be even bigger (6 % of the two-ligand CI).

The biogeochemical ramifications of this underestimation, apparently caused by performing shorter titrations and using simple mathematical models, are that though we attempt to understand the importance of these complexing agents with time-consuming analyses and finicky instrumentation, we are gauging something in between a half and a tenth of what they really measure, ultimately obtaining a trace metal speciation picture that does not reflect the truth and is not as good as it can be. TDI offers the possibility of evaluating several possible interpretations for each titration, without taking more than 30 seconds per interpretation, so that all the instrumental work is used to the maximum of its capacity.

3.2.6. On the internal calibration S-iteration method of Hudson et al. (2003)

Hudson et al. (2003) proposed a modified approach to metal titrations that has been used recently (e.g. van den Berg, 2006; Tian et al., 2006). In the next section, a brief description of this modification of a normal titration mathematical analysis, an evaluation of some relevant datasets using TDI and some conclusions are presented.

The procedure for metal titrations stipulates that additions should be made until a linear response is obtained. In simple cases, for example UV-oxidized trace-metal-free seawater (UVTMFSW) with artificial ligands added (like NTA or EDTA), the titration produced is simple to mathematically interpret. These titrations are generally used to calibrate the method, and additions are made up to ~ five to ten times the known L_T, that is, until the ligand is completely saturated with metal and a linear response is obtained. But in real samples with unknown L_T, where a continuum of ligands of different concentrations and strengths is likely to exist because of the diversity of organic matter present in natural waters, the titration itself is difficult to carry out until a point of completion and thus the mathematical interpretation is more difficult. Strong ligands present in low concentrations are saturated earlier in the titration, i.e. at lower M_{TD} than weaker ligands that exist at higher concentrations. In order to saturate these weaker ligands, the titration needs to be carried out to higher concentrations.

Oceanographers studying trace metal speciation in the past, 20 years have focused on the strong ligands, usually existing at low concentrations, that bind the major fraction of metals like Zn, Cd, Fe and Cu present in solution, i.e. the ligands whose CI is high, those that are calculated to bind more than 90 % of trace metals of biological importance (Donat and Dryden, 2001). Ligands present at higher concentrations but whose binding strengths are low enough to render them not as mathematically important as the strong ligands are usually non-specific and are thought to be related chemically to humic and fulvic substances. Hudson et al. (2003) focused their study on an ample analytical window or windows that can study both the strong and weak ligands. When trying to titrate the strong ligands, a titration is thought to be complete when relatively linear response is obtained, reaching additions of Cu_{TD} ~ 10 nM; in contrast, Hudson et al.

(2003) proposed that complete titrations should be carried out to Cu_{TD} ~ 200 nM or more. This high addition range is very large and unrealistic for open ocean samples, given that the focus is on the small additions carried out between ambient Cu_{TD} and 1 or 2 nM, within the concentration range of L_T in these regimes. In coastal regimes, the Cu_{TD} concentrations can be expected to be higher, and so are the concentrations of fresh, riverine organic matter. Since most titrations have been historically performed over a small range of additions, Hudson et al. (2003) developed a mathematical way to extrapolate the not-linear-yet "linear" final portion of a titration. Their paper discusses several possible ways to correct the initial slope of the linear response portion into an "optimized slope", which is then used as the slope with which the rest of calculations are done, in order to interpret not only the strong ligands present, but also the weaker humic substances as they both affect the trace metal speciation.

I took some recent publications (Van den Berg, 2006; Tian et al., 2006) that use Hudson et al.'s (2003) "optimized slope" criterion and processed some titrations using TDI, with the aim of understanding the need for this extra step. Given that L_T can be estimated first by the x-intercept of the titration, and that estimate is similar to estimates obtained from the Scatchard and Gerringa plots. The slope-correction of the titration step will probably mean, in the case of an incomplete titration a significant change in the concentration of total ligand L_T, which is why that is the most important parameter to discuss here. Van den Berg reports L = 1.38 nM using a one-ligand Ruzic, TDI obtains 1.39 nM (Fig. 15a). Tian et al. reports L = 1.53 nM using a one-ligand Gerringa, TDI obtains 1.50 nM (Fig. 15b). The difference between the published L values and those obtained by TDI is very small, because these two titrations curves are very linear to start with, and complete. Van den Berg's (2006) dataset shows a titration curve that seems to be more complete than Tian et al.'s (2006), with additions made until ~ six times L_T, and thus does not change much when different points are selected for the titrations slope. The dataset of Tian et al. (2006), with additions made until ~ three times L_T, can only be analyzed using the last three titration points as the linear portion of the titration; if the last four points are selected and used as the linear portion, the titration graph shows a linear section that is not linear. This evidences the semi-completeness of this titration.

Garnier et al. (2004) created modeled titration datasets, some with one and some with two ligands, with total additions as low as ~ ten percent more than L_T and some as high as ~ ten times L_T. Analyzing their data with TDI, some titrations show a clear curved look towards the higher M_{TD} end, indicating that they are incomplete (Fig. 15c). Maybe Hudson et al.'s (2003) slope correction can mathematically fix these titrations, but if this was a real titration obtained in the lab, the researcher should do it again until a satisfactory level of completion is obtained. That is, until a longer M_{TD} addition titrates the ligand, and a linear section is obtained. In this sense, TDI interprets the linear, complete or semi-complete titrations, but does not fix nor does a good job at interpreting nonlinear curves characteristic of incomplete titrations.

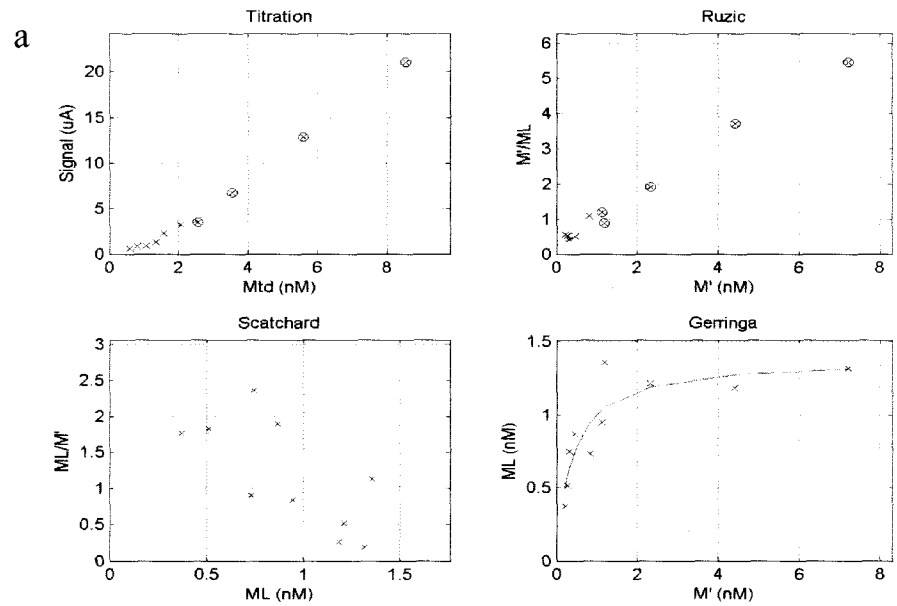

Fig. 15. TDI's graphic output of Van den Berg (2006; a), Tian et al. (2006; b) and Garnier et al. (2004; c), showing complete, semi-complete and incomplete titration curves, respectively. These titrations are carried to approximately six, three and slightly above the L_T.

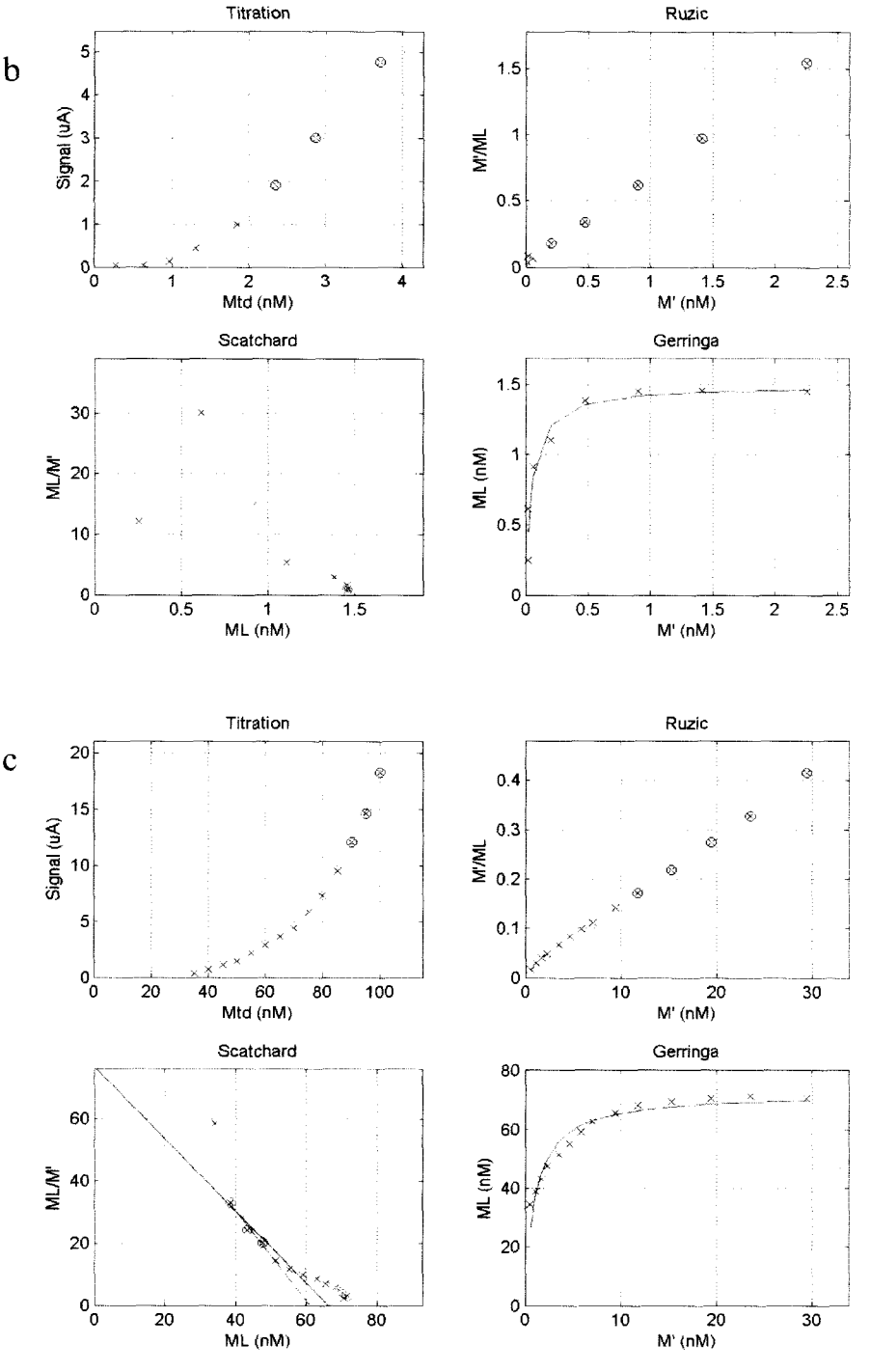

Fig. 15. Continued.

There are other slope corrections similar to Hudson et al. (2003), like Voelker and Kogut (2001) overload calibration or Buck et al. (2005) multi-window analysis. A complete titration will make Hudson et al. (2003) and similar correcting algorithms mathematically unnecessary. A complete titration is what should be analytically obtained to be processed by any mathematical tool the researcher decides to use, preferably with intercomparison of L and K parameters between mathematical approaches. If the titration appears to be incomplete, it should be performed again.

3.2.7. On the hypothesis of Voelker and Kogut (2001) that humics as weak ligands can be difficult to evaluate along with strong ligands with these mathematical methods

Volker and Kogut (2001) stated that the mathematical interpretation of the titration of a sample with heterogeneous complexing ligands (that is, strong ligands in low concentrations and weaker ligands in higher concentrations) is inherently difficult given that preliminary L and K parameters for these ligands limit the interpretation. They also mentioned that in waters with heterogeneous mixtures of ligands the distinction between strong and weak ligands is somewhat arbitrary.

In order to clarify the situation, I attempted to interpret the Garnier et al. (2004) modeled titrations of a mixture of strong and weak ligands with logK' differences between three and four log units that reflect the ligand heterogeneity that Voelker and Kogut (2001) want to analytically explore and mathematically construe. My conclusions confirm Voelker and Kogut's hypothesis. Given the preliminary parameters the Gerringa iteration receives from the Scatchard plot as input, ultimately the parameters produced tend to be somewhat of a merging mixture of both ligands. That is, the strong ligand is not as strong as it should numerically be to reflect the true K values it was defined to have in these modeled data, and the weak is not as weak, either. In other words, these analytical and mathematical methods tend to focus on one analytical window. While CSV can be tweaked to explore different analytical windows (Buck and Bruland, 2005), it can not look at two ends of the spectrum simultaneously, i.e. it can not look at very strong and very weak ligands in the same titration. Rather, the focus is on ligands whose L and K values are close together (within one or two orders of magnitude).

Furthermore, given the relatively low CI of humics in open ocean waters (as a general consensus), the analytical focus should be and is on strong, low concentration, relatively metal-specific ligands, presumably produced by phytoplankton to complex metals of biological importance, rather than on relatively weak, high concentration, non-metal-specific humics. This does not mean that humics should not be investigated; indeed, a more holistic investigation of the effect of both phytoplanktonic and humic ligands on trace metal speciation should compare their importances in various oceanic regimes.

3.3. CONCLUSIONS

1. TDI works as a L and K optimizing, multi-method mathematical tool. Scatchard plot initial L and K estimates are optimized into a Gerringa plot, producing robust, true-minimum L and K parameters. Voelker and Kogut (2001) questioned Miller and Bruland's (1997) first-two and last-two Scatchard plot interpretation methodology because the analytical uncertainty is highest at the plot's extremes. TDI can be tuned to use any titration combination; I used the first three to five and the last three to five points of the Scatchard plot, with the outlier of each data subset being excluded, producing lower uncertainties in the initial L and K estimates. These parameters are then optimized in the Gerringa plot, producing lower uncertainties, that are as good as or better than any other mathematical method, specially for the logK'. In conclusion, I suggest using this multi-method comprehensive tool.

2. TDI's interpretations match previously reported values of both samples and modeled titration curve data. TDI's results have a lower level of uncertainty than any other one-mathematical-method-only approach.

3. Using only one mathematical method is not a good practice because it can produce results that can underestimate the real CI of natural ligands. TDI does not produce this artifact thanks to the Gerringa plot optimization step and, ultimately,

the possibility for the simultaneous evaluation of the graphic and numeric outputs of the titration and the Ruzic, Scatchard and Gerringa plots.

4. I recommend using TDI in the following way. It should be forced to fit two ligands and then fit one ligand, and the results produced should be compared and evaluated. Attempting to super-tune the constraints that separate one- and two-ligand cases is essentially futile because of all the changing factors from one titration to the next.

5. TDI could be used as a mathematical method translator, so that the inherent differences between the different mathematical methods do not add bias to the results. In this sense, data from traditional papers with Ruzic-only interpretations should be de-biased by being run through TDI, and then can be compared with similarly treated Scatchard-only or Gerringa-only datasets.

6. Complete titrations are very important, so that the use of internal calibration methods is not needed. Also, they would help explore humics along with strong ligands. Garnier et al. (2004) compared different titration schemes, and suggested log-addition schemes are better than decade-addition and linear-addition, respectively.

CHAPTER 4

RESULTS

4.1. HYDROGRAPHY

A detailed description of the hydrography of the stations sampled during the IOC 1996 cruise in the South Atlantic is found in Cutter and Measures (1999) and references therein. The hydrography of the region is defined by the physical forces provided by surface currents and deeper water mass movement and advection. Briefly, in the sampled stations there were surface mixed layers of various depths, between 10 and 80 m, influenced by the Amazon River plume and the North Brazil Current (NBC, Stations Amazon 1 and 2 and 6), the South Equatorial Current (SEC, Station Romanche), the South Atlantic Gyre (Station 8) and the Brazil Current (BC, Station 10). Fig. 16a shows a close-up of the surface currents in the Equatorial region of the Atlantic Ocean. Below the surface, different intermediate waters, namely South Atlantic Central Water (SACW) and North Atlantic Central Water (NACW) were found in both hemispheres. Underneath, layers of Antarctic Intermediate Water (AAIW), upper Circumpolar Deep Water (CPDW), North Atlantic Deep Water (NADW, which can be subdivided in its upper and lower portions, u-NADW and l-NADW, respectively) and Antarctic Bottom Water (AABW) were present, aging as they travel away from their respective sources. Fig. 16b shows a cross section of the water masses in the Atlantic Ocean; Fig. 16c focuses on water masses at the sampling stations, whose locations are shown in Fig. 16d. Fig. 16e shows some surface currents for reference. The sources of these water masses are believed to be in the Sub-Antarctic front near the northern Drake Passage (AAIW), near the Labrador Sea (u-NADW), near the Irminger Sea (l-NADW) and near the Weddell Sea (AABW); CPDW is believed to originate from a mixture of deep waters from all oceans, so that contact with surface waters is minimal. While AAIW and CPDW either cross the Equator and turn east (Jochum and Malanotte-Rizzoli, 2003) or merge into NADW (Talley, 1996), major water masses NADW and AABW flow southward and northward, respectively. All four water masses flow mainly in the west side of the South Equatorial

Atlantic, due to the western intensification phenomena.

Chlorophyll-*a* and phaeophytin are proxies for biomass performing primary production and grazing, processes related to the presence of phytoplankton and zooplankton. The relationship between photosynthetic pigments, phytoplankton and zooplankton and Zn and Cd and their complexing ligands is explored in the Discussion chapter, here some basic parameters are defined for each station. The relationship between Zn and silicate and Cd and phosphate are discussed in the Metal / Nutrient section of the Discussion chapter; here, some nutrient data are introduced for each station. Following is a brief description of each station's water column structure, in terms of mixed-layer depth, photosynthetic pigments chlorophyll-*a* and phaeophytin (available in Measures website), water mass and nutrient data (Cutter and Measures, 1999).

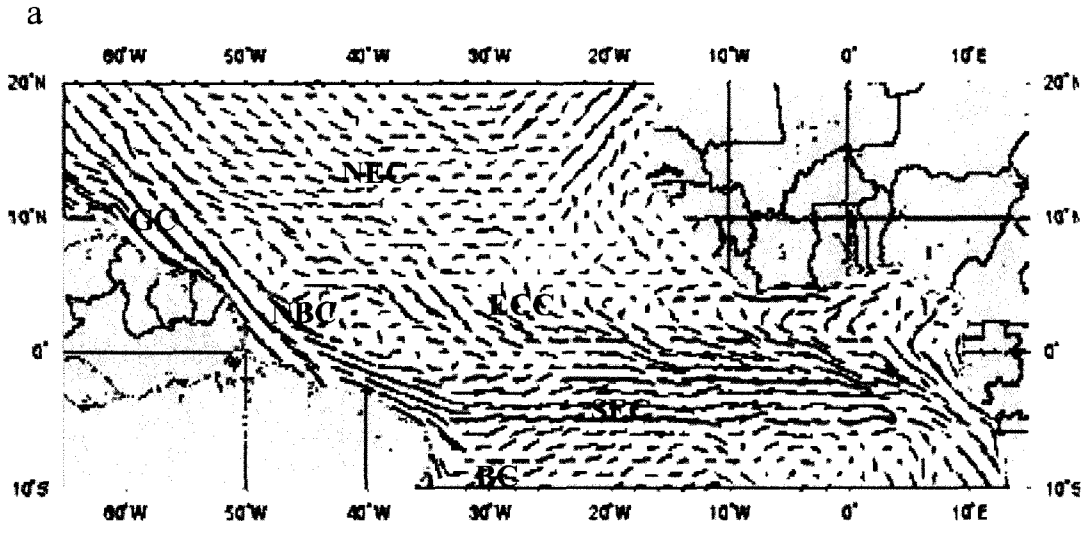

Fig. 16a. Map of surface surrents of the Equatorial region of the Atlantic Ocean (a). GC = Guiana Current, NBC = North Brazil Current, BC = Brazil Current, NEC = North Equatorial Current, ECC = Equatorial Counter Current, SEC = South Equatorial Current. From Bonhoure et al. (2004) and Bischof et al. (2004).

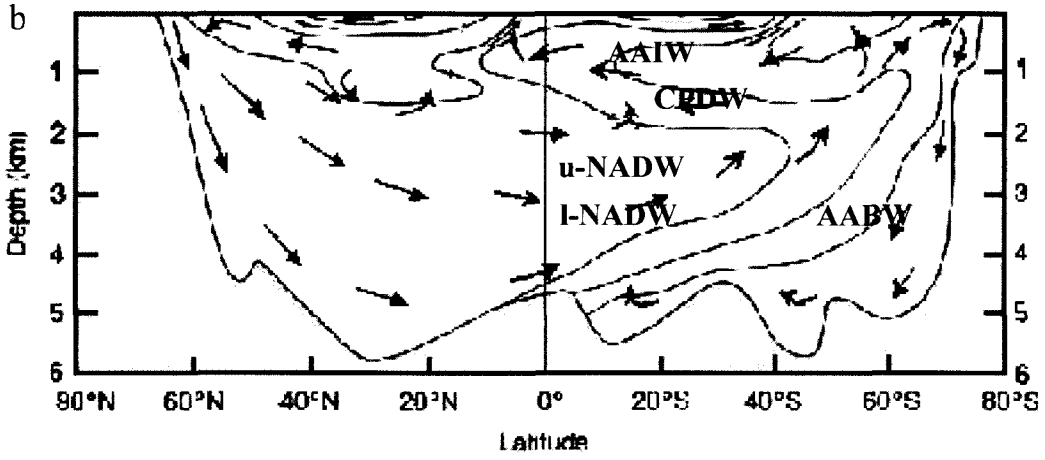

Fig. 16b. Cross sectional diagram of the Atlantic Ocean water mass structure. AAIW = Antarctic Intermediate, CPDW = Circumpolar Deep, u-NADW = upper-North Atlantic Deep, l-NADW = lower-North Atlantic Deep and AABW = Antarctic Bottom waters.

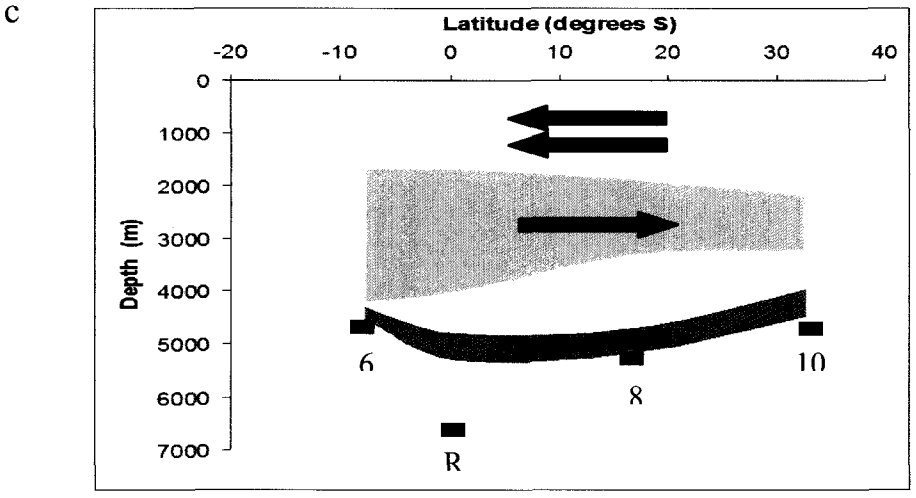

Fig. 16c. Cross sectional diagram of the water masses along the IOC 1996 cruise track shown in Fig. 16d. Shaded areas indicate water masses present at each station (Cutter and Measures, 1999): AAIW (green), CPDW (yellow), NADW or u-NADW and l-NADW (red) and AABW (brown). Arrows indicate direction of travel. Black blocks indicate the depth of the bottom of the water column for each labeled station.

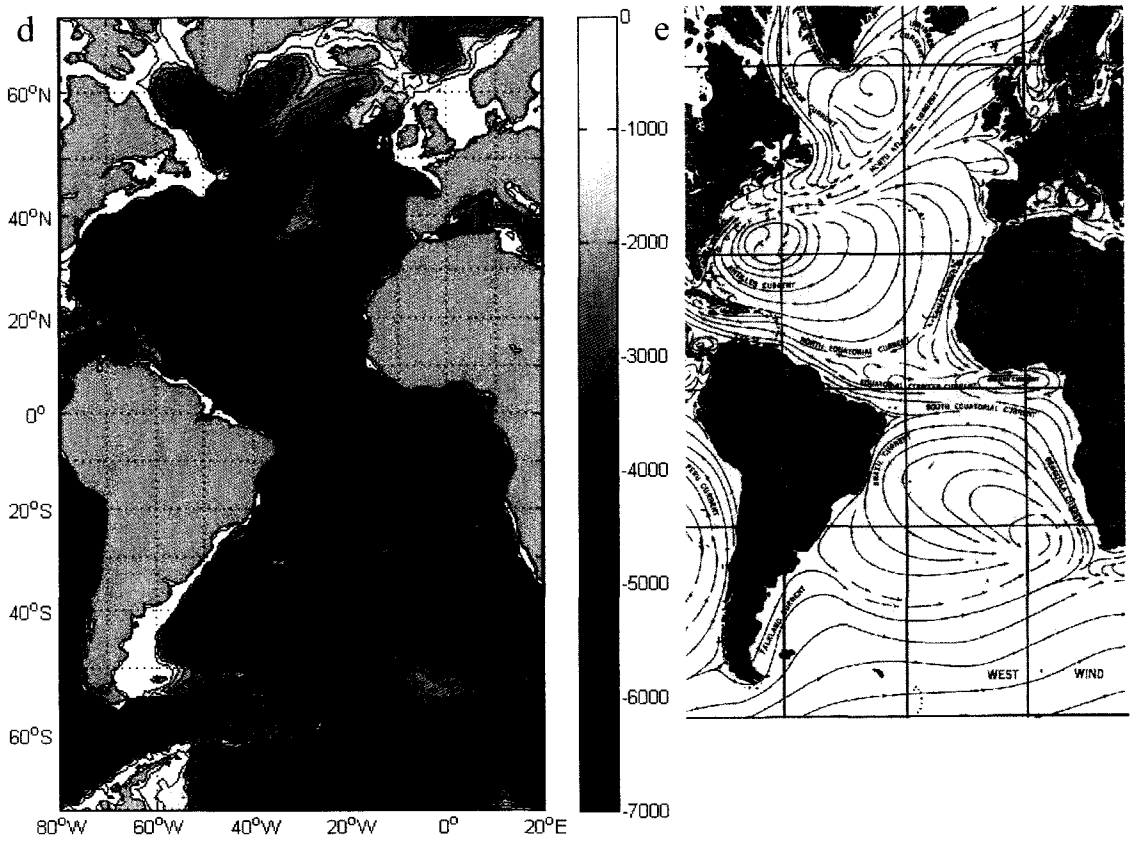

Fig. 16d. Location of 1996 IOC Contaminant Baseline Survey cruise vertical profile Stations Amazon 1 and 2 (A1 and A2), 6, Romanche (R), 8 and 10, shown in a bathymetric contour map. The black line represents the path of water mass transport which was sampled at each of the four stations to obtain the data plotted in Figs. 26 - 31, 33, 38 and 39. Bathymetric features allow the water mass transport shown in Figs. 16b and 16e along the western side of the Atlantic Ocean. Zn speciation was determined at Station B0 by Baars et al. (2010) and at Station E0 by Ellwood and van den Berg (2000); AAIW is formed at B0 and recently-formed NADW is found at E0 (Figs. 38 and 39).

Fig. 16e. Main surface currents in the Atlantic Ocean.

Station Amazon 1 had a 10-m mixed layer over a mixture of SACW and NACW. This station was in the Amazon River plume, and therefore is influenced by it, as a low-salinity, very high silicate (~ 45 μM), few-meters-thick fresh water layer was present at the surface, where the chlorophyll-*a* maximum was located. Phaeophytin showed a 20m subsurface maximum, and a 150m local maximum that did not match with the chlorophyll profile. Phosphate showed a typical nutrient depth profile, with depletion in the surface and increasing values below 100m. The present study focuses on the top 400m of the water column at this station.

Station Amazon 2 had a 60m mixed layer over a mixture of SACW and NACW. This was a more oligotrophic station, with less of a riverine signature, as evidenced by lower surface silicate values (less than 4 μM). The chlorophyll-*a* maximum and phaeophytin maximums were located below the mixed layer, at 69m depth. The phosphate profile closely resembles that of the previous station. This study focuses on the top 400m of the water column at this station as well.

Station 6 had a 40m mixed layer that reflects oligotrophic features as well as atmospheric influence. Below it, the chlorophyll and phaeophytin maximums were located at 80 and 95 m, respectively. Underneath, there was a mixture of SACW, NACW and mode waters. Then, relatively thin layers of AAIW and CPDW were located, centered around 800 and 1000 m, respectively, near the nitrate and phosphate maximum (~700m) and the silicate local maximum (~900m). Below, a wide layer of NADW (91 % northern component) extended from 1700 to 4200m. u-NADW stretched from 1600 to 3000m, while l-NADW went from 3000 to 4200m (Alleman et al., 2001). Below, dilute AABW (71 % northern component; Cutter and Measures, 1999; moderately high silicate ~ 50 μM) was found from 4400m down. From Station 6 and Romanche southward, the water masses originating near Antarctica (AAIW, CPDW and AABW) get wider and younger, while NADW, originating in high latitudes in the north, gets narrower and older. Estimates and measurements of water mass age, varying over a station-to-station range or over the northernmost-to-southernmost station, are discussed later.

Station Romanche, situated in the Inter-Tropical Convergence Zone (ITCZ) and the Romanche Fracture Zone (RFZ), showed some Equatorial upwelling and a 20m mixed layer. The chlorophyll-*a* and phaeophytin maximums, which showed the highest values of all stations (~ 0.9 µg/l), were at 57 m. Below, SACW was found. AAIW extended from 600 to 850m, CPDW from 1000 to 1500m, NADW from 1700 to 4000m and AABW from 4800 to 5300m. The nitrate and phosphate maximum were ~ 700m, within the AAIW, while the silicate local maximum was ~ 1000m, in the upper CPDW. AABW was evidenced by very high silicate values (~ 100 µM) and moderately high nitrate and phosphate that extended up into l-NADW due to advection.

Station 8, further south, showed a 70m mixed layer defined by the SEC, where pigments were evenly distributed. The chlorophyll-*a* maximum was at 138m, and SACW extended down to 500m. Below the surface, AAIW was found between 700 and 850m, CPDW between 900 and 1500m, NADW between 1900 and 3300m and AABW between 4700 and 5200m, with silicate values exceeding 110 µM and high nitrate and phosphate as well. Similar to Station Romanche, the nitrate and phosphate maximum were within AAIW (~ 800m), while silicate local maximum were in the uCPDW (~ 900m).

Station 10, the southernmost station, has an 80m mixed layer of very oligotrophic waters. The chlorophyll-*a* profiles were different from the other stations, as they were high (~ 0.22 µg/l) and constant in the upper 100m, with a maximum at 102m. Also, the phaeophytin profile differed from that of chlorophyll-*a*, showing low (~ 0.1 µg/l) values in the upper 100m that reached a maximum higher than chlorophyll-*a* at ~ 0.3 µg/l. SACW was found below. Underneath this, AAIW extended from 750 to 900m, CPDW from 1000 to 2000m, NADW, with the most dilute 75 % northern component of all stations, from 2200 to 3200m and AABW, with the highest silicate values (~ 130 µM) of all stations, from 3950 to 4460m. The highest silicate values extended into l-NADW (80 µM at 3300m). The local nitrate, phosphate and silicate maximum are ~ 1400m, within CPDW. The northward-moving water masses show the youngest ages (e.g. AAIW 1 - 3 years-old; Roether and Putzka, 1996), compared with the southward-flowing NADW (~ 100 years-old; Hirst, 1999).

4.2. Zn AND Cd TOTAL DISSOLVED CONCENTRATIONS

The method used to determine total dissolved Zn and Cd (Bruland et al., 1979) was tested for blanks and standard reference materials (SLEW-2 and SLRS-3) before running actual samples. Blanks for each batch of samples were evaluated and subtracted to obtain sample Zn_{TD} and Cd_{TD} concentrations. Also, a bulk standard sample was used as a standard to compare while running samples, along with some samples being "spiked" with a known addition of Zn_{TD} and Cd_{TD}. Finally, the recovery of those spikes and the bulk standard sample was evaluated to properly obtain the final Zn_{TD} and Cd_{TD} concentrations. All in all, once the method was tested for blanks, SRMs and recovery, samples were corrected for blanks and recovery. Table 7 shows some figures of merit for the Zn_{TD} and Cd_{TD} determination method.

The Zn_{TD} and Cd_{TD} profiles are the product of the interaction between the physical forcing of surface currents, water mass movement and advection as well as the biogeochemical processes of biological productivity and biological respiration. The Zn_{TD}, Cd_{TD}, silicate and phosphate depth profiles, shown in Fig. 17 are discussed later, with links to specific water mass ages. The Zn/silicate and Cd/phosphate ratios are presented and explored in the Metal/Nutrient section of the Discussion chapter.

Table 7

Figures of merit for the Zn_{TD} and Cd_{TD} determination, following Bruland et al. (1979) method.

Parameter	Zn (nM)	Cd (nM)
Blanks (n = 4)	0.14 ± 0.01	0.002 ± 0.001
LOD (3 x σ)	0.03	0.001
Recovery	97 ± 6 %	105 ± 6 %

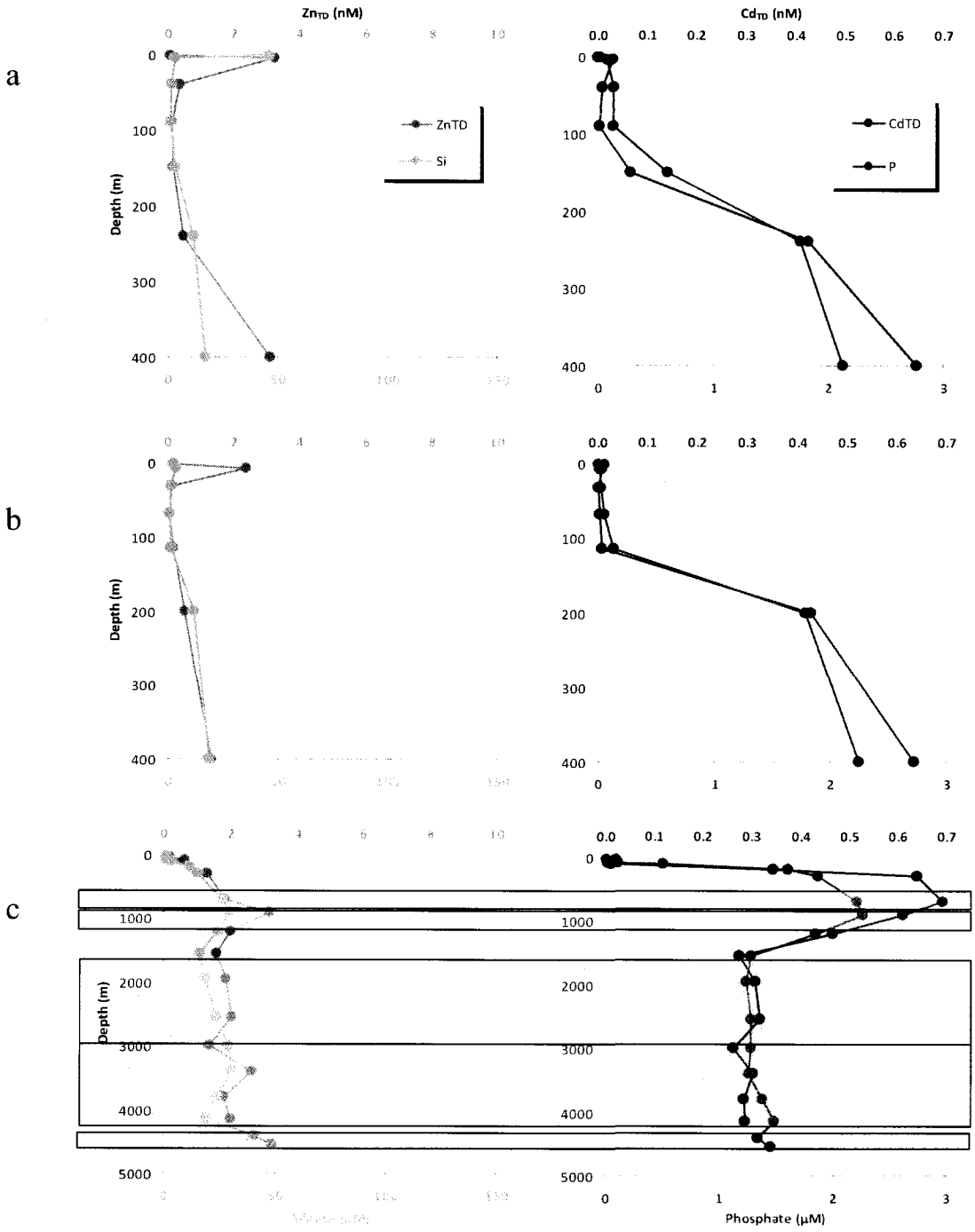

Fig. 17. Zn_{TD}, silicate, Cd_{TD} and phosphate depth profiles of all stations occupied in the IOC 1996 cruise: a) Amazon 1, b) Amazon 2, c) 6, d) Romanche, e) 8 and f) 10. Shaded areas indicate: AAIW (green), CPDW (yellow), NADW or u-NADW and l-NADW (red) and AABW (brown). Note that only the upper 500m were analyzed for Stations Amazon 1 and Amazon 2; note also that Station 10 has no Cd data.

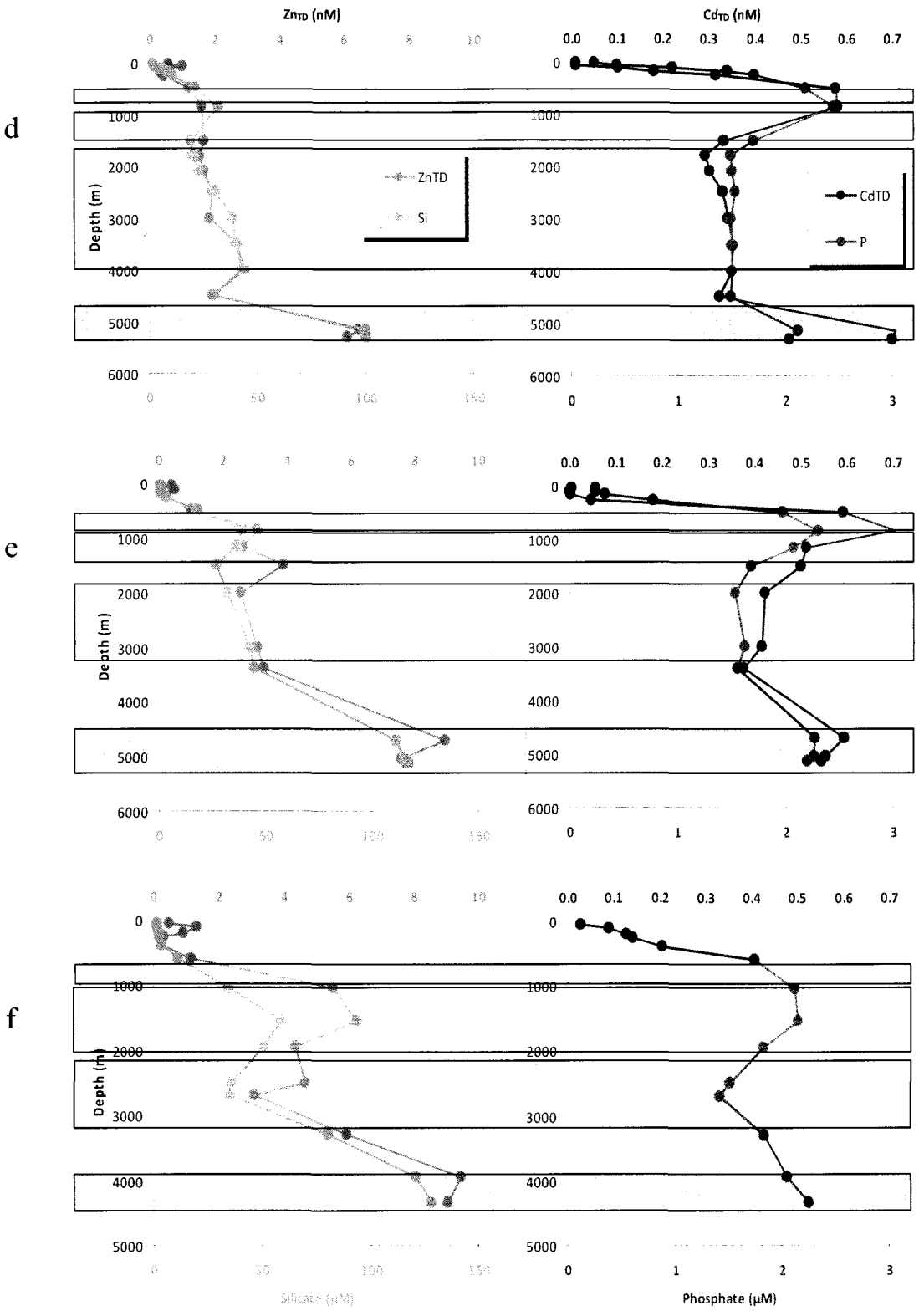

Fig. 17. Continued.

4.3. Zn AND Cd COMPLEXATION DATA

The next two graphs show the TDI output of typical titration, Ruzic, Scatchard and Gerringa plots for Zn and Cd (Figs. 18 and, 19, respectively). These particular titrations indicate the presence of three Zn ligands and two Cd ligands, representative of those present in all the stations.

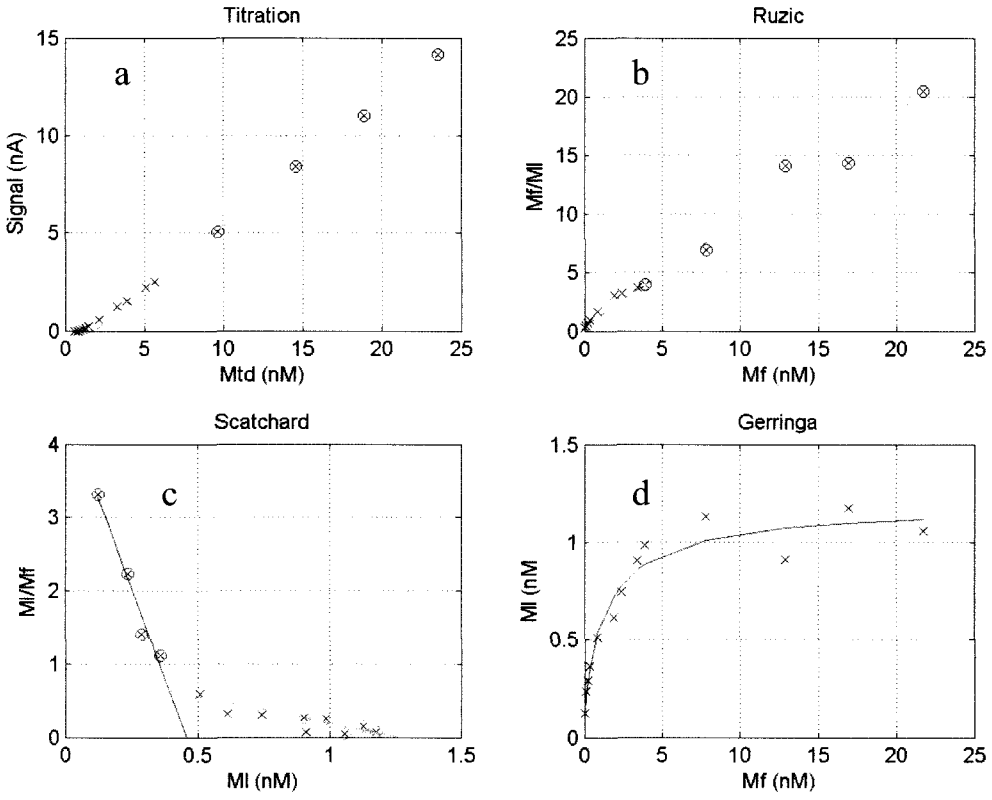

Fig. 18. Typical Zn titration curve (a) and Ruzic (b), Scatchard (c) and Gerringa (d) plots produced by the TDI optimization program. Station Romanche, 15m, showing the presence of three ligands: L1 = 0.753 nM, logK1 = 11.7, L2 = 0.219 nM, logK2 = 10.4, L3 = 0.970 nM, logK3 = 8.8. The concentrations of total dissolved, inorganic and ligand-bound metal are Mtd, Mf and Ml, respectively.

Throughout all the stations sampled, three ligands were detected for both Zn and Cd. Their average logK' values are listed in Table 8 and their vertical profiles are shown in Fig. 20. Based upon their metal-complexing strength, they can be labeled respectively as "very strong" complexing ligands (L1) for Zn and Cd (logK' = 11.7 and 11.5), "strong" ligands (L2: logK' = 10.3 and 10.0) or L2, and "weaker" ligands (L3: logK' = 8.9 and 8.9). For comparison, previously reported stability constants are also listed in Table 8.

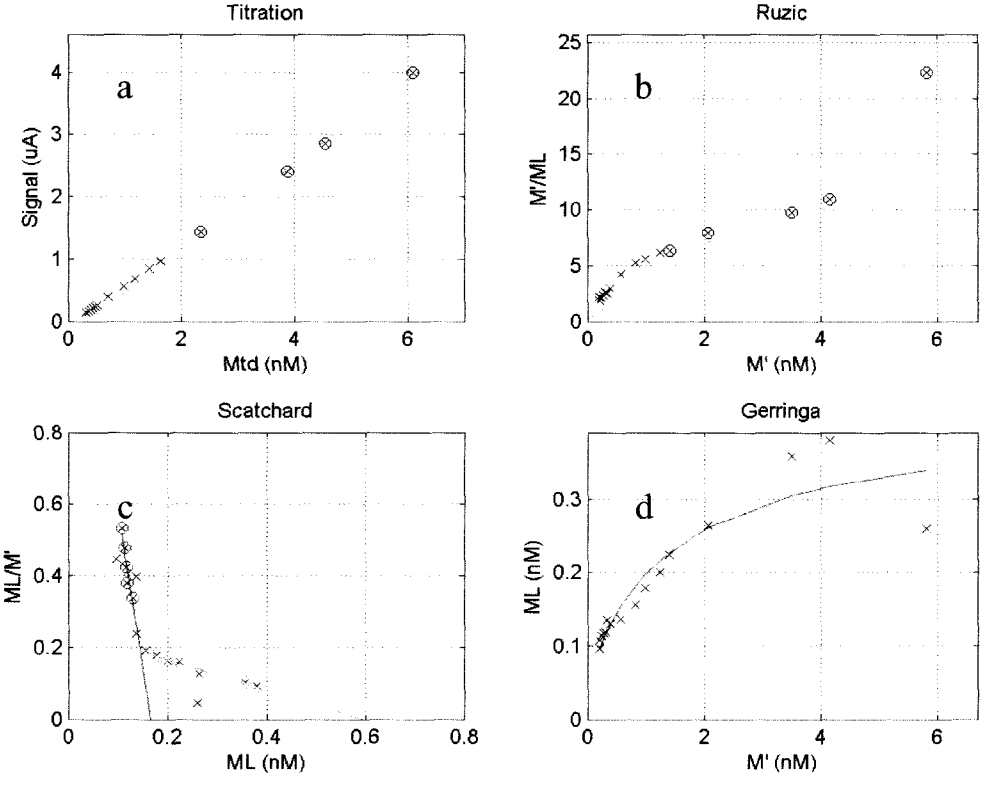

Fig. 19. Typical Cd titration curve (a) and Ruzic (b), Scatchard (c) and Gerringa (d) plots produced by the TDI optimization program. Station 6, 1950m, showing the presence of two ligands: L2 = 0.071 nM, logK2' = 10.3, L3 = 0.347 nM, logK3' = 8.8. The strongest ligand (L1), was not detected in this sample. The concentrations of total dissolved, inorganic and ligand-bound metal are Mtd, Mf and Ml, respectively.

Water column profiles for Zn_{TD} and Cd_{TD} and their complexing ligands are presented in Fig. 21 with water masses shaded for each station. Note that there are no Cd ligand data available for Station 10 because of analytical problems. The presence of ligand(s) in the same water mass in the different stations could indicate transport; further, increasing or decreasing concentrations along the water mass travel path could indicate production or consumption of ligand. The ligand concentrations and the processes that control them are discussed in the Ligand section of the Discussion chapter.

Table 8

Zn- and Cd-complexing ligand stability constants, expressed as logK' ($logK'_{ML,M'}$), in studied stations and compared with literature references (all converted to comparable $logK'_{ML,M'}$). N.D. = not detected at this station. N.A. = data not available. References: a) Bruland (1989), b) Bruland (1992), c) Kozelka and Bruland (1998), d) Ellwood and van den Berg (2000), e) Ellwood (2004), f) Lohan et al. (2005), g) Baars and Croot (2010), h) Henry and Donat (1996), i) Carrasco et al. (2002) and j) Carrasco et al. (2008). Locations: NP = North Pacific, NA = North Atlantic, SO = Southern Ocean, CB = Chesapeake Bay, NB = Narragansett Bay.

Station	logK' Zn L1	logK' Zn L2	log K' Zn L3	logK Cd L1	logK' Cd L2	logK' Cd L3
Amazon 1	11.6	10.6	9.1	N.D.	10.0	9.1
Amazon 2	11.6	10.6	8.8	N.D.	10.3	8.5
6	11.5	10.3	8.8	N.D.	10.4	9.0
Romanche	12.0	10.0	8.9	11.0	10.0	8.9
8	11.9	10.8	9.0	12.0	10.1	9.5
10	11.6	10.3	8.9	N.A.	N.A.	N.A.
All-cruise average	11.7 ± 0.2	10.4 ± 0.3	8.9 ± 0.1	11.5 ± 0.7	10.2 ± 0.2	9.0 ± 0.4
Reference values	11.4	10.0 - 10.6	8.7 - 9.5	11.2	9.9 - 10.5	9.0 - 9.4
Locations	NP	NP,NA,SO,CB	NB,SO,CB,NP	NP	NP,SO	NB,CB,NP
References	j	a, d, e, f, g, h, i	c, g, i, j	j	b, e, j	c, i, j

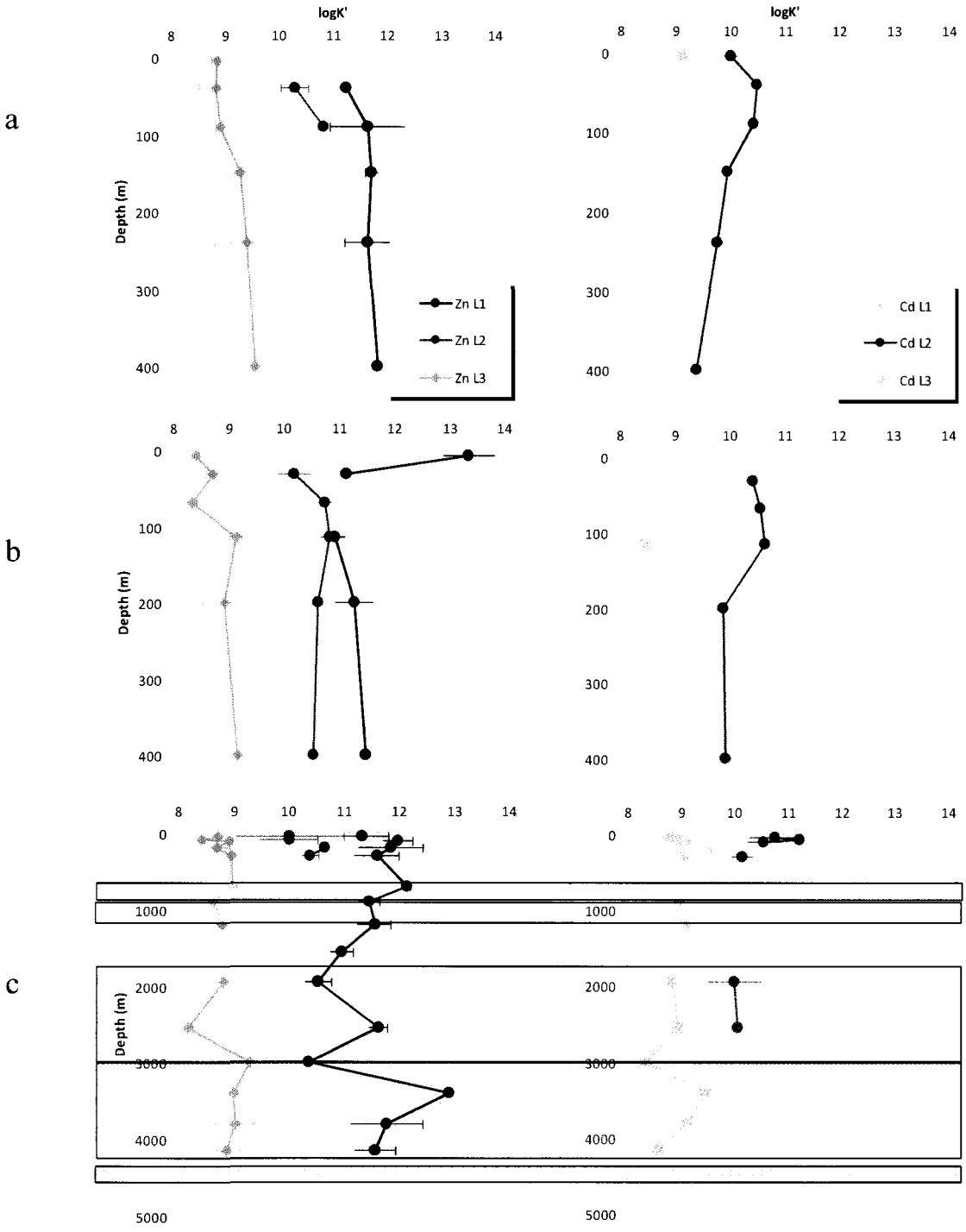

Fig. 20. logK' (with respect to M') depth profile of ligands for Zn and Cd for all stations occupied, a) Amazon 1, b) Amazon 2, c) 6, d) Romanche, e) 8 and f) 10. Shaded areas indicate: AAIW (green), CPDW (yellow), NADW or u-NADW and l-NADW (red) and AABW (brown).

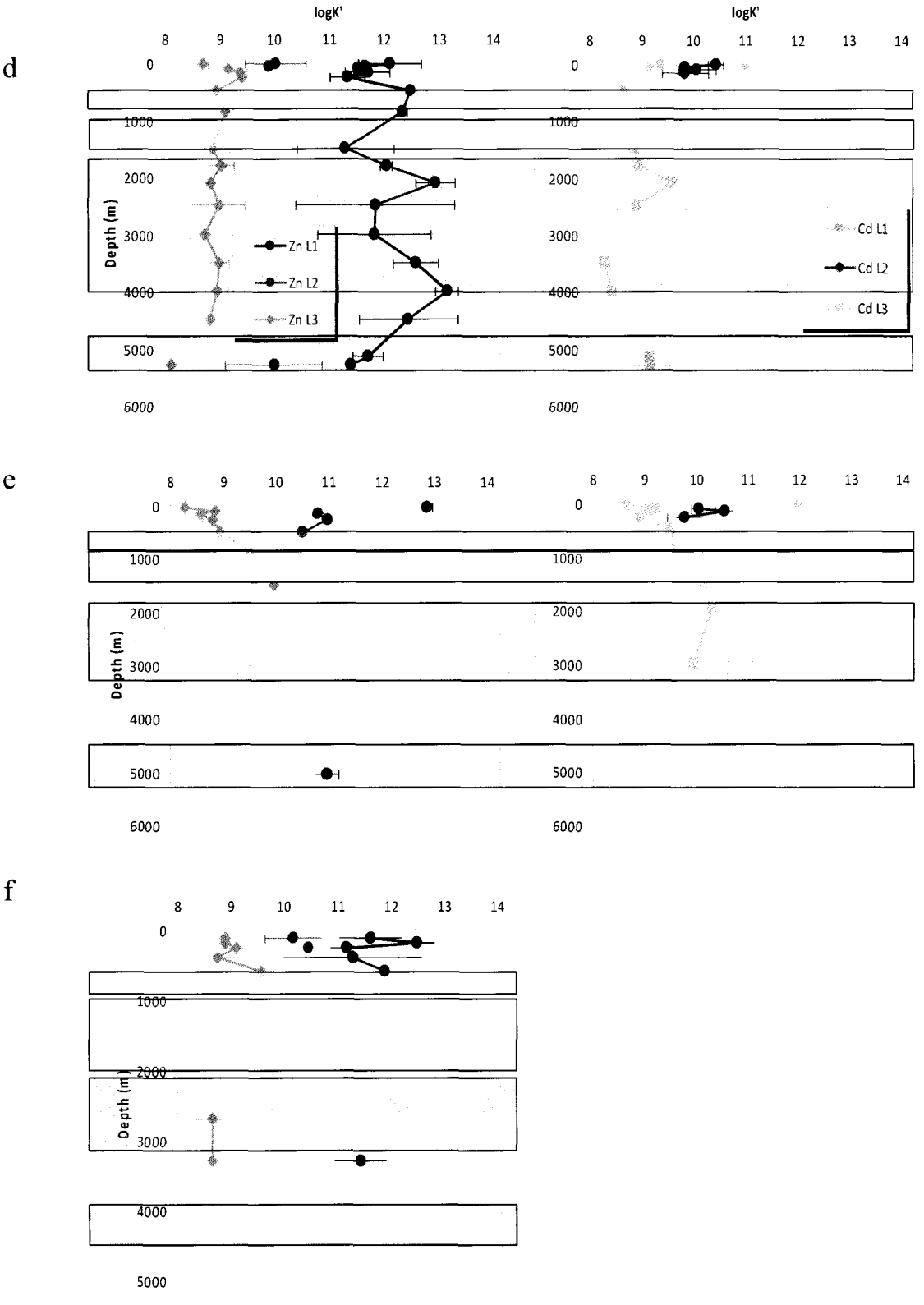

Fig. 20. Continued.

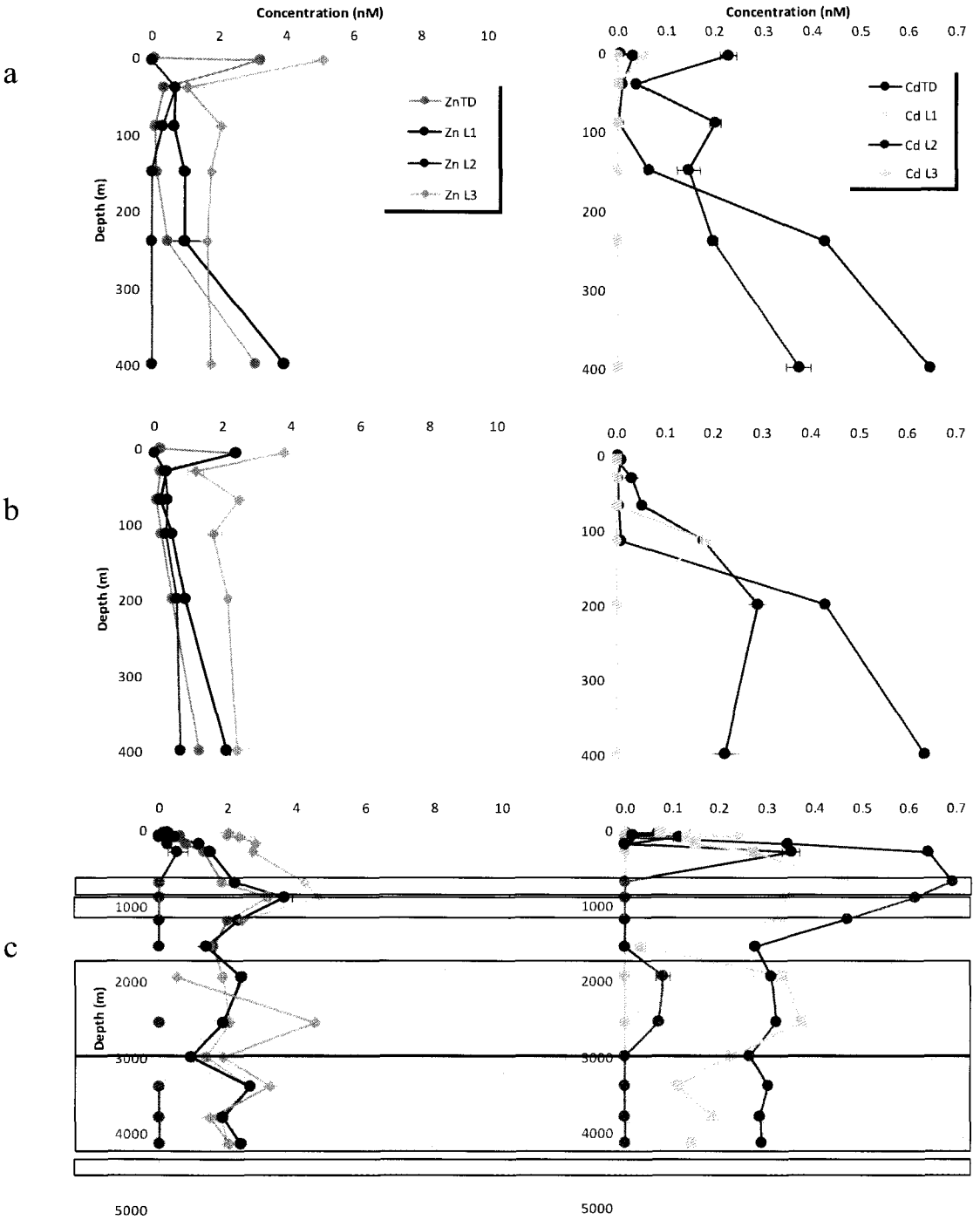

Fig. 21. Water column profiles for the concentrations of Zn_{TD} and Cd_{TD} and their complexing ligands for: Station a) Amazon 1, b) Amazon 2, c) 6, d) Romanche, e) 8 and f) 10. Shaded areas indicate: AAIW (green), CPDW (yellow), NADW or u-NADW and l-NADW (red) and AABW (brown).

d

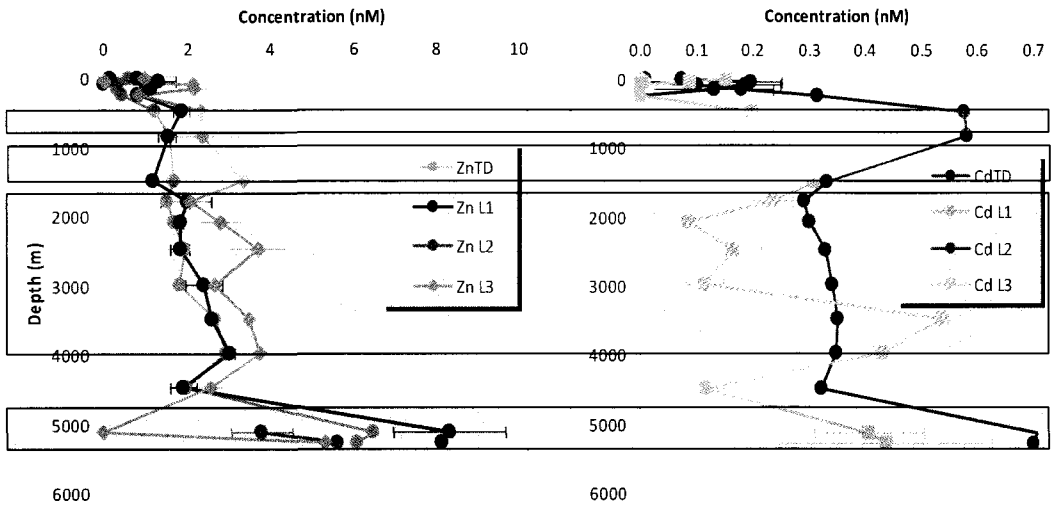

e

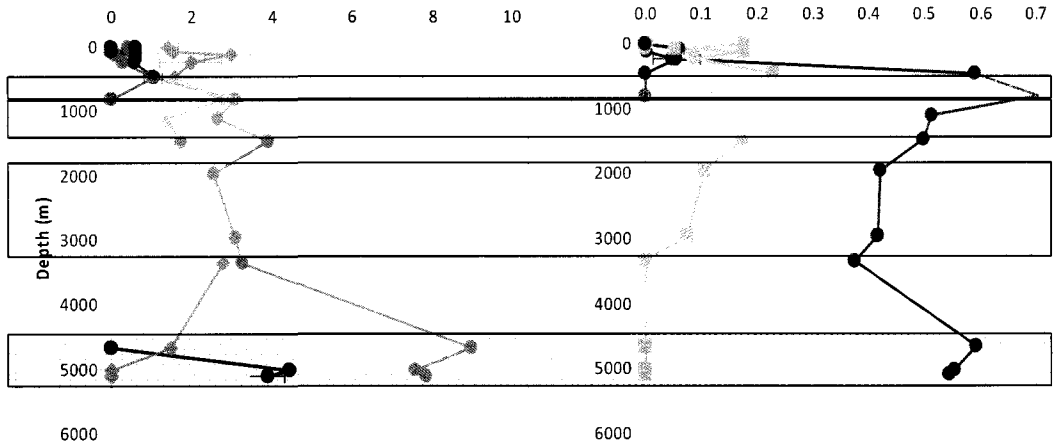

f

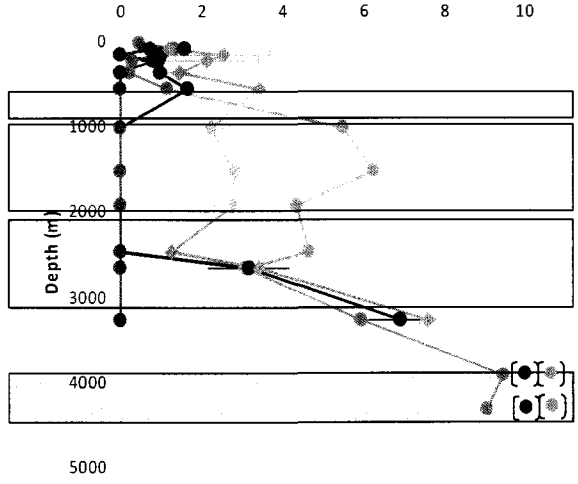

Fig. 21. Continued.

4.4. Zn AND Cd SPECIATION DATA

The chemical speciation of a metal results from the competition between inorganic and organic ligands that create inorganic and organic complexes (MX and ML), depending on the concentration and complexing strength of each of these ligands. The concentrations of the inorganic fractions, Zn' and Cd', and those of the Zn^{2+} and Cd^{2+} ions, are decreased relative to the total dissolved Zn and Cd concentrations by complexation by inorganic and organic ligands. The inorganic speciation of Zn and Cd in seawater were calculated including complexation by inorganic ligands for these samples using the salinity, pH and temperature parameters, thus producing inorganic side reaction coefficients, using a spreadsheet that calculates the ionic strength corrected stability constants and free concentrations of ligands (van den Berg program available at http://www.liv.ac.uk/~sn35/Marine_Electrochemistry.html). Zn's inorganic speciation is dominated by chloride, hydroxide and carbonate complexes, while Cd's inorganic speciation is dominated by chlorides. Zn^{2+} accounts for ~ 50 % of $Zn_{TD,}$ in contrast to the Cd^{2+}, which accounts for less than 3 % of Cd_{TD} (Turner et al., 1981; Morel, 1983; Byrne et al., 1988). The inorganic side reaction coefficients average ~ 2.3 and 37.2 for Zn and Cd, respectively.

Fig. 22 shows the profiles of total dissolved Zn and Cd and Zn^{2+} and Cd^{2+}, while Figs. 23 and 24 focus on the upper 400m and explore the relationship between total dissolved metals, ligands, pigments and free metal concentrations. Since these three figures have logarithmic scales, the dimensions of the natural inorganic side reaction coefficients, defined as a gap between the M' and the M^{n+}, are ~ 0.36 and 1.57 log units. The blue and pink bars in Figs. 22, 23, 24 and 29 indicate the extent of that gap, caused by the iorganic ligands' complexation. These figures plot the total dissolved Zn and Cd, not the Zn' and Cd', so a wider gap between the total dissolved and the free metal concentrations indicates that the organic ligands are complexing a significant portion of the dissolved metal on top of the inorganic ligands present in seawater. A gap as narrow as ~ 0.36 and 1.57 log units between these two lines, at depths where there are no organic ligands present, implies only inorganic complexation is occurring.

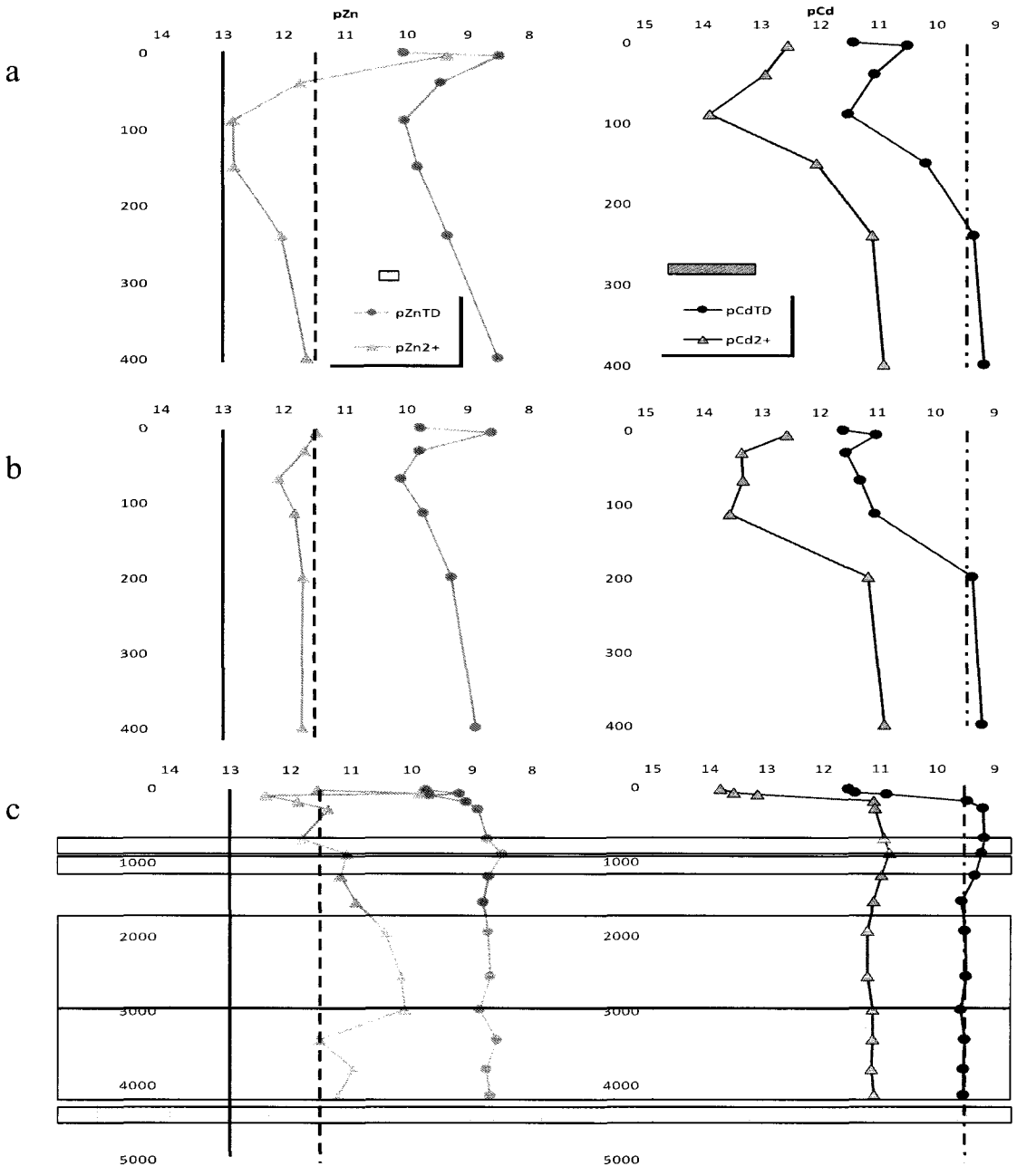

Fig. 22. pZn_{TD}, pZn^{2+}, pCd_{TD} and pCd^{2+} depth profiles of all stations: a) Amazon 1, b) Amazon 2, c) 6, d) Romanche, e) 8 and f) 10. Shaded areas indicate: AAIW (green), CPDW (yellow), NADW or u-NADW and l-NADW (red) and AABW (brown). The solid red line indicates potentially limiting Zn^{2+} concentrations for oceanic species; the dashed line indicates potentially limiting Zn2+ concentrations for neritic species and the dot-dash line indicates potentially toxic Cd^{2+} concentrations for all species. The blue and pink bars above the legend boxes indicate the extent of inorganic complexation.

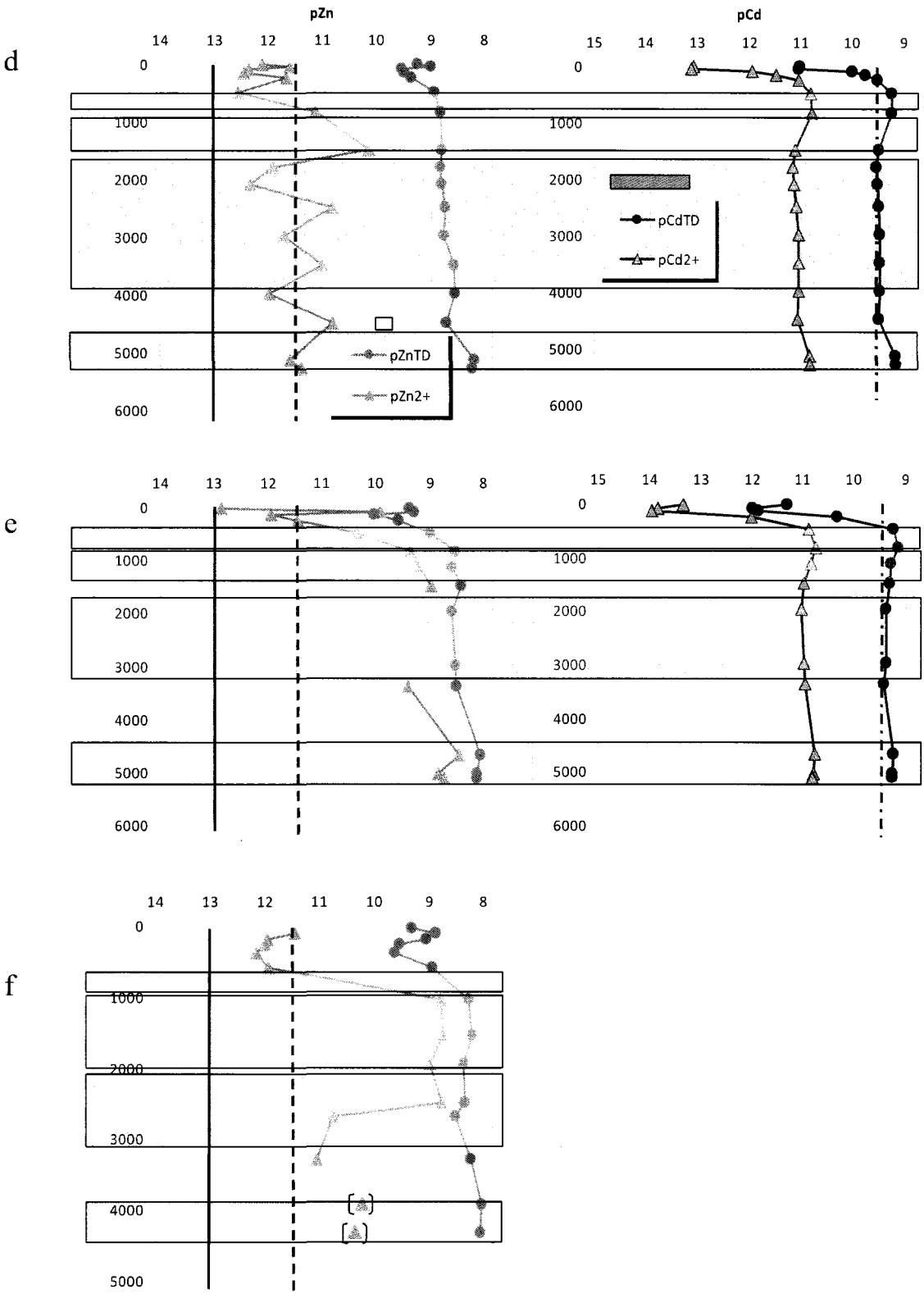

Fig. 22. Continued.

Plotting both M_{TD} and M^{n+} in one graph is only possible if a logarithmic scale is used. Effectively, a span of more than four orders of magnitude is commonly used for a M_{TD} and M^{n+} profile, more so when low surface concentrations of metals, complexed with organic ligands that considerably lower the free metal concentration considerably down are compared with higher concentrations of nutrient-type metals with sometimes only inorganic complexation buffering M_{TD} into relatively high M^{n+} in deeper waters.

Zn is known as an element with several biochemical functions (Morel and Price, 2003), and low Zn concentrations could potentially limit the reproduction rates of phytoplankton. Depending on the phytoplanktonic species adaptation to the habitat where they live, their Zn requirements vary over a large range. For reference, the limiting Zn^{2+} concentration for the average of several neritic and oceanic species ($pZn^{2+} \sim 11.5$ and $\sim$ 13, respectively; Brand et al. 1983) are plotted in Figs. 22, 23 and 29. The general trend is to find Zn^{2+} in the range between the coastal and oceanic limiting concentrations in surface waters, with concentrations increasing with depth. The potential Zn limitation in local and remote (via upwelling of deeper waters) surface waters is discussed in the Speciation section of the Discussion chapter. The expanded depth scale of Fig. 23 and the depth resolution allow for Zn subsurface local maximum to be found in all stations but Amazon 1; this is discussed in the Metal/Nutrient section of the Discussion chapter.

Cd is a metal recently reported to be required for carbonic anhydrase function (Lane et al., 2005), and Cd could also potentially limit phytoplankton reproduction at low enough concentrations. In fact, Co, along with Cd and Zn has been proposed to be part of the "metal trio" that might limit phytoplanktonic activity at low concentrations, with the added intricacy that, under some circumstances like low Zn availability, they can replace each other in some of their biochemical functions at specific efficiencies (Sunda and Huntsman, 1992; Xu et al., 2007). However, no limiting Cd values have ever been reported. At higher concentrations, Cd may act as a toxic element, reducing reproduction rates (Brand et al., 1986). Thus, the toxicity levels for neritic and oceanic phytoplankton species ($pCd^{2+} \sim 9.5$ for both) are also plotted along in Figs. 22, 24 and 29.

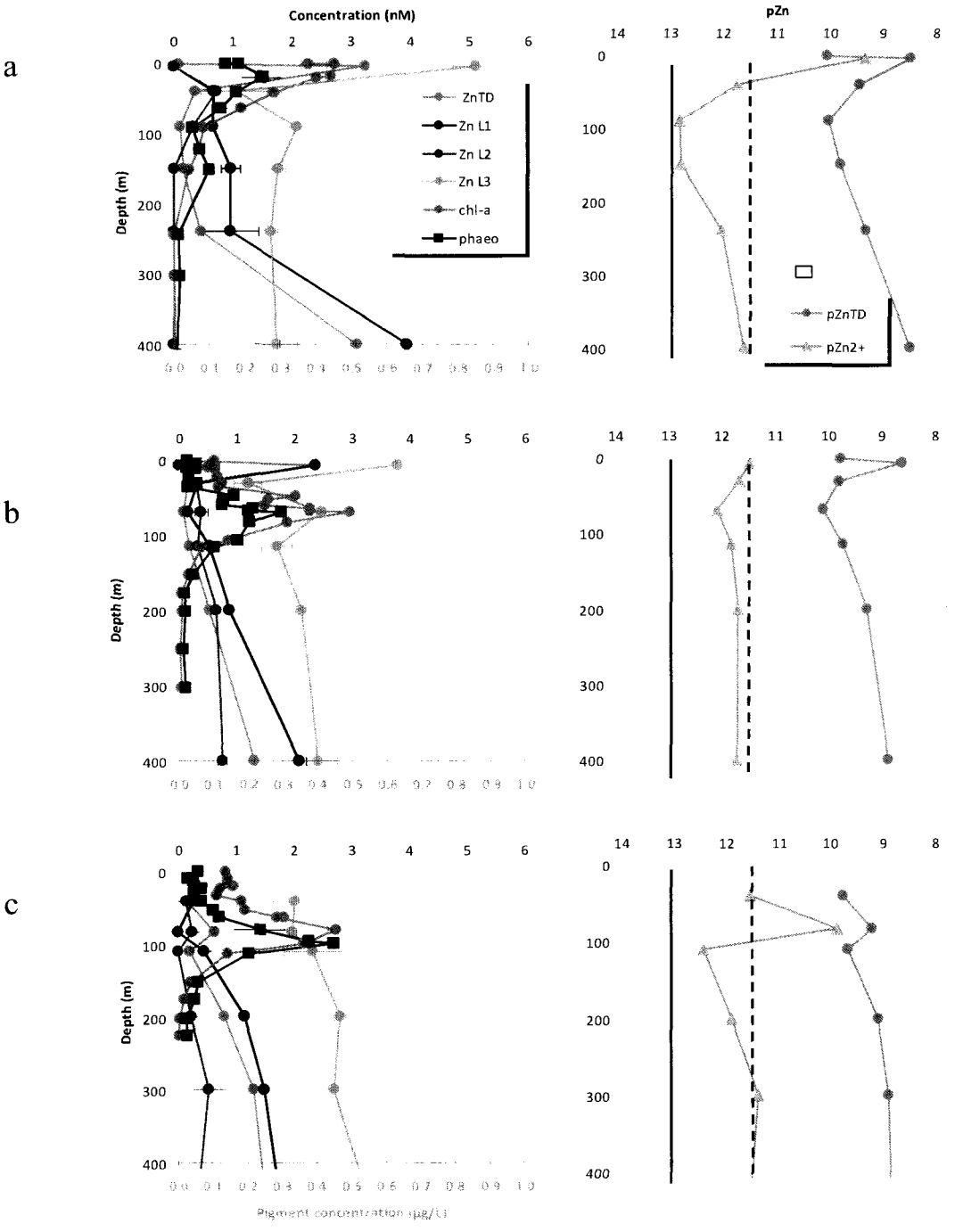

Fig. 23. Upper 400m profiles for the concentration of Zn_{TD} and its complexing ligands, chlorophyll-*a* and phaeophytin and pZn_{TD} and pZn^{2+} for all stations: a) Amazon 1, b) Amazon 2, c) 6, d) Romanche, e) 8 and f) 10. The solid and dashed red lines indicate potentially limiting Zn^{2+} concentrations for oceanic and neritic species. The blue bars above the legend boxes indicate the extent of inorganic Zn complexation.

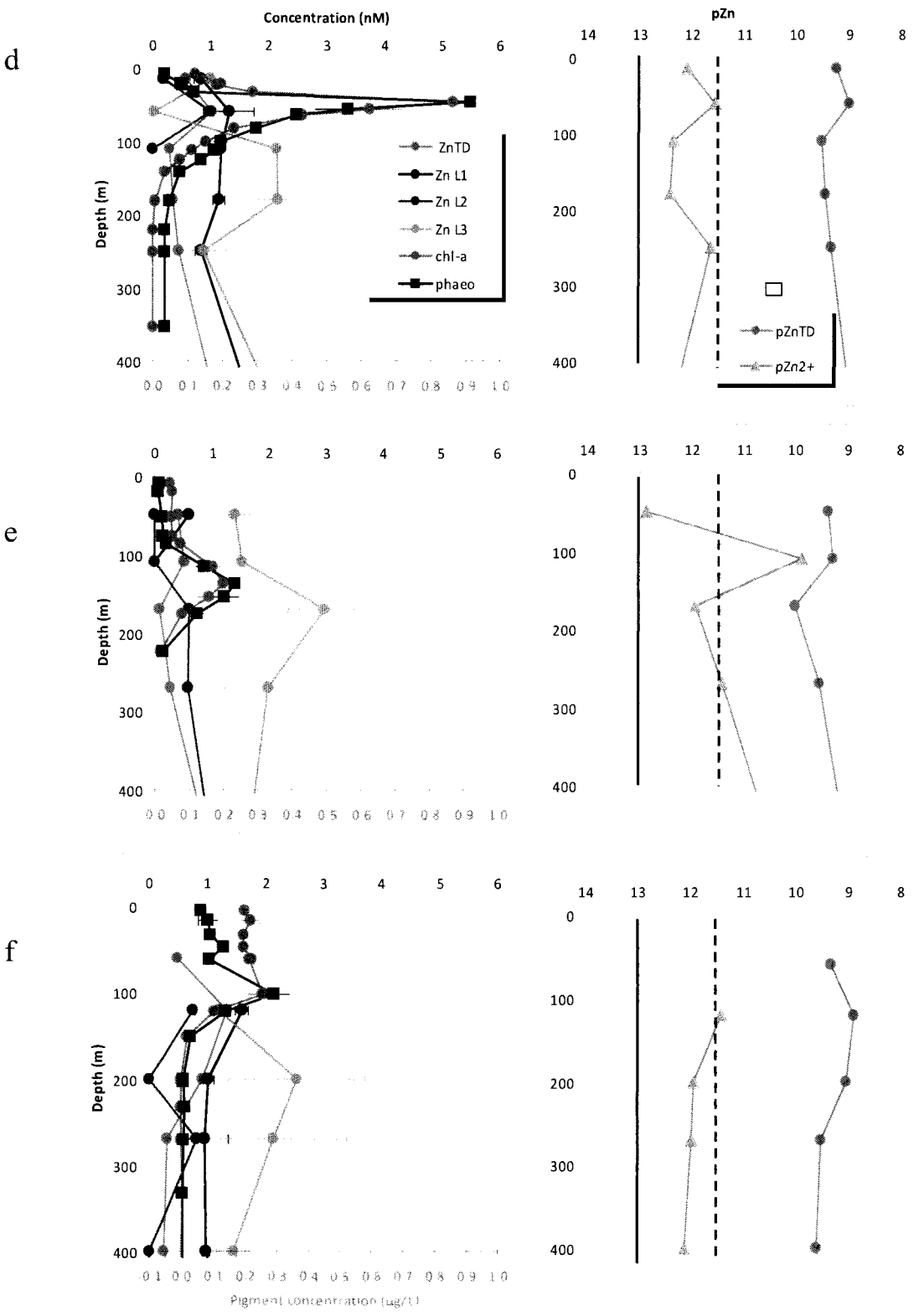

Fig. 23. Continued.

Because of the surface Cd depletion, the general trend is to find Cd^{2+} in ranges lower than Cd^{2+} in surface waters, and increasing concentrations with depth, as Fig. 24 suggests. The dominance of inorganic complexation maintains the Cd^{2+} below the toxic levels at all times; however, the bioavailability of Cd' means that potentially toxic concentrations exist in deep waters and could be upwelled. More about this is discussed in the Speciation section of the Discussion chapter.

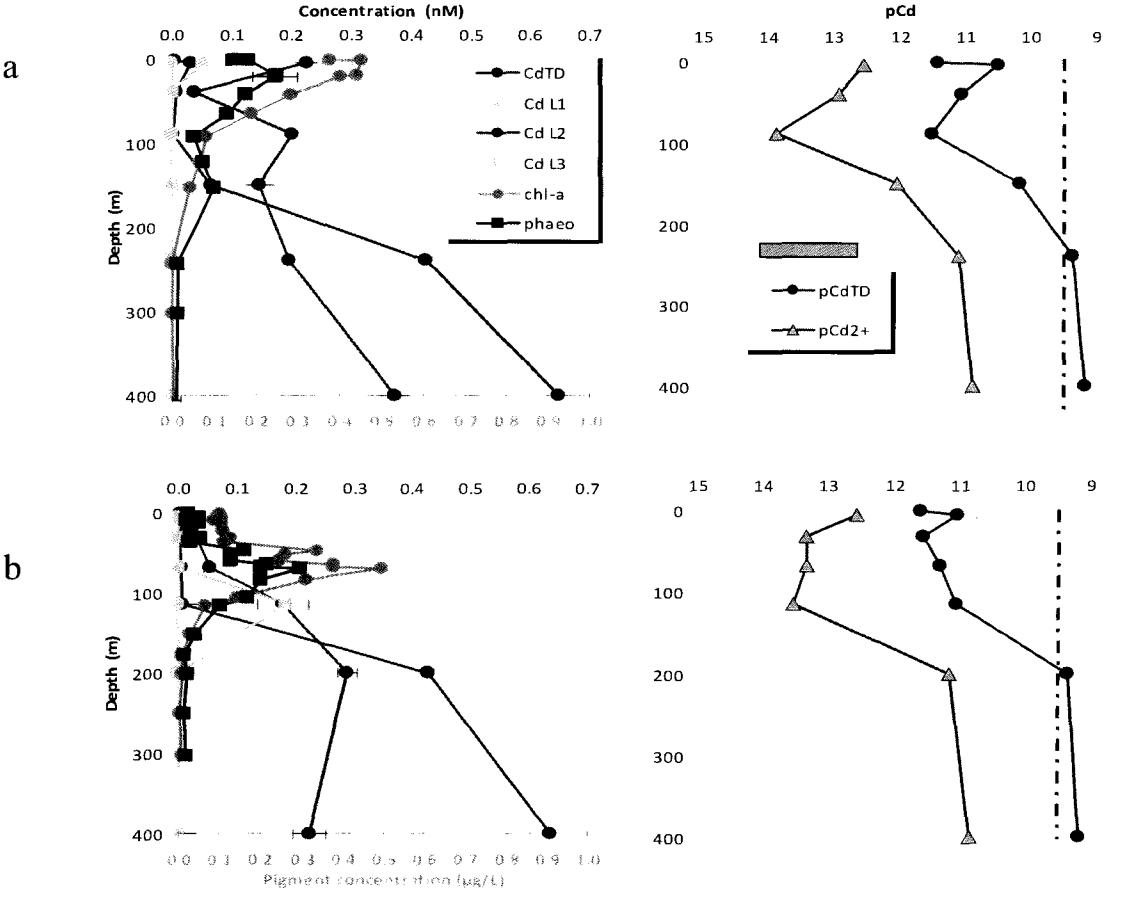

Fig. 24. Upper 400m profiles for the concentration of total dissolved Cd and its complexing ligands, chlorophyll-*a* and phaeophytin and pCd_{TD} and pCd^{2+} for all stations: a) Amazon 1, b) Amazon 2, c) 6, d) Romanche, e) 8 and f) 10. The dot-dash red line indicates potentially toxic Cd^{2+} concentrations for all species. The pink bars above the legend boxes indicate the extent of inorganic complexation.

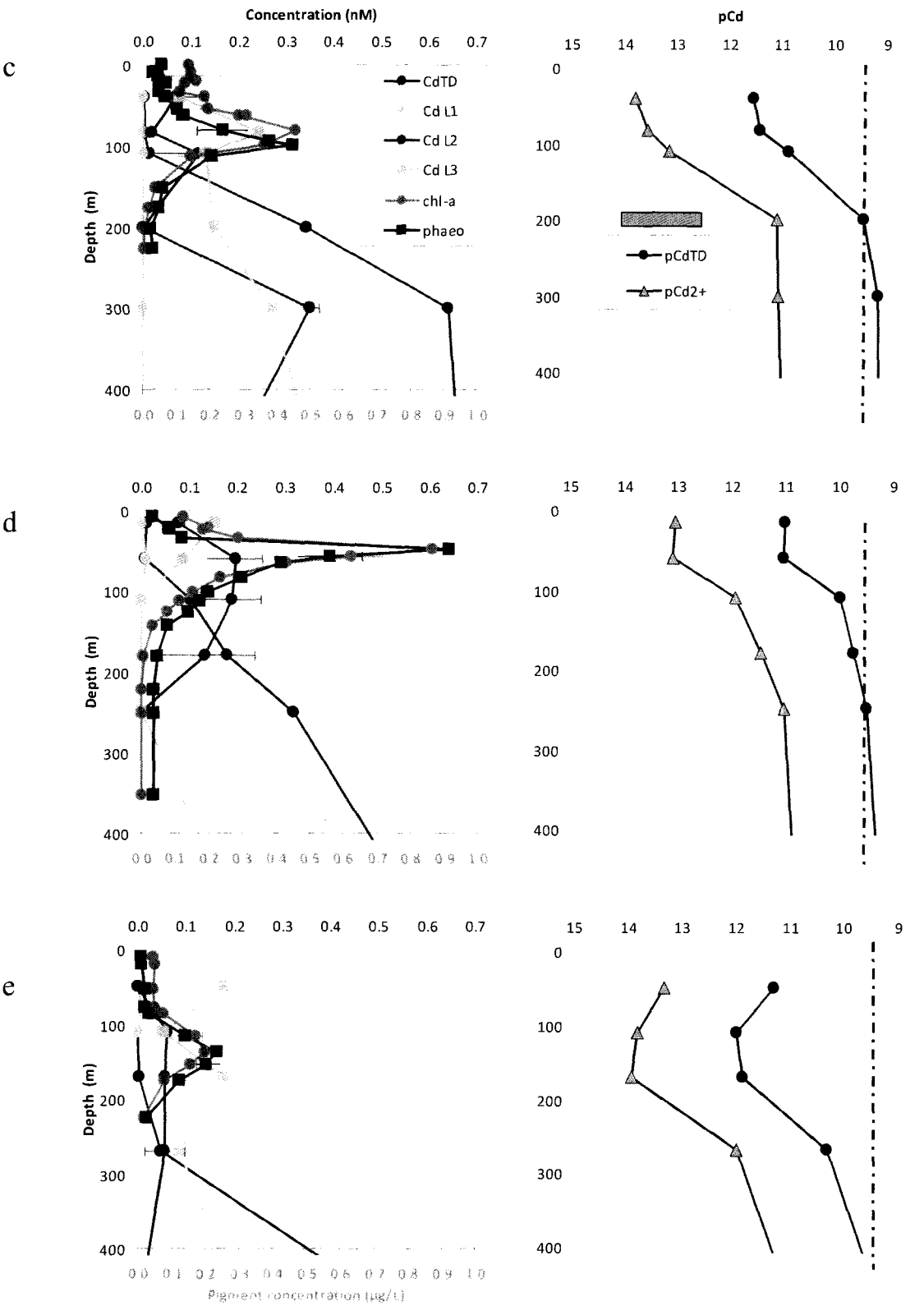

Fig. 24. Continued.

CHAPTER 5

DISCUSSION

5.1. OVERVIEW

Zn_{TD}, Cd_{TD}, silicate, phosphate, Zn/silicate, Cd/phosphate, L, logK, photosynthetic pigments and free metal concentration results shown in the previous chapter are discussed, focusing on relevant processes observed or inferred from those data. A relationship between Zn_{TD}, Cd_{TD}, L, Zn^{2+} and Cd^{2+} and either: a) water mass characteristics, or b) photosynthetic pigments (chlorophyll-*a* and phaeophytin) are explored, aiming at elucidating the biogeochemical processes involved in the formation of Zn- and Cd- complexing ligand(s). Later, the immediate biogeochemical consequence of the presence of ligands, the chemical speciation of Zn and Cd, is evaluated.

The sections to follow in this chapter are:

- analytical figures of merit,
- the Amazon River influence on surface waters,
- water masses and riverine influence on intermediate and deep water masses,
- Amazon River/Equatorial area factor (AEF) influence on intermediate waters,
- Congo River shelf matter factor (CSMF) influence on deep waters,
- the low oxygen depth at Stations Romanche and Amazon,
- Zn_{TD}, Cd_{TD} / nutrients ratios,
- ligands: sources and processes,
- chemical speciation and bioavailability.

First, the influence of the Amazon River on surface waters is discussed with the nutrients, metals and ligands data obtained at the two stations influenced more directly by it. I have performed a thorough analysis of Station Amazon 1 data to predict trends expected at downstream Station Amazon 2. By comparing stations with nutrient, metals

and biological information from the published literature, I discuss the biogeochemical processes occurring at the mouth of the Amazon River, the greatest source of silicate and organic matter to the Atlantic Ocean.

The mixed layers of all stations were sampled at least once, and almost all of the water masses were sampled at all stations, from mixed layer depth down to the bottom. I do not report data for some samples because of either sampling or analytical problems.

Knowing the physical oceanographic characteristics of each station's water column, I identified water masses well-characterized by other researchers. I then plotted the data reported in the Results chapter against latitude along the N-S axis for each water mass (as in Fig. 16b). This enables me to use the latitude axis as a proxy for water mass age, as both northward- and southward-moving water masses border the South American continent. Stations 6, 8 and 10 were not located on the same longitude, but rather near the western boundary of the Equatorial and South Atlantic (Fig. 16d). Thus, these three stations are located along the path of water mass transport. In contrast, Station Romanche is located ~ 10° further east from the water mass path (Fig. 16d), and would be expected to have data trends that diverge to some extent from that shown by the other three stations. These plots and some extrapolations to water mass formation locations are discussed in the Water Mass section.

When nutrient, metal and ligand data were associated with specific water masses, trends were discerned that showed the influences of both Amazon River/Equatorial area factor (AEF) and the Congo River shelf matter factor (CSMF) on intermediate and deep water masses.

All stations showed Zn_{TD} and Cd_{TD} depth profiles as having nutrient-type behavior, characterized by surface water depletion, Zn_{TD} values increasing to a maximum at the maximum silicate dissolution depth, or Cd_{TD} values increasing to a maximum at the maximum phosphate regeneration depth, overlaid by the different water masses present at each station (Fig. 17). These features are oceanographically consistent with previously

reported trends (see Bruland and Lohan, 2004 for a list of references). The Zn_{TD} profiles mimic those of silicate, and the Cd_{TD} profiles mimic phosphate's (Fig. 17). I observed a general trend of high Zn/silicate and low Cd/phosphate in surface waters, and relatively comparable concentrations below ~ 500m, with average Zn/silicate and Cd/phosphate values around 0.08 and 0.24 nM/μM, respectively.

Nearly all samples show the presence of multiple ligands for each metal in surface waters and at all depths (Figs. 20 and 21), as recently reported for Zn and Cd (Baars and Croot, 2010; Carrasco et al., 2008). Specifically, I detected three ligands for each Zn and Cd, with similar complexing strengths to those reported in the literature (Table 8). The stability constants of these ligands are relatively consistent throughout the water column, yet differences larger than 1-log-unit are found in deeper water masses at some stations (Table 8, Fig. 20). In general, the concentrations of both the strongest (L1) and the weakest (L3) of the Zn-binding ligands are mostly equal to or greater than the Zn_{TD} concentrations, in contrast to the concentration of the intermediate strength ligand (L2), present mostly in the upper 800m. AABW waters have high silicate, Zn_{TD} and Zn-binding ligand concentrations (Fig. 21), probably from the water mass formation site. Cd_{TD} exceeds the concentrations of all three of its ligands. While I detected Cd L3 at all depths at all stations, Cd L1 is present only in surface samples of two stations (Fig. 21), and Cd L2 is present in the surface waters of all stations but in the deep waters of only one station. Focusing on the upper 400m (Figs. 23 and 24), some relationships can be drawn between the presence of certain ligands and the relative depth (i.e. surface waters, at or below chlorophyll-*a* maximum).

The presence of the multiple organic ligands reduces the concentrations of the Zn^{2+} and Cd^{2+} to the values shown in Figs. 22 (whole water column) and 23 - 24 (upper 400m). The Zn^{2+} depth profiles are more variable compared to those of Cd^{2+} because of the water-mass-dependent presence of high concentrations of strong ligands, presumably coming from the water mass sources. The Cd^{2+} depth profiles are smoother and less water-mass-influenced than those of Zn^{2+} because of the presence of lower concentrations of weaker ligands and the higher inorganic side reaction coefficient. Figs. 23 and 24

explore the relationship between pigments and ligand concentrations, and their effect on the chemical speciation of Zn and Cd.

The following features appear in the water columns of all stations. In the surface waters, low Zn_{TD} and Cd_{TD} concentrations, high Zn/silicate and low Cd/phosphate, stronger Zn- and Cd-ligands present generally in excess of the Zn_{TD} and Cd_{TD}, and a poor relationship between ligands and photosynthetic pigments. In the subsurface waters, higher Zn_{TD} and Zn/silicate, located at the depth of pigment maximum at the oceanic Stations (80-95m, 57m, 138m, upper 102m, for Stations 6, Romanche, 8 and 10). A subsurface local Zn_{TD} maximum is present, possibly due to particle regeneration (Fig. 23). Strong and weak Zn and Cd ligands are present in excess of the Zn_{TD} and Cd_{TD}, and some of the Zn and Cd ligands are strong correlated with photosynthetic pigments in these waters. In the intermediate and deep waters, Zn ligands are present in excess of Zn_{TD}, but Cd ligands rarely exceed Cd_{TD}. Below 500m, both Zn/silicate and Cd/phosphate stay within a certain range, depending on the age of the water mass.

5.2. FIGURES OF MERIT

The Zn_{TD} and Cd_{TD} concentrations I report and use in this dissertation were determined by Donat research group technician, Cynthia Wickstrom, and postdoctoral research associate, Dr. Rodney T. Powell. Blank concentrations for both Zn_{TD} and Cd_{TD} were in the sub-nanomolar range. Average Zn_{TD} blanks were higher than the Cd_{TD} blanks (0.14 and 0.002 nM, respectively; Table 7). However, the Zn_{TD} blanks were more reproducible than the Cd_{TD} blanks (RSD: ± 7 and ± 22 %, respectively). The 3-sigma LODs (0.03 nM Zn and 0.001 nM Cd) were low enough to allow determination of Zn_{TD} and Cd_{TD} in this region of the Atlantic Ocean.

Solvent extraction recoveries for both Zn_{TD} and Cd_{TD} were very good (97 % and 105 %, respectively), yet somewhat variable (RSD ± 6 % for both metals); thus, they were checked for every batch of samples processed. Very good agreement was found between experimental and certified Zn_{TD} and Cd_{TD} values for SLEW-2 and SLRS-3.

5.3. SURFACE WATERS : AMAZON RIVER INFLUENCE

The IOC 1996 cruise provided a unique opportunity to study the influence of the Amazon River on coastal waters of the Atlantic Ocean near its mouth. Though direct sampling near the river mouth was not possible (due to Brazilian government restrictions), the samples obtained reflect off-shore river plume characteristics (Cutter and Measures, 1999), noticeable as a low salinity, high silicate and Zn layer in both the Amazon 1 and Amazon 2 Stations (Fig. 17 and, more detailed, Table 9). Using the criterion presented by Shipe et al. (2006) - salinity less than 35.5 and silicate higher than 1.5 μM - to classify surface waters of this region as either Amazon River plumewater or oceanic water, the surface waters of both Amazon stations were definitely plumewater. Pertinent nutrient data from the region indicate that the silicate and phosphate concentrations coming from the Amazon River are high enough (~ 144 and 1.4 μM, respectively) so that on the outer shelf neither nutrient limits primary production as much as nitrogen or surface water residence time, especially since less than 4 % of silicate and phosphate are buried in the seabed (DeMaster and Pope, 1996). Trace metal data for the Amazon River show that Zn_{TD} and Cd_{TD} are also elevated (3.8 and less than 0.1 nM, respectively; Shiller and Boyle, 1985; Boyle et al., 1982). Here I report the first measurements of Zn and Cd ligand concentrations and chemical speciation for this region, combined with nutrient and Zn_{TD} and Cd_{TD} data.

Stations Amazon 1 and 2, clearly different from the other stations, showed riverine water features (salinity between 20 and 35.2) in the upper few meters of the water column with high silicate, Zn and Cd concentrations (up to 46 μM, 3.24 nM and 0.032 nM, respectively), yet phosphate concentrations were not elevated (below 0.083 μM; Table 9). Silicate is known to be a terrigenous source indicator, and the surface values are so high that upwelling can not account for them. These results agree with Rutgers van der Loeff and Kattner (1997), who report elevated Cd, Al and silicate (~ 0.040 nM, 80 nM and 2.3 μM) along with relatively low salinity in this same latitude, but ~ 20° further east, presumably of Amazon River origin.

Of all the stations sampled on the IOC 1996 cruise, Station Amazon 1 had the highest surface Zn_{TD} and Cd_{TD} concentrations. This is not surprising because Amazon 1 is the station closest to the Amazon River mouth, located ~ 600 km downstream from the mouth of the Amazon River. What is surprising are the low concentrations of Zn_{TD}, Cd_{TD} and phosphate at 1m depth where the water is the most riverine (Table 9). This may be due to biological uptake in the upper 30m of this station or particle scavenging. The surface chlorophyll-*a* levels are the highest of all stations, in contrast to all other stations which show typical subsurface-maximums, and corroborate this hypothesis. Close to 46 μM dissolved silicate are present, implying the riverine origin of these waters. Not much can be discussed about the Cd or phosphate values, because they are close to their LODs. A more complete picture would have been obtained if suspended particulate matter had been studied. Assuming a roughly 3:7 dilution factor at this point (obtained using the salinities of river water, seawater and this 1m-depth sample, 0, 35 and, 20, respectively, and the "pure" river concentrations of Shiller and Boyle, 1985; Boyle et al., 1982), and assuming that processes other than river water and seawater mixing are minor (DeMaster and Aller, 2001), particulate concentrations of some elements can be calculated by subtracting the dissolved from the total unfiltered concentrations. So, I would predict that 1.54 nM Zn (1.63 - 0.09 nM), 16 μM silicate (62 - 46 μM), 0.036 nM Cd (0.040 - 0.004 nM) and 0.6 μM phosphate should be present in the particulate form at this depth.

Just four meters below, at 5m depth, extremely high Zn_{TD} (3.24 nM) and very high Cd_{TD} (0.032 nM) are present along with high silicate and phosphate (3.06 and 0.083 μM), probably due to respiration of the heavy metal load that was brought by the river, presumably taken up in the 1m depth waters, as the high chlorophyll-*a* values imply. These Zn and Cd values are close to previously reported values in the Amazon River itself (Shiller and Boyle, 1985; Boyle et al., 1982; Table 9), during the same river discharge season. Zn, which tends to flocculate along with Fe at low salinities or to be taken up by phytoplankton, might be in the particulate form at 1m depth, and might desorb and/or dissolve from sinking particles, further downstream from suspended particles as the salinity increases (Windom et al., 1991). The 0.032 nM Cd concentration, the highest surface (shallower than 100m) value for all stations, is similar to literature

river data from other major rivers such as the Orinoco, Mekong, Mississippi, Huang He and Yang Tze (Eisma et al., 1978; Cenci and Martin, 2004; Trefry et al., 1986 and Elbaz-Poulichet et al., 1987), all of which have average Cd concentrations below 0.100 nM, and close to the world average of 0.090 nM estimated by Martin and Windom (1991). Apparently, the Cd provided by the Amazon River, and present in this station, is recycled at a very fast rate, as the high chlorophyll-*a* values indicate. For both Zn and Cd, rapid recycling is suspected to occur within the upper 5 m of this station. Though there is no direct measurement of bacterial respiration (this cruise was primarily intended to sample and analyze metal data), there is evidence that little of the high load of riverine organic carbon is exported as POC within the upper 5m (Charette et al., 1999).

Table 9

Dissolved Zn, Cd, silicate and phosphate and salinity in the upper 150m of Stations Amazon 1 (A1) and 2 (A2), compared with Amazon River values from a) Shiller and Boyle, 1985, b) DeMaster et al., 1996 and c) Boyle et al., 1982.

Station/ Depth (m)	Zn (nM)	silicate (μM)	Cd (nM)	phosphate (μM)	salinity
Amazon River (references)	3.8 a	144 b	< 0.1 c	1.4 b	0
A1/1m	0.09	46.09	0.004	0.002	20.069
A1/5m	3.24	3.06	0.032	0.083	35.210
A1/40m	0.35	1.41	0.009	0.139	36.297
A1/90m	0.09	1.04	0.003	0.132	36.362
A1/150m	0.15	3.26	0.066	0.607	36.389
A2/1m	0.17	2.57	0.003	0.064	35.180
A2/7m	2.38	3.82	0.009	0.016	34.693
A2/32m	0.16	1.5	0.003	0.034	35.688
A2/69m	0.08	1.33	0.005	0.061	36.194
A2/115m	0.19	1.69	0.009	0.139	36.808

Table 10

Zn_{TD}, Zn-binding ligands and Zn^{2+} concentrations in the upper 150m of Stations Amazon 1 (A1) and Amazon 2 (A2). N.A. = not available.

Station / Depth (m)	Zn_{TD} (nM)	L1 Zn (nM)	L2 Zn (nM)	L3 Zn (nM)	Zn^{2+} (nM)
A1/1m	0.09	N.A.	N.A.	N.A.	N.A.
A1/5m	3.24	0	0	5.09	0.469
A1/40m	0.35	0.69	0.71	1.06	0.00178
A1/90m	0.09	0.66	0.31	2.08	0.000145
A1/150m	0.15	0.97	0	1.76	0.000155
A2/1m	0.17	N.A.	N.A.	N.A.	N.A.
A2/7m	2.38	2.38	0	3.79	0.00326
A2/32m	0.16	0.33	0.31	1.20	0.00213
A2/69m	0.08	0.17	0.39	2.48	0.000803
A2/115m	0.19	0.53	0.33	1.70	0.00148

Table 11

Cd_{TD}, Cd-binding ligands and Cd^{2+} concentrations in the upper 150m of Stations Amazon 1 (A1) and Amazon 2 (A2). N.A. = not available.

Station / Depth (m)	Cd_{TD} (nM)	L2 Cd (nM)	L3 Cd (nM)	Cd^{2+} (nM)
A1/1m	0.004	N.A.	N.A.	N.A.
A1/5m	0.032	0.227	0.052	0.000276
A1/40m	0.009	0.038	0	0.000115
A1/90m	0.003	0.201	0	0.000013
A1/150m	0.066	0.147	0	0.000864
A2/1m	0.003	N.A.	N.A.	N.A.
A2/7m	0.009	0	0	0.000259
A2/32m	0.003	0.031	0	0.000044
A2/69m	0.005	0.054	0	0.000046
A2/115m	0.009	0.179	0.185	0.000027

One would expect to see high amounts of POC exported in high nutrient and metal environments with high productivity, unless the recycling rate and efficiency are high. Zn_{TD}, Cd_{TD} and phosphate concentrations increase from 1m to 5m, presumably due to the respiration of particulate matter. Given the high Zn_{TD} concentration and the possible use of Cd for enzymes like CA by the prevailing diatoms (Morel et al., 2003), both Zn and Cd may be used for enzymatic requirements. Despite the relatively high Cd_{TD} concentration at this depth, it is still easier for diatoms to use the 100-times more concentrated Zn.

The 1m depth samples at the two Amazon stations could not be analyzed for chemical speciation, but samples were analyzed from below that depth from Stations Amazon 1 and 2. In Amazon 1 at 1m, the direct river load very likely brings high concentrations of both Zn and Cd (most presumably in the particulate form), so that phytoplankton species living in the upper few meters should be adapted to them. At 5m depth, very high concentrations of both Zn L3 and Cd L2 coincide with high concentrations of Zn_{TD} and Cd_{TD}. Despite the high concentrations of Zn L3 and CdL2, concentrations of Zn^{2+} and Cd^{2+} are extremely high. Water samples below 5m down to 90m show elevated nutrient, Zn_{TD}, Cd_{TD} and chlorophyll-*a* concentrations which decrease with depth (Figs. 17 and 23, Table 9). By 40m, the added complexing capacity of Zn L1, Zn L2 and Cd L3 lower Zn^{2+} and Cd^{2+} to less than 1/250 (below the neritic species limiting Zn concentration threshold) and 1/2 of those at 5m (Tables 10 and 11, Figs. 23 and 24). By 90m, the three Zn-ligands' complexing capacity brings Zn^{2+} to levels that are more than an order of magnitude below the concentrations that are limiting to coastal phytoplankton species, close to concentrations that limit oceanic phytoplankton growth, more than three orders of magnitude lower than at 5m depth (Fig. 23); Cd^{2+} diminishes only slightly more than one order of magnitude in the same depth range (Fig. 24). Below 90m, nutrient, Zn_{TD} and Cd_{TD} concentrations increase. The same M_{TD} - M^{n+} gap is observed from 90m down to the deepest sample analyzed in the two Amazon Stations (400m), ~ 3 and ~ 2 log units for Zn and Cd (Figs. 23 and 24). This M_{TD} - M^{n+} gap here at Amazon 1 is one of the widest of all stations for Zn, in contrast to Cd, for which it is close to the average (Fig. 22), suggesting very high Zn complexing capacity. More about this gap is discussed in the Speciation section.

The distance downstream from Station Amazon 1 to Amazon 2 is merely ~ 120 km, which surface waters travel in ~ 3 - 7 days at the North Brazil Current's (NBC) well-constrained velocity (Bourles et al., 1999; Fig. 16a). So, the chemical composition of Amazon 1 surface waters might represent that of Amazon 2 surface waters only a few days before. This opens up an interesting possibility: exploring a water parcel's chemical speciation in the recent past.

Despite their geographical proximity, Amazon 1 and 2 have sometimes very different oceanographic features. One reason is that freshwater carried by the NBC frequently forms rings or eddies (Goni and Johns, 2001), which could cause heterogeneity at either Amazon Station. However, Goni and Johns (2001) reported that the eddy present closest in time to our sampling dates should have moved further northwest pulled by the NBC to the Guiana Current (GC; Fig. 16a). Another reason for this difference is that Stations Amazon 1 and 2 could be on either side of the front separating the NBC retroflection and the North Equatorial Counter Current (NECC; Ffield, 2005). The NBC eastward retroflection has been reported to occur between July and December each year (Ffield, 2005; Muller-Karger et al., 1988), and these samples were obtained in mid-June, just a short time before the retroflection began. In fact, Cutter and Measures (1999) invoked the possibility that the retroflection already occurred by the time sampling started for the IOC 1996. Thus, the two main heterogeneity-inducing factors may not be directly affecting these two stations, leaving the possibility that Amazon 1 may be influenced by the Amazon River more directly than Amazon 2. This agrees with Shipe et al. (2006), who reported very variable plume and ocean waters in this area, where usually plumewaters mean low salinity and high silicate and oceanic waters mean high salinity and low silicate, with several exceptions (low salinity and low silicate).

Station Amazon 2 is, indeed, different from Amazon 1, for it does not have the low-salinity, high-silicate-and-chlorophyll-*a* surface "wedge" of riverine water over "normal" oceanic water. In fact, the depth profiles of several parameters (Figs. 23 and 24) indicate that Amazon 2 is more similar to Station 6 than it is to Amazon 1, while surface waters at this station Amazon 2 are similar to Amazon 1, but diluted because of

the additional distance from the source and the physical phenomena that might affect the former more so than the latter.

At 1m depth there is a layer of low Zn_{TD} and Cd_{TD}, high silicate and phosphate (2.57 and 0.064 μM) and high salinity (~ 35.2). The high silicate and relatively high phosphate (Fig. 17) suggest riverine unfluence, yet the oceanic salinity would mean that the nutrients brought from the Amazon River this far downstream are diluted. One would think there would be high primary productivity or biomass and possibly high concentrations of particulate nutrients and metals; but the very low chlorophyll-*a* in the surface 1-m sample (and down to ~ 30m, averaging ~ 0.1 mg/L) indicates that biological activity is low in the upper 30m and high in the deeper ~ 30 to 100m range, where chlorophyll-*a* peaks (Figs. 23 and 24).

There is a subsurface layer of high Zn and silicate and low Cd and phosphate at 7m depth, which contrasts with those at 1m depth. Here, salinity is a bit lower (~ 34.69) and the Zn_{TD} and silicate concentrations increase to 2.38 nM and 3.82 μM, respectively, within ~ 30 % of what they are in Amazon 1 at 5m (3.24 nM and 3.06 μM; Fig. 17). Interestingly Zn/silicate ratios are 40 % lower here, implying a preferential Zn uptake or a preferential silicate recycling or both. Cd is low and stays low until ~ 150m, well below the pigment maximum depth (~ 69m). This might indicate a preferential Cd uptake with respect to Zn, or maybe regeneration of dissolved Zn, as Cd is taken up or removed as these waters are brought from Amazon 1 to Amazon 2.

Much like Amazon 1, Zn_{TD} and silicate concentrations below 7m in Amazon 2 are above "typical" surface concentrations. The additional Zn_{TD} and silicate (more than one order of magnitude and twice more at 7m than at the next depth analyzed, 32m) decrease down to 69m depth. Below 69m, both Zn_{TD} and silicate concentrations increase with depth (Fig. 17). The Cd_{TD} and phosphate concentrations increase from 1m to 7m is not as large as that over the same depth interval at Amazon 1. Cd_{TD} does not increase until below ~ 115m, while phosphate starts to increase only moderately below ~ 32m, but only increases significantly below ~ 115m, too. Although there are no particulate data for this

station, I predict high POC export here, knowing that at Station Amazon 1 and under high silicate concentrations, diatoms produce high export (Charette et al., 1999).

The depths of Amazon 2's mixed layer (~ 60m) and chlorophyll-*a* maximum (~ 70m) are drastically different from those at Amazon 1 (~ 10m and at ~ 1m, respectively), but they are similar to the depths of these features at oligotrophic stations. Consequently, nutrient and metal recycling at both stations might be expected to influence their vertical profiles; yet, they are not too different (Fig. 17). Figs. 23 and 24, Tables 10 and 11 provide evidence for suggesting the difference between these two stations as Zn and Cd sources to the Atlantic Ocean. While Amazon 1 has very high surface Zn_{TD} concentrations that may be complexed by organic ligands (bringing the Zn^{2+} concentration close to a limiting threshold concentration between 90 and 150m), Amazon 2's surface inputs show a very similar Zn_{TD} profile, but a more uniform Zn^{2+} profile than that at Amazon 1, probably because of the deeper phytoplankton community (shown by the ~ 70m chlorophyll-*a* maximum). Phytoplankton at 7m in Amazon 2 are in contact with complexing ligands (maybe brought by the river) and with coastal-species-limiting concentrations of Zn^{2+}, more than two orders of magnitude lower than those on Amazon 1. This could explain the pigments' profiles. Similar excess Zn L3 concentrations occur at the surface of both stations, possibly brought by the river. As in Amazon 1, these ligand concentrations are present at the chlorophyll-*a* maximum but not at Amazon 2; Zn L3 and Zn L2 show maximums coincident with that of chlorophyll-*a*. The presence of Zn L1 in large excess over Zn_{TD} at Amazon 1 between 40 and 240m, compared with its slight excess in Amazon 2, accounts for the bulk of this difference, and thus, explains the wider gap between Zn_{TD} and Zn^{2+} mentioned above. As a result, Zn^{2+} is frequently below the limiting threshold for coastal species at Amazon 2, and below that threshold and close to the limiting threshold for oceanic species between 40 and 250m at Amazon 1, one and a half orders of magnitude lower (Fig. 23 and Table 10).

Amazon 1 surface waters above 90m appear to be a more important source of Cd_{TD} and Cd^{2+} than Amazon 2 (Fig. 24). While Amazon 1 brings more Cd_{TD} than Amazon 2, the portion that is complexed by Cd L2 and Cd L3 present in the upper 90m is

large, and both Cd_{TD} and Cd^{2+} decrease gradually from the surface to 90m. In contrast, in the upper 69m waters at Amazon 2, Cd_{TD} is as low as the oceanic stations 6, Romanche, 8 and 10 with a small, one-point high concentration at 7m and increasing concentrations below. Thus, Cd is only complexed with L2 in the upper 69m; L3 appears only at 115m, below the chlorophyll-*a* maximum, causing the Cd_{TD} - Cd^{2+} gap at this depth to reach the highest value of all stations (~ 2.5 log units), followed by Amazon 1 at 90m (~ 2.4; Fig. 24 and Table 11).

5.3.1. Ligands' profiles

Comparing the ligands' profiles (Figs. 23 and 24, Tables 10 and 11), Zn ligand concentrations exceed Zn_{TD} in all the 400m profile at both Stations Amazon 1 and 2; in contrast, the Cd ligand concentrations exceed Cd_{TD} only in the upper 150m. Thus, at the subsurface depths at Amazon 1, both Zn^{2+} and Cd^{2+} concentrations may be co-limiting (Zn limiting values are established and Cd's are not), possibly limiting neritic species' growth. At Amazon 2, Cd^{2+} may limit some phytoplankton species. Despite these Cd^{2+} values being low, they are located at the chlorophyll-*a* maximum depth, similarly to oceanic stations 6 and 8. This implies that, despite Cd's suggested nutrient role (Lane et al., 2005), some phytoplankton species may grow and reproduce more in the lowest concentration of Cd. This argument hints to potential chlorophyll-*a* maximum occurring at the lowest pCd^{2+} depths because of lower Cd toxicity.

Despite the lack of chemical speciation data from Amazon River water, (i.e. the 1m depth samples or closer to the mouth of the river) the samples below the riverine waters in both Amazon stations show very large concentrations of a weak Zn ligand in excess of the Zn_{TD} concentration, and strong and weak Cd ligands also in excess of Cd_{TD}. These ligands may be brought to the surface waters by the Amazon River itself or could be produced by phytoplankton living in surface waters of these stations. The latter is supported by Station Amazon 1's unique high-at-surface chlorophyll-*a* profile that correlates with the presence of Zn L3. Station Amazon 2 shows high concentrations of Zn L1 and Zn L3 in the surface that do not correlate with either photosynthetic pigment but reach a maximum at 7m, suggesting riverine sources of ligands. Two Cd ligands are

present at 5m at Amazon 1, but curiously none are present in surface waters at Amazon 2. This may indicate that riverine Zn ligands are more refractory than those for Cd.

The stability constant data of surface-water ligands show relatively weak complexes (station average logK's: Zn L3 9.1, Cd L2 10.0 and Cd L3 9.1), with the exception of Zn L1 (logK' 11.6). The stability constants I measured are similar to those of other Zn- and Cd-binding ligands from oceanic, coastal and estuarine environments (Table 8). However, they differ from those reported recently for rivers (logK' ~ 13; Hoffman et al., 2007) and from classic values reported for humic-substance (logK' ~ 7; Morel, 1983). The average logK' for Zn L1 for both Amazon stations is 11.6. Ligands found as far south as Station 10 (33° S) and as far east as Station Romanche (20° E) in this study, and in the West North Pacific (logK' ~ 11.4; Carrasco et al., 2008) are of similar strength. This suggests that Zn L1 may be produced *in-situ* throughout the South Atlantic and maybe the North Pacific. The most riverine station, Amazon 1, does not show the presence of this ligand in surface waters, supporting the hypothesis of a non-riverine origin for this ligand. Bruland (1989) reported a slightly weaker (logK' ~ 10.6) ligand in North Pacific surface waters distributed homogeneously in the upper 600m.

Another ligand found in oceanic environments is Cd L2, reported in the South Pacific (Ellwood, 2004), with a logK' value ~ 10.2, very close to this study's results (~ 10.0). This ligand may be produced *in-situ* in Stations Amazon 1 and 2; or maybe the ligands brought by the river waters have very similar binding characteristics to the ligands produced in surface waters of the South Pacific.

The Zn and Cd ligands reported by Bruland (1989) and Ellwood (2004) are in large excess of the low Zn_{TD} and Cd_{TD} concentrations, and might be cases of "acquisition ligand", that is, a ligand produced reputedly by phytoplankton to help in the assimilation process of a scarce yet essential metal (as opposed to a "detox" ligand, a ligand produced reputedly by phytoplankton to reduce the large bioavailable concentration of a metal of potential toxicity). For example, in Ellwood (2004) report in the Southern Ocean, total dissolved Zn, Cd and Co were present at picomolar concentrations and a primary

productivity limitation based on inhibition of the CA system would be plausible unless a mechanism of acquisition allows phytoplankton to take up the very little Zn, Cd or Co present. In contrast, at the Amazon stations, both Zn_{TD} and Cd_{TD} are very high (5 to 10 times higher than those that are being compared against), and the production of Zn L1 and Cd L2 found in surface waters, though in excess of both metals, would not likely be part of an "acquisition" strategy as phytoplankton might not be struggling to get Zn or Cd. The environments being compared here (the North Pacific, the South Pacific and the Amazon River plume) are so different that the phytoplankton living in them could be expected to be also very different (Piontkovski et al., 2003). Thus, the reasons for phytoplankton to produce ligands for each metal could be very different, too. Also, the distribution of these ligands is rather homogeneous in the limited depth profiles available for the Pacific and Southern Ocean, as opposed to the variability observed in the Amazon stations' profiles. Also, the ligands brought by the river waters may have similar binding characteristics to the ligands produced in other surface waters of the North and South Pacific as a simple coincidence.

The Zn L3 and Cd L3 determined in this study have stability constants (logK' 9.1 and 9.1, respectively) similar to those reported in the Narragansett Bay, an estuary with riverine, continental and anthropogenic influences (logK' 8.9 and 9.0; Kozelka and Bruland, 1998). There, relatively weak Zn and Cd ligands were found throughout the higher end of the salinity gradient (salinity ~ 25 to 30) along with very high Zn_{TD}, Cd_{TD} and nutrient concentrations. The similarity in the environmental conditions of the Amazon stations and the Narragansett Bay (salinity, nutrient, Zn and Cd concentrations) may suggest similar ligand production conditions. In both environments, the concentrations of ligands are around that of Zn_{TD} and about 10 times greater than that of Cd_{TD}. However, the Zn_{TD} and Cd_{TD} concentrations are around 10 times higher in the Bay, and the "detox" ligand production mechanism is more logical for phytoplankton coping with high metal concentrations.

The hypothesis that Cd ligands present in waters with elevated Cd concentrations are "detox" ligands is strengthened by the presence of an excess of a strong Cu-

complexing ligand (logK' ~ 10.2) in waters having Cu_{TD} concentrations ~ 2 nM in Station Amazon 1 at 5m depth (Consolvo, 2000). This Cu-ligand is comparable to the strongest Cu ligand found by Kozelka and Bruland (1998) in Narragansett Bay, yet not as strong as the ligand produced by Cu-stressed phytoplankton species *Synechococcus* and *Emiliana huxleyii* (logK' ~ 11 - 13; Moffet and Brand, 1996; Leal et al., 1999), whose wide distribution (Coale and Bruland, 1988; Dryden et al., 2007; Moffett and Dupont, 2007) makes it a typical case of a detox phytoplankton-produced ligand.

The horizontal salinity gradient present in Amazon stations (salinity 20 to 35) and in the Narragansett Bay Stations (salinity 25 to 30) showed similar trends of Zn ligands concentrations: the ligand concentrations decrease moderately as Zn_{TD} and riverine influence decreases and salinity increases. A similar comparison for the Cd ligands show contrasting trends: in the Amazon stations the ligand is present in upper-50m of the low salinity station and is absent at the high-salinity end, while in the Narragansett Bay, the Cd-ligand concentrations remains rather constant despite salinity changes. The similar Zn-ligands distributions suggest similar riverine sources, while the differences in the Cd-ligands might indicate different reactivities, and possibly different sources and processes.

Comparing the ligands detected in the Amazon stations with a group of ligands from environments whose metal and nutrient concentrations span over more than 3 orders of magnitude (Bruland, 1989; Ellwood, 2004; Kozelka and Bruland, 1998), the concentrations of Zn^{2+} and Cd^{2+}, complexed by these ligands, remarkably remain within a window that allows phytoplankton survival (pZn^{2+} ~ 10 - 12 and pCd^{2+} ~ 11 - 13). Regions near rivers, where high concentrations of both metals (pZn^{2+} ~ 9 and pCd^{2+} ~ 10) occur, suggest phytoplankton adaptation to the environment because of the presence of the metal complexing ligands.

Terrestrial humic substances, long reported to weakly complex to metals due to low stability constants (Morel, 1983), have recently been shown to be weak Zn and Cd ligands (logK' lower than 6 for both Zn and Cd; Abate and Masini, 2002; Garrigosa et al., 2008; Christensen and Christensen, 2000). Methodological and analytical constraints for

Cu ligands were re-evaluated by Kogut and Voelker (2001) and Voelker and Kogut (2001) after humic and fulvic standards (Suwanee River humic standards) were determined to contain a Cd ligand with logK' ~ 9 (Xue and Sigg, 1999), comparable with Cd L3 in this study (logK' ~ 9.0).

Is Cd L3 (or Zn L3 by extension) related to riverine organic matter that can be understood through knowledge of humic substances? The concentration of organic matter coming from the Amazon River is very large and some fraction of that DOC pool might be the ligands observed in this study at the most riverine Station Amazon 1. Some of the Amazon stations' depth profiles of Zn L3 and Cd L3 resemble each other, but the ligand concentrations are so different (the Zn L3 concentration is roughly ten times larger than that of Cd L3), that the hypothesis that they are the same substance should be discarded. What remains is another question: what is the real complexing capacity of the Amazon River's organic matter? Since high concentrations of Zn- and Cd-ligands occur in surface waters of Stations Amazon 1 and 2, are these ligands really riverine/terrestrial in origin? Or, are these ligands produced by phytoplankton living in waters influenced heavily by the riverine/terrestrial inputs brought in by the Amazon River? Based on this study's results, I can not make many definitive conclusions about these questions; the ligands present in surface waters in the Amazon Stations could be either allochthonous (riverine) or authocthonous (phytoplanktonic) in origin.

5.3.2. Regional and widespread potential influence

The source of nutrients and subsequent phytoplankton blooms in the NECC region is a matter of debate (Hu et al., 2004); some researchers suggest eddy upwelling and others, Amazon water dispersal. Despite the debate, the influence of these elevated Zn_{TD} and Cd_{TD} concentrations may reach as far as the surface waters travel. Depending on the season, this is to the Caribbean Sea via the NBC/GC, or to the Central Equatorial Atlantic via the NECC (Hu et al., 2004; Ffield, 2005; Muller-Karger et al., 1988; see Fig. 16a). The latter possibility makes the Rutgers van der Loeff and Kattner's (1997) speculation plausible - that the influence of the Amazon River water is evident in a high Cd, Al and silicate concentration surface station ~ 20° to the east.

Certainly, the Amazon River has an important influence on the chemistry of the Atlantic Ocean. Dissolved matter travells directly in the surface waters of the Equatorial Atlantic, and settling particles and dissolved matter are upwelled by eddies. The Amazon River produces large amounts of particulate matter which enters the Equatorial Atlantic circulation system and might influence not only the surface waters but also deeper water masses, as the particulate matter sinks. Station Amazon 1 is an active site of carbon export (Charette and Moran, 1999), probably related to siliceous organisms (Shipe et al., 2006); and Station Amazon 2 might be similar, though there are no carbon export data. Suspended sediment discharge from the Amazon River has increased over the past three decades (Martinez et al., 2009) probably due to deforestation and/or erosion of the Amazon rainforest. Extrapolating to the future, the influence of the Amazon River can be only expected to get larger in quantity with time, though possibly different in quality.

Recent studies suggest the Congo River is a major riverine-matter input in the Eastern Equatorial Atlantic region (Vangriesheim et al., 2009). Interestingly, the riverine inputs take place in two separate realms: surface and deep waters (~ 4000m; Braga et al., 2004; Vangriesheim et al., 2009).

The next section studies the water mass structure, while in the following three mini-sections there is one section devoted to the Amazon River and another devoted to the Congo River, including why this study's results indicate the Amazon River settling particles may be influencing not only surface waters, but also intermediate water masses, and why organic matter originating from the Congo River might be observed in deep waters.

5.4. INTERMEDIATE AND DEEP WATERS: WATER MASSES AND OTHER INFLUENCES

Based on physical parameters discussed in the Hydrography section of the Results chapter, the depth profiles obtained can be separated into water masses and each water mass tracked as it travels along its N-S path on the western side of the Equatorial South

Atlantic by Stations 6, 8 and 10. The water mass diagram (Fig. 16b) shows the water masses found in the Atlantic Ocean; the similar diagram for Stations 6, Romanche, 8 and 10 (Fig. 16c) corroborates the presence of the same water masses in the shorter N-S transect (8° N to 33° S). Despite not fitting directly along the N-S path of the water masses (~ 10° to the east), Station Romanche shows a very similar water mass structure and is also plotted. The water masses at each IOC 1996 station are described at length in the Hydrography section in the Results chapter.

The shaded areas in Figs. 17, 20, 21 and 22 delineate the water mass depth ranges at each station; these data are re-plotted in Figs. 25 - 29 for each separate water mass; some data, manipulated and compared with data from the literature, are shown in Figs. 31, 33, 38 and 39. Each water mass reported here includes generally data from two separate depth samples; few include one point only. The water mass physical properties (temperature, salinity and density) are shown in Table 12. The actual station data are compared with literature values. Density, expressed as Sigma theta or Sigma four (σ_t or σ_4) horizons or isopycnals, is used to tag water masses.

Briefly, the σ_t value of the "pure" form of each water mass (i.e. the southernmost AAIW, CPDW and AABW and the northernmost NADW), ~ 27.17, 27.57, 27.85, 27.89 and 27.85, were used to tag the AAIW and CPDW isopycnal horizons. u-NADW, l-NADW and AABW were harder to distinguish. Cutter and Measures (1999) used the temperature and silicate data to distinguish between l-NADW and AABW, since the σ_t values were very close. Yeats (1998) presented a survey of metal and nutrient data for the Atlantic Ocean, and used the sigma theta based on the 4000m reference point (σ_4) instead of σ_t to distinguish between u-NADW, l-NADW and AABW, a common practice for deeper water masses. Yeats' σ_t and σ_4 labels for these five water masses (σ_t: 27.25 and 27.50 for AAIW and CPDW; σ_4: 45.80, 45.85 and 45.95 for u-NADW, l-NADW and AABW) match well with the CTD σ_t and the σ_4 values I calculated for the same water masses in the IOC 1996 Stations (σ_t: 27.17 and 27.57 for AAIW and CPDW; σ_4: 45.76, 45.87 and 46.03 for u-NADW, l-NADW and AABW). Further, the salinity, temperature, oxygen and nutrient data presented in Cutter and Measures's (1999) hydrography paper

corroborate these labels. Given the limited depth point data available, the one or two depth points used per water mass yield average σ values that are close to the σ_t or σ_4 values I used to label the water masses.

The physical parameters of each water mass change slightly as it travels away from its sources, mostly due to mixing with water masses above or below. Thus, the slightly increasing temperature, salinity and density of AAIW, CPDW and AABW as they travel northward (Table 12) are expected. Cutter and Measures (1999) used the "percent northern component" nomenclature, which indicates the similarity between the original water mass formed and the water mass found at each point of its journey, to quantifying the percent of a water mass originating from the North Atlantic source. This purity indicator is important for this study, since a strong focus is given to the influence of a water mass (or some other factors) over another.

5.4.1. Water mass signature concentrations

The concept of finding water mass signature concentrations is not new. Saager et al. (1997) and Laes et al. (2003) used it to interpret the distributions of several dissolved metals in the Atlantic Ocean; Mason and Sullivan (1999) and Cutter and Cutter (2001) used it to study the chemical and redox speciation of some metals and metalloids in this same cruise; thus, I use some ideas borrowed from their work and I make some comparisons between their data and this study. The idea is to use the concentrations of diverse parameters in the water masses to calculate processes occurring within the moving water mass, so that the end-member concentrations can be extrapolated, both in the past at the water mass formation location and time and in the future at the eventual, distant upwelling estimated locations and times.

Figs. 25 to 29 show the evolution of several parameters with latitude as water masses travel. Fig. 25 shows the total dissolved Zn, silicate, Cd and phosphate concentrations; Fig. 26, the Zn/silicate and Cd/phosphate; Fig. 27, the concentrations of Zn- and Cd-ligands; Fig. 28, the stability constants of these ligands; and finally, Fig. 29 shows the Zn_{TD}, Cd_{TD} and the Zn^{2+} and Cd^{2+} (in a negative logarithmic scale), with

potentially limiting and toxic concentrations of Zn and Cd indicated. These figures are shown in this section and are discussed later at different points of the discussion, organized around processes.

Table 12

Temperatures, salinities and densities (σ_t or σ_4) for the water masses found in intermediate and deep waters at the IOC 1996 cruise stations, compared with literature values from Emery (2008) and Yeats (1998)*. Actual values represent generally the average of two separate depth sampling points per water mass.

Water Mass		Station 6	Station R	Station 8	Station 10	"Pure" σ_t or σ_4 density horizon	Literature values
AAIW	Temp (°C)	5.3	5.8	5.3	4.2		2.0 - 6.0
	Salinity	34.80	34.57	34.52	34.29		33.8 - 34.8
	σ_t	27.19	27.24	27.24	27.17	~ 27.17	~ 27.25*
CPDW	Temp (°C)	4.9	4.1	3.8	2.7		1.0 - 2.0
	Salinity	34.88	34.97	34.77	34.60		34.6 - 34.7
	σ_t	27.61	27.76	27.65	27.57	~ 27.57	~ 27.50*
u-NADW	Temp (°C)	3.1	3.0	2.9	3.0		Upper 1.5- 4.0
	Salinity	34.80	34.95	34.91	34.90		34.8 - 35.0
	σ_t	27.85	27.85	27.82	27.80	~ 27.85	~ 27.8
	σ_4	45.76	45.73	45.71	45.68	~ 45.76	~ 45.80*
l-NADW	Temp (°C)	2.1	2.0	2.4	2.7		Lower 1.5- 4.0
	Salinity	34.96	34.89	34.90	34.92		34.8 - 35.0
	σ_t	27.89	27.89	27.86	27.84	~ 27.89	~ 27.8
	σ_4	45.87	45.87	45.80	45.83	~ 45.87	~ 45.85*
AABW	Temp (°C)	1.7	0.6	0.4	0.2		- 0.9 - 1.7
	Salinity	34.88	34.76	34.72	34.68		34.6 - 34.7
	σ_t	27.89	27.87	27.86	27.85	~ 27.85	~ 27.8
	σ_4	45.91	46.01	46.03	46.03	~ 46.03	~ 45.95*

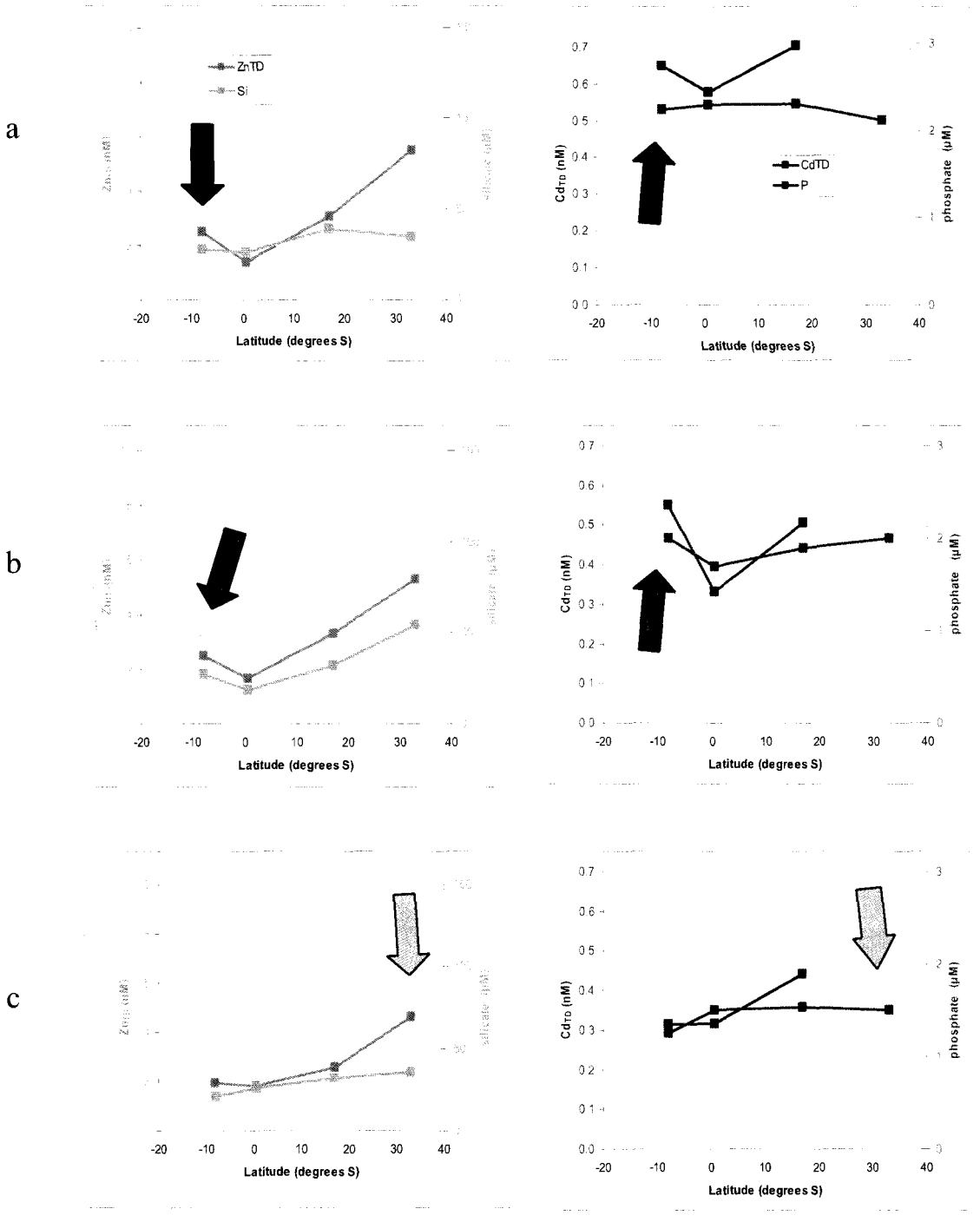

Fig. 25. Zn_{TD}, silicate, Cd_{TD} and phosphate plotted against latitude at Stations 6, Romanche, 8 and 10 in specific water masses: a) AAIW, b) CPDW, c) u-NADW, d) l-NADW and e) AABW. Arrows highlight external factors: influences by the Amazon River/Equatorial region (AEF, red arrows), Southern water masses (SWMF, blue arrows) and Congo River remineralized shelf matter (CSMF, green arrows).

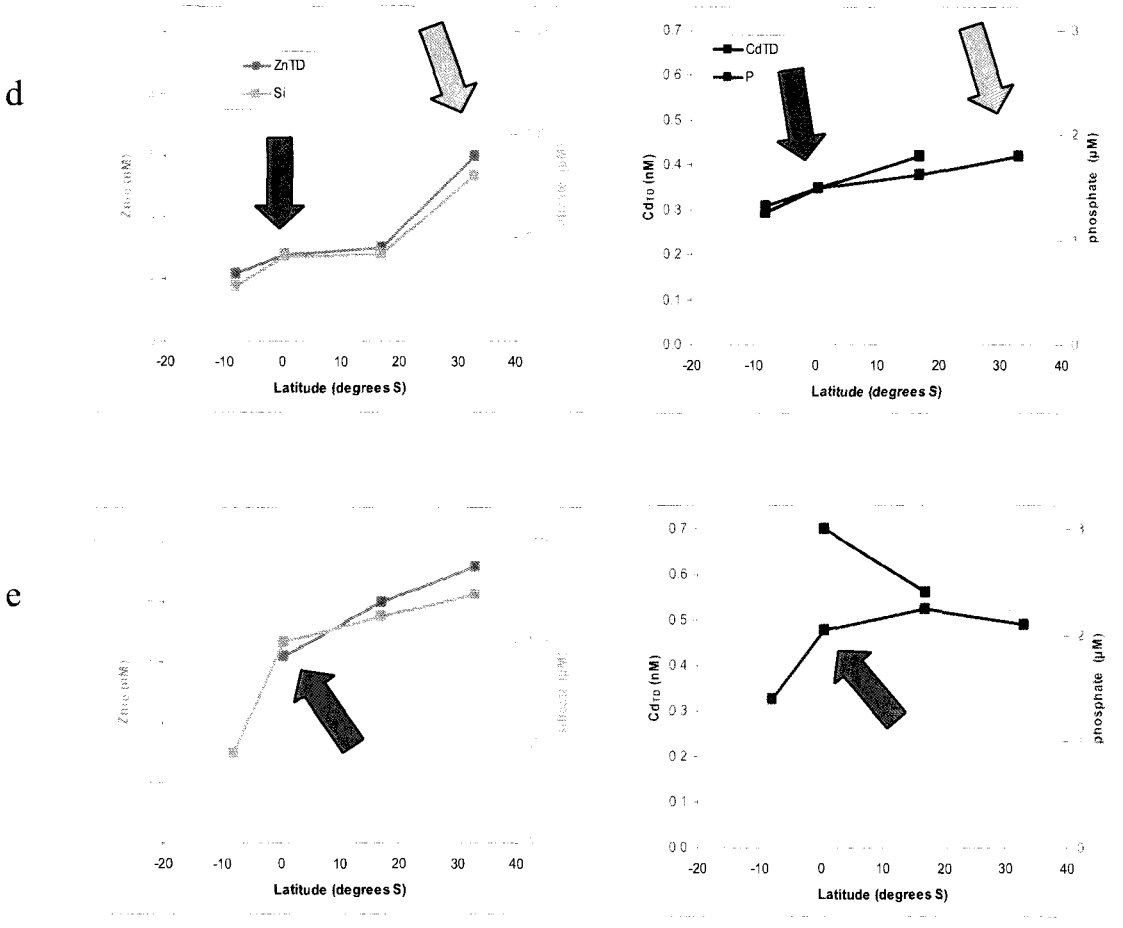

Fig. 25. Continued.

Fig. 21, showing the depth profiles of metals and ligands, is more complete (i.e. has more points) than Fig. 20, showing the ligands' stability constant depth profile. Not all the depths where ligands were present in Fig. 21 have data from which to obtain stability constants: some datasets, either too noisy or mathematically difficult to interpret by TDI or with the ligand saturated and a natural high concentration of metal, only allow for an estimation of the total ligand concentration. Also, the ligands in few of these samples can not be separated mathematically, and the two ligand concentration and logK' are merged into just one ligand parameters. Fig. 28 uses data from Fig. 20, and thus some points are missing because of this reason.

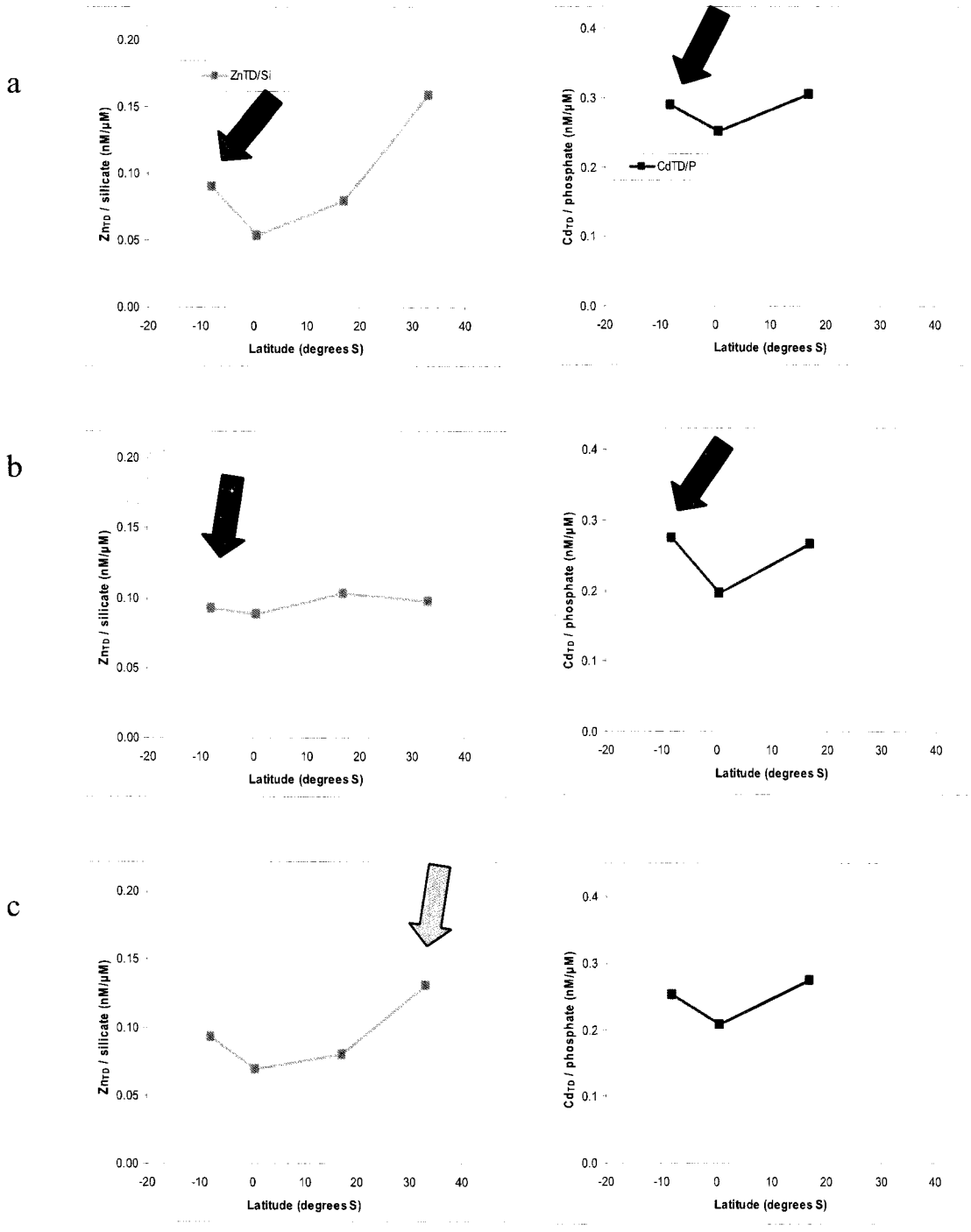

Fig. 26. Zn/silicate and Cd/phosphate plotted against latitude at Stations 6, Romanche, 8 and 10 in specific water masses: a) AAIW, b) CPDW, c) u-NADW, d) l-NADW and e) AABW. Arrows highlight external factors AEF, SWMF and CSMF (see Fig. 25 for explanation).

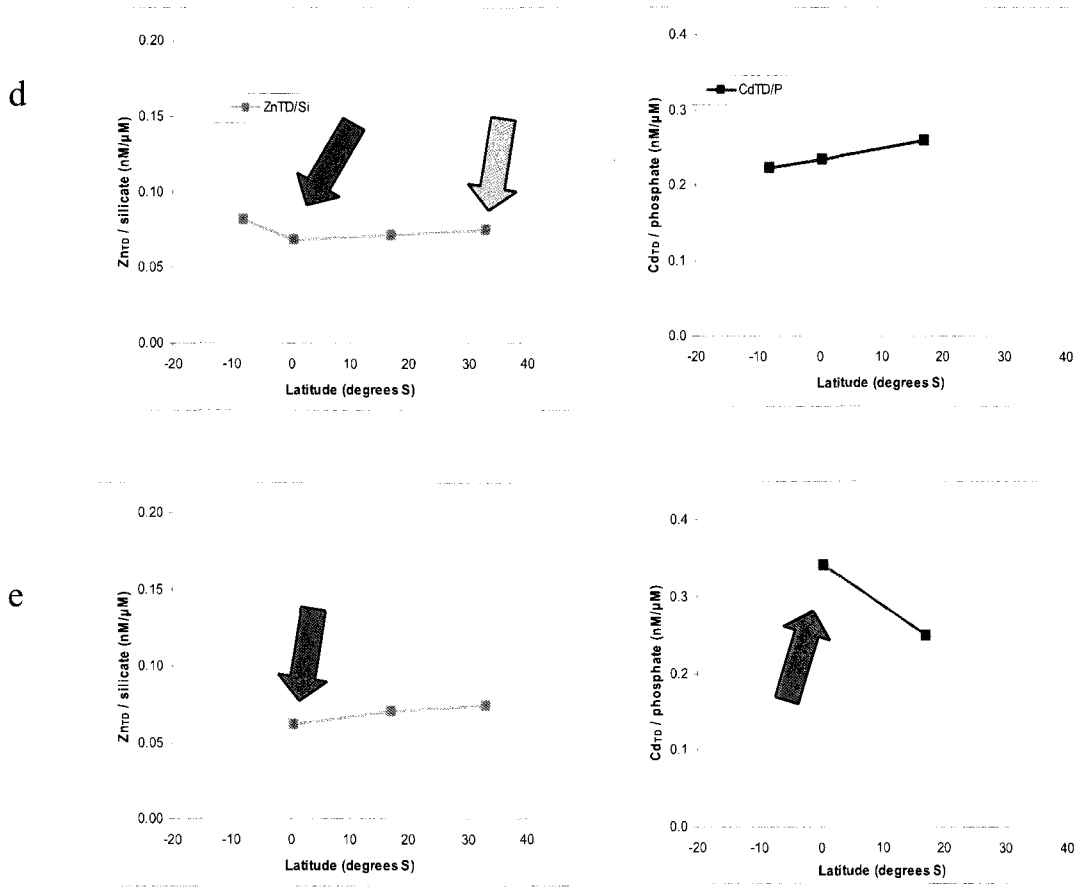

Fig. 26. Continued.

5.4.2. Water mass age

In order to better understand the processes occurring in these water masses, a time frame for water mass travel is required. This is obtained from three methodologies, based on radiocarbon (C14), CFCs and CCl_4 and tritium (H3). Circulation patterns are clear and relative water mass ages are well constrained (Schlitzer, 2007). AAIW is the youngest of the water masses discussed in this study (Huhn et al., 2001), followed by AABW (Huhn et al., 2008b), both u- and l-NADW (Huhn et al., 2008, Andrie et al., 2002) and CPDW, the oldest (Well et al., 2003). CPDW is a water mass that takes from the Antarctic Circumpolar Current (ACC), a water mass that may have been circulating around

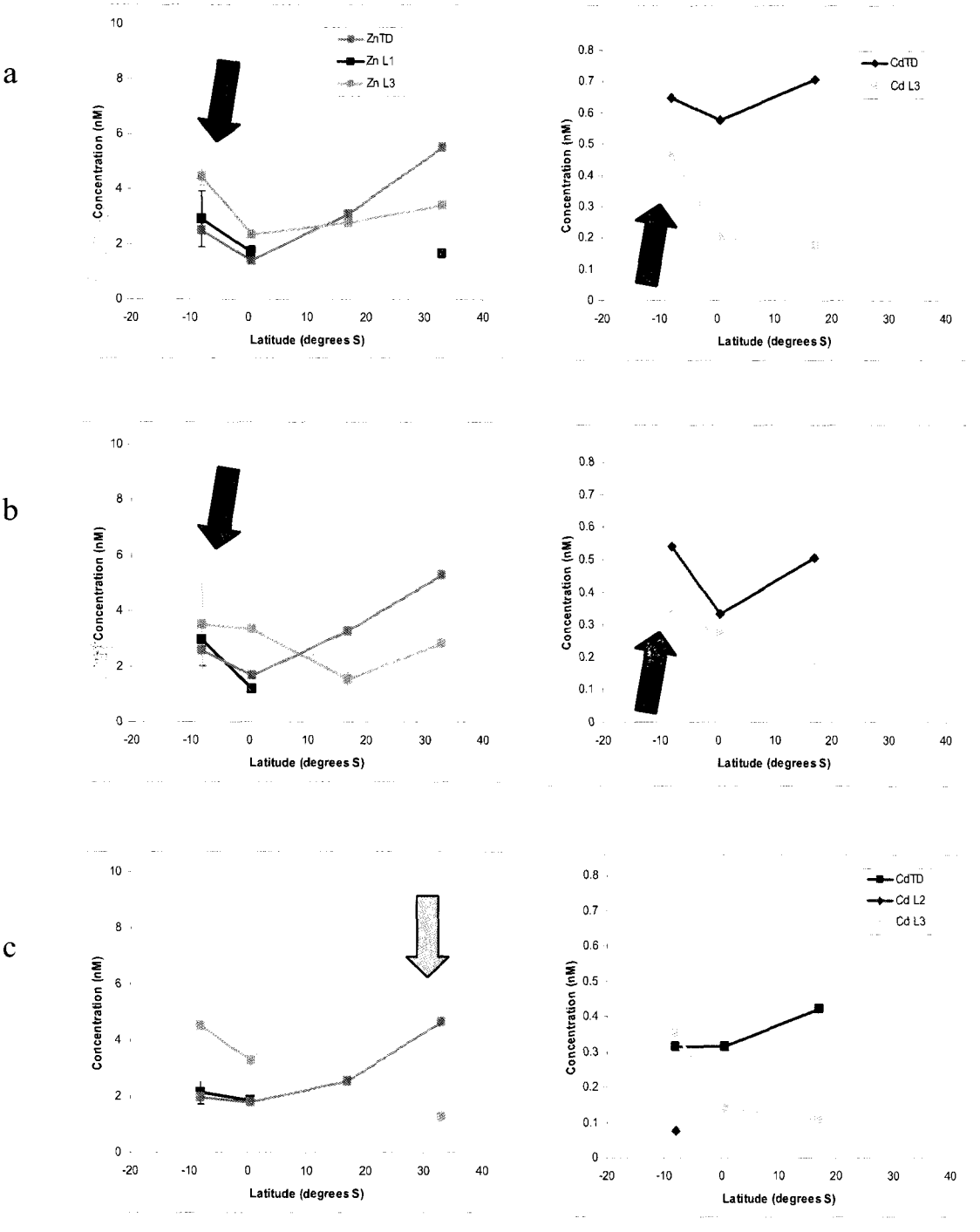

Fig. 27. Concentration of Zn_{TD}, Cd_{TD} and Zn and Cd ligands plotted against latitude at Stations 6, Romanche, 8 and 10 in specific water masses: a) AAIW, b) CPDW, c) u-NADW, d) l-NADW and e) AABW. Arrows highlight external factors AEF, SWMF and CSMF (see Fig. 25 for explanation).

d

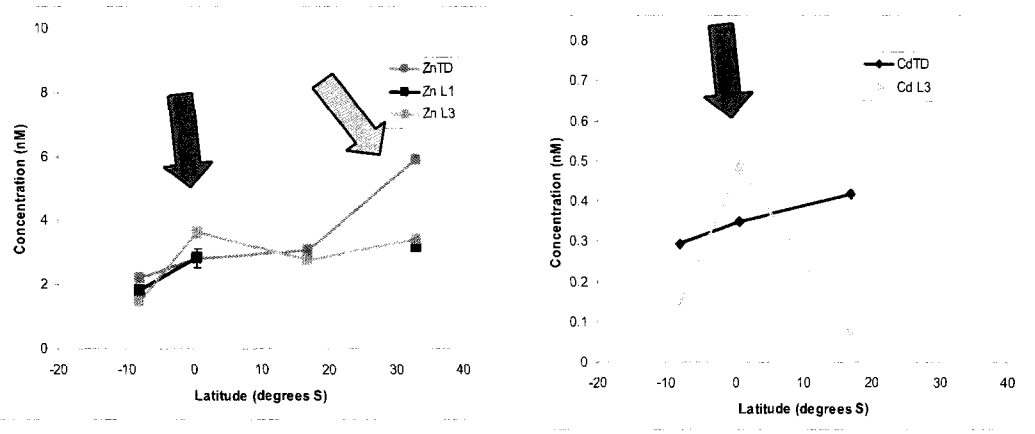

e

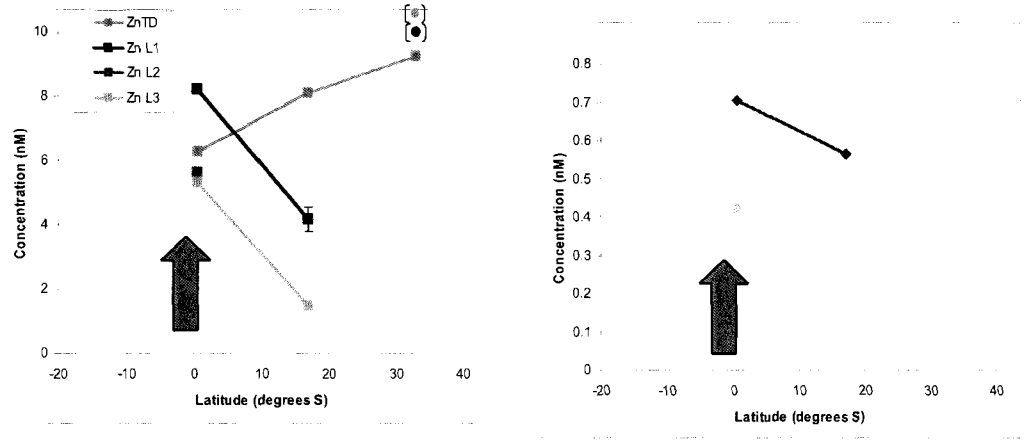

Fig. 27. Continued.

Antarctica and that may originate from a mixture of deep waters coming from the Indian, Pacific and Atlantic Oceans, thus its old age. Both u-NADW and l-NADW are ~ 40 years old by the time they reach Station 6, and ~ 85 years old by the time they reach Station 10. Andrie et al. (2002) stated that u-NADW is ~ 3 years younger than l-NADW because of the extra distance travelled (Irminger to Labrador Sea, see Fig. 16e for location reference). Mason and Sullivan (1999) used a similar time range (10 to 50 years) for the AAIW to transit between these same IOC 1006 stations in their report. Huhn et al. (2008) estimated transit time between Station 6 and Station 10, the extreme north and south stations for this study, as 40 years in average, which is the transit time I will use for all water masses in this study.

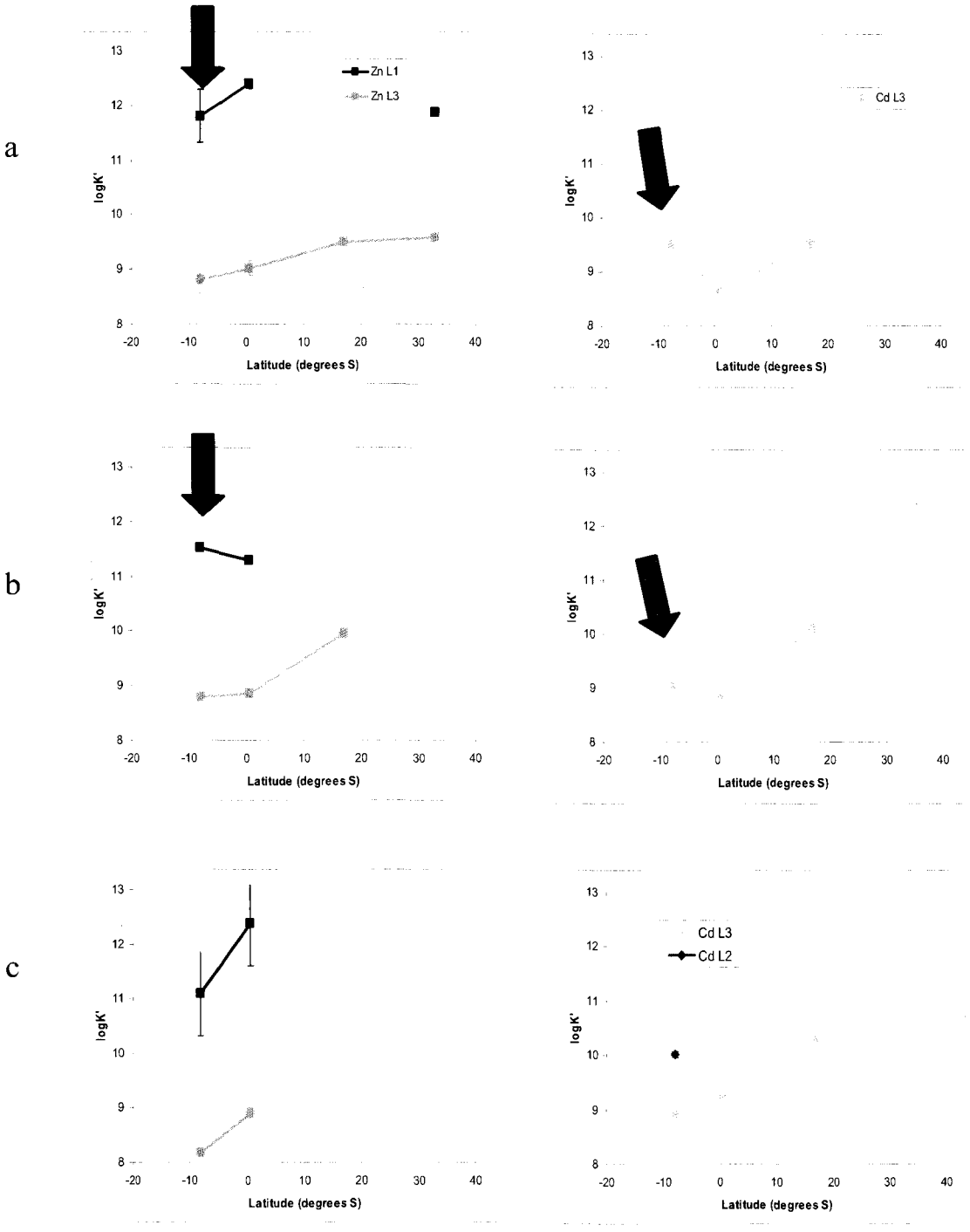

Fig. 28. Stability constants (expressed as logK') of Zn and Cd ligands plotted against latitude at Stations 6, Romanche, 8 and 10 in specific water masses: a) AAIW, b) CPDW, c) u-NADW, d) l-NADW and e) AABW. Arrows highlight external factors AEF, SWMF and CSMF (see Fig. 25 for explanation). Note that not all the depths where ligands were present in Fig. 27 show stability constants.

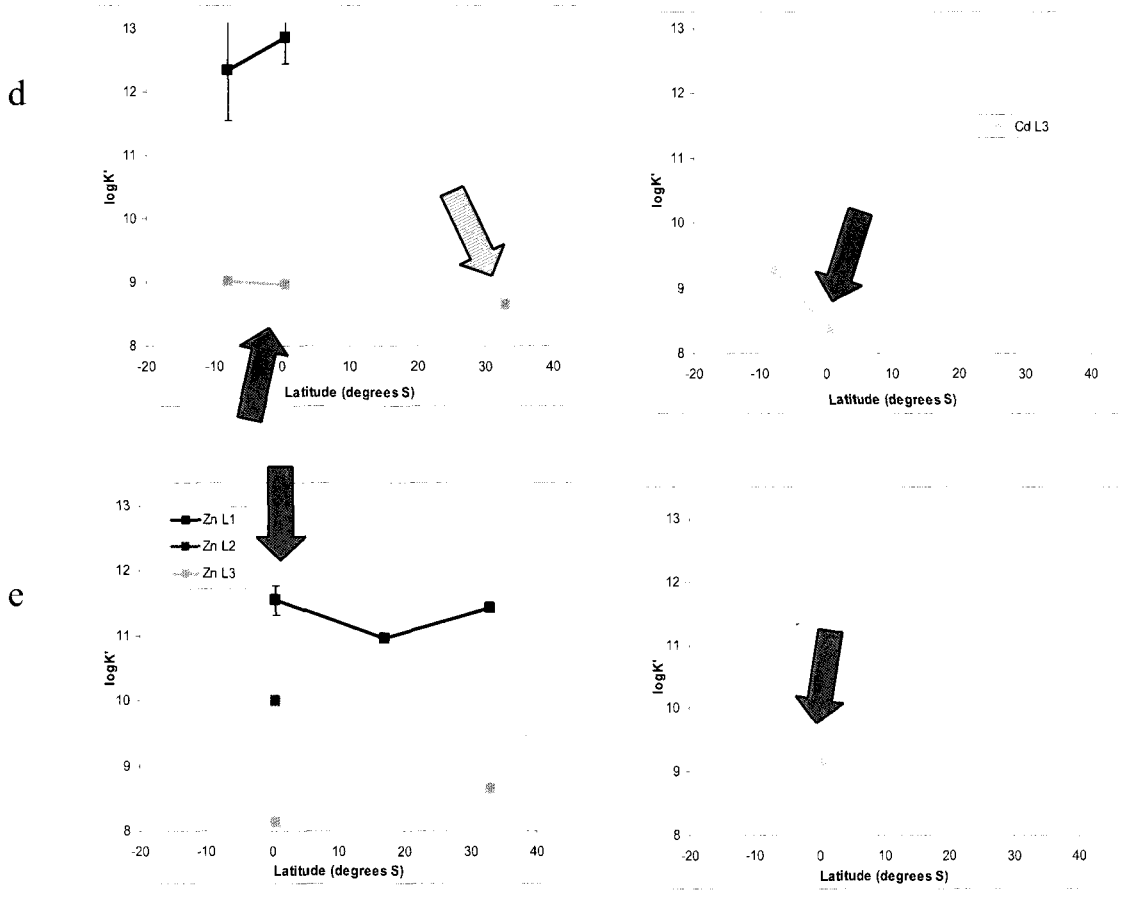

Fig. 28. Continued.

5.4.3. Water masses' salient nutrient and metal features.

A brief description is found in the Cutter and Measures (1999) hydrography paper.

AAIW is characterized as having very low salinity, low temperature and very high oxygen, compared with CPDW in stations studied here. The high oxygen concentrations show its recent contact with surface waters. Its nutrient and oxygen concentrations are masked with nutrients from both maximum respiration and dissolution depths, which are located at depths similar to those of AAIW. Concomitantly, both Zn_{TD} and Cd_{TD} show

a

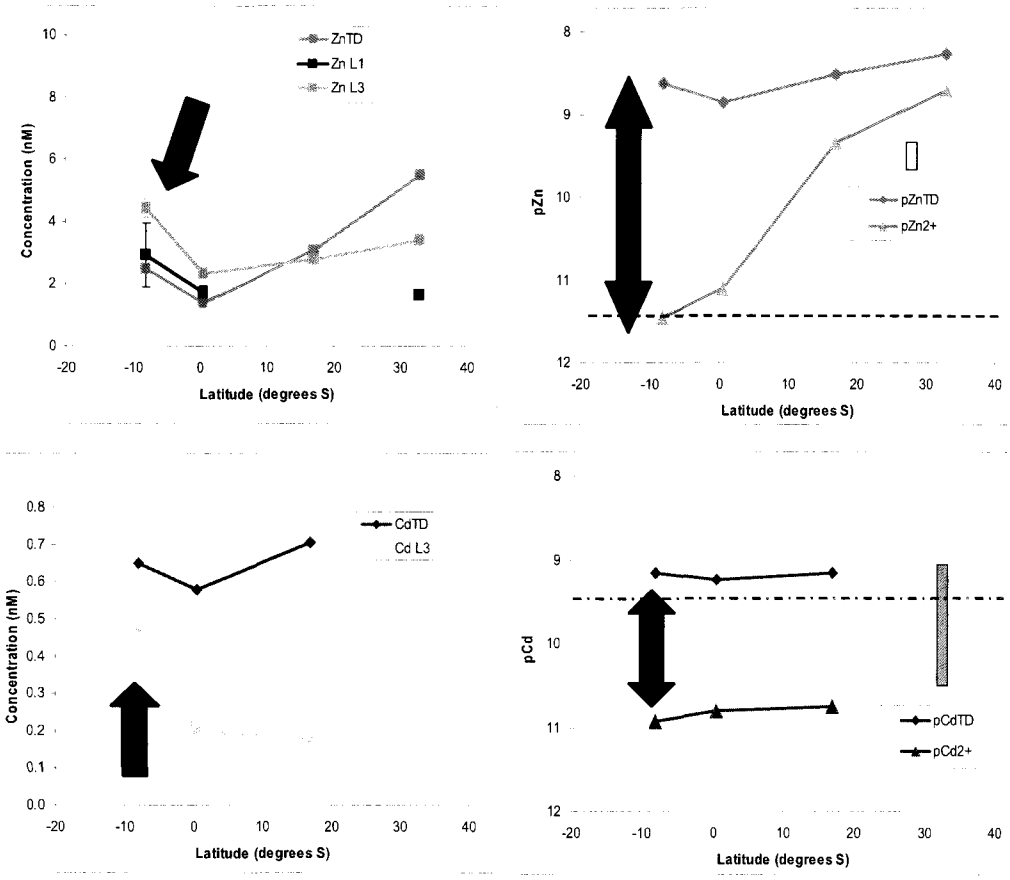

Fig. 29. pZn_{TD}, pZn^{2+}, pCd_{TD} and pCd^{2+} compared with concentration of Zn_{TD}, Cd_{TD} and Zn and Cd ligands plotted against latitude at Stations 6, Romanche, 8 and 10 in specific water masses: a) AAIW, b) CPDW, c) u-NADW, d) l-NADW and e) AABW. Arrows highlight external factors AEF, SWMF and CSMF (see Fig. 25 for explanation). The dashed and dash-dot red lines, respectively, indicate potentially limiting Zn^{2+} concentrations for neritic species and potentially toxic Cd^{2+}concentrations for all species. The blue and pink bars above the legend boxes indicate the extent of inorganic complexation.

b

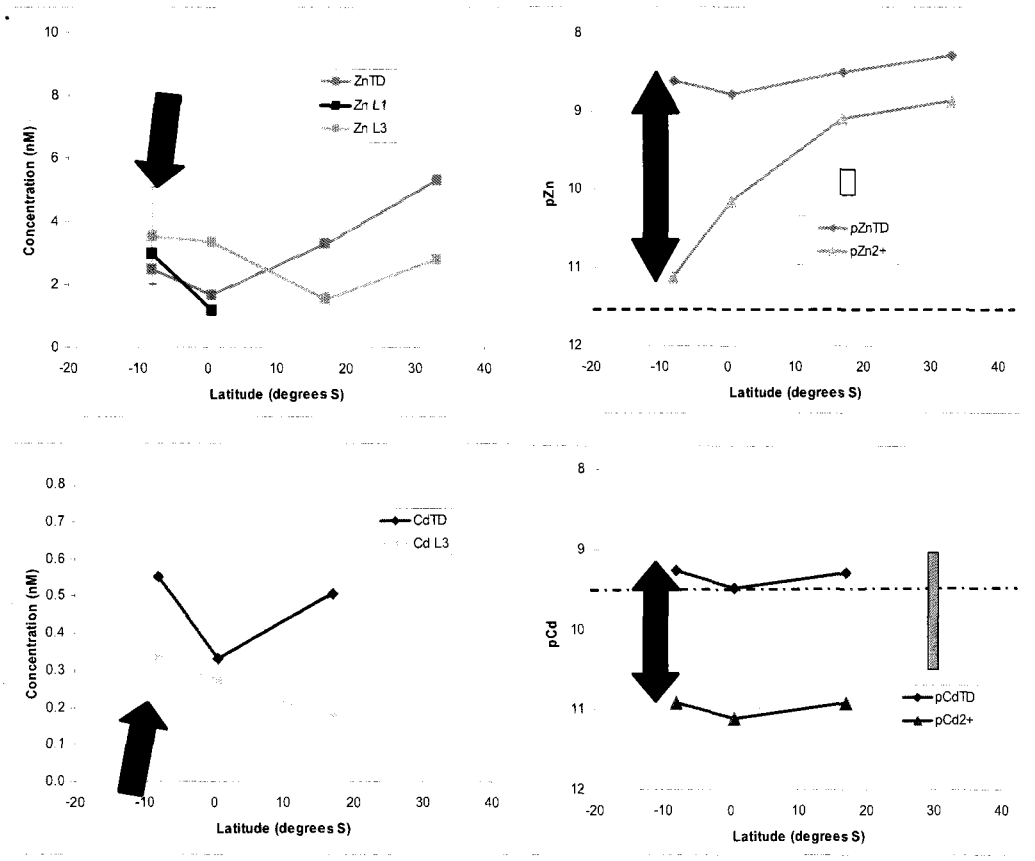

c

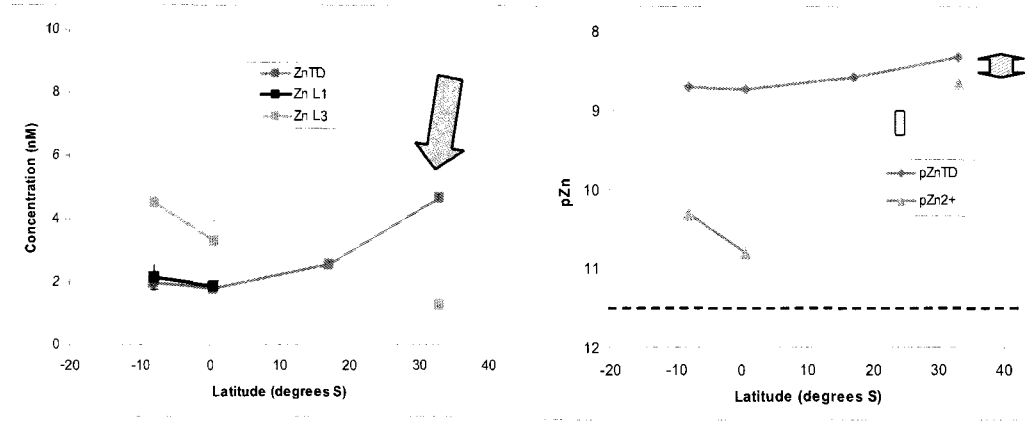

Fig. 29. Continued.

c

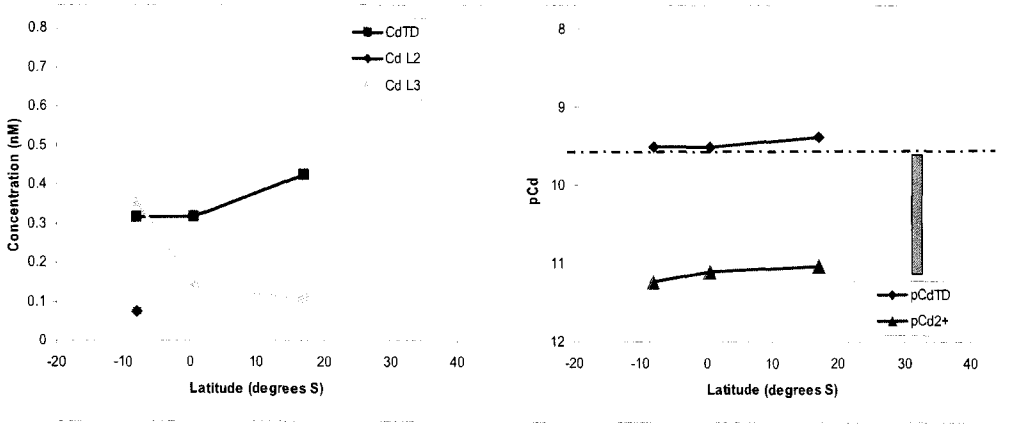

d

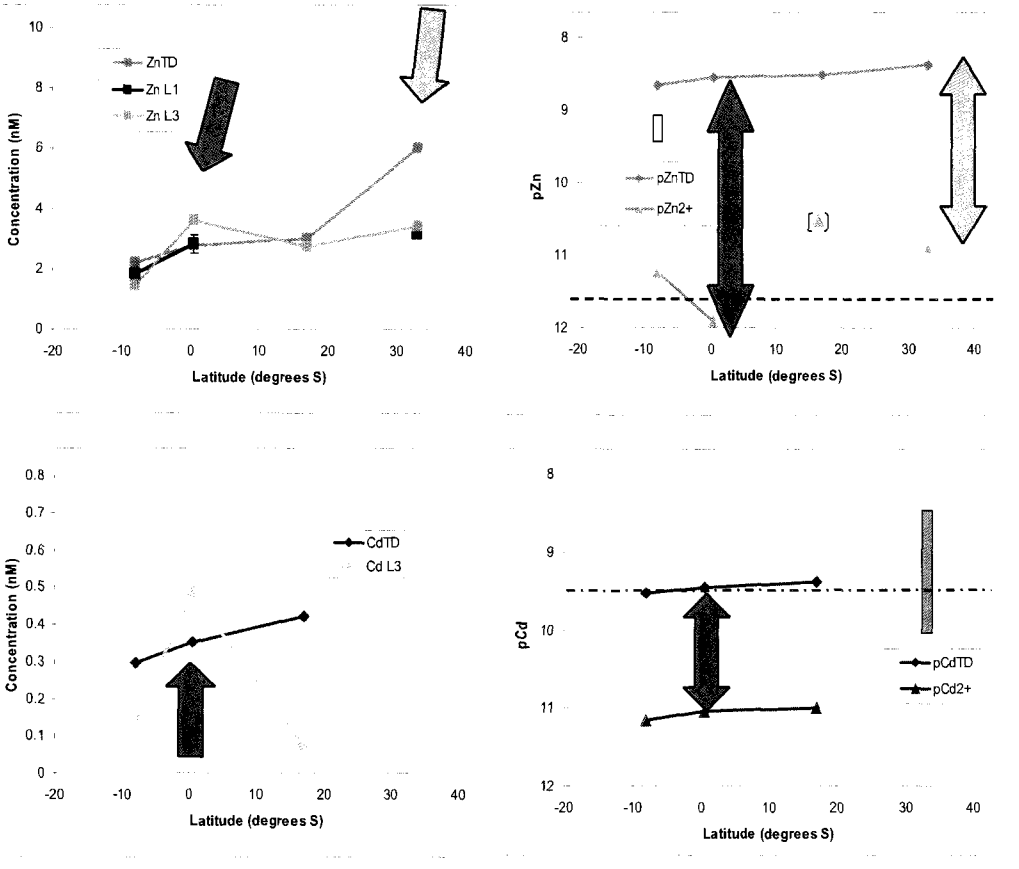

Fig. 29. Continued.

e

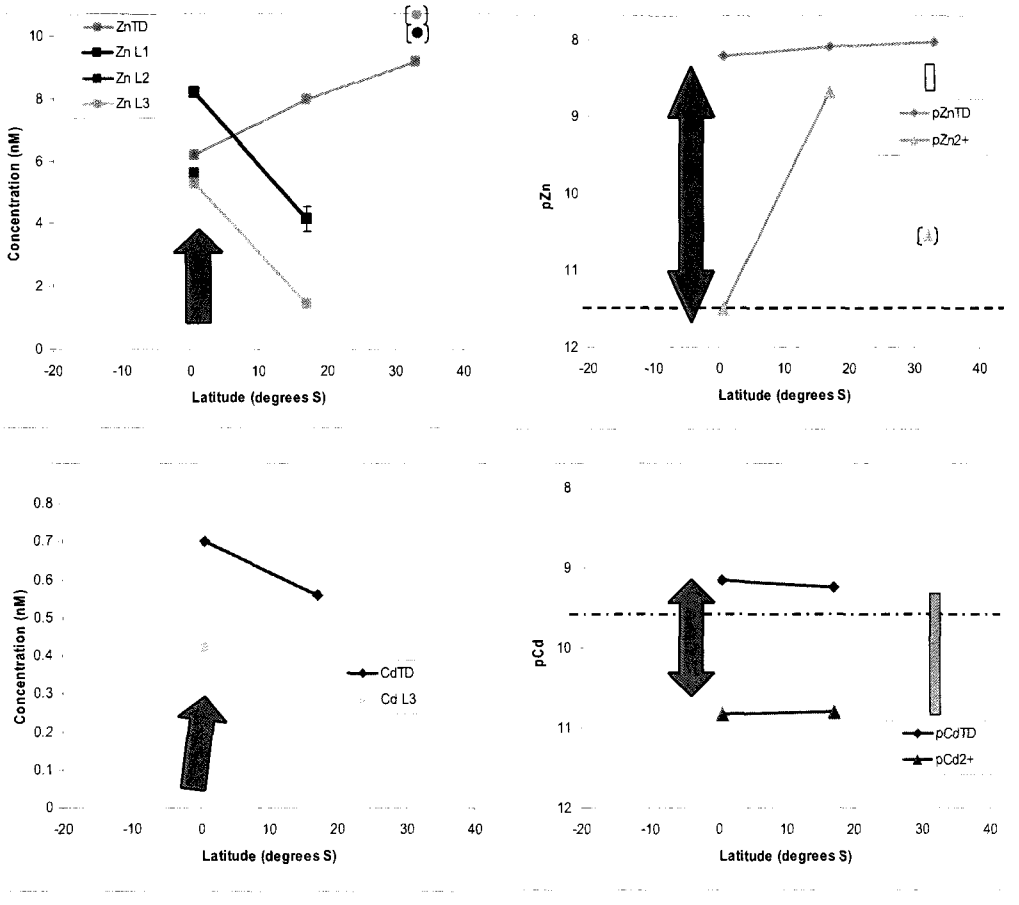

Fig. 29. Continued.

maximum concentrations in this water mass (Fig. 17). Windom et al. (1988) reported similar trends, where the Zn_{TD} and Cd_{TD} maximums occur at nutrient maximum, resulting from trace metal regeneration and organic matter decomposition in an estuary, that is, along a horizontal transect instead of a vertical transect.

Mason and Sullivan (1999) used AOU (Apparent Oxygen Utilization, a value expressed in μM oxygen that represents the difference between calculated oxygen concentration at saturation and the actual oxygen concentration, widely used to gauge bacterial respiration) depth profiles from the South Equatorial Atlantic across 30° W as a

proxy for bacterial respiration. When this study is compared with their AOU depth section, only Station 10 shows water apparently not modified by bacterial activity and supposedly similar in nature to the source; AAIW at Stations 6, Romanche and 8 is affected by increased AOU, potentially modifying not only the nutrients and total dissolved metals, but possibly the ligand(s) present (bacterial respiration gauges chemical processes by which particulate matter is consumed and metals and nutrients released, altering the balance of dissolved nutrients and ligands that bind to them). Regardless of this constraint, Yeats (1998) reported Cd_{TD} and phosphate values at isopycnals very close to those used in this study (σ_t 27.25 vs. 27.17), and his values are in agreement with those from this study. There are no Zn_{TD} and silicate data from AAIW, but Corami et al.'s (2005) data from the Surface Antarctic Mode Water (SAMW), arguably a predecessor of AAIW, indicate ~ 5 nM Zn_{TD}. This is in the ~ 5 nM range of the Zn_{TD} recently reported by Baars and Croot (submitted). Source point concentrations are ~ 40 μM silicate (Smith et al., 2009), ~ 0.6 nM Cd_{TD} and ~ 2.1 μM phosphate (Yeats, 1998).

CPDW is apparent as the high silicate, nitrate and phosphate, low oxygen that occurs with low salinity and temperature in the water column of the stations studied here above NADW and below AAIW. Its high silicate concentrations (~ 77 μM at source point, Well et al., 2003) and low oxygen relate this water mass to the ACC. There are no Zn_{TD} or Cd_{TD} data from this water mass directly, but Zn_{TD} measured in the ACC across the Drake Passage is ~ 4 nM (Baars and Croot, 2010). This is a bit lower than values reported by Loscher (1999) and Corami et al. (2005) from the Weddell and Ross Seas, respectively. Increased AOU also affects the CPDW moving north; Stations 6 and 8 may be affected. Source point concentrations are ~ 6 nM Zn_{TD} (Loscher, 1999; Corami et al., 2005), ~ 77 μM silicate (Well et al., 2003), ~ 0.7 nM Cd_{TD} and ~ 2.2 μM phosphate (Yeats, 1998; Well et al., 2003).

NADW is observed as the low silicate, nitrate and phosphate and high oxygen that occurs with high salinity and temperature in the water column of the stations studied here above AABW and below CPDW. Using σ_4 values, NADW is separated into u-NADW (coming from the Labrador Sea, σ_4 ~ 45.80) and l-NADW (coming from the Irminger

Sea, $\sigma_4 \sim 45.85$; Yeats, 1998). The same distinction has not been made yet in terms of metal and nutrient concentrations and probably the concentrations in these two water masses are not too different (see data in Cutter and Measures, 1999). Zn_{TD} is estimated ~ 2 nM in Labrador Sea Water (LSW), which is more than 97 % northern component (Ellwood and van den Berg, 2000). The source concentrations used in this study are the average of Saager et al. (1997) and Yeats (1998), ~ 12 μM silicate, ~ 0.20 nM Cd_{TD} and ~ 1.0 μM phosphate.

AABW, originating near the Weddell Sea, is characterized by the high silicate, nitrate and phosphate that occurrs with low salinity and temperature near the bottom of the water column below NADW. It has the highest silicate concentrations in the world's ocean (~ 120 μM, Saager et al., 1997) and also very high Zn_{TD} (~ 5 - 6 nM, Westerlund and Ohman, 1991; Corami et al., 2005). Cd_{TD} averages 0.7 nM and phosphate 2.3 μM (Yeats, 1998; Saager et al., 1997). Close to Antarctica, AABW's features are so strong it actually influences l-NADW and maybe u-NADW (where high silicate values are observed), but these features fade as it moves away from its source in the Atlantic Ocean.

Source point concentrations of Zn_{TD}, Cd_{TD}, silicate and phosphate for the water masses studied are summarized in Table 13. End points are the locations where each water mass upwells, whether this is nearby or remote. Fig. 16c suggests that AAIW upwells somewhere in the low latitude North Atlantic. In contrast, CPDW gets mixed with NADW; NADW gets mixed with AABW and CPDW somewhere in high southern latitudes and may upwell to a certain extent; and AABW gets mixed with NADW somewhere around the Equator (though it might reach higher latitudes of the North Atlantic; Johnson, 2008). When water masses mix, their chemical properties are averaged, thus the chemical signatures discussed in this section can be followed.

5.4.4. Physical and biogeochemical processes

As each water mass travels away from its source, physical and biogeochemical processes occur that, combined, might alter the nutrients, metals and ligands concentrations in the dissolved and particulate matter in the following ways:

- advective water mixing,
- particle formation, settling and transport
- particle dissolution,
- nutrient and metal uptake and respiration, and
- ligand formation and decay.

A brief description of these processes follows, with information pertinent to gauging how significant they are in the oceanographic region studied here.

a) Advective mixing:

From a purely physical perspective, advective mixing causes nutrients, metals and ligands coming from two water masses with different concentrations to merge into one "average" water concentration. Traditionally thought to budget young water masses' nutrients, simple mixing physics were shown to govern older water masses' nutrient and metal concentrations, as opposed to *in-situ* or cumulative regeneration which were minor factors (Saager et al., 1997).

In order to investigate the effect of advective mixing in this study, I revisited the metal, nutrient and metal/nutrient water mass plots (Figs. 25 and 26) and expanded them to the source points (data in Table 13) and likely end points for each water mass. Figs. 30 and 31 are the products of this water mass extension study. In general, AAIW, CPDW and AABW show decreasing nutrient and metal concentrations as they move away from their sources, in contrast with the NADW system (u- and l-NADW) whose concentrations increase as the move closer to Antarctica. This implies a heavy influence of the silicate-and-Zn-rich Southern Ocean water masses (indicated by the blue arrows in Figs. 30 and 31 and referred hereafter as SWMF, Southern Ocean originated Water Mass Factor). For the southern originated water masses (AAIW, CPDW and AABW, shown in Figs. 30a, b and e), there seems to be a disconnect between the very linear Zn and silicate decreasing concentration from Station 10 to Station 8 to Station Romanche and their source concentrations; either the source concentrations are higher than reported or maybe there is a large sink of Zn and silicate in the water masses (between ~ 10 and 50

Table 13

Approximate formation latitude and average literature Zn_{TD}, silicate, Cd_{TD} and phosphate concentrations for intermediate and deep water masses found on the IOC 1996 cruise. Approximate latitudes from Sarmiento and Gruber (2006); concentrations from Broecker et al. (1991), Saager et al. (1997), Baars and Croot (submitted), Loscher (1999), Well et al. (2003), Westerlund and Ohman (1991), Bruland and Lohan (2003), Ellwood and van den Berg (2000), Corami et al. (2005), Smith et al. (2009) and Yeats (1998).

Water Mass	Approximate formation latitude	Zn_{TD} (nM)	silicate (μM)	Cd_{TD} (nM)	phosphate (μM)
AAIW	~ 60° S	~ 5	~ 40	~ 0.6	~ 2.1
CPDW	~ 65° S	~ 6	~ 77	~ 0.7	~ 2.2
u-NADW	~ 60° N	~ 2	~ 12	~ 0.2	~ 1.0
l-NADW	~ 65° N	~ 2	~ 12	~ 0.2	~ 1.0
AABW	~ 70° S	~ 6	~ 120	~ 0.7	~ 2.3

percent) between their source point latitudes (~ 60 - 70° S) and 33° S, where Station 10 is and the apparent linear concentration starts.

There are two apparent phenomena that distort the linear nutrient and metal concentrations trends in these water masses. One of them is located at the intermediate waters (AAIW and CPDW) of Station 6, and the other is located between l-NADW and AABW at Station Romanche. They are indicated by the red and green arrows, respectively, from Figs. 30 and 31 and on. Near the mouth of the Amazon River in the Equatorial Atlantic, there is one source point that shows increased Zn_{TD} and Cd_{TD}, and to a lower extent silicate and phosphate concentrations. In contrast, at Station Romanche, there is an apparent weaker source point of Zn_{TD} and silicate mainly, that could be related to Congo River originated organic matter, remineralized and transported. Both of these inputs, referred hereafter as AEF (Amazon river/Equatorial high productivity and net flux

a

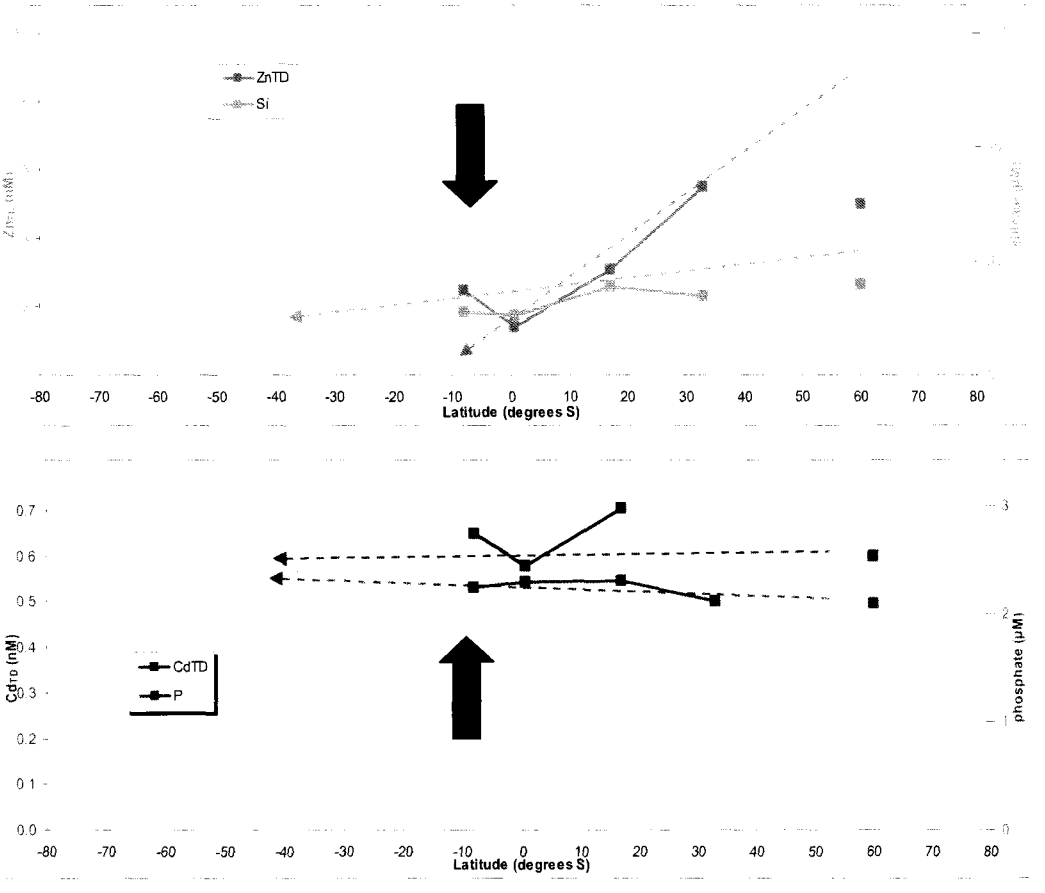

Fig. 30. Zn_{TD}, silicate, Cd_{TD} and phosphate plotted against latitude at Stations 6, Romanche, 8 and 10 in specific water masses: a) AAIW, b) CPDW, c) u-NADW, d) l-NADW and e) AABW; extended to the source points for each water mass. Source concentrations plotted and an arbitrary linear estimation of water mass travel signal strength for each parameter, indicating direction of travel and an approximate "end latitude" (latitude where water mass will merge into some other water mass). Arrows highlight external factors AEF, SWMF and CSMF (see Fig. 25 for explanation).

b

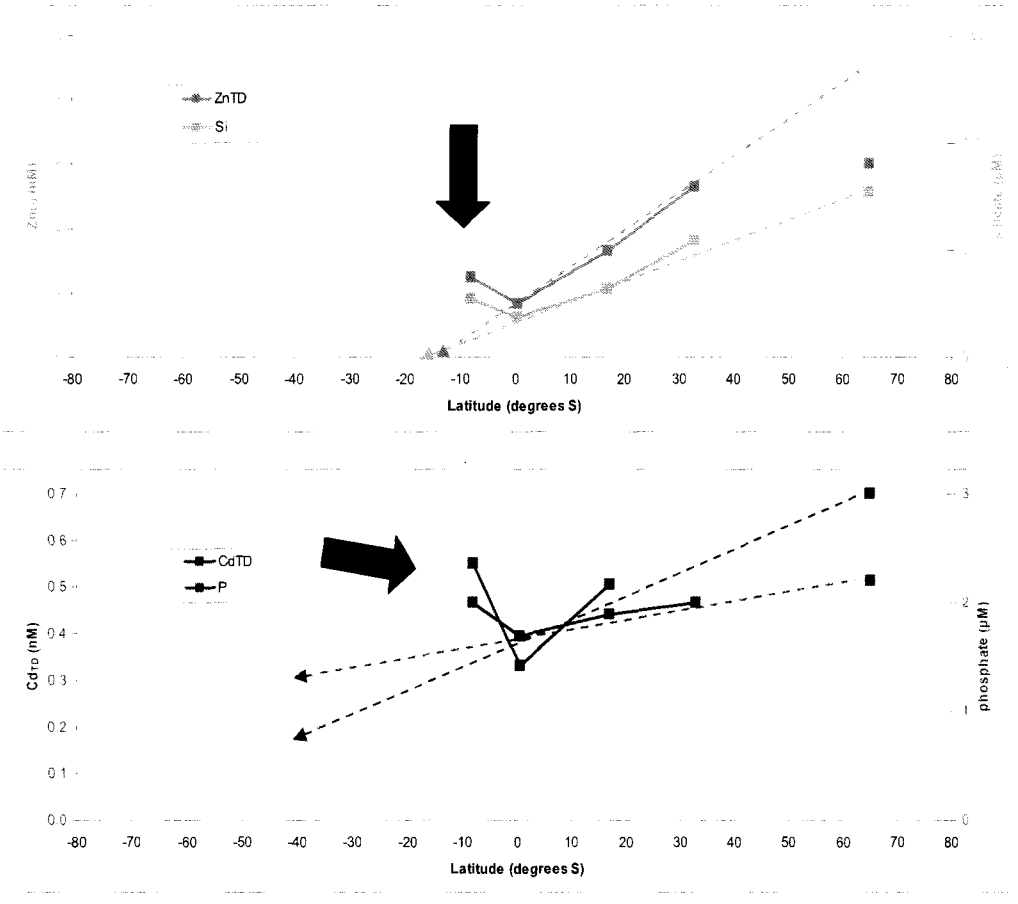

c

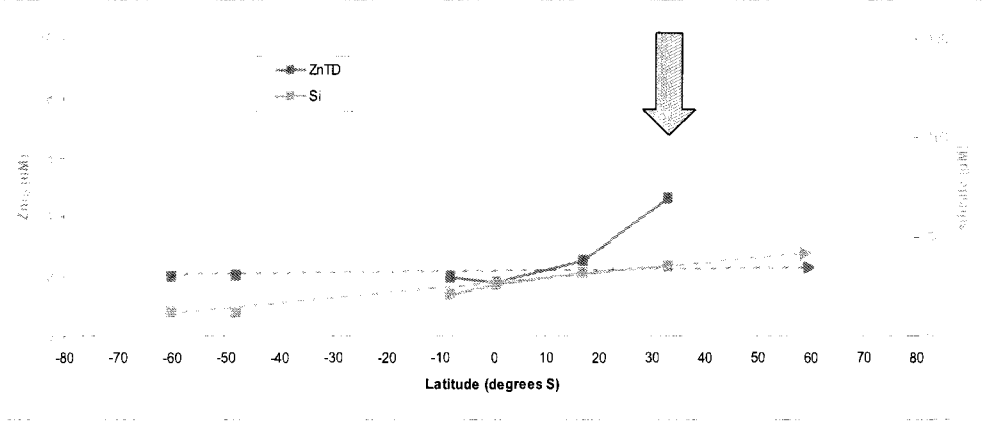

Fig. 30. Continued.

c

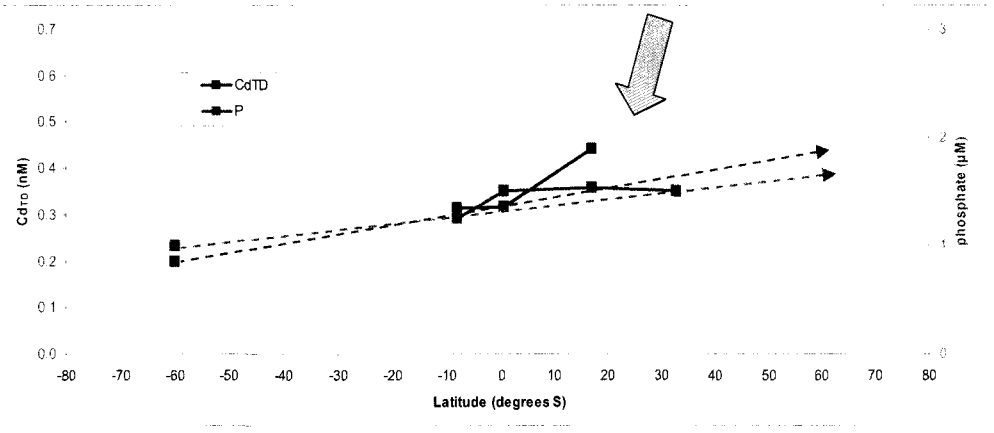

d

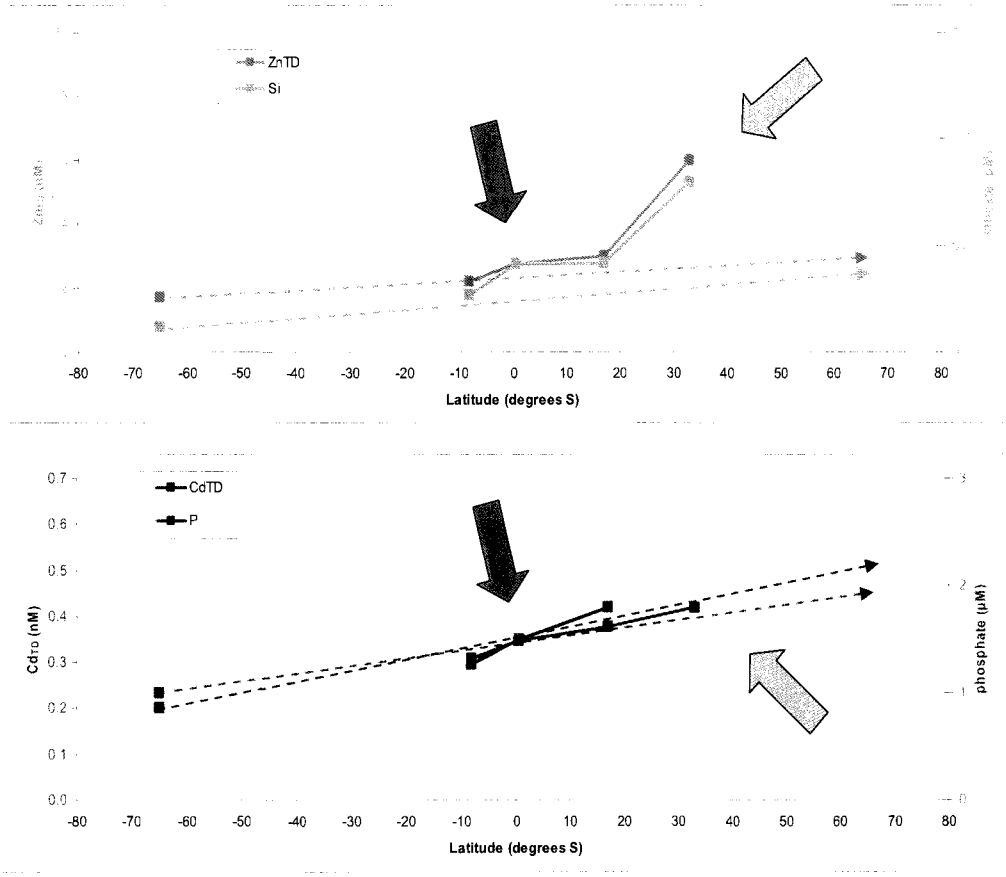

Fig. 30. Continued.

e

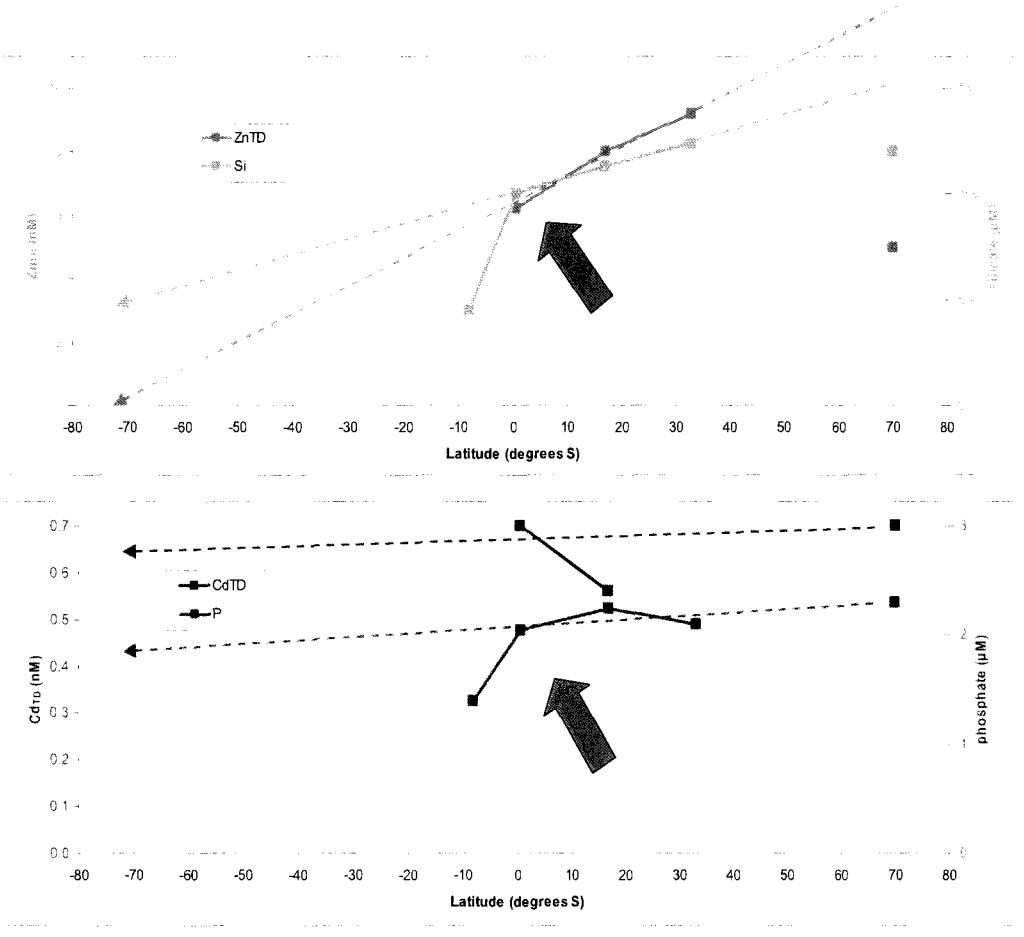

Fig. 30. Continued.

Factor) and CSMF (Congo river Shelf remineralized Matter Factor), are discussed extensively in the next sections, as well as SWMF.

Fig. 31 indicates a disconnect between Zn/silicate and Cd/phosphate in the southern origin water masses. In general, Zn/silicate shows higher variability than Cd/phosphate within water masses as they flow. Further, AAIW, u-NADW and l-NADW suggest an apparent preferential silicate remineralization, as the Zn/silicate ratio decreases as these water masses age. In contrast, CPDW and AABW show apparent preferential Zn remineralization. These observations are attempted on the linear trend section that

a

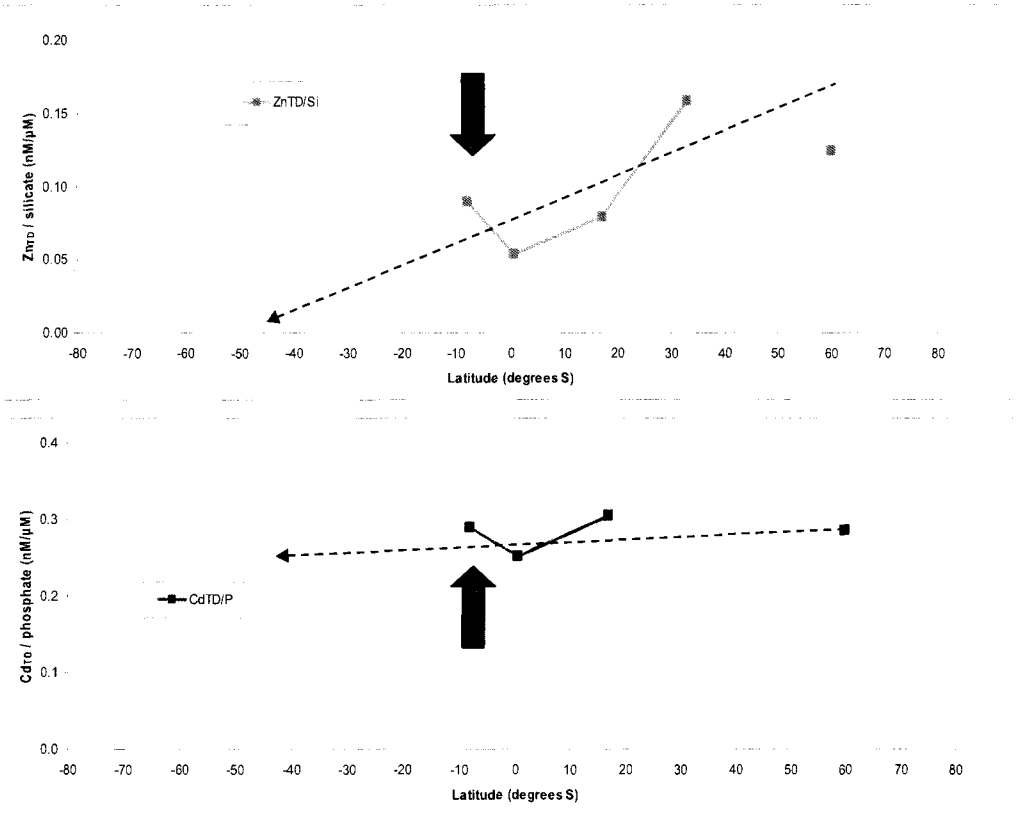

Fig. 31. Zn_{TD}/silicate and Cd_{TD}/phosphate ratios plotted against latitude at Stations 6, Romanche, 8 and 10 in specific water masses: a) AAIW, b) CPDW, c) u-NADW, d) l-NADW and e) AABW; extended to the source points for each water mass. Source ratios plotted and an arbitrary linear estimation of water mass travel signal strength for each parameter, indicating direction of travel and an approximate "end latitude" (latitude where water mass will merge into some other water mass. Arrows highlight external factors AEF, SWMF and CSMF (see Fig. 25 for explanation).

b

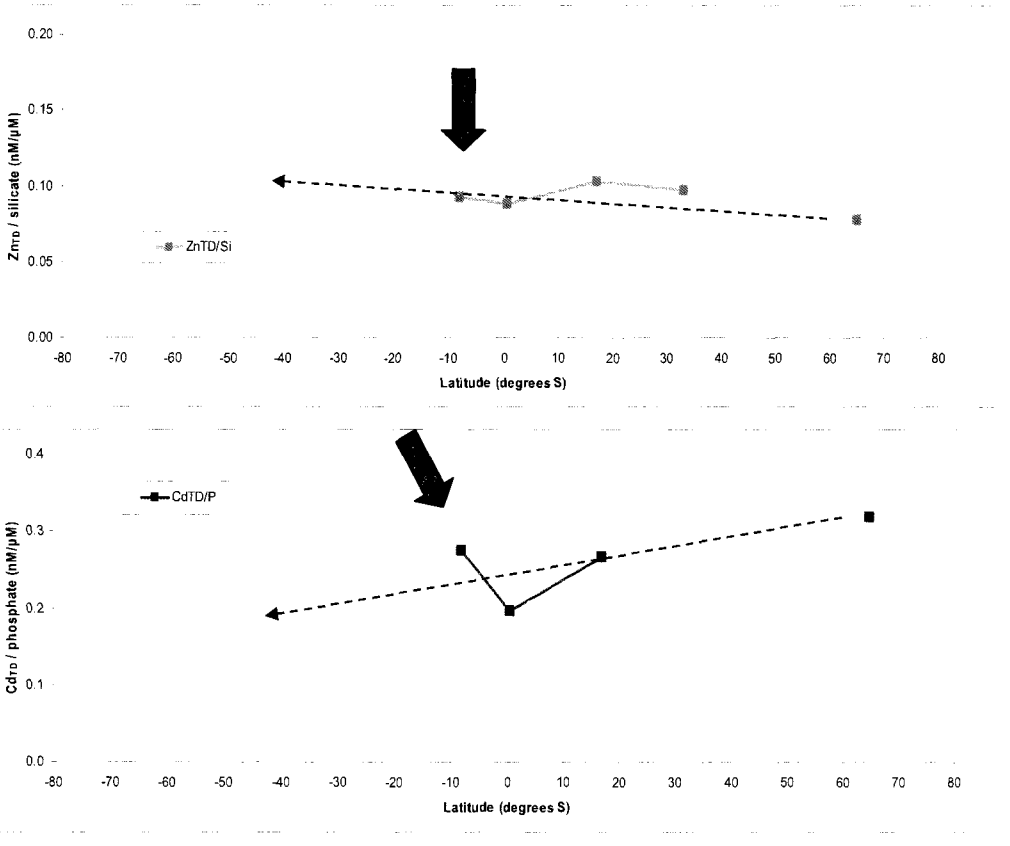

c

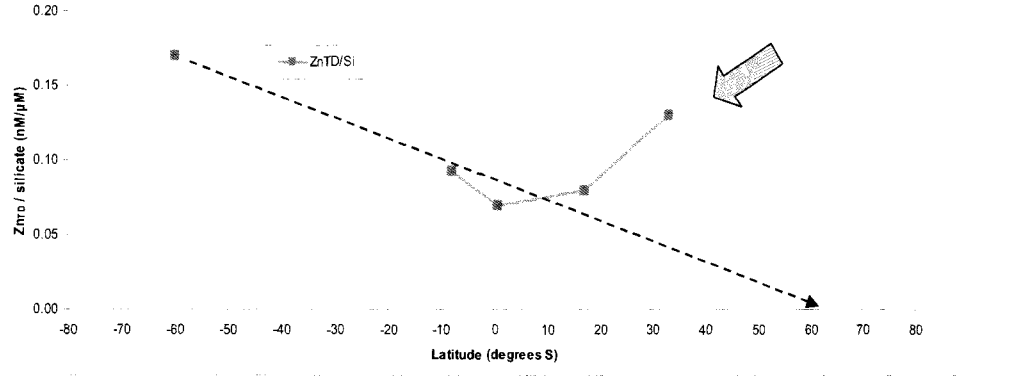

Fig. 31. Continued.

c

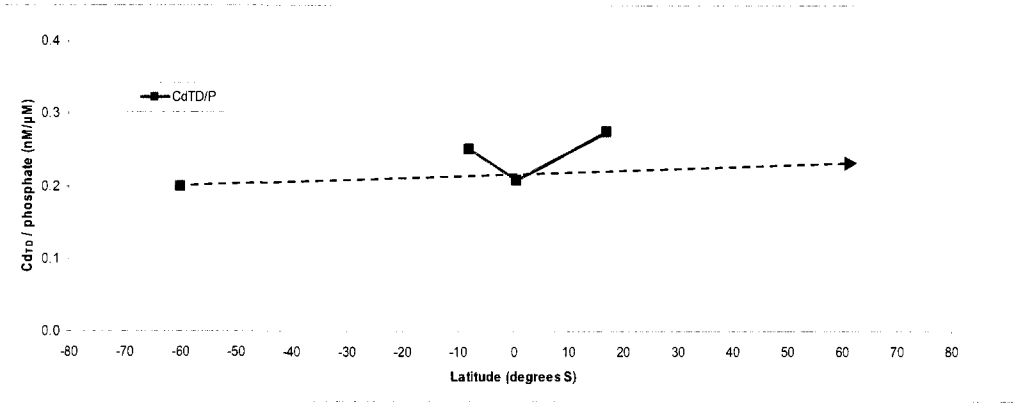

d

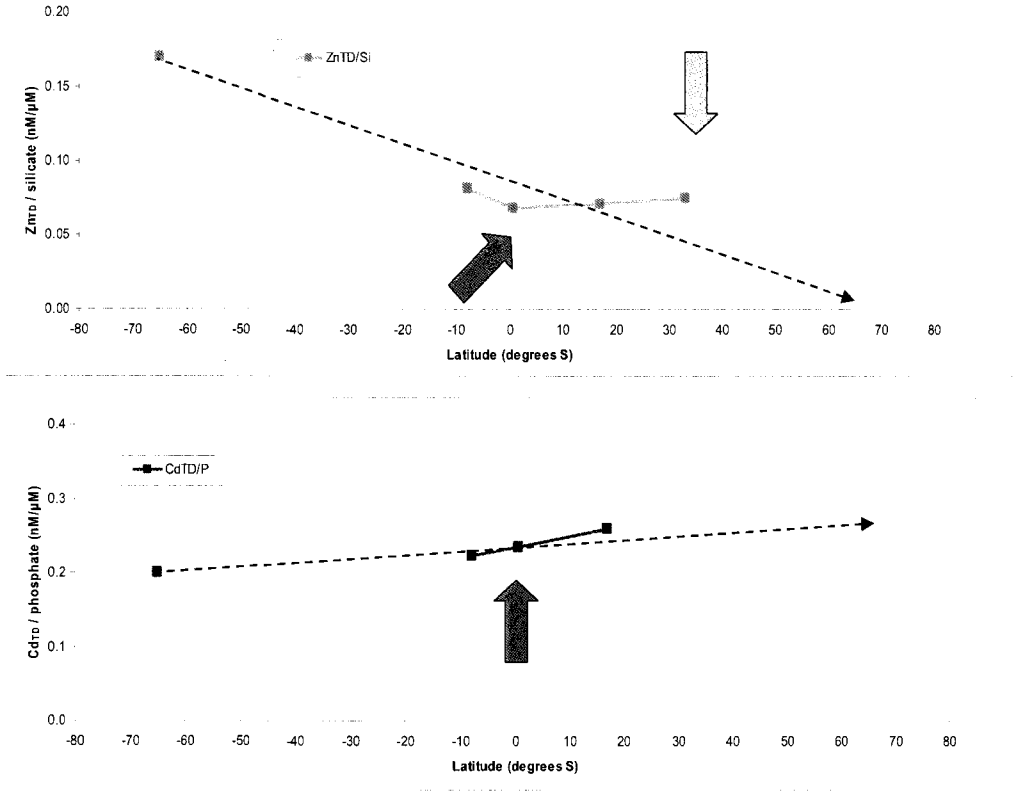

Fig. 31. Continued.

e

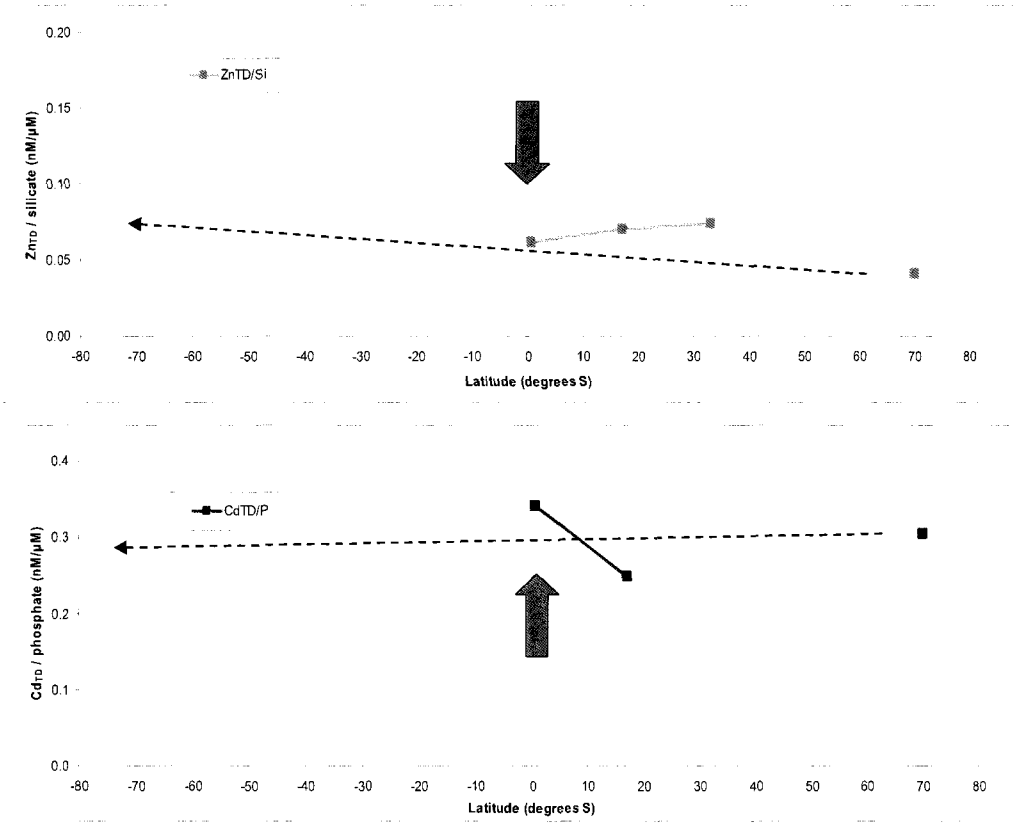

Fig. 31. Continued.

excludes the sources mentioned before (i.e. AEF, SWMF and CSMF), leaving fewer points to construe these linear trends. There is a later section in this chapter completely devoted to the Zn_{TD}/silicate and Cd_{TD}/phosphate.

Cutter and Measures (1999) calculated the percent of northern component for NADW and AABW present in deep waters at Stations 6, Romanche, 8 and 10 using deeper-than-2000m phosphate and oxygen data (following methodology from Broecker et al., 1991). With that information (shown in Table 14) and the point source concentration data (shown in Table 13), the "expected" concentrations of Zn_{TD}, silicate, Cd_{TD} and phosphate at each station can be calculated for these two water masses.

An initial plot of measured vs. expected parameter (Fig. 32) suggests that physical mixing governs the silicate and phosphate distributions. In contrast, for Zn and Cd, other processes besides water mass mixing need to be invoked, especially for Zn and Cd in AABW, presumably: a) the Zn-and-silicate rich AABW influence on NADW at Station 10, the highest point for all NADW element datasets except Cd, for which there is not one, represented as an empty blue diamond in Fig. 32 and pointed out by the light blue arrow in Figs. 33a and b; and b) particulate matter near the benthos on most of the bottom-sweeping AABW, which apparently provides a strong extra input of Zn only in the southernmost Station 10 and to a lower extent in Station 8. Remarkably, this benthic-enriched AABW silicate is the closest to have a measured-to-expected ratio ~ 1, followed by the phosphate in both NADW and AABW.

Fig. 33 contrasts the measured nutrient and metal concentrations with those calculated with the northern component and source concentrations, plotted along latitude. Data from l-NADW, "average" NADW and AABW are shown. Measured datasets are available for l-NADW and AABW; for the "average" NADW, measured nutrient and metal concentrations for u-NADW and l-NADW were averaged, to produce a dataset more directly comparable to that calculated using Cutter and Measures' (1999) data.

The influence of more nutrient- and metal-depleted u-NADW makes the "average" NADW more similar to the concentrations of expected NADW, so the focus is given to Fig. 33b rather than 33a from this point on to refer to NADW. Ignoring the two additional inputs on NADW, the trend is generally showing both more nutrients and metals than expected at Stations 6 and 8. In contrast, in AABW both silicate and phosphate are found at concentrations very close to the expected concentrations. Measured Zn_{TD} concentrations are almost twice as great as those expected in AABW at Station 10 and the source point, with a trend that gradually agrees more as the water mass ages. Particulate matter near the benthic layers in southern locations (i.e. station 10) may be related to this phenomenon, which occurs for Zn only. Alternatively, the AABW Zn_{TD} concentration might be higher than the reported ~ 5 nM (Westerlund and Ohman, 1991 and Corami et al., 2005), and more towards the ~ 8 - 10 nM reported for Lower

Table 14

Northern component percentage for NADW and AABW in the oceanic Stations (6, Romanche, 8 and 10). Data from Cutter and Measures (1999). Approximate formation latitudes from Sarmiento and Gruber (2006). Station latitudes from Table 1.

Water Mass	Approximate formation latitude	6 (8°N)	Romanche (0.59° N)	8 (17° S)	10 (33° S)
NADW	~ 65° N	91	66	70	75
AABW	~ 70° S	76	20	6	0

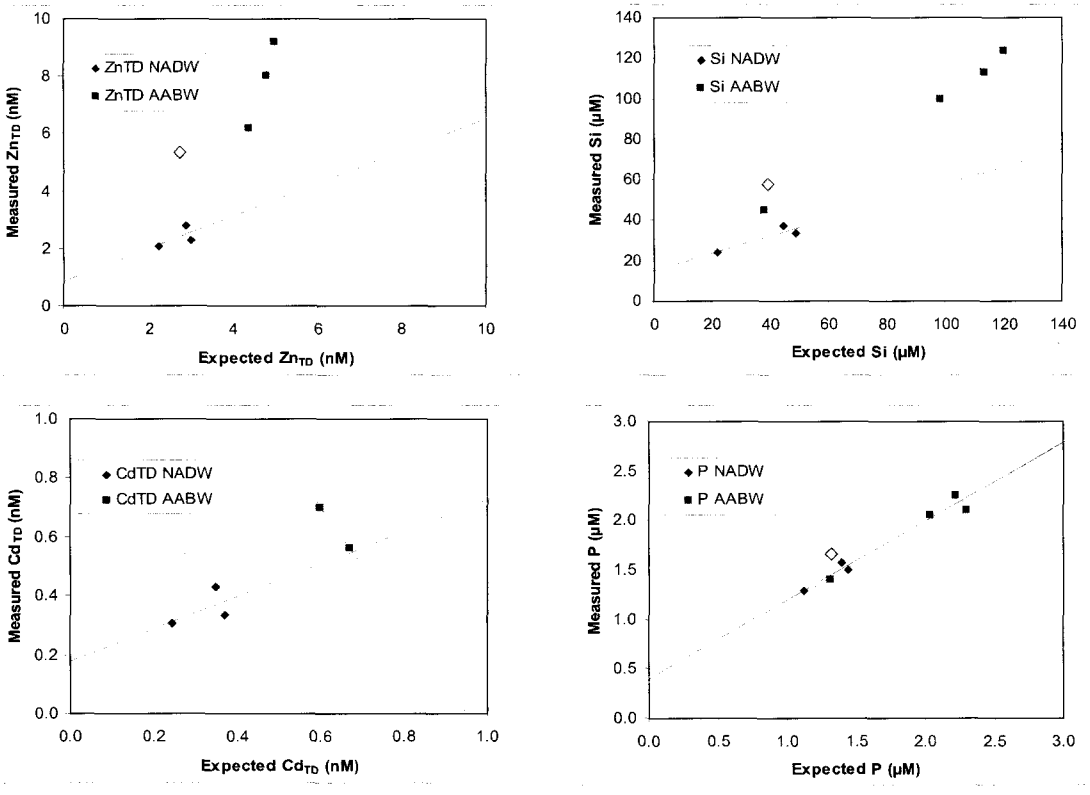

Fig. 32. Measured Zn_{TD}, silicate, Cd_{TD} and phosphate concentrations in "average" NADW and AABW as a function of "expected" concentrations, calculated from source concentration and northern component data (Tables 13 and 14).

a

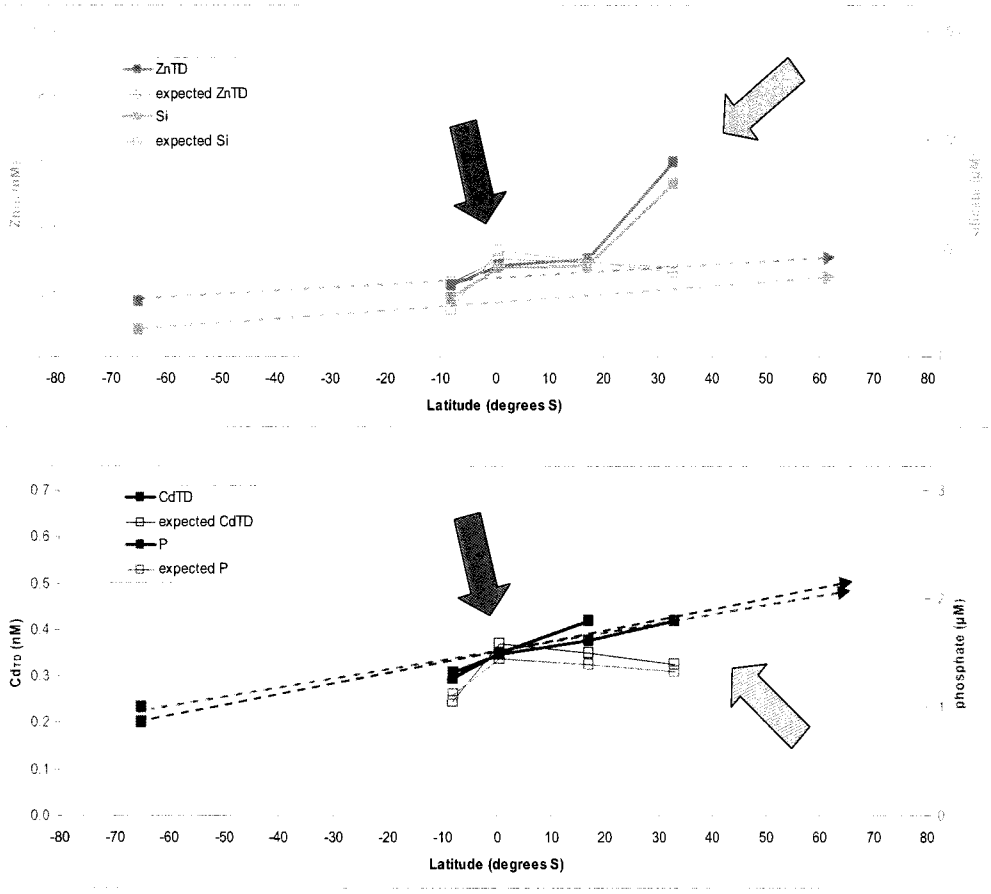

Fig. 33. Measured Zn_{TD}, silicate, Cd_{TD} and phosphate plotted against latitude at Stations 6, Romanche, 8 and 10 in specific water masses: a) l-NADW, b) "average" NADW (u-NADW and l-NADW averaged) and c) AABW; extended to the source points for each water mass compared with "expected" values. Source concentrations plotted and a linear estimation of water mass travel signal strength for each parameter, indicating direction of travel and an approximate "end point latitude" (latitude where water mass will merge into some other water mass). For comparison, the "expected" Zn_{TD}, silicate, Cd_{TD} and phosphate, calculated with the percent of northern component each water mass has at each station, according to Cutter and Measures' (1999) hydrography data, are plotted along (in empty symbols according to each metal or nutrient). Arrows highlight external factors AEF, SWMF and CSMF (see Fig. 25 for explanation).

b

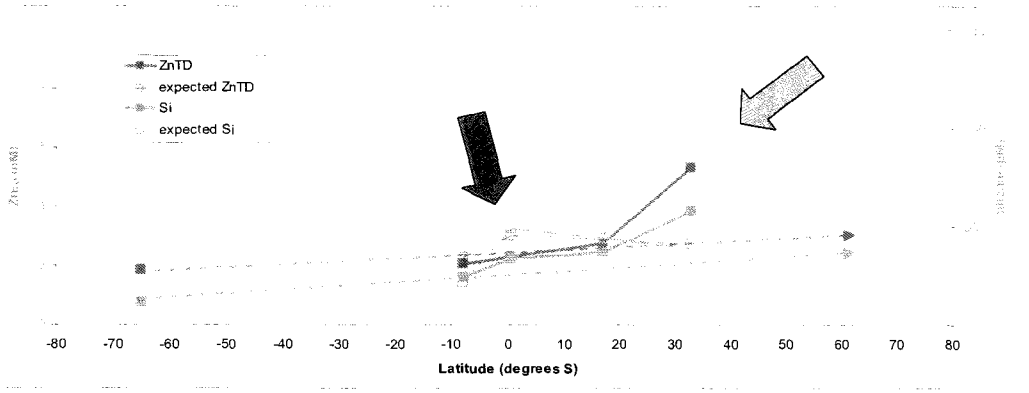

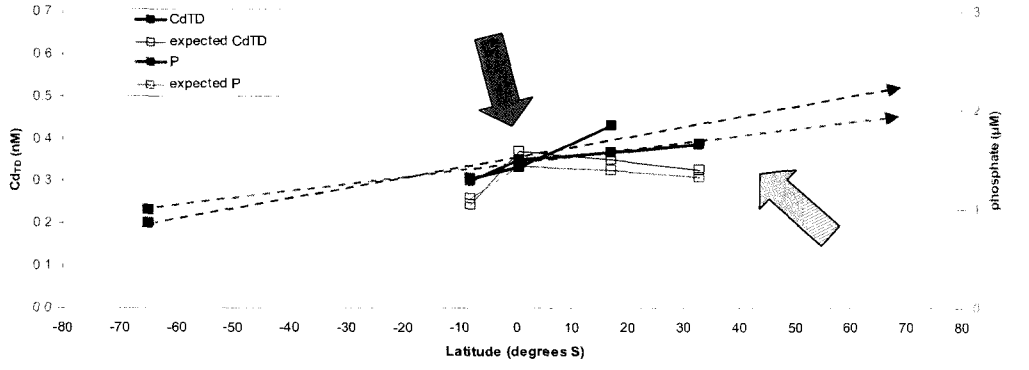

c

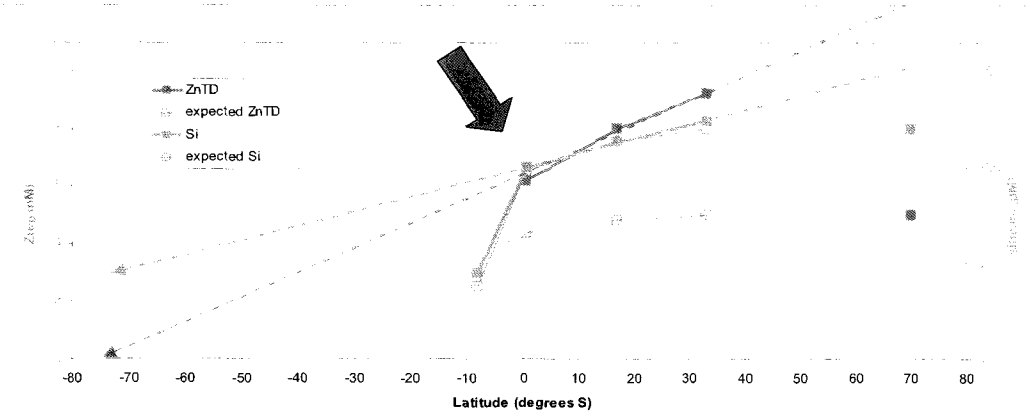

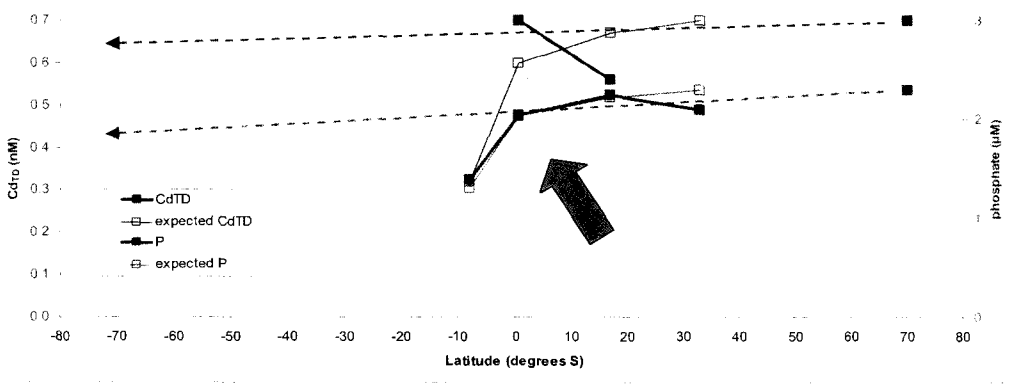

Fig. 33. Continued.

Circumpolar Deep Water (LCDW; Loscher, 1999). Studies performed in the Ross and Weddell Seas and in the Drake Passage (Corami et al., 2005; Loscher, 1999; Sanudo et al., 2002; Baars and Croot, 2010) did not find AABW's concentrations, as bottom waters directly related to AABW were either not sampled or not analyzed for Zn. However, expecting the AABW Zn_{TD} concentration to be higher than those at LCDW is not unreasonable, as Cu_{TD} and phosphate are (Loscher, 1999); this would be a more than 10 nM Zn_{TD} concentration, which would agree more with the AABW graph (Fig. 33c) than the actual ~ 5 nM Zn value.

Interestingly, with the northern component added into the calculations, the apparent Zn_{TD} and silicate extra input that I attributed to CSMF in this study (green arrows in Figs. 33b and c) seems to have ~ 30 % lower concentrations than the "expected" concentrations in the NADW at Station Romanche; also, measured Cd_{TD} is ~ 10 % lower than the expected value. The AABW silicate expected and measured values are very close to each other, and the Zn_{TD}, if ~ 10 nM source point concentration were used instead of 5 nM, would be exactly the same as the concentrations measured. In summary, the Zn_{TD} and silicate source suggested in CSMF in Figs. 25d, 25e, 30d and 30e, does not seem to be real once a component analysis (i.e. a dilution study) is performed. Thus, the simplest assumption, a linear increase or decrease in concentrations in water masses as they age, does not hold true in this case because water mass mixing seems to occur non-linearly with latitude. Alternatively, non-linear water mixing would produce a non-linear plot of its properties, which I have not explored in this dissertation, but which should be considered as a possibility.

b) Particle scavenging:

On the other hand, biogeochemical processes of diverse nature occur. Both nutrients and metals can be particle reactive to a certain extent, being adsorbed onto a particle. The particle can theoretically be classified as one with similar density to the water mass it will then travel with, or as a dense enough particle that settles down to deeper waters. Later, the metal or nutrient could eventually dissolve out of the particle near the depth where the particle is formed, further down or in the benthic region.

Another theoretical distinction can be drawn between biological uptake (into a phytoplanktonic particle) and physical adsorption (onto or into a mineral or dead-plankton particle). Corami et al. (2005) determined both particulate and dissolved Zn and Cd (among other metals) in the Ross Sea; their results show that in this very productive area of the world's oceans, where AABW is formed, less than 10 % Zn and Cd is present as particles. In contrast, a river might be different because of organic matter flocculation. DeMaster and Pope (1996) suggested this is not the case for the Amazon River, since nutrients apparently do not have any barrier that keeps them from spreading over the Atlantic Ocean, presumably in the dissolved form. In comparison, the Congo River, though a relatively less significant sediment source to the Equatorial Atlantic than the Amazon River, provides both particulate and dissolved organic matter to the region in two separate layers in surface and deep waters. The deep layer is characterized by organic matter remineralized at depths ~ 4000m, originating a distinctive low-oxygen, high-nutrients, relatively thin water mass (Vangriesheim et al., 2009). Water masses like this one, rich in organic matter that has had time to mature in the continental shelf, can transport particulate and dissolved metals very long distances, and thus can affect substancially primary productivity hundreds of kilometers downstream from the source point, like Planquette et al. (2009) has suggested for the Crozet Islands or Lam et al. (2006), Nishioka et al. (2007) and Carrasco et al. (2008) for the Sea of Okhotsk.

Upper 250m data for particle scavenging and particulate organic carbon export for this IOC 1996 cruise (Charette and Moran, 1999) is re-plotted in Fig. 34. This graph provides valuable information to estimate potential particle settling effects on chemical speciation that is discussed in depth in the following section, devoted to the Amazon effect on intermediate waters. Briefly, the Th_{234}-based results show that the POC flux at Station Amazon 1 was among the highest of all stations studied in this cruise. Further, the high POC flux is high from 50m and stays high well bellow 250m, increasing to a maximum value at 500m (value not shown in the graph), in a trend that distinguishes this station from the rest. Stations 6 and Romanche show localized high POC fluxes centered around 50 and 25m, which get respired almost completely by the time the particles reach ~ 220 and 75m, respectively, leaving no net POC flux to intermediate waters. In contrast,

Amazon 1 shows net POC flux to deeper-than-500m waters. Amazon 1's unique chlorophyll-*a* profile (Fig. 35a) and phytoplankton species (mainly diatoms, Pointkovski et al., 2003) further suggest that silicate-rich diatoms might be a major portion of this POC export flux, as there is a surface chlorophyll-*a* maximum and subsurface POC flux.

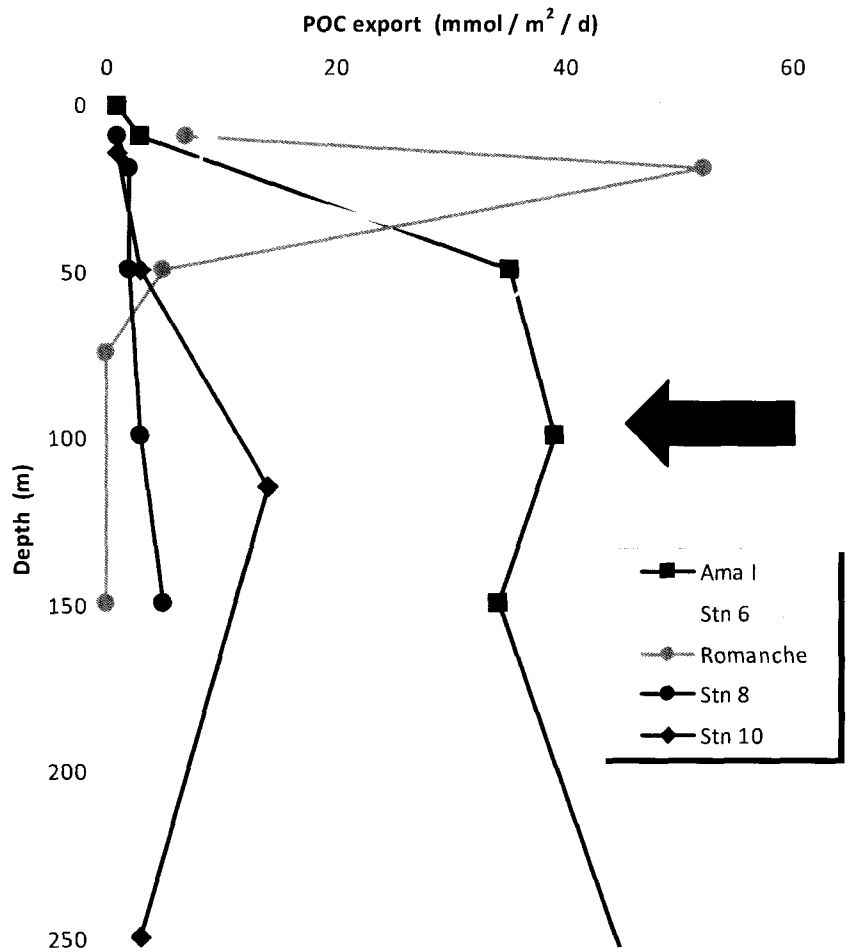

Fig. 34. Particulate Organic Carbon (POC) export (in mmol/m^2/day) depth profiles in the upper 250m of all IOC 1996 stations, except Amazon 2. From Charette and Moran (1999). Red arrow indicates net POC export in Amazon 1 Station.

In contrast, Stations 6, Romanche and 8 show chlorophyll-*a* subsurface maximums (Fig. 35a) which correlate approximately with the local POC flux maximum. Curiously, Station 10 resembles the Amazon 1 profile and Amazon 2 resembles the open-ocean stations despite its proximity to Amazon 1. This shows once again the different biogeochemical features of the Amazon Stations. Additionally, surface transect data (not shown here) from Charette and Moran (1999) show that around 5 - 6° N near Station Romanche there was a high concentrations of particulate matter related to Saharan dust, not present in any of the station profiles.

c) Colloidal fraction:

Zn has a small fraction in the colloidal size (less than 7 %), most of which is associated with large colloids in Narragansett Bay (Wells et al., 2000). Organically complexed Zn is not as particle reactive as inorganic Zn (Wells et al., 2000), presumably due to the ligand keeping Zn in solution. Thus, organically complexed Zn and Cd are in the dissolved phases mostly (Wells et al., 1998; Ellwood, 2004). The dynamics of the region of study, which includes Zn and Cd in river–seawater mixing regions in the mouth of the Amazon and organically bound Zn and Cd travelling in aging water masses, could provide valuable information.

d) Primary productivity, zooplankton grazing and bacterial respiration:

Both nutrients and metals can be affected by biological processes. Primary productivity turns dissolved nutrients and metals into living particulate phytoplankton as they are taken up, zooplankton grazing moves particulate matter from a phytoplankton pool to a larger zooplankton pool, and bacterial respiration turns organic and inorganic particulate matter into dissolved nutrients and metals.

Chlorophyll-*a* and phaeophytin data from this IOC 1996 cruise (Figs. 35a and b) are used as proxies of biomass and zooplankton grazing. Phaeophytin molecules are chlorophyll molecules with the magnesium atom in it replaced by hydrogen after being ingested and excreted by a zooplankton (Lorenzen, 1967; Welshmeyer et al., 1984) because of the gastric juices' acidity. The phaeophytin/chlorophyll-*a* ratio is a logical

a

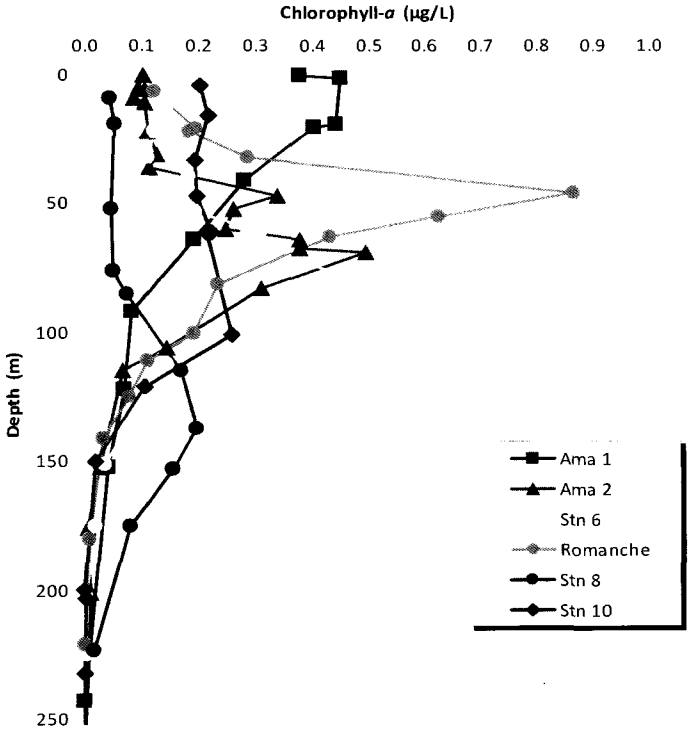

b

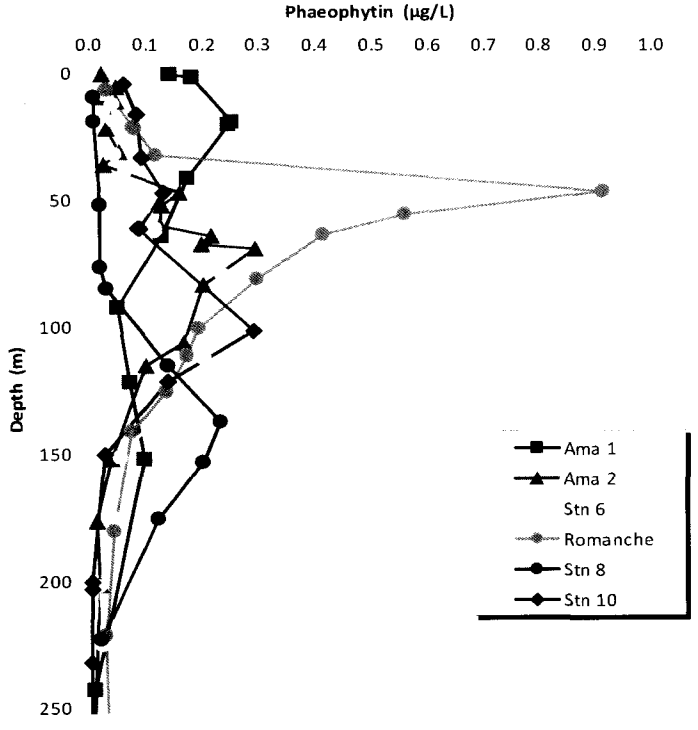

Fig. 35. a) Chlorophyll-*a*, b) Phaeophytin (in µg/L) depth profiles in the upper 250m of all IOC 1996 stations. From ancillary data.

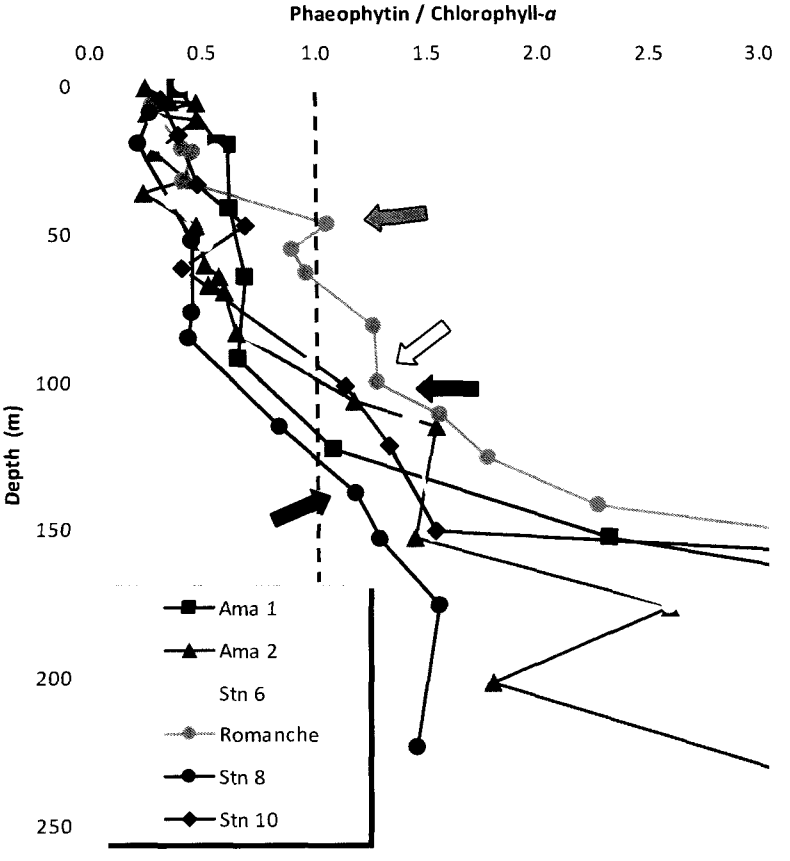

Fig. 36. Phaeophytin/chlorophyll-*a* ratios in the upper 250m from all IOC 1996 stations. From ancillary data. Arrows indicate the phaeophytin maximum depths (below a ~ 1.3 value) for Stations 6, Romanche, 8 and 10. See discussion for explanation.

biological indicator that shows the balance between grazing and productivity (Downs and Lorenzen, 1985). Fig. 36 shows the phaeophytin/chlorophyll-*a* ratios in the upper 250m at all six stations sampled.

Fig. 35 depicts the depth profiles of chlorophyll-*a* and phaeophytin from ancillary data. The most notable feature is Station Amazon 1 surface chlorophyll-*a* maximum which, in contrast to the rest of stations, shows subsurface maximum between ~ 50 and ~ 125m depth (Fig. 35a). The highest chlorophyll-*a* value is at Station Romanche, followed

by the other Equatorial Stations Amazon 1 and 2 and 6. The more oligotrophic Stations 8 and 10 show deeper, lower intensity chlorophyll-*a* maximums. On the other hand phaeophytin profiles (Fig. 35b) indicate considerable grazing occurring at Stations Romanche, 6, 8 and 10, in contrast to the lower grazing shown at the Amazon Stations. This reinforces the hypothesis of diatomaceous particle net export from near the Amazon River. These pigment data are more thoroughly discussed in the Ligand section, aiming at finding relationships between ligands and either phytoplankton biomass, zooplankton grazing or bacterial respiration.

Fig. 36 shows the phaeophytin/chlorophyll-*a* ratio profile in the upper 250m of the water column of all stations. Pigment ratios above 1.3 for each station are denoted by an arrow, below which the ratio increases to very high ranges. These high ranges represent depths below which grazing and/or respiration dominates the biogeochemical processes. The trend for this ratio throughout the water column shows higher values for Station Romanche, lower for Stations Amazon 2, 6 and 10 and lowest for Stations Amazon 1 and 8. Station Romanche has a local maximum at ~ 50m (which surpasses the phaeophytin/chlorophyll-*a* ratio of 1) and a deeper maximum at ~ 90m and below.

Some important biological ancillary data from Piontkovski et al.'s (2003) South Atlantic 40-year data record, as well as from Shipe et al. (2006) and Smith and DeMaster's (1996) data for the Amazon plume region is summarized in Table 15. Briefly, closer to continents and riverine inputs, the primary production and chlorophyll-*a* values are very high and variable, evidenced as large percentages of larger cells, notably diatoms. Both the Amazon plume and the Benguela/Angola Current show this trend, as opposed to the central gyre region, where low productivity and chlorophyll are observed in mostly small cell colonies.

On the other hand, AOU is used to constrain bacterial respiration. AOU from each station, for the exact location and month of the year from 2005's NOAA World Ocean Atlas (Garcia et al., 2006) is plotted in Fig. 37, which shows the AOU in three depth ranges: the upper 400m, intermediate and deep water masses.

In the surface waters (Fig. 37a), the profiles of Stations 6 and Romanche show high AOU below the depths where POC export occur (Fig. 34), possibly explaining the zero-net-export mentioned before. On the other hand, Station Amazon 1 shows little AOU in the upper ~ 150m, increasing to a maximum at ~ 220m, coinciding with the POC export minimum; all in all the kind and size of particles might be what makes this a positive-net export station. The profile of Station Amazon 2 resembles that of Amazon 1 and, with its chlorophyll-*a* distribution, this should be a net export station, too, if diatoms also live in the sub-surface silicate-rich waters above ~ 32m.

The intermediate and deep water masses (Figs. 37b and 37c), trackable by the σ_t and σ_4 source label values used in Table 12 and the shaded colors used in Figs. 17, 20, 21 and 22 show the AOU effect on the intermediate and bottom waters (AAIW, CPDW and AABW) more than on the deep waters (u-and l-NADW). As predicted, the equatorial stations are more affected than the higher latitude ones. This agrees with Mason and Sullivan's (1999) AOU data from the ~ 30° W transect, an estimate to this cruise's latitudinal locations. AAIW is affected more in Stations 6 and Romanche and to a lower

Table 15

Some biological parameters of the dominant phytoplankton species in regions near the IOC 1996 stations. South Atlantic data from Piontkovski et al., 2003; Amazon plume data from Smith and DeMaster, 1996 and Shipe et al., 2006.

Current/Region	IOC1996 Station	Relative Primary production	Average Chl-*a*/SD (μg/L)	Large (>5μm) species %	Phytoplankton Species
Amazon Plume	Amazon 1 and 2	Highest variable	Up to 25.5 variable		Diatoms (Bacillariophyceae)
Benguela/Angola current		High	3.0/1.5	> 95	Diatoms (*Chaetoceros*)
South Equatorial Current	Romanche	Medium	0.15/0.05	20	Pyrrophyta, Chrysophyta
Central gyre	8	Lowest	0.09/0.04	8	Pyrrophyta, Chrysophyta
Subtropical Brazil Current	10	Low	0.30/0.10	22	Diatoms and Chrysophyta

extent in Station 8. CPDW seems to be affected by AOU in equal amount for all stations, except for Station 10, which should have purer CPDW characterized by low oxygen values caused by the ACC water not being exposed to the atmosphere recently. The deep waters show other interesting feature, a local AOU maximum between u- and l-NADW in Stations 6 and Romanche (resolution on other stations is poor and it can not be

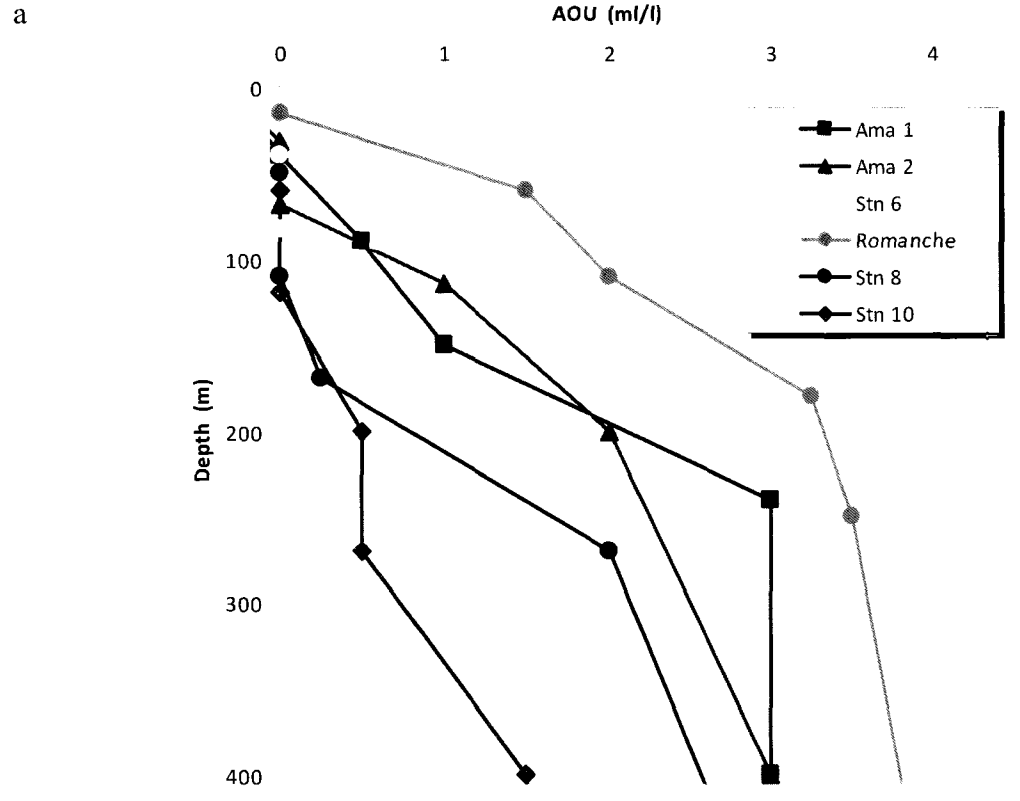

Fig. 37. Approximate Oxygen Utilization (in ml/l) in a) upper 400m in all IOC 1996 stations, b) intermediate and c) deep water masses in Stations 6, Romanche, 8 and 10. Shaded areas indicate water masses: AAIW (green), CPDW (yellow), NADW or u-NADW and l-NADW (red) and AABW (brown), see Table 12 for σ_t and σ_4 label values. Data from Garcia et al. (2006).

b

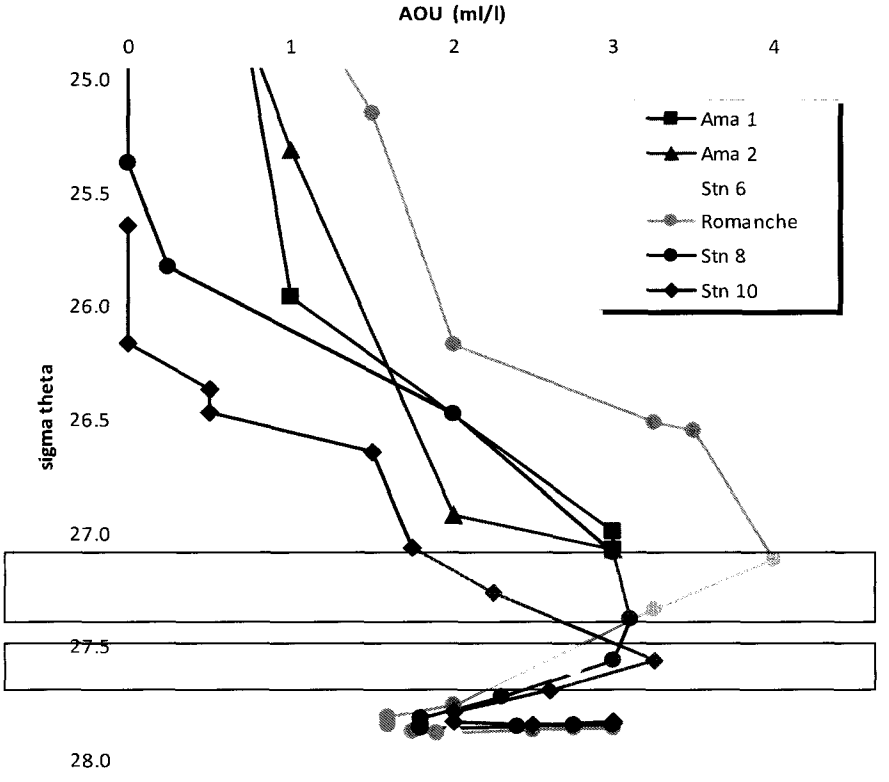

c

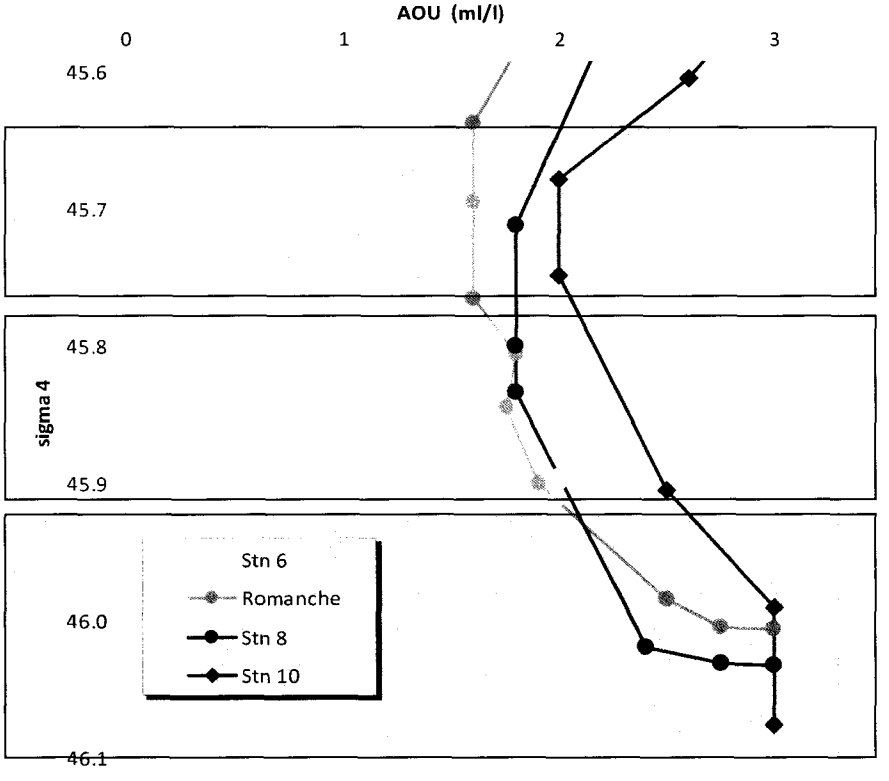

Fig. 37. Continued.

elucidated if a similar feature exists) that might be a counter argument for the Congo riverine organic matter. AABW shows high AOU values for Stations 10 and Romanche, probably related to the benthos or the same reasons that make CPDW high AOU (i.e. some water from the ACC) despite both AABW and CPDW being younger than, for example, both u- and l-NADW at either station.

e) Chemical decay and formation processes:

Metal-complexing ligands may undergo chemical decay processes or the opposite, formation as organic matter ages and a metal complexing ligand is produced. First, a distinction needs to be made between organic matter in general and metal-complexing organic ligands. The ligands are such a small part of the total organic matter pool, as indicated by their respective nM and μM concentration ranges, that the chemistry that governs dissolved organic ligand production and decay may be different from the chemistry that governs dissolved organic matter (DOM) decay. DOM, as a whole, relates more to organic matter, arguably terrigenous in origin and geobiopolymeric in nature; strong ligands are hypothesized to be produced by organisms to actively acquire or detoxify some bioactive metals. However, there is evidence of a Fe complexing ligand produced by viral destruction of phytoplankton, (i.e. the "bug gut" sort of ligand; Poorvin et al., 2004), and of Zn and Cd complexing ligand from other non-specific metal complexing substances (i.e. humic substances; Christensen and Christensen, 2000), but they are generally weaker ligands. The high metabolic cost of producing such strong metal-binding substances makes it unlikely that the strongest ligands be "accidental" metal binding substances.

The degradation of organic matter by photic (e.g. Spencer et al., 2009) and non-photic processes (e.g. Hernes and Benner, 2002) has been studied. In general, most terrestrial organic matter that makes it to the sea gets degraded and respired, and the small amount (global average ~ 50 μM) that survives the photochemical attack is reputedly very refractory and old (Eglinton and Repeta, 2003). In contrast, only two studies have reported on the degradation of strong metal binding ligands (e.g. Rijkenberg et al., 2006; Gerringa et al., 2008) and both studies focused on Fe-binding ligands. Their results are

variable and not much can be linked with Zn- and Cd-ligands because of the different redox chemistry that Fe undergoes in comparison to Zn and Cd. Presumably, they are different chemical entities.

Mason and Sullivan (1999) reported on the degradation of methylated Hg species; they estimated net formation or decay rates in specific water masses are estimated using concentrations and travel time between the same IOC 1996 stations. We have little definitive knowledge about the chemical identities of Zn and Cd complexing ligands, and we know even less about the chemistry behind the possible degradation processes they may undergo. In this study, I used the the same pragmatic approach as Mason and Sullivan (1999): sources are explored and increasing or decreasing concentrations are attributed to formation or decay processes. Using an estimate of the amount of time it takes for a water mass to travel from one station and other, net formation or decay rates are calculated.

5.4.5. Data interpretation and uncertainties

Figs. 25 - 29 show the Zn_{TD}, Cd_{TD}, silicate, phosphate and ligand concentrations, the Zn_{TD}/ silicate and Cd_{TD}/phosphate ratios, the stability constants of Zn and Cd ligands and the chemical speciation of Zn and Cd at each water mass. The following pages describe my interpretation of these data.

NADW and AABW, the two deepest water masses in the Atlantic Ocean, have relatively well-constrained geochemical features. Water can only advect between them due to the fact that AABW is the bottom water mass and that the NADW complex system has u-NADW encapsulating l-NADW underneath. Thus, they are easier to constrain than CPDW or AAIW. When the northern component analysis and the subsequent "expected" vs. measured nutrient and metal data trends were explored for NADW and AABW (Figs. 32 and 33), it became clear that there is some uncertainty inherent to interpreting the nutrient, Zn, Cd, ligand and chemical speciation data (Figs. 25 - 29) without considering both a) the relative dilution of each water mass at each point of its path, plotted in these figures in a simplified version as a latitude transect, and b) the source point's

concentrations of Zn_{TD}, Cd_{TD} and nutrients, with the added uncertainty those numbers pose on "linearized" trends as water masses age (Figs. 30 and 31). A very conservative approach would have been to report only the station's data and compare it with some sources, not attempting to discover or rationalize a trend. So, the trends discussed next should be taken with their uncertainties in consideration.

Unfortunately, there are very few chemical speciation studies that involve waters deeper than ~ 500m; and even fewer that involve water masses directly comparable with those analyzed in this cruise (Ellwood and van den Berg, 2000; Baars and Croot, 2010). This may be because deeper waters were believed not to have significant ligand concentrations (Bruland, 1989; 1992). Only recently have deep waters been studied for chemical speciation (for Cu: Moffett and Dupont, 2007; for Zn and Cd: Carrasco et al., 2008). This study, thus, presents results on Zn, silicate, Zn ligand concentrations and stability constants and Zn speciation that can only be compared specifically to Baars and Croot (2010) for the AAIW and Ellwood and van den Berg (2000) for the u-NADW. Those comparisons are shown in Figs. 38 and 39. For the rest of water masses (CPDW, l-NADW and AABW), a comparison with the nutrients and metals source point concentrations is the best that can be done at this point (Figs. 30 and 31 which extend Figs. 25 and 26) as there are no data from these water masses to extend Figs. 27, 28 and 29.

The data shown in Figs. 25 and 26 has been discussed previously in the description of Figs. 30, 31 and revised again on Fig. 33. Briefly, water masses originating in the Southern Ocean show high concentrations of nutrients, Zn and Cd that decrease as they age. In contrast, both u- and l-NADW show concentrations that apparently increase as they travel south, presumably caused by the influence of southern components. Over this general south-to-north gradient, two point sources can be discerned: a) one point source near the Amazon River mouth at equatorial latitudes, where extra nutrients and metals are observed (high Zn_{TD} and Cd_{TD}, moderately high silicate and phosphate) in AAIW and CPDW at Station 6, and b) another, more subtle point source in l-NADW and AABW at Station Romanche, possibly connected to Congo River shelf material

remineralized and transported here (high silicate, Zn_{TD} and phosphate, and apparently no Cd_{TD}). After a more detailed analysis, the second apparent source is found to be a Zn sink instead (Fig. 33). Red and green arrows in Figs. 25 - 29 and others highlight each of these external sources, respectively the Amazon River/Equatorial region (AEF) and the Congo River remineralized Shelf Matter (CSMF), while the blue arrow indicates the heavier influence of Southern Water Masses (SWMF), introduced earlier in this discussion.

My assumption here is that Zn and Cd ligands were produced in the surface waters when the water masses were formed in response to the Zn_{TD} and Cd_{TD} concentrations present at the point source at the moment of water mass formation. Fig. 27 follows the concentrations of metals and ligands as water masses travel.

5.4.6. Ligand saturation: an apparent artifact

An issue that arises from the use of ASV to determine ligand concentrations and stability constants and the fact that deeper waters have higher Zn_{TD} and Cd_{TD} concentrations is that the ligands could be saturated. In such a case, it is difficult to mathematically distinguish different ligands that might be present, and in some cases it becomes impossible to obtain a stability constant and only the total ligand concentrations can be estimated. Baars and Croot (2010) encountered this problem when trying to interpret metal titrations of samples they obtained from the Southern Ocean directly in and across the Drake Passage (further south of 48° S and south of 56° S). I encountered a similar situation in analyzing deep samples from high latitude that also contained high Zn_{TD} and Cd_{TD} concentrations. That is, the deepest sample from the southernmost location was the most prone to saturation of Zn and Cd ligand by elevated Zn_{TD} and Cd_{TD} concentrations and, as such, metal titrations were harder to interpret when compared with shallower samples from locations from lower latitudes. A direct consequence of this is that there are more L than log K' data, as discussed before. This is observed when comparing Figs. 21e and 21f with Figs. 20e and 20f; here, deep, southern Stations 8 and 10 have ligand concentrations in the profiles, but only a few logK' data.

Over the complete cruise track, I am able to distinguish three Zn ligands and three Cd ligands. I have compared the Zn ligand concentrations and stability constants from the Atlantic Ocean to those of the ligand reported by Baars and Croot (2010) for the Southern Ocean - they report one ligand with logK' ~ 10 and one inert ligand they did not discuss because of different methodology - and with the Zn ligand reported by Ellwood and van den Berg (2000) for the North Atlantic Ocean, also with a logK' ~ 10. In general, a similar trend is observed for the Zn and Cd ligand concentrations as for the two metals, i.e. decreasing ligand concentrations as northward-moving water masses age or flow away from their source points and increasing concentrations as southward-moving water masses approach the Southern Ocean influence. Cd ligand plots show more scatter than those for Zn ligands, probably because of the lower concentration of both Cd_{TD} and Cd ligands, which would make Cd complexation analysis more difficult than for Zn.

At locations with higher Zn_{TD} and Cd_{TD} concentrations, their ligands were present at slightly lower concentrations than the metal they bind, so the ligand has an apparent net decay rate lower than the metal's "decrease" rate (metals can undergo biological or particle scavenging or are diluted as advective mixing occurs between water masses). This trend can be observed in the plots of Zn L3 and Zn_{TD} in AAIW, l-NADW or AABW (Figs. 27a, d and e). Knowing the amount of time it takes for these water masses to travel from Station 10 to Romanche (approximately 30 years), a simple calculation yields the following decay or decrease rates: ~ 0.14, ~ 0.04 and ~ 0 nM/yr for Zn_{TD}, Zn L3 and Zn L1 in AAIW (Fig. 27a), the water mass with the smoothest plots, the least tendency to undergo the ligand saturation issue mentioned earlier and thus, the easiest to work out.

Another way of studying this phenomenon is using the M_{TD}/L ratio, like Gerringa et al. (2010) did with Fe in Southern Ocean waters to identify them and track them in a very similar way to what has been done in this study. For the other water masses and for Cd, either more scattered plots or lack of enough data points (for Cd there are no Station 10 data) or the dominant effect of the influencing factors (in deeper waters) makes it difficult for this calculation to be performed and to obtain decay or decrease rate values which confidently represent the water mass trend.

5.4.7. The three influencing factors

The three influencing factors (AEF, SWMF and CSMF), which showed differences among themselves when the nutrient, Zn_{TD} and Cd_{TD} plots are analyzed, show further defining differences when ligand concentrations are studied.

First, AEF is a larger source of complexing ligands than it is of metals for Zn (on average, ~ 6.9 nM ligand total, L_T, is present in clear excess of the average ~ 2.5 nM Zn_{TD}), but not for Cd (~ 0.40 nM L_T for ~ 0.60 nM Cd_{TD}), as shown in Figs. 27a and b for AAIW and CPDW at Station 6. Because of the size of the error bars, the trend observed for changing L_T for Zn and Cd with depth in these two water masses (that could be extended to the next deeper water mass, u-NADW, Fig. 27c) does not show conclusive results. Still, very similar or slightly decreasing L_T and L3 concentrations could imply a shallower origin and a potential relationship with particulate fluxes of organic matter (Charette and Moran, 1999) and trackable in origin to the Amazon River or to the equatorial Atlantic region to intermediate (the depth where AEF is observed) and possibly deeper waters (as hinted by the L_T and L3 concentrations in u-NADW).

Secondly, the SWMF influence is focused on Station 10 only and then could only be evaluated for Zn because of missing Cd data. In contrast to AEF, the Zn-binding ligands' concentrations remain lower than Zn_{TD} itself (averages ~ 4.0 nM L_T for ~ 5.3 nM Zn_{TD}, Figs. 27c and d). l-NADW shows a larger SWMF effect than u-NADW (6.6 nM L_T for 6.0 nM Zn_{TD} compared with the 1.3 L_T for 4.6 Zn_{TD}). Note that for l-NADW, L_T is slightly higher than Zn_{TD}, due to this station's proximity to the metal and ligand source, the Southern Ocean region.

Finally, the CSMF influence, much like that of AEF, appears to be more a source of ligands than of metals. In fact, in l-NADW at Station Romanche (Fig. 27d), there is ~ 6.4 nM L_T for only ~ 2.8 nM Zn_{TD}, as well as ~ 0.48 nM L_T for ~ 0.35 nM Cd_{TD}. But the most outstanding evidence of an important localized source of organic complexing ligands is in AABW at Station Romanche where ~ 19.1 nM L_T are found to be complexing ~ 6.3 nM Zn_{TD}. Note that such high L_T concentrations have never been

reported in oceanic waters; for comparison Donat et al. (2002) reported ~ 20 nM L_T for ~ 7 nM Zn_{TD} in the water column of the Chesapeake Bay mouth, a zone where benthic fluxes are reportedly important sources of ligands and metals. AABW at Station 10 could not be successfully analyzed because of the ligand saturation effects, but out of its depth profile (Fig. 21f) ~ 10 nM L1 and ~ 11 nM L3 have been estimated (based on the heavy southern component influence on l-NADW and on the linear Zn and ligands increase with depth) and are shown in parentheses in Figs. 21f, 22f, 27e and 29e. These values in AABW at Station 10 would mean ~ 21 nM L_T for ~ 9.3 nM Zn_{TD} are found in the southernmost AABW station studied in the IOC 1996 cruise. These high values can be understood at this latitude in this specific water mass, which forms when Weddell Sea bottom waters move north, sweeping the continental shelf of Antarctica at ~ 3000m (Johnson, 2008) and producing a very nutrient- and metal- and presumably also ligand-rich water mass. As AABW travels northward, at Station 8, ~ 5.6 nM L_T for ~ 8.1 nM Zn_{TD} are the remains of what I believe to be the water mass with the highest concentrations of Zn, Cd and ligand, compared with the other water masses present. A projected linear decay from Station 10 to 8 to Romanche would leave zero ligands by the time this water mass reaches Station Romanche, suggesting that those ~ 19.1 nM L_T come directly from a localized external source. Notice that the Zn_{TD} decreases linearly from Station 10 to Station 8 to Station Romanche, confirming that CSMF at AABW (as well as at NADW, analyzed carefully in Fig. 33) is not a source of Zn_{TD}, but of Zn ligands.

The logK's shown in Fig. 28 correlate well with those from globally reported Zn and Cd ligands (Table 8). The Baars and Croot (2010) and Ellwood and van den Berg (2000) studies were performed in locations that are very closely related to source points for water masses analyzed and discussed in this study. Due to ligand saturation, there are more data from intermediate depth water masses than from deeper water masses; also, there are more data for Zn ligand than for Cd ligands. In general, a gradual decrease of ligand stability constant is apparent as water masses move away from their source points. Clear examples are found in AAIW, CPDW and to a certain extent in l-NADW and AABW. There seems to be no SWMF effect for this. Fig. 28a shows logK' for Zn L3 decreasing from ~ 9.6 to ~ 8.7 log units in AAIW as it moves northward; Fig. 28d shows

logK' for Zn L3 decreasing from ~ 9.0 to ~ 8.6 in l-NADW as it moves southward; and Fig. 28e shows logK' for Zn L3 decreasing from ~ 8.5 to ~ 8.1 in AABW as it moves northward. This apparent systematic decrease in ligand strength is discussed in extent later using Fig. 38, where a 5-point decreasing trend is interpreted for AAIW, the water mass that shows this trend more clearly, when the source point logK' of Baars and Croot (2010) is included. The limited Cd data show a similar general trend for logK' for Cd L3, though having only three stations' data (no Cd data for Station 10) makes the interpretation difficult.

Given that AEF and CSMF are sources of ligands more than of metals, there is a lesser degree of ligand saturation in the samples influenced directly by these factors and thus, it is possible to obtain logK' values. However, since the preceding or following samples in the water mass path are prone to ligand saturation, there are fewer points to compare logK' against (Figs. 28d and e). Thus, influencing factors are more difficult to distinguish from the general trend using stability constants than when using ligand concentrations. AEF appears to locally introduce Zn L1 (with a distinctly stronger, logK' ~ 3 orders of magnitude higher than the relatively weak ligand Zn L3 present in all stations in both AAIW and CPDW) and to increase the logK' for Cd L3. SWMF shows merely one point at l-NADW, with a logK' for Zn L3 that follows the ligand strength decrease trend. Finally, CSMF appears to provide strong ligands Zn L1 and Zn L2 (like AEF), while Zn L3 seems to be present in the southernmost point of both water masses. In sum, not only are AEF and CSMF sources of ligands more than metals, they appear to be localized sources of strong ligands over the general decaying trend of weaker ligands.

Fig. 29 summarizes graphically the matters of study reported in here. On the left graphs, the concentrations of Zn_{TD} and Cd_{TD} and the concentrations of Zn- and Cd-binding ligands are shown, combining weakening, aging ligands from water mass source points (with time scales in the order of hundreds of years) with the stronger, presumably fresher, younger ligands (particle flux, on time scales of weeks to months) coming from the external influence factors discussed previously (AEF and CSMF mostly, and SWMF to a certain extent, too). The graphs on the right show the Zn^{2+} and Cd^{2+} concentrations,

the direct result of the ligands' presence on Zn and Cd's chemical speciation.

The left graphs in Fig. 29 show the Zn_{TD}, Cd_{TD} and ligand concentrations in a normal linear scale. The external influences (indicated by the color-coded arrows mentioned before) can be compared with general water mass trends discussed previously. The right graphs show the M_{TD} and M^{n+} data, plotted in a negative logarithmic scale (pM_{TD} and pM^{n+}) for both Zn and Cd. Reference neritic phytoplanktonic species limiting Zn^{2+} and general species toxic Cd^{2+} concentrations are plotted along as dashed and dash-and-dot lines. The blue and pink bars represent the extent of inorganic complexation of Zn and Cd in seawater (at environmental salinity, pH and temperature) expressed in log units. These average 0.36 and 1.57 log units for Zn and Cd in seawater (at salinity = 35, pH = 8.2, temperature = 278 K). As introduced in the Results section, a wide M_{TD} - M^{n+} gap represents a major difference between the concentrations of Zn_{TD} and Zn^{2+} and Cd_{TD} and Cd^{2+} because of organic complexation of Zn_{TD} and Cd_{TD} in addition to inorganic complexation. A narrow gap, at depths where there is little or no organic ligands present, represents a small difference between the concentrations of Zn_{TD} and Zn^{2+} and Cd_{TD} and Cd^{2+} because of minimum or no organic complexation, as only inorganic ligands complex Zn and Cd. The double headed arrows indicate the location and the approximate degree to which this M_{TD} - M^{n+} gap extends in the specific locations where the external influences are observed; they are color-coded in the same way that the external influences are. Finally, in parentheses in Fig. 29d, a point of l-NADW estimated from a slightly underlying water mass, and in Fig. 29e, estimated points (explained in detail in the description of Fig. 27).

Because of the logarithmic scale used in the right half, the Zn_{TD} and Cd_{TD} changes from one station to the next seem less pronounced than in the left graphs. The amount of total complexed Zn, visually represented in the Zn_{TD} - Zn^{2+} gap, has a larger variability (~ 3.65 to ~ 0.40 log units) than the amount of total complexed Cd, the Cd_{TD} - Cd^{2+} gap, (~ 1.78 to ~ 1.54 log units) in these water masses. Thus, Zn speciation gets more heavily affected than Cd's by both water mass trends (as can be observed in Figs. 29a and b, as the amount of total complexed Zn increases as AAIW and CPDW move from Station 10

to 8 to Romanche, Zn gaps get wider) and external influencing factors (as can be seen in Figs. 29a - e in the locations where double-pointed arrows show that the amount of total complexed Zn increases, where the Zn gap widens).

Focusing first on Zn, the clearest example of the preferential ligand preservation trend in an aging water mass is observed in AAIW as it moves from Station 10 to Station 8 and then to Station Romanche. On this transect, as Zn_{TD} decreases from ~ 5.5 to ~ 1.4 nM and Zn L3 decreases from ~ 3.4 to ~ 2.4 nM only, the consequence is the increased extent of total complexed Zn (the Zn_{TD} - Zn^{2+} gap widens) observed in Fig. 29a. This water mass trend is disrupted by the time AAIW reaches Station 6, where higher Zn_{TD} and much higher organic ligand concentrations are brought in by AEF, causing great extent of total complexed Zn, indicated by the very long double headed red arrow.

Baars and Croot followed Zn_{TD} and Zn L3 in surface waters along the Zero meridian in the Southern Ocean from ~ 68° S to ~ 46° S (Baars and Croot, submitted) and compare their data to Ellwood's (2004) Subantarctic Pacific data at ~ 37° S. Southern locations have a high Zn/L ratio that decreases as surface waters move northward. That is, Zn_{TD} decreases drastically while L does not decrease much. As a consequence Zn^{2+} concentrations decrease a lot from the southernmost to the northernmost locations.

The results from this study are from AAIW and time frames of transport are different from that of Baars and Croot (submitted), in the order of months for surface waters vs. decades for intermediate waters. Spite this difference there is a similar phenomenon of preferential ligand preservation. On the other hand, the relative similarity of preferential ligand preservation in surface and interemediate waters also means that the Zn ligands measured in the surface waters have probably little photolability; and, since both ligands originate in very similar and close locations near the Southern Ocean, the ligands in intermediate waters, by extension, may be non-photolabile too.

In a localized manner, AEF and CSMF, the influencing factors that bring in more ligands than metals into the studied water masses, produce greater amounts of total

complexed Zn (wide Zn_{TD} - Zn^{2+} gaps), with Zn^{2+} being reduced to values close to or even below limiting. Specifically, AEF produces very low Zn^{2+} in Station 6 at AAIW and CPDW (Figs. 29a and b). Similarly, CSMF appears to produce very low Zn^{2+} in Station Romanche at l-NADW and AABW (Figs. 29d and e).

Looking into the Zn_{TD}/L_T ratio in different water masses influenced by AEF, a lower ratio is observed in AAIW, the ratio gets slightly higher in CPDW, and it decreases in u-NADW (the uncertainties of some of the parameters involved in these water mass calculations do not allow for making conclusive statements, though). The length of the double-headed red arrow in the right Zn graphs of Figs. 29a, b and c decreases from ~ 2.8 to ~ 2.5 to ~ 1.6 log units as AAIW, CPDW and u-NADW are compared; suggesting the extent of organic complexation produced by AEF gets smaller with depth, presumably because of ligand respiration, adsorption onto particles or ligand decay processes.

The CSMF influence also causes a low Zn_{TD}/L_T ratio in both l-NADW and AABW, because of the presence of high concentrations of Zn L1 and L3 (and L2 in AABW). The ligands present bring the Zn^{2+} concentration below and close to the limiting concentration in l-NADW and AABW. These, the greatest amounts of total complexed Zn in all water masses in this IOC 1996 study, average ~ 3.4 and ~ 3.3 log units and are observed in the double headed green arrows in Figs. 29d and e. The hypothesis that benthic fluxes at Station Romanche influence the bottom waters is weakened by the fact that the very similar amounts of total complexed Zn in both l-NADW and AABW can not be explained by potential benthic fluxes; in fact, this may indicate a common process occurring for both water masses or a process that occurs in between these two water masses, maybe the ~ 4000m deep organic rich Congo River water, and spreads out vertically.

In contrast to the two influencing factors just discussed, SWMF clearly brings more Zn_{TD} than L. This influencing factor is observed in u-NADW mostly as Zn_{TD} (at higher concentrations than the only ligand present, L3; Fig. 29c) and in l-NADW as both Zn_{TD} and ligands (both L3 and L1, coming presumably from the closer source points;

Fig. 29d). Thus, the amount of total complexed Zn is contrastingly lower in u-NADW compared with l-NADW (~ 0.3 and ~ 2.5 log units). In this extent, the amount of total complexed Zn in l-NADW resembles that in AABW (~ 2.4 log units), though this can not be assessed with much certainty because of the estimated ligand concentrations in AABW at Station 10.

Adding both the water mass trend and the pointsome influences together, the general trend is a large amount of total complexed Zn (i.e. low Zn^{2+}) at lower latitudes and lesser total complexation (i.e. higher Zn^{2+}) at high latitudes. Exceptions to this trend are l-NADW and AABW, where high Zn_{TD} and very high concentrations of very fresh (less than 10 years old) L_T coming presumably from the south provides locally a source of low Zn^{2+} at Station 10 in these deep and bottom water masses.

Focusing on Cd, the situation is less clear because of the lack of Cd information from Station 10 which does not allow for evaluation of SWMF for Cd, and also because the changes in the amount of total complexed Cd in all of these water masses from station to station are very subtle. The latter means that the Cd gap is relatively constant, ranging between ~ 1.78 to ~ 1.54 log units. The sources do not appear to be as consistent and reproducible as they were for Zn. AEF appears to be a metal-in-excess-of-ligand source in both AAIW and CPDW. CSMF does not show clear trends, because at l-NDAW it appears as a clear maximum of Cd L3 in excess of Cd_{TD} at Station Romanche that does not match with AABW's data, which shows Cd_{TD} in excess of L3.

The left graphs show some ligand point ligand sources that could mean potentially large localized changes in speciation at the influential factor stations. However, the right graphs show a slightly noticeable wider Cd gap for AEF at AAIW and for CSMF at AABW (Figs. 29a and e). The rest of water masses and locations show a general trend which consists of inorganic complexation keeping Cd^{2+} approximately 1.5 orders of magnitude below toxic levels (Cd plots in Fig. 29). Indeed, though there are no values for Cd mediated limitation, if they were below ~ 11 log units (that is, 0.010 nM Cd^{2+} concentrations), some samples could potentially have limiting concentrations of Cd.

Ellwood (2004) investigated *in situ* the Zn_{TD} and Cd_{TD} concentrations in surface waters of the Pacific sector of the Southern Ocean, where as low as 0.0003 nM Cd^{2+} concentrations were reported, with no apparent limitating effect on the phytoplankton living there. Remarkably, in response to very low Cd_{TD} (~ 0.010 nM), there was a hundred plus times higher concentration of a ligand (more than 1 nM), a good example of "acquisition" ligand. This ligand can be compared with Cd L1 or L2 from this study in terms of stability constant (logK' is between 9.8 and 10.9; Table 8); and it can also be compared with the L1 and L2 reported by Carrasco et al. (2002) in the Chesapeake Bay and Elizabeth River, where Cd^{2+} ~ 0.001 nM resulted from complexing 0.1 nM Cd_{TD} with ~ 1.0 nM L_T (logK1 ~ 11, log K2 ~ 10). In this IOC 1996 study, relatively homogeneous ~ 0.010 nM Cd^{2+} is found throughout the water masses. This concentration is unlikely to limit phytoplankton growth when the water masses are upwelled, unless they are exposed to more removal processes.

More on the potential limiting effects of Zn^{2+} and Cd^{2+} concentrations is discussed in the Speciation section towards the end of the discussion chapter.

5.4.8. Point source concentrations

Finally, Figs. 38 and 39, the most complete comparisons of data from this study with literature data available for specific water masses, are discussed here. Fig. 38 combines information shown in Figs. 25 - 29 for AAIW and compares it with Baars and Croot (submitted) and Croot et al. (submitted) data from AAIW's reputed point source in the Drake Passage (~ 57° S, 61° W). Fig. 39 shows the same kind of information for u-NADW and Ellwood and van den Berg (2000) data for recently formed waters from near u-NADW source point in the Eastern North Atlantic (~ 48° N, 12° W).

For AAIW's source point concentrations, the average of 400 - 900m from Station 241 of Baars and Croot (submitted) and Croot et al. (submitted) is used. These waters are confirmed to be related to AAIW by positively comparing with the point source Zn_{TD} concentration. Also, AAIW forms as the upper 900m of the ACC cross the Drake Passage and part of it turns northward along the western boundary of the South Atlantic

Ocean (Talley, 1996; Stramma and England, 1999; Lankhorst et al., 2009). For u-NADW, the 1991m depth sample from Station Challenger 13 (Ellwood and van den Berg, 2000) is used. These waters are confirmed to be related to u-NADW by checking that LSW is found between 1700 and 2000m in that location (van Aken, 2000) and later double checking with silicate values.

Fig. 38 shows AAIW. Zn_{TD} saturates L in AAIW waters in the source point and the southernmost Stations 10 and 8 (Fig. 38b), indicating the Southern Ocean origin of this water mass. AAIW is not as intense as AABW, but it is still noticeable as both Zn_{TD} and high silicate concentrations (Fig. 38a) which causes the ligand saturation issue that makes the determination of more than one ligand difficult. Zn_{TD} decreases as AAIW moves northward, but both Zn L3 decreases at lower rates and Zn L1 shows no change in concentration at all in that transect (Fig. 38b). By the time AAIW has reached Station Romanche, this has caused each ligand's concentration to exceed that of Zn_{TD}. At Station 6, AEF appears to bring more Zn L1 and L3 than Zn_{TD}, causing the amount of total complexed Zn to reach the maximum value (see double-headed red arrow in Fig. 38d), as both a strong and a weak ligands are observed (logK1' ~ 12, logK3' ~ 9; Fig. 38c). At Station 10, there was approximately the same low concentration of Zn L1 than in Station Romanche; the extremely high Zn_{TD} kept the amount of total complexed Zn at a low range in Station 10. I hypothesize this L1 is brought by AAIW from its source; Baars and Croot (submitted) could not observe it in such saturated-ligand conditions.

5.4.9. Apparent systematic decrease in ligand strength

A very important thing to discuss in the AAIW dataset is the apparent linear decrease in logK' for Zn L3. The concentrations of Zn L3 in AAIW at the five stations are in the 1.5 - 4.5 nM range (Fig. 38b), with an apparent linear concentration decrease from Station 10 to Station Romanche; these concentrations are probably affected by dilutions related to the percent of northern components, as discussed earlier. However, I suggest the emphasis should be put on the logK3' decline of 1.2 log units, as it has a more manifest effect in the complexing index and thus, the greater amount of total complexed Zn. In fact, the stability constant of this ligand decreases linearly with latitude from its

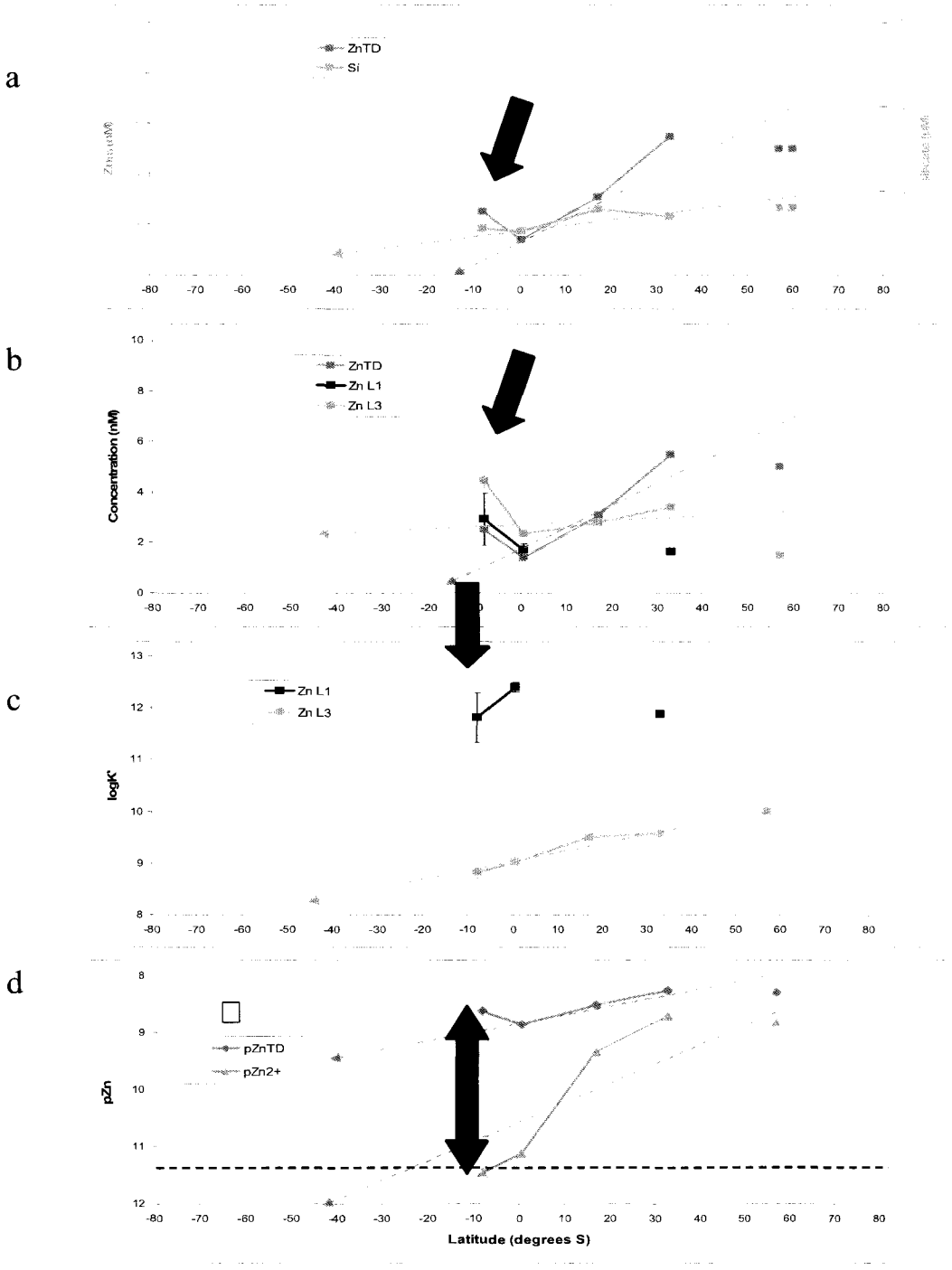

Fig. 38. Zn_{TD} and silicate (a), ligand concentrations (b) and stability constants (c), pZn_{TD} and pZn^{2+} (d) plotted against latitude at Stations 6, Romanche, 8 and 10 in AAIW, compared with Baars and Croot (2010) and Croot et al. (submitted) similar data near the Drake Passage (~ 57° S, Station B0 in Fig. 16c) and point source Zn_{TD} and silicate concentration (~ 60° S). Red arrows represent the AEF influence observed at Station 6.

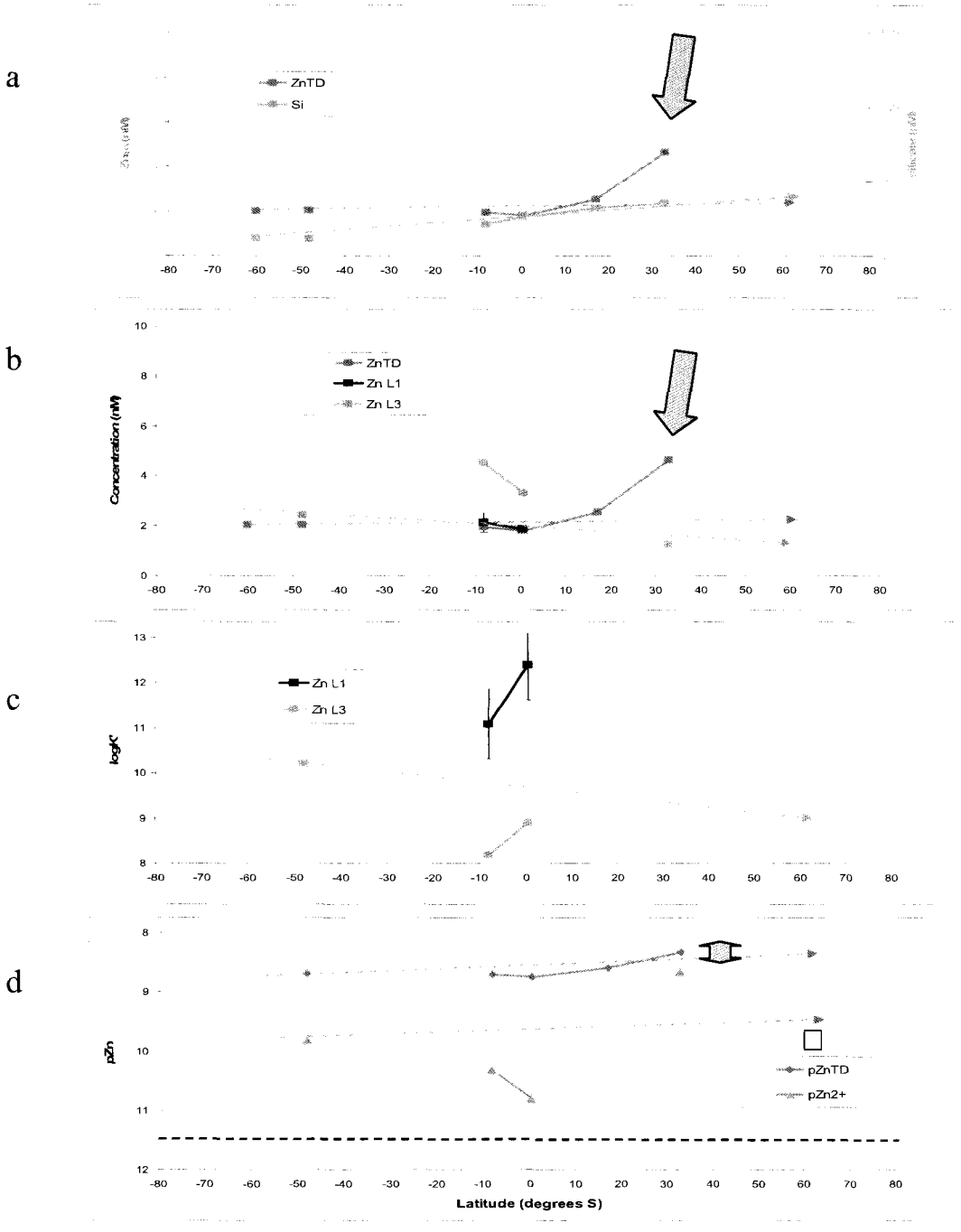

Fig. 39. Zn_{TD} and silicate (a), ligand concentrations (b) and stability constants (c), pZn_{TD} and pZn^{2+} (d) plotted against latitude at Stations 6, Romanche, 8 and 10 in u-NADW, compared with Ellwood and van den Berg (2000) data from the North Atlantic (~ 48° N, Station E0 in Fig. 16c) and point source Zn_{TD} and silicate concentrations (~ 60° N). Blue arrows represent the SWMF influence observed at Station 10.

point source value (logK' ~ 10; Baars and Croot, submitted) to the lowest value at Station 6 (logK' ~ 8.8; Fig. 38c). If the same chemical substance is being transported by AAIW, this would be the first time evidence of this kind has been shown that supports the idea of a strong metal-complexing ligand decaying not only in concentration, but more importantly, in binding strength. From now on, I will use the terms "ligand concentration decrease" and "ligand strength decrease" to refer to the decrease in L and logK', respectively; while "ligand decay" refers to both. Though the first two terms could be related to the same biogeochemical process(es), they will be distinguished from each other when needed, or considered together when needed with the third term.

The ramifications for this alleged phenomenon are diverse. There may be a strong Zn-complexing ligand L1 in surface waters spread out worldwide (as Bruland, 1989; Carrasco et al., 2008 and this study suggest). In intermediate and deep water masses, there may be an apparent systematic decrease in ligand strength which could be turning some of the strong ligand into some weaker derivatives, i.e. converting L1 into L2 or L2 into L3, in a time frame of decades as these chemical substances are carried away and age with the water mass. Despite the intended unbiased determination of the logK' values (i.e. the use of TDI), given the arbitrary choice of logK' value that separates one ligand from another, ultimately the labels L1, L2 an d L3 are given by the researcher. Thus, a ligand with a logK in the L3 class may have been present in the same water as a ligand with a logK in the L2 class (average logK2' in the whole cruise is ~ 10.4, and this ligand's logK' at the source point is 10.0) which could be turning into L3 (average cruise logK3' is 8.9, compared with this ligand's decayed logK' at the northernmost station is 8.8) in this northward moving water mass.

Interestingly, Zn- and Cd-complexing ligands in the West North Pacific show the same trend. Hernes and Benner (2002) followed the lignin signature of organic matter originating from forests and then wash into the Amur River. This organic matter is eventually sedimented and remineralized on the Sea of Okhotsk shelf. Their North Pacific deep water profiles showed evidence of lignin being brought by North Pacific Intermediate Water (NPIW) to stations close Hawaii in the North Pacific. This is a very

great distance, more than 30° towards the east, and is equivalent to roughly the same distance travelled by AAIW from point source to Station 6. Carrasco et al. (2008) found evidence of decreasing Zn L2 concentrations brought along with NPIW at ~ 800m depth. They also reported Zn L1 brought from the East China Sea along another intermediate water mass, Sub Tropical Mode Water (STMW), at ~ 300m depth; STMW gets riverine matter inputs from both the Huang He and Yang Tze Rivers, reputedly resuspended and remineralized on the East China Sea shelf. NPIW showed very high ligand concentrations that decrease with distance (~ 14.5 to ~ 5.0 nM L2). STMW showed relatively constant concentrations (between ~ 1.6 and ~ 1.1, with no clear trend). More importantly, the same decreasing logK' trend was seen in both intermediate water masses; logK' decreased as NPIW moved away from its source point from ~ 10.2 to ~ 9.2 and in STMW from ~ 12.3 to ~ 11.2. In that North Pacific study, both L2 and L3 weaken. These observations are made in intermediate water masses because the relatively low concentrations of metals allow for better determinations than those made in deeper water masses, where the high metal concentrations would very likely produce the ligand saturation (in turn producing only one ligand estimate and no logK').

This phenomenon raises several questions. Taking into consideration the limited data presented in CPDW, l-NADW and AABW, there seems to be evidence of the same decreasing logK' phenomenon occurring in most if not all water masses studied here in the Atlantic Ocean. How much more can the data in Fig. 38c be extrapolated?, i.e. how low does the logK' decrease as a water mass ages? What exactly are the chemical changes that modify the binding strength and the concentration of the ligand in an apparent gradual fashion? What are the environmental ramifications of this phenomenon both in a regional and in a global scale?

The answers to these questions lie in the chemical structure of the ligand, of which only preliminary progress has been made lately. Few things are known about the general structure of the iron-binding ligand, and even less about the Zn-binding ligand. Ellwood (2004) determined the Zn-complexing ligand in the Southern Pacific (equivalent to this study's Zn L2) to be smaller than 100 KDa in size (i.e. truly dissolved), like the ligands

Bruland (1989, 1992) found in the North Pacific for Zn and Cd. Other studies relate weaker Zn-binding ligands (probably L2 and L3) to phytochelatin (Wei et al., 2005), CA (Sarthou et al., 2001) and viral attack on phytoplankton (Poorvin et al., 2004). More information about the structure of the ligands remains to be discovered.

Point sources of u-NADW (Fig. 39a) show lower Zn_{TD} and silicate. In contrast to AAIW, L3 is in excess of Zn_{TD} in an apparent trend in the transect north of the Equator (Stations 6 and Romanche). As the water mass passes by Station 8 (no ligand data available, but increased Zn_{TD}) and further south by Station 10, the influence of SWMF exerted by the overlying CPDW and AAIW cause the Zn_{TD} concentrations to increase, while Zn L3 apparently decreases. At Station 10, Zn_{TD} saturates the ligand(s) present, allowing me only to estimate the ligand(s)'s concentration, not its logK'. This can be observed as an apparent lack of data in Fig. 39c. At equatorial latitudes there is a noticeable source of ligands mostly and little Zn (Fig. 39b). Of those ligands, only Zn L3 is found in the same water mass further south and north, which might mean that L1 could be also part of the AEF influence, specially as its concentration ranges and logK's resemble those of overlying water masses (see discussions of Figs. 27 and 28). The ligand strength decrease mentioned before can not be observed clearly because of ligand saturation which did not allow for the determination of logK3' at Station 10 and the lack of data from Station 8 (due to an apparent contamination problem). However, there seems to be a decreasing logK' trend with latitude (Fig. 39c), less clear but somewhat similar to AAIW.

At Stations 6 and Romanche too, the influence of AEF is observed as an increased amount of total complexed Zn (Fig. 39d). This is not as great as in AAIW (Fig. 38d) or other external influences (see Fig. 29 for examples). Ignoring the localized influence of AEF, the amount of total complexed Zn in u-NADW shows a decreasing trend with water mass age (Fig. 39d). As both ligand concentrations and binding strength decrease, Zn_{TD} increases as the SWMF influence is observed when the water mass approaches high south latitudes (blue arrow and double headed arrow in Fig. 39). Both AEF and SWMFs strongly influence this water mass's Zn complexing ability.

In conclusion, all water masses have somewhat clear trends that are affected by external influences. These influences, although expected to be important (i.e. the Amazon River is known to be a source of organic matter), are major and define the local Zn and Cd chemical speciation.

The following three small sections discuss these localized but important influences, namely AEF, CSMF and the presence of low oxygen concentrations in waters off Africa in Station Romanche.

5.5. AMAZON RIVER OR SURFACE EQUATORIAL PARTICULATE FACTOR (AEF) INFLUENCE ON SURFACE AND INTERMEDIATE WATERS

In a previous section, the influence of the Amazon River on surface waters of the Equatorial Atlantic was discussed, after discussing the profile of the more obvious riverine waters, waters with low S and high silicate, which bring also high concentrations of Zn and Cd ligands. Exploring Stations Amazon 1 and 2 in terms of ligands was challenging, because these two stations show different ligand depth profiles, yet somewhat similar pZn^{2+} and pCd^{2+} profiles (Figs. 23a, 23b, 24a and 24b). High concentrations of Zn L1 and L3 and Cd L2 and L3 were found in waters directly traceable to the Amazon River itself. Below the low salinity waters, the maximum concentrations of some of these ligands were at or below the chlorophyll-*a* maximum or the POC export maximum. The river contribution of Zn- and Cd-binding ligands, expected to be high in concentration but low in logK' because of the riverine humic substances, is not very clear because it is difficult to analyze what is brought by the river from what is produced *in situ* by phytoplankton, presumably responding to very high Zn and silicate concentrations. Rutgers and van der Loeff (1997) hypothesized that high Al, silicate and Cd concentrations found in the Eastern Equatorial Atlantic were related to the influence of the Amazon River, which I think is entirely plausible.

The Amazon River's particulate matter potentially influences intermediate and deeper water masses, as Charette and Moran (1999) suggested. They state that the flux in

the Equatorial Atlantic between 5° N and 5° S is mainly driven by Saharan dust. Yet, they show that Amazon 1 is an active site of net carbon export (Fig. 34) and, though there are no data for Station Amazon 2, I predict it is somewhat similar to Amazon 1, with patchy export related to siliceous organisms (Shipe et al., 2006) and with some physical phenomena providing for variability between stations. The POC fluxes of Charette and Moran (1999) along with the chlorophyll-*a*, the phaeophytin and the AOU profiles in the upper 250m of these stations (Figs. 34, 35a, 35b and 37a), suggest that Stations 6 and Romanche provide some POC flux between surface and ~ 100m, with no net flux below ~ 200m from either station. Stations 8 and 10 might have some net export, but not of the magnitude of Amazon 1. Charette and Moran (1999) only plotted data for the upper 250m, but there is a point for Amazon 1 measured at ~ 500m (not shown in their plot) that indicates that this net POC flux persists by that depth. In an average water column, most of the remineralization and consumption of POC occurs below the chlorophyll-*a* maximum depth (Figs. 35a and 37a), effectively reducing the net POC flux within the upper ~ 150m (Fig. 34). This is what appears to have happened in Stations 6 and Romanche which show high chlorophyll-*a* at 75m and 50m (Fig. 35a), respectively, high POC flux ~ 20m above those chlorophyll-*a* maximum depths (Fig. 34) and high AOU starting as shallow as 50m that stays increasingly high throughout the water column's upper 400m (Fig. 37a), very likely resulting from respiration of the particles produced in the surface.

The phaeophytin profiles (Fig. 35b) provide evidence of efficient grazing recycling at Stations 6, Romanche, 8 and 10; in contrast, Station Amazon 1, with phaeophytin concentrations as low as half of those of chlorophyll-*a*, shows little grazing evidence and thus, potential for export from the upper, very productive 20m. Interestingly, there is a deep grazing maximum at ~ 150m (Fig. 35b) that matches with a slight decrease in local POC flux at that depth (Fig. 34).

Station Amazon 1 is different from the rest of stations: it has a surface chlorophyll-*a* maximum in the upper ~ 50m (Fig. 35a), low surface grazing rates and a deep grazing local maximum at ~ 150m (Fig. 35b), an apparent maximum particle

respiration around 200m (Fig. 37a), but apparently not enough respiration to consume all the particles falling. In fact, the particle flux, high between 50m and peaking at 100m, is not as high as Station Romanche (Fig. 34). The particle flux decreases at 150m because of the increasing AOU and the local grazing maximum. Below 200m, AOU increases and stays at that rate until right above AAIW (Fig. 37b), allowing for particles to yield a considerable positive net particle flux (Fig. 34). Knowing that the POC flux reaches this intermediate depth, it is reasonable to expect that it might reach deeper into intermediate water masses like AAIW and CPDW, as suggested before in the water mass analysis section.

Stations Amazon 1 and 2 were only sampled in the upper 400m, so Zn and Cd ligands were not measured in either intermediate or deep waters. However, nearby Station 6, still heavily influenced by the Amazon River, might receive a heavy particle load from both riverine organic and mineral origin (Charette and Moran, 1999). Particles from nearby Stations Amazon 1 or 2 might get horizontally transported towards Station 6, causing the high ligand concentrations in Station 6 between AAIW and CPDW for both Zn- and Cd-binding ligands (Fig. 21c). This is in fact the highest L_T for both Zn and Cd reported in intermediate water masses (including AAIW and CPDW) in all stations in this study (~ 8.3 nM and 0.46 nM total ligands for Zn and Cd). This depth corresponds to the extra Zn, Cd and nutrient input observed in Station 6 profiles (Fig. 17c). The origin of these elevated concentrations could be riverine or related to AAIW/CPDW. Most likely, they are partially related to AAIW/CPDW, as the Zn_{TD} and Cd_{TD} concentrations, which decrease with distance from the the source point, suggest (Figs. 25a, 25b and 38b). However, there is some Zn_{TD}, silicate, Cd_{TD} and phosphate being provided by AEF's influence too. Exploring the origin of the elevated concentrations of Zn- and Cd- ligands, some evidence is found that suggests the ligands are riverine in origin, and spread out to a certain extent. This evidence is the presence of Zn L1 and L3 at both Stations 6 and Romanche (Figs. 27a and b), which agrees with the Charette and Moran's (1999) hypothesis that the Equatorial Atlantic region is a source of particles that might provide contrastingly high concentrations of Zn- and Cd-binding ligands of high metal affinities: Zn L1, Zn L3 (Fig. 28a) and a slightly stronger, maybe fresher Cd L3 (Fig. 28b).

An immediate ramification of AEF being a source of Zn and Cd ligands is that the ZnTD and CdTD in these waters are largely complexed, especially Zn, decreasing Zn^{2+} to almost limiting concentrations (Figs. 29a and b). A potential remote ramification is that an eventual upwelling or mixing of AAIW with mode waters will provide low Zn^{2+} concentrations. Thought debatable, AAIW is believed to be upwelled in the low latitudes of the North Atlantic (Talley, 1996; Jochum and Malanotte-Rizzoli, 2003; Lankhorst et al., 2009), while both AAIW and CPDW also get entrained in shallower SACW and deeper u-NADW, respectively. AAIW is the most probable candidate for being upwelled not too long after being influenced by AEF, in the mid-latitude North Atlantic. Thus, if Zn proved to be limiting in those waters, it might be related to the influence of AEF on AAIW.

The eventual upwelling of low Zn^{2+} waters might not have as much of an environmental effect, if the take in consideration the possible metal-binding ligands photolability. Though some anecdotal evidence suggests photolability of some of these Zn- and Cd-binding ligands (Carrasco, unpublished), at this point it can not be categorically stated or denied that these ligands would be destroyed by UV light if and when upwelled. Baars and Croot (submitted) suggest that Zn L3 which originates near the Southern Ocean gets transported along surface waters along the zero meridianover a time-span of weeks to a few months, and there is little apparent photolability of these Zn ligands. Although most similar studies for ligands for Cu and Fe have been done in estuaries, there are some reports that the ligands are influenced by UV light (Laglera and van den Berg, 2006; Shank et al., 2006; Barbeau, 2006; Rijkenberg et al., 2005) and there are some that show similar ligands are not significantly affected (Sander et al., 2005, Rijkenberg et al., 2006).

In summary, two important things to notice about AEF are: a) its influence on AAIW and CPDW and maybe even u-NADW, as the ligand concentrations and similar logK's suggest; and b) its ligand influence being larger than its Zn_{TD} and Cd_{TD} influence. These two things imply that there could be important particle fall out in the region, as Charette and Moran's (1999) POC data suggest, and that these particles are rich in

organic matter, as Conkright et al. (2000) and Hu et al. (2004) imply. Thus, I report the presence of Zn and Cd ligands in intermediate depth water masses AAIW and CPDW at Stations 6 and Romanche, and I hypothesize them to be related to particles falling from near the Amazon River mouth or the Equatorial Atlantic high productivity region.

5.6. CONGO RIVER CONTINENTAL SHELF REMINERALIZED MATTER FACTOR (CSMF) INFLUENCE ON DEEP WATERS

The Congo River is the second largest river in terms of water discharge and size of the drainage basin and the second largest riverine source of DOM to the world's oceans, as it drains the world's second largest rain forest area and flows through the world's largest swamp forest area (Spencer et al., 2009 and references within). As such, it is more lignin-rich than the Amazon and Mississippi Rivers, indicating significant vascular plant sources (Spencer et al., 2009; Hedges et al., 2000; Benner and Opsahl, 2001). For comparison, black water tributaries of the Amazon River similar to the Rio Negro River have comparable lignin concentrations (Ertel et al., 1986). The Congo River does not have a large sediment discharge when compared with the Amazon. However, recent reports show two separate depths (surface and deep) where dissolved and particulate organic matter is brought to the Equatorial Atlantic (Vangriesheim et al., 2009). Spencer et al. (2009) focused on the surface organic matter and its photolability; for this study, I focus on the deep thin layer.

Congo River DOM at ~ 4000m depth was reported in the Guinea Basin of the Eastern Atlantic Ocean (Braga et al., 2004); Vangriesheim et al. (2009) studied this deep thin layer, apparently formed in the abyssal plain at ~ 4000m depth around 7.5° E, where settling particles flow down from the Congo Canyon, accumulate and get remineralized. In their paper, this is supported by subtle oxygen and silicate anomalies. Oxygen is ~ 10 μM lower and silicate is ~ 6 μM higher than waters immediately above and below, representing a ~ 5 % oxygen deficit and ~ 12 % silicate excess, respectively. Comparable oxygen and silicate anomalies have been reported for this specific site in other papers (Rabouille et al., 2009; Ragueneau et al., 2009). Other nutrients like phosphate and

nitrate show similar excesses (~ 5 %). Remineralization was confirmed with DIC, pH and C and O isotopes (Vangriesheim et al., 2009). There are reports that suggest this organic-rich water changes direction often, and that it spreads in north and south direction (Braga et al., 2004; Vangriesheim et al., 2009) shoaling a few hundred meters when spreading west (Vangriesheim et al., 2009). I hypothesize that the water I observed in this study's easternmost Station Romanche between l-NADW and AABW is related to this deep layer spreading westward, and the evidence is presented next.

Station Romanche is located right on top of the Romanche Fracture Zone (RFZ), a major opening in the mid-Atlantic ridge where deep water masses may exchange between the Brazil Basin in the Western Equatorial South Atlantic and its eastern counterparts, the Sierra Leone and the Guinea Basins (see Fig. 16d for the topographic information). For reference, Station 8 is located in the center of the Brazil Basin, and Station 10 is located on top of the Vema Channel, the south major bottom-water opening of the Brazil Basin, located in its southernmost tip. Mercier and Speer (1998) and Ferron et al. (1998) suggested fluctuating and variable fluxes across the RFZ, and they recommend tracking movement across the RFZ with temperature (~ 1.4° C) instead of salinity and density, which are less useful to distinguish it (see Table 12).

Cutter and Measures' (1999) hydrography paper shows subtle oxygen and silicate anomalies between ~ 3000 and 3500m at Station Romanche, somewhat alike Vangriesheim et al. (2009). More so, the temperature registered at 3000, 3500 and 4000m depth at Station Romanche, 2.4, 2.2 and 1.8° C, is different from the colder AABW and the warmer l-NADW waters below and above (average temperatures: 0.6 and 2.8° C). The very similar densities of these two water masses (Table 12) probably allows for diffusion between both of them.

Figs. 17d, 25d and 25e show somewhat elevated Zn_{TD}, silicate, and Cd_{TD} concentrations at this station and depth ranges. These get mostly reduced when a northern component analysis is performed (Fig. 33). Thus, this water layer, whose origin is riverine and which is organic-rich, would bring organic matter but not silicate to the

region. More importantly, very high Zn- and Cd-ligand concentrations in l-NADW and higher concentrations in AABW reduce Zn^{2+} concentrations in l-NADW to the lowest values measured at all stations and all deep water masses and in AABW, to very low value (Figs. 21d, 29d and 29e). These extremely low Zn^{2+} concentrations are around and below the limiting threshold set by Brand et al. (1983).

A potential remote ramification of the presence of this ligand-rich water layer is similar but not identical to those of AEF. When these deep water masses get mixed with shallower water masses, they will provide very low, potentially limiting Zn^{2+} concentrations. l-NADW and AABW will likely mix into deep ACC/CDW or l-NADW, respectively. The effect of the low Zn^{2+} concentration in l-NADW will probably be minimized when mixing with Southern-Ocean-influenced water masses, usually Zn- and silicate-rich, happens before the formation of the deep ACC/CDW complex. The low Zn^{2+} provided by AABW to l-NADW could potentially follow the same path. However small the apparent effect of these two water masses' low Zn^{2+} concentration might be, the global Zn budgets should account for this.

The ligands' depth profiles at Station Romanche (Fig. 21d) suggest that the phenomenon observed in these two depths may not be connected, as there is one sample between l-NADW and AABW at ~ 4500m that shows lower Zn_{TD} and Zn and Cd ligand concentrations than both the samples immediately above and below. Maybe the influence of CSMF is more directly observed in l-NADW than in AABW. Maybe the organic ligands measured in AABW at Station Romanche are related to bottom material accumulated in the RFZ, instead.

On the other hand, the deep water masses' AOU profile (Fig. 37c) appears to show that in l-NADW at stations 6 and Romanche there is a slightly increased AOU depth range around σ_4 45.8. This is not directly the depth where the high-organic-ligand layer is located, but the depth immediately above it, in between u- and l-NADW. These AOU data, though not conclusive, may be indicating this ligand-rich thin layer is related to an enhanced respiration layer at the u-NADW/l-NADW interphase. This could pose an

alternative explanation to the observed phenomenon, acting as a counter argument for the Congo River organic matter hypothesis. At this point I can only speculate that either origin of the thin layer water is possible. More studies need to be done to clarify this.

In summary, two important things to remember about CSMF are: a) its influence on l-NADW and AABW, with more pronounced effects on l-NADW; and b) its ligand influence being larger than its Zn_{TD} or Cd_{TD} influence. These two things suggest remineralized particles provide DOM in the abyssal plain of the Guinea Basin, then are transported to the westernmost point of the Sierra Leone Basin, and later cross the RFZ to the Brazil Basin along a thin layer in the ~ 3500 - 4000m depth range. I report the presence of Zn- and Cd-ligands in l-NADW and AABW at Station Romanche, and I hypothesize these ligands are provided by this organic-rich thin layer of water which originates from Congo River particulate matter remineralized in the abysal plains of the eastern Guinea Basin.

5.7. THE HYPOXIC INTERMEDIATE DEPTH AT STATION ROMANCHE, SOME METAL / LIGAND IMPLICATIONS

Completely not-related to intermediate or deep water masses aforementioned, but at the same Station Romanche is one phenomenon that deserves to be analyzed carefully. The presence of a low-oxygen subsurface depth range where important biogeochemical processes related to metals might occur and a potential hint about ligand production might be deciphered.

Hypoxic, suboxic and oxygen minimum zones (OMZ) are locations that show less than 100, 10 and 1μM oxygen, respectively (Stramma et al., 2008); for comparison, surface water oxygen saturation concentrations are commonly around 200 μM. This low oxygen is caused in part by increased productivity in the surface waters, accompanied by increased respiration a few meters below, where the oxygen deficit is perceived. OMZs in tropical regions of the world's ocean have grown over the past few decades, and the Equatorial Atlantic is one of those regions (Stramma et al., 2008). In OMZs, important

biological effects have been suggested (Stramma et al., 2010), very likely related to redox chemistry in certain metals (i.e. Nameroff, 2002). Iron redox and chemical speciation have been studied in these conditions, with suggestions of redox-status-specific ligands (Hopkinson and Barbeau, 2007; Lohan and Bruland, 2008; Moffett et al., 2007). Sulfide has been suggested as a possible metal-non-specific ligand in such conditions; logK' values for several bioactive metals including Zn and Cd, with logK' ~ 6.1 and 8.4, respectively (al Farawati and van den Berg, 1999).

In all IOC 1996 stations, the only hypoxic layer is present at Station Romanche between ~ 200 and 400 m, where oxygen concentrations are below 100 μM. Specifically, at 250 and 350 m, the oxygen concentrations were ~ 96 and ~ 80 μM, respectively (ancillary data). These oxygen concentrations are not necessarily suboxic, but following the criterion of Stramma et al. (2008), they were hypoxic and could potentially become suboxic in the next decades.

A detailed analysis of the surface and subsurface waters at Station Romanche follows, focused on the surface conditions that produce these low oxygen concentrations. Subsurface waters in Station Romanche show some of the highest chlorophyll-*a*, phaeophytin (Fig. 35) and local POC fluxes (Fig. 34) of all stations, as well as the highest AOU values (Figs. 37a and b) throughout the upper 400m of the water column. In this station's subsurface waters, there are large amounts of phytoplankton productivity, grazing and particles and, in all the upper-water column, large amount of respiration. Both chlorophyll-*a* and phaeophytin reach a maximum at 50m (Figs. 35a and b). Fig. 36, below 75m suggests high grazing rates compared with other stations in this study. The POC maximum is located at ~ 25m, somewhat disconnected from the pigments maximums (Fig. 34). Because there is no net POC flux below 75m, the suspended particles should be undergoing extensive respiration below the chlorophyll-*a* maximum. High respiration rates cause AOU in Station Romanche to be the highest of all stations compared in this study in the upper ~ 600m (Figs. 37a and b). For comparison, AOU at ~ 50m in Station Romanche is as high as it is at ~ 400m in Station 10.

Thus, oxygen profiles (Cutter and Measures, 1999) show that the ~ 200 - 400m depth range has the lowest oxygen concentrations of all stations. The oxygen concentration is as low as 80 μM, almost half of subsurface waters below the Amazon River plume in Stations Amazon 1 and 2 (as low as 130 μM) where major amounts of respiration are expected to occur as riverine organic matter is respired.

Fe shows redox chemistry that relates to the oxic conditions in seawater (Morel and Price, 2003; Hopkinson and Barbeau, 2007). In contrast, Zn and Cd have no redox chemistry in seawater. Still, the sample in this hypoxic layer at 250m (~ 96 μM oxygen) showed Zn and Cd complexation and speciation features when compared with the next deeper sample from 500m (where oxygen concentrations were low, ~ 123 μM, but not as low as in the 250m sample). These features are discussed next.

The depth profile of the upper 400m can be broken into the following segments: the particle export maximum (~ 20m; Fig. 34), the pigment maximum (~ 50m; Fig. 35) and the oxygen minimum layer (~ 180 to 700m, with oxygen below 150 μM; ancillary data). Analyzing the Zn and Cd ligand profiles (Figs. 23d and 24d, left graphs), the following is observed: the particle export maximum depth correlates with Zn L3 and Cd L3; the chlorophyll-maximum depth correlates with Zn L2 and a very low concentration of Cd L1; the waters below the chlorophyll-maximum show a clear increase of Zn L3 and only Cd L2 complexing Cd_{TD}, suggesting a disconnect from stronger ligands in the chlorophyll-maximum depth; at 250m, the hypoxic sample shows the lowest concentration of both Zn- and Cd-ligands; finally, the 500m sample shows increasing concentrations of Zn L1, Zn L3 and Cd L3, as oxygen concentration increases to ~ 130 μM (ancillary data).

As a consequence of the Zn and Cd ligand concentrations changing with depth, the chemical speciation of Zn is affected more than that of Cd (Fig. 22d, Figs. 23d, 24d, right graphs). The hypoxic 250m sample shows a Zn^{2+} local maximum, almost an order of magnitude higher than samples in the upper 500m. Other sample with high Zn^{2+} is the chlorophyll-maximum depth at 50m, where the Zn subsurface maximum produces Zn_{TD}

in high concentrations (Fig. 23d). More about this Zn subsurface maximum is found in the following section. In contrast to Zn, the profile of Cd^{2+} at station Romanche does not show any major difference from other station's profiles (Fig. 24). Despite the changing concentration of Cd ligands, the chemical speciation of this metal appears to be efficiently controlled by the inorganic ligands below 200m.

With the depth profile of the upper 500m of station Romanche, the preliminary and limited correlations between low oxygen concentration and Zn and Cd ligands are suggested:

- Zn L2 and Cd L1 appear to relate to phytoplankton productivity (chlorophyll-maximum depth),
- Zn L3 and Cd L2 appear to relate to grazing or respiration (waters below chlorophyll-maximum),
- Ligand destruction, consumption or decay appears to relate to low oxygen concentrations (hypoxic layer analyzed at 250m depth).

Here, preliminary evidence suggests that the presence of stronger Zn and Cd ligands is related to live phytoplankton (probably "acquisition" or "detox" ligands) and relatively weaker ligands are related to grazing or respiration ("bug gut" ligands). In contrast to an Fe-ligand, whose strength and concentration increases in a different suboxic region, presumably related to active production by phytoplankton living in these conditions (Hopkinson and Barbeau, 2007); the Zn and Cd ligands discussed here appear to be affected by low-oxygen concentrations in detrimental ways, as their decreasing concentrations suggest.

Additionally, the effect on ligands in OMZs would increase with OMZ intensification, potentially producing stronger surface-to-low-oxygen-depth gradients in terms of Zn^{2+} and Cd^{2+}. Sulfide, which binds to these two metals with affinities (al Farawati and van den Berg, 1999) lower than those of the ligands found in surface waters

and in deeper waters in higher oxygen concentrations, would become more important as conditions get more anoxic in the OMZs throughout the world's oceans.

5.8. METAL / NUTRIENT RATIOS

In Fig. 17, I presented the Zn_{TD}, Cd_{TD}, silicate and phosphate profiles for each individual IOC 1996 station. Then, these data were separated into water masses in Figs. 25 and 26, using water-mass-representative points or averages for clarity purposes. In contrast, Figs. 40, 41, 42 and 43 show the complete water column datasets for all stations simultaneously, to allow more direct comparison.

The depth profiles of Zn_{TD}, Cd_{TD}, silicate, phosphate and AOU are plotted in Fig. 40. These plots and the Zn_{TD}/silicate and Cd_{TD}/phosphate water column profiles are replotted with the water masses discriminated using the density label values. The focus is divided into three subsections: the upper 400m, the intermediate waters and the deep waters (Figs. 41, 42 and 43, respectively). Finally, Zn_{TD} vs silicate and Cd_{TD} vs phosphate plots for all stations are presented in Fig. 44.

5.8.1. General trends

The general trend shows high Zn_{TD}/silicate and Cd_{TD}/phosphate ratios in the Amazon Station surface waters; high Zn_{TD}/silicate and low Cd_{TD}/phosphate in subsurface waters; medium high Cd/phosphate in waters deeper than the high subsurface Zn_{TD}/silicate; and low Zn_{TD}/silicate and Cd_{TD}/phosphate in intermediate and deep waters (Figs. 41c, 42c and 43c). Zn_{TD}/silicate deviates from that general trend by showing subsurface high ratios (Fig. 41c), caused by high Zn_{TD} concentrations (Fig. 41a). Despite the variability, "deep" values below ~ 800m depth are pretty comparable, with average Zn_{TD}/silicate and Cd_{TD}/phosphate values below 0.08 and 0.24 nM/μM (Figs. 42c and 43c), which compare well with regional and global ocean estimates (Ellwood, 2008; Hendry et al.2008; Hendry and Rickaby, 2008; Elderfield and Rickaby, 2000).

The surface Amazon Stations show both relatively high Zn_{TD}/silicate and

a

b

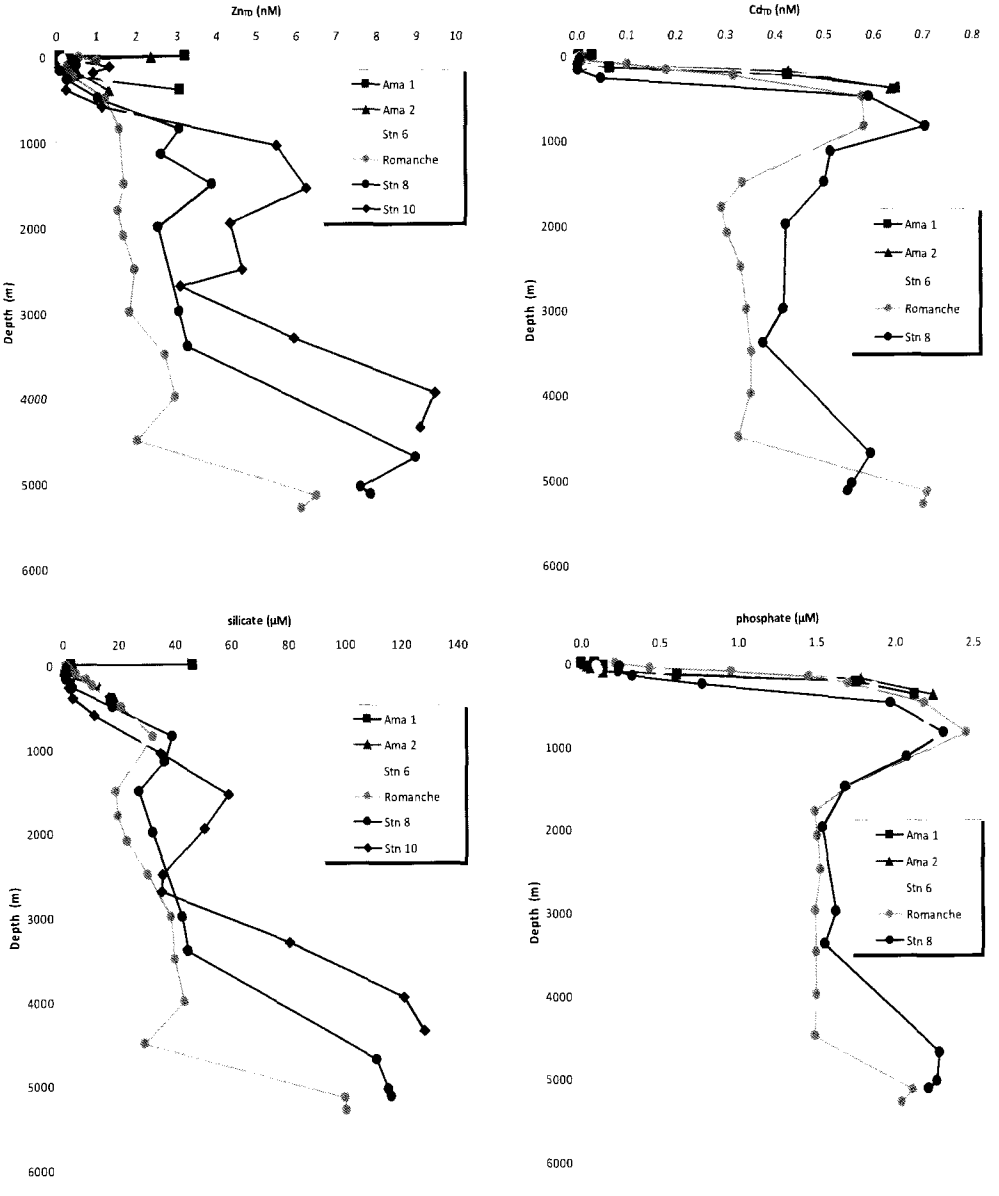

Fig. 40. Complete water column profiles of Zn_{TD} and Cd_{TD} (a), silicate and phosphate (b) and AOU (c) in all IOC 1996 stations.

c

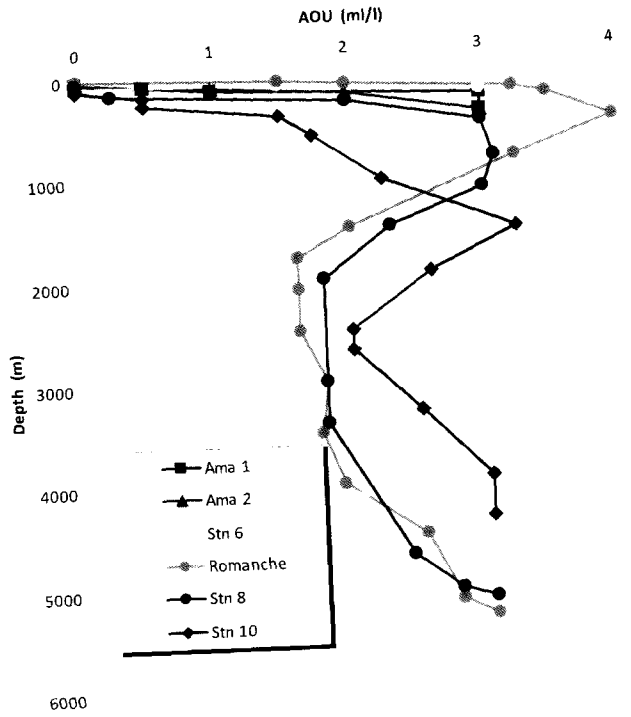

Fig. 40. Continued.

Cd_{TD}/phosphate (Fig. 41c), suggesting increased Zn loads of riverine, terrigenous or anthropogenic origin and, to a lower extent, Cd loads too. Theese relatively high metal/nutrient signatures mean that the Amazon River brings Zn-and-Cd-enriched, in comparison to nutrients to the Atlantic Ocean, on top of the expected riverine silicate signature, as can be observed in the depth profiles (Figs. 40a and b), more so if the continental shelf does not preclude the riverine input from spreading out (DeMaster and Pope, 1996). Thus, observations like those of Rutgers van der Loeff and Kattner (1997) in which high Cd, Al and silicate at a location ~ 20° to the east, speculated to be related to Amazon River water, are backed by this study's results.

5.8.2. Elevated Zn_{TD} at subsurface waters

The oceanic stations (Stations 6, Romanche, 8 and 10, of which there are complete depth profiles) show subsurface elevated Zn_{TD}/silicate ratios above 150m (Fig. 41c)

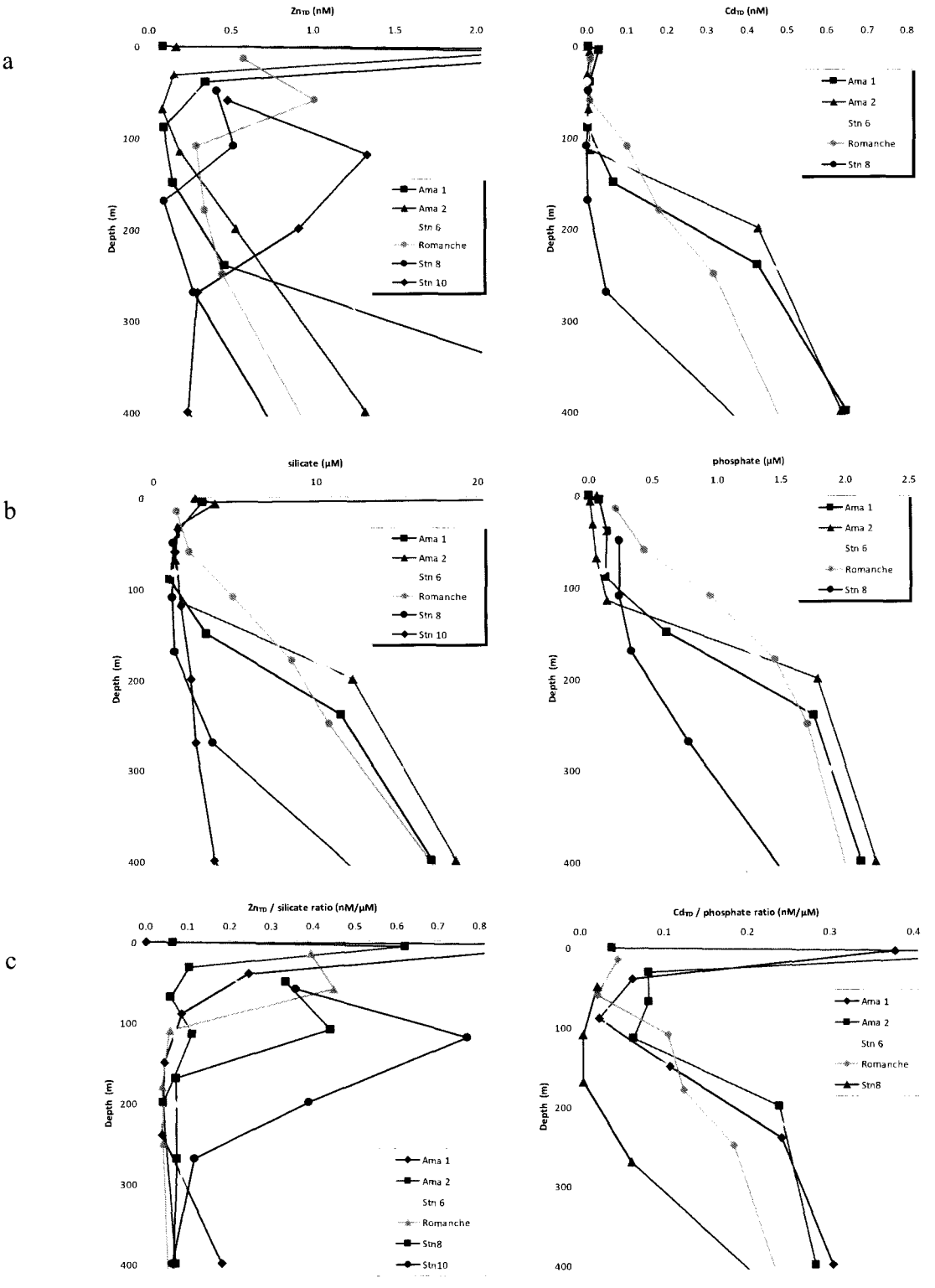

Fig. 41. a) Zn_{TD}, Cd_{TD} (in nM), b) silicate, phosphate (μM) and c) Zn_{TD}/silicate and Cd_{TD}/phosphate (nM/μM) in upper 400m in all IOC 1996 stations.

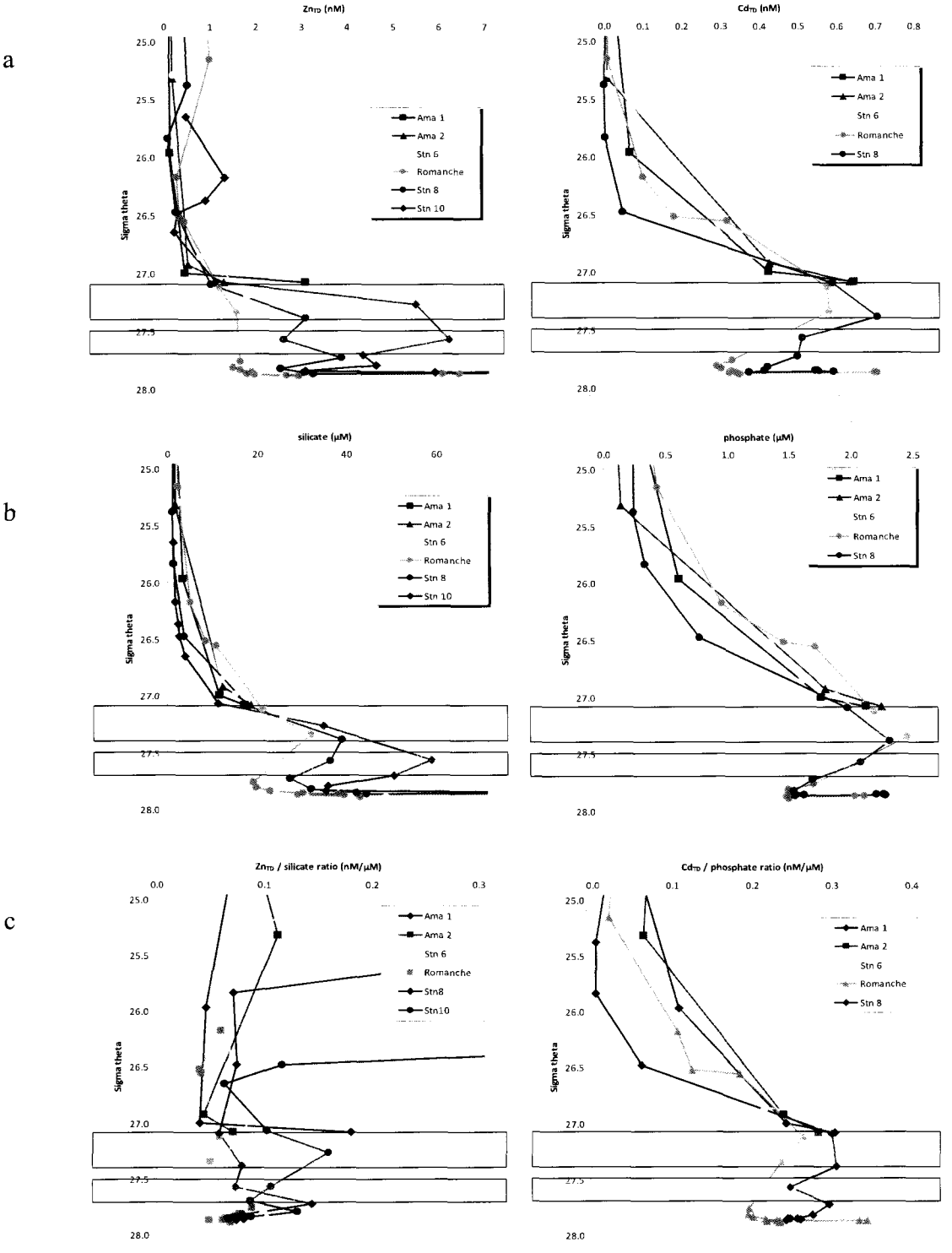

Fig. 42. a) Zn_{TD}, Cd_{TD} (in nM), b) silicate, phosphate (µM) and c) Zn_{TD}/silicate and Cd_{TD}/phosphate (nM/µM) in intermediate waters in all IOC 1996 stations. Shaded areas indicate: AAIW (green) and CPDW (yellow), see Table 12 for σ_t label values.

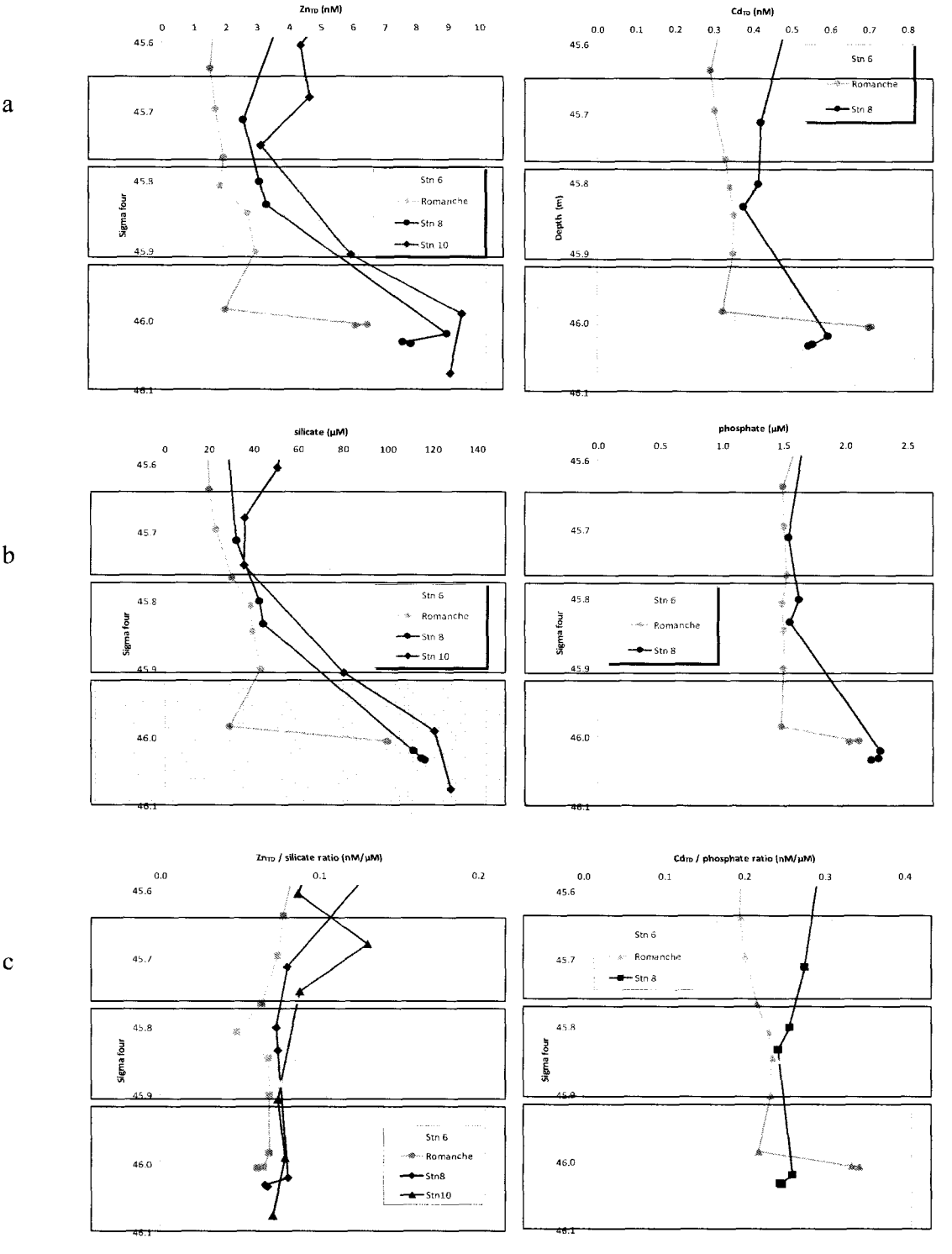

Fig. 43. a) Zn_{TD}, Cd_{TD} (in nM), b) silicate, phosphate (μM) and c) Zn_{TD}/silicate and Cd_{TD}/phosphate (nM/μM) in deep waters in all IOC 1996 stations. Shaded areas indicate u-NADW (red), l-NADW (red) and AABW (brown). See Table 12 for σ_4 label values.

which correlate with elevated Zn_{TD} at subsurface waters (Fig. 41a) at or below chlorophyll-*a* and phaeophytin maximums (Fig. 35). Station Amazon 2 shows a little Zn_{TD}/silicate maximum around 120m, but Station Amazon 1 is dominated by the surface inputs (Fig. 41c). These Zn_{TD}/silicate maximums seem to be driven by elevated Zn_{TD} in those stations at that depth range (Fig. 41a) that show a disconnect from the relatively low silicate (Fig. 41b). The elevated subsurface Zn_{TD} concentrations (specifically ~ 0.5, 0.8, 0.4 and 0.9 nM Zn_{TD} above the average of the depths right above and right below) are located at 80, 60, 110 and 120m. These points are all below each station's mixed layer depth (40, 20, 70 and 80m; Cutter and Measures, 1999), and at or below the chlorophyll-*a* maximum depths (80, 57, 138, upper-100m, ancillary data; Fig. 35a). Thus, I hypothesize they are related to a depth where locally high Zn regeneration may be occurring, as Croot et al. (submitted) and Ellwood (2008) have reported for other oceans.

In the Southern Ocean, Ellwood (2008) suggests two Zn_{TD} regeneration pools, both related to silicate-rich diatoms: a soft, labile pool and a second hard, refractory pool. I hypothesize the Zn_{TD} maximum located in subsurface waters may relate to the soft and labile pool, in contrast to the silicate dissolution maximum depth, which may relate to the hard and refractory pool. Intermediate water masses transport exported Zn from high latitude waters in the region studied in Ellwood's (2008) study; in the IOC 1996 samples, there is no local maximum between the subsurface Zn_{TD} maximum points and AAIW, where the South Atlantic Central Water (SACW) is located (Cutter and Measures, 1999), as this Zn_{TD} maximum concentration point occurs at a shallower depth.

The subsurface maximum Zn_{TD} concentrations at different stations follow what resembles a decreasing-concentration and shoaling trend (Station 10 > Station 8 > Station 6; Fig. 41a) that follows the trends of intermediate water masses AAIW and CPDW for Zn_{TD}, Cd_{TD} and ligand concentrations (Figs. 27a and b). The depths at which these subsurface Zn_{TD} maximums occur may indicate that regeneration of a relatively labile Zn pool is occurring ~ 40m below the mixed layer, close to the upper border of the SACW. The location of this Zn-rich micro-layer in the water column suggests a potential buoyancy constraint: zooplankton that live at this depth may float up to the mixed layer

to eat phytoplankton, later sink down to this depth and excrete fecal material containing Zn-enriched phytoplankton.

In fact, when the chlorophyll-*a* and phaeophytin profiles (Fig. 35) are compared, it becomes clear that phaeophytin, a proxy for grazing (Lorenzen, 1967), reaches a maximum below chlorophyll-*a* (phaeophytin maximum occurring at 100, 57, 138, 100m, Fig. 35b; chlorophyll-*a* maximums at 80, 57, 138, upper-100m, ancillary data; Fig. 35a) and that there is a relatively solid relationship between phytoplankton grazing by zooplankton and the Zn_{TD} local maximum at subsurface waters for Stations Romanche, 8 and 10. These two depths are within 10m, a pretty reasonable proximity to make the inference that they are related, especially given the depth resolution of this study. The phaeophytin/chlorophyll ratio (Fig. 36), a commonly used proxy for grazing, shows the balance between grazing and productivity. The ratio is low in the upper part of the euphotic zone as primary productivity is higher than grazing. The ratio exceeds the 1:1 ratio at the depths where phaeophytin balances chlorophyll, as it does at the depths indicated by the arrows in Fig. 36, where phaeophytin reaches its local maximum concentrations. Below those depths, the ratio gets higher, as less photosynthesis and more degradation processes occur, both microzooplankton grazing and bacterial respiration. So, Zn seems to be regenerated in subsurface waters very near the depth of maximum phytoplankton grazing.

This is not surprising, since chlorophyll degrades to phaeophytin when microzooplankton ingest phytoplankton and then excrete, and the chemical transformation is an acid attack on the chlorophyll to turn it into phaeophytin by exchanging a Mg ion for an H ion. Similarly, Zn present in phytoplankton would be acid leached out of the particle and dissolved by the action of the acid juices in the digestive tract of the microzooplankton. In contrast, there is no clear relationship between these Zn local maximums and respiration, as the AOU maximums are much deeper than these maximum depths (Fig. 37a). Elevated Zn subsurface values at or below chlorophyll-*a* maximum have also been observed in the Western North Pacific IOC-2002 (Carrasco et al., 2008) and the Southern Ocean (Croot et al. submitted).

In contrast to Zn_{TD}/silicate, the high Cd_{TD}/phosphate in subsurface waters appear deeper than the Zn maximum (200 - 300m) and are less pronounced (Fig. 41c). The Cd_{TD} concentrations (Fig. 41a) seem to be the decisive factor for this, suggesting that Stations Amazon 1, Amazon 2 and 6, with Amazon River or Equatorial influence, have a noticeable increase in the Cd_{TD} concentrations between 200 and 300m, well below chlorophyll, phaeophytin and AOU maximums and deeper than the Zn subsurface local maximum point related to grazing. This is a depth that shows Cd_{TD} and phosphate values approaching the maximum phosphate respiration depth values for Station 6. There are no Zn and Cd data deeper than 400m for Stations Amazon 1 and 2; however, nutrient and oxygen data down to 700m depth (Cutter and Measures, 1999) suggest similar nutrient maximum and oxygen minimum depths ($\sigma_t \sim 27.2$) to those in the AAIW at Station 6.

This sheds light on the relationship between Cd_{TD}/phosphate and respiration. In surface waters, there is almost complete Cd_{TD} depletion in all stations except where the Amazon River's signature can be observed (Fig. 41a); thus, all the Cd may be in the particulate form. With increasing depth, as Cd and phosphate are respired, the low concentrations increase. Fig. 37a shows that in the upper 400m, AOU for Stations Amazon 1, Amazon 2 and 6 is higher than that at Stations 8 and 10. At the stations and depths where high respiration occurs, there is high Cd_{TD}/phosphate (Fig. 41c) very likely resulting from particulate respiration. Below ~ 150m, Cd_{TD} and phosphate profiles closely resemble each other (Figs. 40a, 40b, 41a, 41b, 42a, 42b, 43a and 43b). Comparing these profiles with the Zn and silicate two-pool concept suggests different processes are involved in each metal and nutrient, as apparently there is one single pool of Cd and phosphate regeneration that gets affected by respiration, which drives the concentration and ratios of both elements.

The apparent Cd depletion observed in the upper ~ 100m of the Cd and phosphate upper-400m depth profile plots (Fig. 41a) can be produced by increased Cd uptake related to either Fe limitation (Cullen, 2006; Ellwood, 2008) or Zn limitation (Morel et al., 1994; Sunda and Huntsman, 1998; Ellwood, 2008). There is no evidence of Fe limitation at the IOC 1996 stations (Powell and Donat, 2001). However, there may be local areas of

potential Zn limitation in the upper 400m, especially where there is no influence of the Zn subsurface local maximum (Fig. 41a); the Zn^{2+} data in Fig. 27 suggests this may occur in Station Amazon 1 between ~ 100 and 200m, in Station 6 ~ 100m, in Station Romanche between ~ 100 - 200m and in Station 8 ~ 500m.

One thing to notice in the subsurface Cd_{TD}/phosphate is that in Station Romanche above the hypoxic layer, phosphate seems to be preferentially respired in comparison to Cd. There is a relatively high concentration of phosphate in the upper 100m (high Cd_{TD} at ~ 100m only) where all other stations have more depleted concentrations (Figs. 41a and b). The POC profiles (Fig. 34) provide a good hint about the processes occurring: at 25m there is the highest particle export of all stations and between 50 and 100m these particles get completely respired, to the extent that there is no POC export by ~ 75m depth (Charette and Moran, 1999). This particle respiration is observed in the upper 100m of the AOU profile (Fig. 37a) where Station Romanche shows a high AOU that contrasts with all other stations' zero values. The high phosphate can be observed as a smooth increase in the phosphate profile around and below those depths (Fig. 41b), that produces a lower Cd_{TD}/phosphate profile (Fig. 41c). At ~ 100m, the high Cd_{TD} increases are over-imposed on the low Cd_{TD}/phosphate profile. Despite this AOU offset being observed down to AAIW (Fig. 37b), the phosphate offset is only observed in the upper-100m range. Below the ~ 100m mark, the high phosphate and low Cd cause a low Cd_{TD}/phosphate (Figs. 41a, b and c).

Similarly, Station 6 has high particulate export that gets effectively respired (see Figs. 34, 37a and b), but the respiration depth range is deeper than for Station Romanche as particulate matter gets respired completely between ~ 50 and 225m (Charette and Moran, 1999); the AOU offset persists further into and below AAIW (Fig. 37b). In this case, given the proximity of this station to the Amazon River and the high concentrations of Cd being brought by the river into the Atlantic, the Cd and Cd_{TD}/phosphate appear to be the highest of all stations at 300m (Figs. 41a and c). Station 6's upper 400m Cd and phosphate profiles closely resemble those of Stations Amazon 1 and 2 (Figs. 41a and b), suggesting similar sources and processes. The particulate load of Station Amazon 1 does

not get completely respired despite high AOU levels (Fig. 37a) and a large part of it is effectively exported to waters deeper than the 250m shown in Charette and Moran's (1999) profiles. Thus, the dissolved Cd and phosphate observed in Station 6's profiles should reflect a part of the total amount of biogenic matter produced *in situ* near the mouth of the Amazon River. The Cd to phosphate proportions are mostly preserved, though, and I hypothesize that this export causes the Cd_{TD}/phosphate of Stations Amazon 1 and 2 to resemble those of Station 6 (Fig. 41c). Station Romanche shows, as discussed above, distinctly low Cd and high phosphate in the depth range where respiration is greatest, possibly because it might be influenced by a different riverine source - the Congo River (Vangriesheim et al., 2009) - and to a lower extent because of the large distance from the source.

5.8.3. Intermediate waters

Both the Cd_{TD} and the Cd_{TD}/phosphate increase in all stations from the surface and subsurface values until they reach their intermediate water values (Figs. 42a and c). These maximum values are the product of three processes: a) the locally-variable effect of vertical transport of particulate organic matter falling from the euphotic zone and being respired as it sinks, b) advection and upwelling from deeper waters of high nutrient and metal concentrations (in the Pacific Ocean more than in the Atlantic, as deeper water masses get older and accumulate respired nutrients), and c) horizontal transport of organic matter being respired in intermediate water masses. The two first processes involve vertical transport of POC and DOC and are the most commonly studied; the third factor has been given importance recently. Given that Cd_{TD} in seawater closely correlates to phosphate, suggesting Cd's major presence in soft tissue (Collier and Edmond, 1984; Noriki et al., 1999), the depths of Cd_{TD} and Cd_{TD}/phosphate maximums are at or near the maximum phosphate respiration and the minimum oxygen depths. In contrast, given that Zn associates with both soft and hard tissue (Collier and Edmond, 1984; Ellwood, 2008), besides the Zn local subsurface maximum there is a Zn_{TD}/silicate maximum located around the maximum silicate dissolution depth, near the maximum phosphate respiration depth. Usually the phosphate maximum depth is shallower than silicate's, with variability depending on water mass structure; similarly, Cd_{TD} maximum is usually shallower than

Zn_{TD}'s (Lohan and Bruland, 2003).

The high-resolution complete silicate and phosphate depth profiles (Cutter and Measures, 1999) show silicate maximums around ~ 1000, 900, 900 and 1600m for the oceanic stations (Stations 6, Romanche, 8 and 10) that occur at AAIW, at AAIW, at AAIW and at CPDW. In contrast, the local phosphate maximums are at ~ 800, 900 and 800m for Stations 6, Romanche and 8 that occur all at AAIW. To calculate the Zn_{TD}/silicate and Cd_{TD}/phosphate ratios (Figs. 40, 41, 42 and 43), points from the complete nutrient depth profiles were extracted for the depths where there are Zn or Cd data. These low-resolution silicate and phosphate depth profiles show maximum depths (Fig. 40b) similar to those of the complete depth profiles. The depths of local or global Zn_{TD} maximums, located at 900, 850-1500, 850 and 1500 and 1550m (for all four oceanic stations) occur at AAIW, at CPDW and below CPDW, at AAIW and below CPDW and at CPDW. In contrast, the Cd_{TD} maximums, located at 700, 500-850, and 850 for Stations 6, Romanche and 8, all occur at AAIW (Fig. 40a). The nutrient maximum depths are compared with the depths of global or local Zn and Cd maximums. There might be some discrepancies in the metal data probably because of lower depth resolution, higher level of analytical difficulty and potential Zn and Cd contamination problems. A biological reference is provided by the AOU maximums for the oceanic stations, located at 700, 500, 850 and 1550m, occurring at AAIW, at AAIW, in between AAIW and CPDW and at CPDW (Fig. 40c).

Comparing the nutrient maximum depths, there is an offset between phosphate and silicate maximums: phosphate maximums are slightly shallower than silicate's in most stations, as expected. In general, silicate, phosphate and AOU (Figs. 40b and c) are similar - within a 100 - 200m depth range - for all stations except Romanche where the AOU is shallower than nutrients because of particle respiration in the upper 100m and the hypoxic conditions present around ~ 200 - 400m (see section above for more information). Similarly, when the Zn_{TD} and Cd_{TD} maximums depths are compared, they are relatively similar to each other. However, Cd_{TD} maximums are slightly shallower than Zn_{TD}'s due to the relationship between Zn and silicate and Cd and phosphate

previously discussed.

When the nutrient maximum depths are compared with the Zn and Cd maximum depths, the parallel behavior of these two metals and nutrients is evidenced by the similarity between the Cd and phosphate maximum depths. The same parallel is observed for Zn and silicate maximum depths with an interesting caveat: while there is a Zn maximum to match every silicate maximum, there are two stations (Romanche and 8) that show extended Zn maximums from ~ 800m to ~ 1500m. This may occur because of the influence of Zn-rich CPDW which is right above these depths in both stations (Fig. 17). Alternatively, this may be a deeper, even more refractory, third Zn pool getting dissolved or respired at deeper depths than silicate. This contrasting Zn and Cd depth profile behavior has been reported for both subsurface local maximums and maximum values near the respiration maximum in the Southern Ocean by Ellwood (2008).

When comparing the metal/nutrient maximum depth data, the AOU maximum depths described in the previous page are used as a reference point. The Zn_{TD}/silicate maximums, located at 900, 1500, 1500 and 1050-2500m, occur below AAIW, below AAIW, below both AAIW and CPDW and below both AAIW and CPDW (Fig. 42c). In contrast, the Cd_{TD}/phosphate maximums for the first three stations, located some distance above at 700, 850, 850m, occur above, at and below AAIW (Fig. 42c).

In intermediate and deep water masses, Zn and silicate concentrations are high in AAIW and CPDW (Figs. 42a and b) and very high in AABW (Figs. 43a and b). This is not surprising since these water masses are the origin of the SWMF influence which is observed more intensely in Stations 10 and 8, the southernmost stations on this cruise and thus the closest to the source point of each water mass involved in SWMF. Also, when comparing the three water masses, AABW appears to be the one with the most elevated Zn and silicate concentrations, followed by CPDW and, finally AAIW (Figs. 42a and b, 43a and b, left graphs). In contrast, for Cd and phosphate AAIW is a slightly stronger source than CPDW, probably because the vertical processes (i.e. maximum respiration depth) overcome the horizontal processes (i.e. concentrations changing as the water mass

moves). All in all, there is less station-to-station change for Cd and phosphate (Figs. 42a and b, 43a and b, right graphs) than for Zn and silicate.

Regardless of the different concentrations of metals and nutrients, the Zn_{TD}/silicate ratio stays relatively homogeneous, especially in deep water masses (Figs. 42c and 43c). In contrast, the Cd_{TD}/phosphate ratios are less homogeneous than Zn_{TD}/silicate (Figs. 42c and 43c). The relatively constant Zn_{TD}/silicate ratios are in agreement with global Zn_{TD}/silicate estimates (Ellwood, 2008; Hendry et al., 2008). The global Cd_{TD}/phosphate is quasi linear (Cullen, 2006; de Baar et al., 1994; Frew and Hunter, 1992; Hendry et al., 2008; Yeats, 1998) and has been interpreted using non-linear Raleigh fractionation (Elderfield and Rickaby, 2000); a comparison of data from this study with the extensive global dataset suggests the IOC 1996 dataset, with Equatorial and South Atlantic data, fits right between the literature North Atlantic and the Southern Ocean datasets.

Both Zn_{TD}/silicate and Cd_{TD}/phosphate ratios in deep waters (Fig. 43c) show little variability. Despite AABW bringing very high Zn_{TD} and silicate and slightly increased Cd_{TD} and phosphate (Figs. 43a and b), the ratios are relatively constant with depth, even more than in intermediate waters (Fig. 42c). The Zn_{TD}/silicate in both NADW and AABW are very similar, especially near the very bottom of the water column. More so, an increasing trend on the Cd_{TD}/phosphate values along both u- and l-NADW path (Fig. 43c), from northernmost Station 6 to southernmost Station 10, suggests higher metal/nutrient ratios in older waters. These results are in agreement with the Atlantic-to-Pacific continuum of increasing Cd_{TD}/phosphate ratios caused by preferential Cd uptake with respect to the phosphate (Elderfield and Rickaby, 2000 and references within). The latter causes particles to be Cd-enriched, and deep waters to accumulate Cd-rich particles as they age, ultimately producing higher Cd_{TD}/phosphate in older waters as these particles are respired.

Elderfield and Rickaby (2000) plotted Cd_{TD} and phosphate data down to 3000m only, focusing their observations on NADW, intentionally ignoring AABW, which flows

and ages in the opposite direction, in order to elaborate the Atlantic-to-Pacific continuum of increasing Cd_{TD}/phosphate ratios model. There are only two Cd/phosphate datapoints from AABW in this study (Fig. 43c, right plot) and they show noticeably higher ratios in older waters which have experienced more cumulative respiration, according to the expected trend. Indeed, the Cd_{TD}/phosphate ratio increases in AABW as it moves away from its sources too. Note that the simplified version used in Elderfield and Rickaby's (2000) model does not reflect real complications like the diffusion of northern and southern components in these water masses, i.e. there is no "pure" water mass here, but a continuum of mixtures.

Two specific disclaimers about these ratios in deep waters are discussed next. First, at l-NADW there are two points at ~ 3000m in Stations 6 and Romanche that show a noticeable low Zn_{TD}/silicate value, produced by low Zn_{TD} (Figs. 43c and 40a) with respect to silicate. At this point, it is difficult to state much about these two points; I speculate they might be the product of increased dissolution/respiration between the two NADW water masses. Secondly, in intermediate and deep waters, the profiles from Station Romanche do not follow the trend of the other stations. As mentioned earlier, the location of Stations 6, 8 and 10 make them part of the continuum of water mass travel path along the western intensified boundary, and Station Romanche is some distance off from it; the data coming from Station Romanche should be interpreted with care, falling between stations 6 and 8. To this extent, though the Zn_{TD}, silicate, Cd_{TD} and phosphate plots in deep waters suggest that data from Station Romanche fits right in between the other stations (Figs. 40a and b, 43a and b), Zn_{TD}/silicate and Cd_{TD}/phosphate plots do not clearly show that same trend (Fig. 43c). Similar discrepancies are found in intermediate water masses (Fig. 42). Also, it should be kept in mind that Station Romanche has subsurface hypoxic conditions that might make respiration and other biogeochemical processes different from the rest of stations. In the previous section, the ligand decay in this station was linked to the low oxygen concentrations and the metal/nutrient ratios may be affected too.

5.8.4. Zn_{TD} vs. silicate and Cd_{TD} vs. phosphate

First, some notes on what data are included and what data are excluded of the bulk dataset linearizations. For Zn_{TD} vs. silicate (Fig. 44a), data from Stations Amazon 1 and 2 are not included because they do not show correlation with the rest of data and rather reflect the high Zn_{TD} or high silicate inputs coming from the Amazon River, especially in the surface. Samples from Stations 6, Romanche, 8 and 10 directly in AAIW, CPDW and AABW were not initially included in the main plot. Once these data are contrasted, it is clear that the AAIW/CPDW subset does not fit with the main dataset as the Zn_{TD}/silicate slope of this subset is much higher than the main dataset's (0.107 vs. 0.069 nM Zn_{TD} /μM silicate). The slope of the complete AAIW/CPDW data subset is 0.107 nM/μM and is denoted by a blue circle cluster near the origin. In contrast, the AABW data subset fits almost perfectly with the main dataset, as their slopes differ only slightly (0.065 and 0.069 nM Zn_{TD} /μM silicate); these data are indicated with a blue circle cluster located in the upper right corner of the graph.

The procedure followed for Cd_{TD} vs. phosphate data selection was the following. Data points for which the phosphate was below ~ 0.75 μM are not considered (following Ellwood, 2008), and are generally surface and subsurface samples that do not reflect the proper Cd_{TD} to P ratio. Datapoints from water under the AEF influence, initially excluded from the main plot because of their slightly higher slope (0.45 vs. 0.39 nM Cd_{TD}/μM phosphate), are included in the bulk dataset linearization; these points, indicated with the red circle cluster, are located at Stations 6 and 8 in intermediate waters as high Cd_{TD} and phosphate.

There are no water-mass-specific Zn_{TD}/silicate literature data for this oceanic region (as there are for Cd_{TD}/phosphate for nearby regions) which these data can be compared with. Instead, the source point data for Zn_{TD}/silicate and Cd/phosphate compiled in Fig. 31 is used for reference. Additionally, Yeats (1998) compared the Cd_{TD}/phosphate ratios for all five water masses discussed in this study, compiled from several studies in the North and South-East Atlantic Ocean; those data are directly compared with this study's.

There are some changes in the metal/nutrient ratios that occur in station-to-station transects of the water mass path and also, and there are transect water mass linearized estimates from the four oceanic stations (6, Romanche, 8 and 10), which do not necessarily represent a statistically solid average trend of all station-to-station transects, but rather an arbitrarily-defined whole-cruise transect estimation. The station-to-station transects are the lines that connect stations in Figs. 25 - 31, 33, 38 and 39, and the whole-cruise transects are the arbitrarily-defined trend lines that most of these figures have which connect the source point with the IOC 1996 stations with the theoretical end point along the path of the water mass. Also, the Zn and silicate analyses are more prone to inaccuracies in comparison with the Cd and phosphate data (Geotraces Intercalibration Meeting, Norfolk, March, 2010), mainly because of a silicate polymerization issue that may affect Zn in frozen samples, so that the Zn and silicate data could have lower accuracy. Additionally, the point source Zn, Cd and nutrient data gathered in Table 13 and plotted in Fig. 31 and other figures were obtained with a variety of analytical methodologies, so there could theoretically be an issue with comparing these data, too.

In general, the data from this study and the data gathered from point sources show agreement between the inter-station transect change for the Zn_{TD}/silicate and the Cd_{TD}/phosphate as the water masses travel and age (Fig. 31). This means that in station-to-station transects where there is an increase of one ratio, the other one increases too, except in a couple of instances in deeper l-NADW and AABW where an offset is observed. This station-to-station transect agreement suggests relatively similar chemical processes occurring for Zn_{TD}/silicate and Cd_{TD}/phosphate. The first, basic parameter to compare in the whole-cruise transect estimation is the sign of the trend slope, i.e. if it shows an increasing or decreasing ratio. The slopes for Zn_{TD}/silicate and Cd_{TD}/phosphate in general do not agree for any water mass (Fig. 31), i.e. all stations show that while the whole water mass trend for one ratio is to increase, the other ratio decreases. This suggests a weakness in the whole-cruise transect estimation. Zn_{TD}/silicate appears to be more variable from station to station than Cd_{TD}/phosphate (Zn_{TD}/silicate ranges from ~ 0.05 to 0.17 nM/μM, while Cd_{TD}/phosphate ranges from ~ 0.20 to 0.35 nM/μM). In some of these station-to-station transects, the metal/nutrient ratios increase as the water mass

a

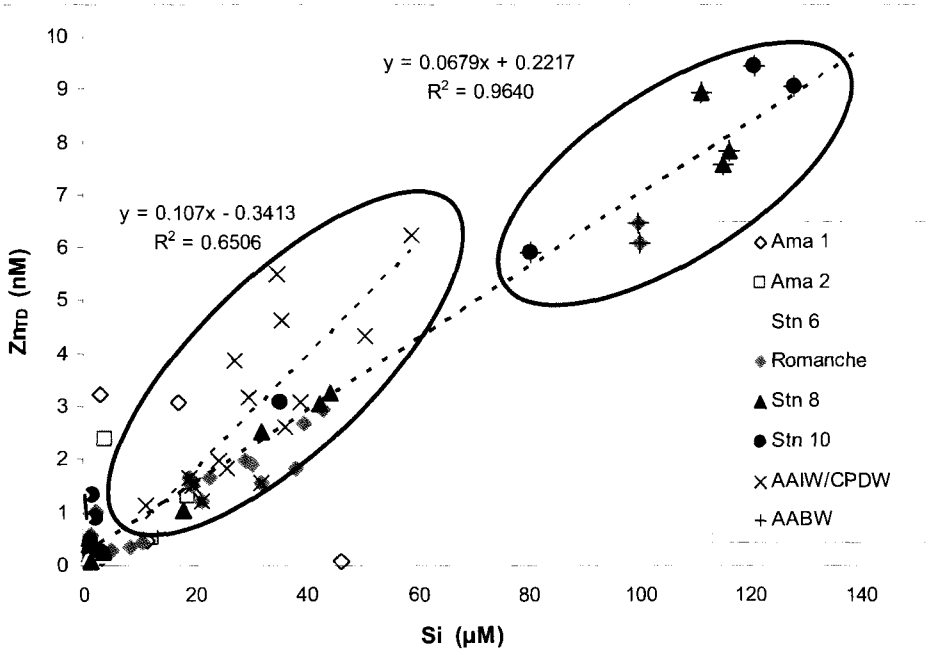

b

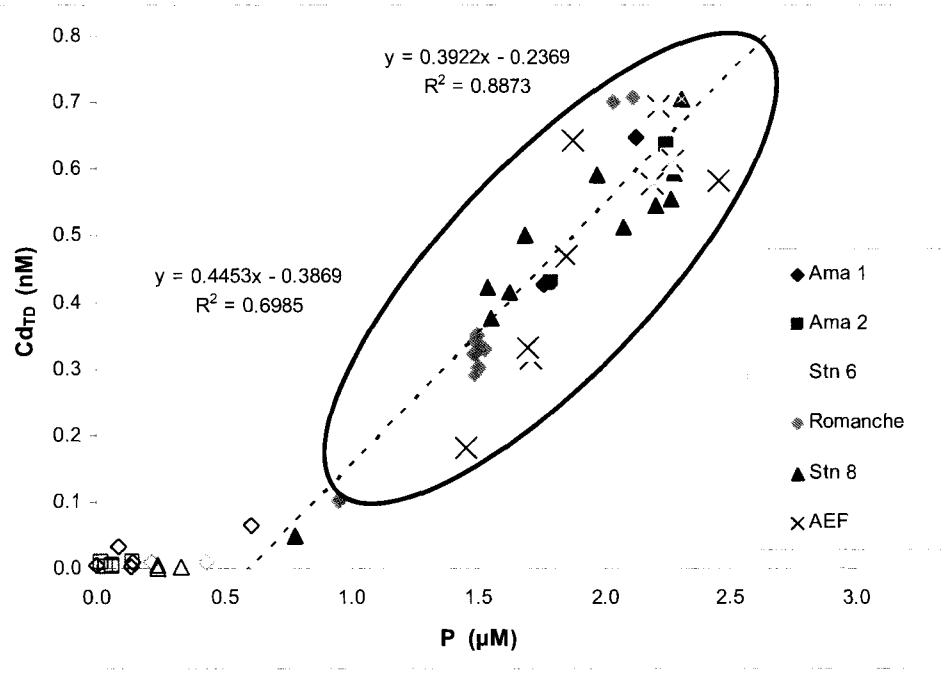

Fig. 44. a) Zn_{TD} vs silicate and b) Cd_{TD} vs. phosphate at all IOC 1996 stations. Not included in the bulk linearization datasets: for Zn_{TD}, Stations Amazon 1 and 2 (empty symbols), samples from Station 10 and 8 directly in AAIW and CPDW (blue exes); for Cd_{TD}, all empty points with less than 0.75 µM phosphate (empty symbols), points influenced by AEF in Stations 6 and 8 (red exes).

ages, while in some others they decrease, in response to local factors like AEF and CSMF, as Fig. 31 shows, with the external influences drawn on top of the whole-cruise trend metal/nutrient ratio for both Zn and Cd. As discussed earlier, SWMF, in contrast, did not seem to have a major effect on either Zn_{TD}/silicate or Cd_{TD}/phosphate

Direct Amazon River data shows a low Zn_{TD}/silicate ratio (~ 0.026 nM/μM; Table 9 and references therein). In contrast, surface waters near the direct riverine sources show all three possible combinations (high-Zn-low-silicate, low-Zn-high-silicate and proportional Zn and silicate points; Fig. 44a, near the origin). Given that in surface waters there are very high chlorophyll values, a large particulate/dissolved fractionation is expected at least in local terms, both horizontally and vertically. Subsurface waters in the same Stations Amazon 1 and 2 show data that fit with the main Zn_{TD} vs. silicate data plot; Station 6 data shows some variability but not points that diverge severely from the main plot slope (Fig. 44).

AAIW and CPDW appear to be Zn enriched in comparison with other water masses. This is initially deduced from the Zn_{TD}/silicate intermediate depth profile (Fig. 42c) and is corroborated with the Zn_{TD} vs. silicate plot (Fig. 44) that shows a significantly higher slope for the AAIW/CPDW subset (0.107 nM/μM) compared with all other water masses (0.0687 nM/μM). I speculate the reason for this relates to the organic matter respiration/silicate dissolution maximum depth generally falling within these two intermediate water masses. Another reason may be the increased Zn load in these water masses, as classic work by Martin et al. (1990) in the vicinity of the Drake Passage and recent work by Croot et al. (submitted) show high concentrations of Zn_{TD} in waters that will influence these two water masses. Also, AAIW and CPDW originate in the Southern Ocean, so high silicate concentrations are expected, too. AAIW differs from CDPW in the fact that AAIW is exposed to the surface (evidenced by high oxygen concentrations) and has lower Zn/silicate, as there is relatively fresh organic matter to be respired and silicate particles to be dissolved. CPDW originates from intermediate waters that have been circulating around Antarctica in the deeper sections of ACC and has not been exposed to surface waters recently. Thus, there is more organic matter to be respired in

AAIW than in CPDW. The AOU depth profiles show that more respiration occurs in AAIW than in CPDW along the Station-6-to-Station-10 transect (Fig. 37b), probably because the AOU maximum falls in AAIW more often than in CPDW. This way the low Zn_{TD}/silicate at source points in AAIW (Fig. 31) would increase to high values near Station 10. From then on to Stations 8 and Romanche, the Zn_{TD}/silicate ratios decrease as high concentrations of Zn_{TD} would presumably be taken up by bacteria. At Station 6, the Zn_{TD}/silicate ratio increases probably because of high Zn_{TD}/silicate ratios in the particulate matter sinking in the region near the mouth of the Amazon River.

In fact, the Amazon River itself has a low Zn_{TD}/silicate ratio (0.026 nM/μM, estimated using Shiller and Boyle, 1985 and DeMaster et al., 1996 data) probably because of the dominance of the silicate load and, though there are noparticulate Zn_{TD}/silicate data, I suggest it is low too. This occurrs despite preferential Zn dissolution by grazing (Fig. 36 shows a phaeophytin/chlorophyll-*a* ratio that, though lower than 1, is the highest of all stations and constant in the upper 100m) and the slightly deeper high respiration (Fig. 37a shows elevated respiration for Station Amazon 1 below ~ 150m, reaching a maximum at ~ 225m and staying that high until the AAIW depth, Fig. 37b).

Of the three water masses originating in the Southern Ocean, AAIW and CPDW have a high Zn_{TD}/silicate signature and AABW does not. In fact, the Zn_{TD} vs. silicate plot (Fig. 44a) shows that AABW's Zn_{TD}/silicate slope is similar to the rest of water masses. Why does not AABW show Zn enrichment as well? The answer might lie in the physical processes that are involved in the formation of AABW and how they make this water mass different from the other two.

AABW forms when Weddell Bottom Water spills over the lip of the Weddell Abyssal Plain and starts to move north (Osterhus and Gammelsrod, 2009). All along the bottom of the Antarctic shelf and further along its path, AABW is in contact with the benthic region which, in the Weddell Sea and the Southern Ocean, has a high proportion of silicate-rich diatomaceous ooze. This study suggests that local interaction between the AABW and the benthos might be responsible for some fluctuations in the metal and

ligand concentrations (Fig. 27e). For the same reason, AABW's Zn_{TD}/silicate may be affected too. In fact, AABW would have to be getting either enriched in silicate, depleted in Zn or both near the bottom of the water column.

Zn/silicate opal ratios relate to the Zn/silicate in organic tissue of a model diatom, *T. pseudonana*, which reflects the Zn^{2+} concentration in solution in the water where the diatom grew, which in turn is related to the Zn_{TD}/silicate in those waters (Ellwood and Hunter, 2000). An important finding of Ellwood and Hunter (2000) is that ~ 3% of Zn taken up by diatoms goes into their opal structure, meaning that ~ 97% goes into soft tissue, which is easily respirable or dissolvable. This way, low Zn/silicate in particles in the bottom of the Southern Oceans, along with high Zn_{TD}/silicate in waters would probably mean there is a balancing Zn flux from the water mass into the benthos. This is observed in the very last two points in each depth profile at Stations Romanche, 8 and 10 in this study (Figs. 17d, e and f). In those points, the bottom sample has lower Zn_{TD} concentration than the sample right above it at the three stations. This may reflect low benthic Zn_{TD} concentrations. Thus, AABW, being the only one of the three Southern Ocean water masses that becomes Zn depleted as it flows because of interaction with the benthos, does not show the Zn enrichment the other two water masses show and rather, as it becomes silicate enriched, appears to have a "normal" slope that fits with the rest of stations' Zn to silicate data.

Finally, the mathematical parameters that define the Zn_{TD} vs. silicate and the Cd_{TD} vs. phosphate relationships (slope, y-intercept, r^2 and n) in relevant literature references are shown in Table 16. They are compared with this study's results (plotted in Fig. 44) in the following part of this section.

For the Zn_{TD} vs. silicate plot, the parameters for the main plot and the AABW are close enough to be merged into one dataset, as the slopes differ by ~ 15%. In contrast, the AAIW/CPDW subset has a significantly different slope (55% higher) and is not included in the main bulk dataset plot. For Cd_{TD} vs. phosphate, the main plot's parameters are close to the AEF's influence (~ 13% off), and they were merged into one

plot. The three data subsets are rather small and variable, as their low n and r^2 suggest.

Zn and silicate are linearly related in deep waters, with increasing concentrations of both along the global oceanic conveyor belt's deep waters as more silicate particles dissolve with time. In this study, despite the high concentrations of both Zn_{TD} and silicate in AABW (Figs. 43a and b), the ratios remain constant (Fig. 43c). Using the solid average world ocean Zn_{TD} vs. silicate relationship and the extensive silicate data available, Zn_{TD} was estimated globally (Bruland and Lohan, 2003); the IOC 1996's results fall very close to the world estimates. A closer comparison of the Zn_{TD} vs. silicate dataset from the Southern Ocean, South Pacific and Drake Passage (Croot et al. submitted; Ellwood, 2008; Martin et al., 1990) shows that this study's main dataset fits within their range. On the other hand, both the Ross Sea shelf non-productive deep waters (shallower than 300m) and the Weddell Sea's (shallower than 300m) datasets (Fitzwater et al., 2000; Nolting et al., 1991) show comparable elevated slopes, possibly because of increased grazing and respiration of diatomaceous phytoplankton in the shallow waters of these very productive waters where intermediate waters like AAIW and CPDW are believed to be formed.

In contrast to Zn_{TD} vs. silicate, Cd_{TD} vs. phosphate shows a non linear relationship that could be interpreted as Cd fractionation, as Cd is preferentially adsorbed onto particles and taken up by phytoplankton in surface waters. Thus, POM is enriched in Cd compared with surface water and, as a consequence, Cd_{TD}/phosphate increases along the conveyor belt's deep waters as more particles fall and get respired with time (Yeats, 1995; Elderfield and Rickaby, 2000). In this study, despite the not-so variable Cd and phosphate concentrations in NADW and AABW (Figs. 43a and b), the Cd_{TD}/phosphate ratios show a relatively variable trend (i.e. Station 6 data are lower than Station 8 in Fig. 43c). The average Cd_{TD}/phosphate in deep waters for all stations (~ 0.24 nM/μM; Fig. 43c), being the average of Equatorial and Southern Atlantic Ocean data, fits between Atlantic and Indian Ocean data Cd_{TD}/phosphate ratios, ~ 0.18 and 0.31 nM/μM (Elderfield and Rickaby, 2000). More specifically in the Atlantic Ocean, the water mass analysis of Yeats (1998) suggests that AAIW/CPDW are slightly Cd-depleted compared

Table 16

Literature values of the linear regression parameters for Zn_{TD} vs. silicate and Cd_{TD} vs. phosphate compared with data from this study and shown in Fig. 44 (see it for main plots and exceptions). References: a) This study, b) Croot et al. (submitted), c) Ellwood (2008), d) Martin et al. (1990), e) Fitzwater et al. (2000), f) Nolting et al. (1991) g) Bruland and Lohan (2003) and h) Yeats (1998) and references therein.

Current/Region	Slope	y-intercept	r^2	n	References
Zn_{TD} vs. silicate					
This study, main Zn vs. silicate plot	0.069	+ 0.167	0.968	50	A
This study AAIW/CPDW	0.107	- 0.341	0.651	15	A
This study AABW	0.080	- 0.984	0.730	8	A
Southern Ocean	0.040	+ 0.67	0.859	130	B
South Pacific (< 1000m)	0.077	+ 0.201	0.914	97	C
Drake Passage	0.059	+ 0.199	0.946	10	D
Ross Sea shelf					
Productive surface waters	0.017	- 0.264	0.600	6	E
Non-productive deep waters	0.095	- 2.187	0.914	31	E
Weddell Sea (< 300m)	0.10	+ 0.94	0.640	55	F
Average World Ocean	0.063				E
Average 3000m estimate	0.05	+ 0.8			G
Cd_{TD} vs. phosphate					
This study, main Cd vs. phosphate plot	0.392	- 0.237	0.887	33	A
This study AEF	0.445	- 0.387	0.699	9	A
South Pacific (< 1000m)	0.444	- 0.262	0.943	98	C
Drake Passage	0.650	- 0.855	0.973	10	D
Ross Sea shelf > 0.75 μM phosphate	0.597	- 0.570	0.934	35	E
Atlantic Ocean					
AAIW ($\sigma_t \sim 27.25$)	0.334	- 0.129	0.971	30	H
CPDW ($\sigma_t \sim 27.5$)	0.382	- 0.195	0.961	30	H
u-NADW ($\sigma_4 \sim 45.8$)	0.419	- 0.234	0.967	28	H
l-NADW ($\sigma_4 \sim 45.85$)	0.403	- 0.233	0.984	26	H
AABW ($\sigma_4 \sim 45.95$)	0.419	- 0.233	0.958	25	H

with the other three water masses present in this study. In this study, there are not enough data from each water mass to produce robust plots; however, CPDW appears to have lower slopes than l-NADW and AABW, confirming Yeat's hypothesis.

The Cd_{TD} vs. phosphate relationship can also be interpreted as a combination of linear relationships and a "kink" at ~ 1.3 μM phosphate (Yeats, 1998 and others). In this study, this kink is not observed (Fig. 44), probably because of samples reflecting their Equatorial and South Atlantic location's slopes which are somewhere in between the Atlantic and the Southern Ocean's slopes in Elderfield and Rickaby's (2000) compilation of data. This means that the interpretation that invokes two separate linees for different oceanographic regions is not supported by these data, and the "kink" seems to be rather gradual, potentially supporting Elderfield and Rickaby's (2000) Rayleigh fractionation hypothesis. Further, the average fractionation factor of the main plot is estimated to be ~ 2, in very good agreement with the ~ 2.5 modern global ocean estimate.

5.9. LIGANDS : SOURCES AND PROCESSES

In this section, possible relationships relating to the presence of complexing ligands, in surface, intermediate and deep waters are analyzed. First, the possible chemical identity of the ligands is discussed; later, different potential ligand sources. An analysis of the processes related to ligand decay follow, with emphasis on the residence time of ligands. Finally, there is a note on the specificity of the ligands for Zn or Cd.

5.9.1. First oceanic report of more than one ligand for Zn and Cd

This is the first time two or three strong Zn- and Cd-complexing ligands are reported in oceanic environments. This is because of two reasons, one related to the method and one to the nature of the samples.

First, the mathematical tool used in this study (TDI) allows for discernment between two or even three ligands that complex a metal. Historically, linear approaches have been and continue to be used now. The Ruzic linear method was the only linear

method used in Bruland (1989), Ellwood and van den Berg (2000) and Ellwood (2004). Bruland (1992) used both Ruzic and Scatchard linear methods, for one ligand only. Kozelka and Bruland (1998) used Scatchard linearization and more than one ligand was reported for Pb and Cu; they also used a method that extrapolated linear section of incomplete titrations, designed by Hudson et al. (2003). The mathematical tool used in this study uses Ruzic and Scatchard linearizations to visualize the data and then the Scatchard linear plot to decide if one or two ligands are present. The raw L and K' parameters produced by the Scatchard plot are then fitted to the Gerringa non-linear method to obtain optimized L and K' parameters. The errors in Ls and K's are reduced to a minimum which compares favorably with those of linear methods (Table 5).

Secondly, a comparison of the logK's produced in this study with previously reported data (Table 8) suggests that strong and weak ligands are found in this location because of its oceanographic diversity. In this location, riverine organic matter coming directly from the Amazon River, remineralized organic matter coming from the Congo River, intermediate and deep water masses originating in both polar regions and surface waters from different regions create a potential for finding diverse organic matter such that the three Zn- and Cd-complexing ligands are reported in one single study.

Previous metal-complexation studies reporting more than one Zn or Cd ligand were performed in coastal and estuarine environments where weak ligands were observed. Van den Berg (1985) reported two Zn ligands in the surface coastal Irish Sea with logK's 8.4 and 7.5 and high $Zn_{TD} \sim 26$ nM. This resembles the high-metal-and-ligand-concentration that Kozelka and Bruland (1998) found in the Narragansett Bay, where only one Zn ligand and Cd were measured (logK' 9.0 and 8.9), contrasting with three for Cu and two for Pb.

On the other hand, Zn and Cd complexation in both surface and deep waters have only been studied recently, including this study and those of Ellwood and van den Berg (2000), Carrasco et al. (2008) and Baars and Croot (2010). Ellwood and van den Berg (2000) presented the first evidence of Zn- and Cd-complexing ligands in deep waters in

the North Atlantic. This may be in part because the paradigm until the 1990's was that metal-binding ligands were mostly present in surface waters and that their presence in intermediate and deep waters was not important for the metal chemical speciation of bioactive elements that show nutrient-type profiles (Bruland, 1989 and, 1992).

5.9.2. Ligand concentration water mass structure

An Fe complexation and speciation study of the IOC 1996 cruise shows the presence of an Fe ligand in deep waters, though with less water column resolution (Powell and Donat, 2001). They state there is not much variability in ligand concentration related to water mass structure, though some notable similarities and differences with this study help to draw some relationships between ligands for Fe with those for Zn and for Cd. Powell and Donat (2001) found very high percentages (more than 99 %) of Fe complexed with a strong ligand mainly because the ligand was in excess of the Fe_{TD} concentration; this dissertation shows very water-mass-dependent complexation for Zn and a more consistent speciation for Cd dominated by inorganic complexation in intermediate and deep waters. They reported the upper 70m of the Amazon River not to be a major source of Fe-complexing ligands to the open ocean; I studied a 400m water column in the two Amazon Stations and observed ligands present in the surface waters that may be produced by phytoplankton or brought by the river water, and subsurface ligands that seemed to be related to respiration processes. Looking for information about the three influencing factors, they report Station 6 at ~ 900m has very high Fe L concentration that matches my data showing the highest Zn and Cd ligand concentration of all intermediate water profiles, which I hypothesize relates to the POC-flux-mediated AEF influence. Donat and Powell's (2001) study does not report data between 3000 and 5300m in, and thus the influence of CSMF is mostly overlooked; this is in clear contrast with this study's results which show very high Zn_{TD} and three Zn ligands in the highest L_T concentration of all depths reported in this study (~ 6.3 nM Zn_{TD} and ~ 19.1 nM L_T) coming from water masses influenced by Souther Ocean originated organic matter. Their Fe_{TD} and Fe L in AABW at Station 8, similar to this study's Zn ligands, show low ligand concentrations at 4700 and higher concentrations at the bottom of the water column, which I hypothesize relates to interactions with the benthic region.

Another similarity between these two studies is the high ligand concentrations for ligands for both Fe and Zn reported in u-NADW at Station Romanche.

Cutter and Cutter (2001), Cuttter et al. (2001) and Mason and Sullivan (1999) reported the organic complexation of Se, As and Sb and Hg in the IOC 1996 cruise. Organic ligands that complex Se may be "acquisition" ligands since Se is a required element, in contrast to the ligands that complex As and Hg, reputedly "detox" ligands because of these elements' deleterious effects. The latter makes As and Hg ligands not directly nor necessarily comparable to the metals discussed in this study; regardless, these elements' ligands are discussed in the interest of studying processes related to complexing ligand formation and decay. The ligands that bind As and Hg (and Sb by chemical similarity to As) are methyl radicals; thus, monomethylated (MM) and dimethylated (DM) molecules of such elements are formed (molecular weights: 15 and 30 Da). These methylated forms of the metals are reputedly produced by bacteria to facilitate the ingestion of toxic elements by higher trophic level members.

Cutter and Cutter (2001) showed the presence of organic ligands for Se in surface waters only, suggesting a relationship with phytoplankton. The only exception is AAIW and CPDW at Station 10, the southernmost station, where apparently the short-lived ligands (residence time is less than 10 years) occur, probably carried by these relatively young intermediate depth water masses. As these water masses flow north, the ligands decay and their presence is not observed at Station 8 nor at any other station further north. Rapid ligand concentration decrease occurs in this case.

Similarly, Cutter et al. (2001) followed the MM and DM forms of As and Sb which appear to be formed in surface waters only. Though the Amazon River does not seem to be a source of either element, Station Amazon 1 shows the highest concentration of methylated forms of As. The subsurface local maximum of MMAs and DMAs in Station 10 at around 200m is notable also, for it matches with this study's high levels of organic complexation of Zn (Figs. 21f and 23f) and increasing AOU levels (Fig. 37a).

Both Amazon 1 and Station 10 examples suggest bacterially-mediated formation of methylated forms of As and Sb.

While Cutter and Cutter (2001) and Cutter et al. (2001) pointed to surface waters as the main source of ligands for Se, As and Sb, Mason and Sullivan's (1999) data indicate no MMHg nor DMHg in either surface waters, nor in Amazon Stations. They show evidence of ligands coming from water masses originating recently in the Southern Ocean. AAIW, CPDW and AABW show decreasing ligand concentrations from Station 10 to Station 8, suggesting these methylated forms have longer residence times than those of Se which were observed only in Station 10. Another methylated-Hg source accounted for in their paper is the particulate matter in equatorial latitudes that produces high microbial activity (AEF in this study), indicated as increased AOU in intermediate depths at Stations Romanche and 6. Finally, NADW, being ~ 100 years old by the time it reaches the stations occupied in this cruise, shows very little concentrations of methylated Hg forms in all stations except Station Romanche at 3500m where the second highest DMHg value of all stations and depths in a sample where Hg_{TD} is not particularly high was unaccounted for by the authors; I suggest it may indicate high concentrations of remineralized organic matter from CSMF influence.

All in all, comparing this study's data to all previous studies dealing with metals' and metaloids' complexation and speciation on the IOC 1996 cruise, Powell and Donat (2001), Cutter and Cutter (2001), Cutter et al. (2001) and Mason and Sullivan (1999), some localized influences are indicated in their results that match with this study's, specifically the three influencing factors AEF, SWMF and CSMF.

Additionally, when comparing: a) Powell and Donat's (2001) relatively homogeneous Fe L concentrations, b) this study's results that show Zn and Cd ligand concentrations changing with time along aging water masses, c) Mason and Sullivan's (1999) ligands for Hg at Station 10 and 8, and d) Cutter and Cutter's (2001) ligands for Se at Station 10 only, the logical conclusion is that there are different complexing ligands for different elements with different reactivities and different net decay rates that are

transported and age along water masses originated in high latitudes. In fact, the Fe ligand seems to be more refractory and resistant to degradation than Zn and Cd ligands, which in turn are more refractory than those for Hg, which are in turn more refractory than those for Se in the observed water masses in the Equatorial and South Atlantic Ocean.

Regarding local sources of high concentrations of ligands, this study's results suggest the presence of ligands in surface waters (i.e. Zn L1 and Zn L3 in Station Amazon 1 and 2, Cd L1 at Station Romanche and 8), in intermediate or deep waters (i.e. those affected by AEF and CSMF influences) or near the bottom of the water column (i.e. the benthic factors that seem to be affecting Station Romanche and 8 bottom waters). Besides these ligands, there are ligands whose similarity to ligands of global distribution in terms of L and logK' suggest they could be globally spread out. Particularly, strong ligands Zn L2 and Cd L2 have been observed mostly in open-ocean environments before (North Pacific, North Atlantic and Southern Ocean), while weaker Zn L3 and Cd L3 have been observed in both open-ocean (North Pacific and Southern Ocean) and estuarine environments (Chesapeake Bay and Narragansett Bay).

5.9.3. Chemical Identity of the Ligands

Some substances have been suggested to be related to the ligands. This section presents a literature review of the most important, pondering why they are or not related to Zn and Cd ligands in this study. Some of them have been studied in terms of their *in vitro* metal complexing properties, while some field studies have determined their concentrations. Both L and logK' parameters of suspect substances sulphide, thiols, phytochelatins and CA have been investigated in seawater.

The binding strength of sulphide to Zn, Cd and Cu was studied (al-Farawati and van den Berg, 1999) and the logK's for each metal (6.1, 8.4 and 12.9) suggest sulphide is strong enough for being Cu L1, but is much weaker than other naturally existing Zn- and Cd-complexing ligands. Further, sulphide's concentrations in the few tens of picomolar (average ~ 0.06 nM in the North Atlantic; Cutter, 1999) confirm that they could not be the ligands discussed in this study which are on the nM range. In estuarine environments,

sulphide appears to play a role in the redox speciation of Zn and Cd (Gerringa et al., 2001) which I suggest may be relevant to OMZ regions.

Phytochelatins, polymers of thiol excreted by phytoplankton as a way to deal with metal stress (Dupont and Ahner, 2005), were studied in the Chesapeake Bay and Elizabeth River (Carrasco et al., 2002; Donat et al., 2002); the correlation of the presence of ligands and phytochelatins was strong (Wei et al., 2003). Zn L2, Zn L3, Cd L3 and Cd L4 were present in that study (logK' 10.4, 8.7, 9.4 and 8.4; Donat et al., 2002). Phytochelatins are a good suspect for the "detox" ligand, since their dissolved concentrations were in the order of nM in that study (Wei and Ahner, 2005), though their particulate concentrations can be much higher.

For the "acquisition" ligand, Sarthou et al. (2001) studied *in vitro* the affinity of bovine carbonic anhydrase (CA) in seawater. They found CA to bind to Zn in similar strength to Zn L3 (logK' 8.6). On the other hand, the possible inter-replacement of Zn, Cd and Co for one CA (Xu et al., 2007) implies that this enzyme would be somewhat of a non-specific ligand. This is in contrast to this study's results of ligands for Zn and Cd ligands, which are present in different concentrations ranges and in different permutations (high-Zn-ligand-high-Cd-ligand, high-Zn-ligand-low-Cd-ligand, low-Zn-ligand-high-Cd-ligand and low-Zn-ligand-low-Cd-ligand). These enzymes are present inside and outside the phytoplankton cells, thus its intra- vs. extra-cellular concentrations could be related to particulate vs. dissolved ligand concentrations.

Some substances are believed to be related to the Zn and Cd ligands. At this point there is no study that can prove categorically that they are the same chemical entity. Further, the evidence for correlation of some of these substances with the presence of the ligand in estuarine environments does not necessarily prove or disprove the same substances would be present in open-ocean environments.

5.9.4. Ligands sources

Irrespective of their chemical nature, next a brief review of the potential ligand

sources is listed. This study's results are related to some of these sources, so emphasis is given to possible relationships that could help discern the nature of these ligands. For comparison purposes, the ligand sources are divided into three theoretically separated, but in reality very interlinked, groups: a) live phytoplankton, b) dead or lysed phytoplankton and c) non-planktonic sources. Each group comprises a series of processes that might overlap with other group, while some are very specific and clear.

a) Live phytoplankton.

Ligands related to live phytoplankton would presumably be present in surface waters, i.e. in the euphotic zone. If some processes occur to the phytoplankton present and they are affected, they would be in the next conceptual group described (dead or lysed phytoplankton).

Moffet and Brand (1996) showed that under Cu stress, certain phytoplankton species produce ligands to cope with potentially toxic Cu concentrations (i.e. "detox" ligands). On the contrary, Lohan et al. (2005) suggested Zn-binding ligands are produced in low Zn conditions and in a matter of hours (less than one day) by active production, not by cell lysis, to assist assimilation under Zn limiting conditions (i.e. "acquisition" ligands). Also ligands for Fe have been reported to be related to diatom exudates (Zhang et al., 2004).

In this study, some phytoplankton, like the species living in the surface of Station Amazon 1, are so intensely defined by the riverine-source-influenced environment that it is hard to say that they are a phytoplanktonic source, as they are in reality more of a ramification of the riverine source. That is, the borderline between allochthonous riverine and authocthonous phytoplanktonic organic complexing ligands is difficult to distinguish. As such, they are discussed in the non-planktonic sources section.

The logical parameter to gauge live phytoplankton is chlorophyll-*a*, which is to be compared with the ligand concentrations in this section. Phaeophytin and

AOU are used as proxies of zooplankton grazing and respiration (including both bacterial and zooplanktonic, as oxygen consumption does not discriminate between them) in the dead-plankton as ligand source section; note that phaeophytin maximum has been discussed in a previous section in relation to a Zn_{TD} local maximum, presumably caused by local maximum Zn regeneration. The phaeophytin/chlorophyll-*a* ratio is used as a proxy of grazing overcoming primary productivity. When the ligand maximum depth coincides with the chlorophyll-*a* maximum depth, phytoplankton are suggested to produce the ligand; in contrast, when the ligand maximum depth is below that of the chlorophyll-*a* maximum, it is suggested that either bacteria living underneath the phytoplankton eat them and liberate the ligand or zooplankton grazing liberate the ligands by excreting digested phytoplankton. Alternatively, Gerringa et al. (2006) suggested a distinction between diatoms and *Synechococcus* or picoeukaryotes based on their relative position with respect to the chlorophyll-*a* maximum. While the former are located at the chlorophyll-*a* maximum, the latter are located below it. This could create a potential conflict with the bacteria or zooplankton hypotheses mentioned above.

In their study of Fe ligands in the North Eastern Atlantic, Gerringa et al. (2006) proposed a distinction between metal binding ligands based upon their depth relative to the chlorophyll-*a* maximum depth. They distinguish the following four depth ranges:

- In the surface mixed layer (SML)
- Above maximum of deep chlorophyll-*a* maximum (MDCM)
- At MDCD
- Below MDCM

The data obtained in this study does not have enough surface depth resolution to distinguish between the first two depth ranges; there is usually one sampling point in the mixed layer which also falls above the MDCM and then the next point in the depth profile is the chlorophyll-*a* maximum. Thus, SML and

above MDCM are together. This study's plots of Zn and Cd ligands and photosynthetic pigments (Figs. 23 and 24) depict the following ligand depth distributions:

- In the SML/ above MDCM:
  Zn L1 and Zn L3 are present in some stations, being L3 in excess of Zn_{TD}.
  Cd L2 and Cd L3 are present in a couple of stations.
- At MDCM:
  Zn L2 is present in some stations.
  Cd L2 and Cd L3 are present in some stations; Cd L1 is present only in this depth range.
- Below MDCM:
  All Zn ligands are present in some stations; Zn L3 is present a few tens of meters below MDCM, concomitant with the phaeophytin maximum.
  Cd L2 is found more often here than Cd L3.

There are scarce literature data to compare this study's results with. As mentioned in the third chapter, the simple mathematical methodology frequently used to obtain the L and K' parameters tends to simplify the results and produce one ligand for each metal. Reviewing the ligands compiled in Table 8, the most commonly seen ligand in oceanic environments is Zn L2 and the general trend is to observe a relatively uniform depth distribution (e.g. Jakuba et al., 2008; Ellwood, 2004; Bruland, 1989). However, Ellwood and van den Berg (2000) showed high Zn L2 at SML/above MDCM which decreases around and below MDCM and increases again in deeper waters; Baars et al. (2010) showed low Zn L2 and Zn L3 at SML/above MDCM increasing at MDCM and increasing even more below it. Cd ligands have been shown to be either uniformly distributed in a curious case of an apparent ligand that binds to both Zn and Cd (Ellwood, 2004) or to have a specific depth range where they are present, like in Bruland's (1992) study showing Cd L2 present only in waters around the MDCM.

The mathematical methodology of Baars et al. (2010) allowed finding more than one ligand, but the common presence of saturated ligands did not; in the end they report Zn L2 and a weaker ligand Zn L3 but only after using separate electroanalytical techniques to characterize each ligand. Carrasco et al. (2008) used the same mathematical and instrumental methodology used in this study and thus, their results are the most comparable to this study's. They find Zn L1 distributed above, at and below MDCM in different stations with a trend that appears to be difficult to interpret. In contrast, Zn L3 is present mostly below MDCM, being related to either respiration or grazing processes. For Cd, Cd L1 is present mostly below MDCM, while Cd L2 and Cd L3 are present at the SML and also below the MDCM.

The ligand depth distribution has not often been analyzed using Gerringa et al.'s (2006) scheme. In general, combining the data obtained in this study from the Equatorial South Atlantic with Carrasco et al.'s (2008) data from the Western North Pacific, the following trends appear to exist:

- In the SML/above MDCM:
  Cd L2 and Cd L3 are present often.
- At MDCM:
  There is some discrepancy between Pacific and Atlantic data showing Zn L1 and Cd L1 here.
- Below MDCM:
  Zn L3, Zn L1 and Cd L2 are present in both basins.

Though a comparison of environmental, biological and ecological niches as different as those encountered in the datasets compared is not very conducing, the cross-basin comparison is still valid as such. The general results this comparison produces indicate that the strongest ligands (Zn L1 and Cd L1) are produced *in situ* in some locations in direct relation to phytoplankton, for they are present at the MDCM. Recently, Bown et al. (2010) reported a Co ligand that positively

correlates with chlorophyll-*a*, too. Conversely, the presence of less strong Zn L3 and Cd L3 both above and below the MDCM may indicate the ligands are being produced by a minor phytoplankton species that lives above MDCM or by respiration or grazing.

Focusing on this study's results, Fig. 45 shows the presence of some Zn and Cd ligands at or below the chlorophyll-*a* maximum across all the stations occupied. In Fig. 45a, good correlation between Zn L2 and chlorophyll-*a* at the MDCM suggests that the ligand concentration could be linearly estimated at that specific depth range based upon the chlorophyll-*a* concentration. On the other hand, three separate environmental surface water regions are defined: the Amazon River influenced region (Station Amazon 1), the equatorial and tropical latitude (Stations Amazon 2, 6 and Romanche) and the higher latitude region (Stations 8 and 10); of those regions, the equatorial and tropical region seems to have a lower ligand concentration per chlorophyll-*a* molecule than the higher latitude region. The more prevalent phytoplankton species in each station (Table 15) do not show common species within each of these regions, but the ligand may not necessarily be produced by a major, prevalent phytoplankton species; rather minor species could be producing the ligands to outcompete other major species.

b) Dead or lysed phytoplankton.

Another potential ligand source is phytoplankton that has underwent chemical processes related to biological agents. Since Fe has been studied more, there is evidence for a supposed "acquisition" Fe ligand produced by microzooplankton and copepod grazing (Sato et al., 2007) or by viral phytoplankton lysis (Poorvin et al., 2004). For Zn, ligands have been related to dead *Emiliana huxleii* (Muller, 2003). Also, "detox" ligands for Cu have been reported to be produced by heterotrophic bacteria (Gordon et al., 2000). Knowing that phytoplankton are consumed by zooplankton and sink to the bottom of the water column as fecal pellets, a step further in the biogeochemical degradation continuum of live phytoplankton to dead phytoplankton to grazed phytoplankton is investigating for metals and ligands being

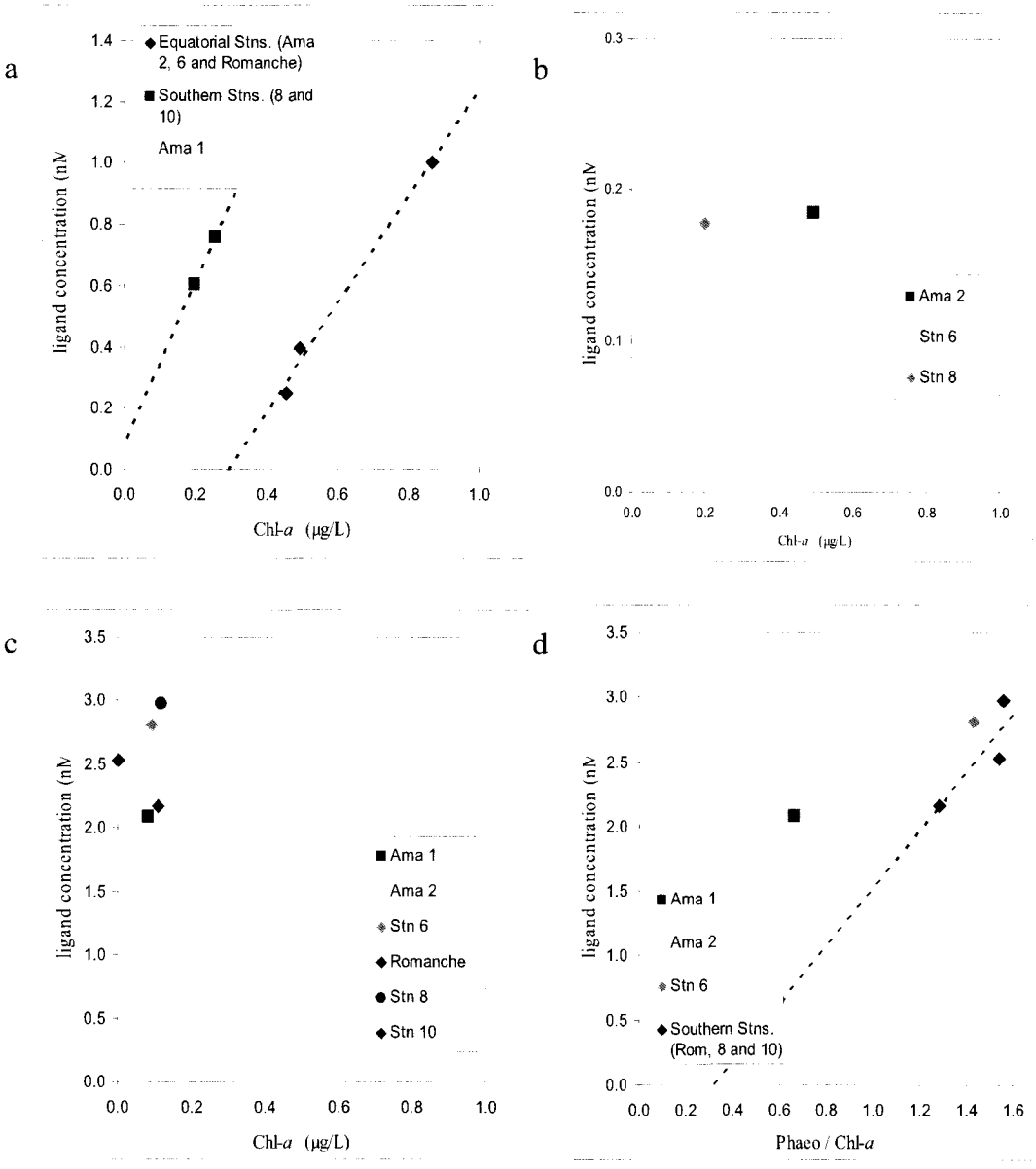

Fig. 45. Some Zn and Cd ligands correlated with chlorophyll-*a* at or below the chlorophyll-*a* maximum: a) Zn L2 at MDCM (maximum of deep chlorophyll-*a* maximum), b) Cd L3 at MDCM, c) Zn L3 below MDCM and d) Zn L3 below MDCM correlated against the phaeophytin/chlorophyll-*a* ratio.

fluxed in or out of the benthos both locally (Carrasco et al., 2002) and in a bigger, basin-wide and potentially global scale picture scheme, out of continental shelves (Carrasco et al., 2008, Lam et al., 2008). For this study, there are data for a grazing proxy (phaeophytin) to compare the ligand data against, yet there are no data for viruses.

Figs. 45b and c attempt unsuccessfully to find correlations between Cd L3 and Zn L3 (at and below MDCM respectively) and chlorophyll-*a*. There are not many points in the Cd L3 plot, and there is not correlation among the few available (Fig. 45b). For the Zn L3 below MDCM plot, there are data points from all stations, suggesting that Zn L3 at this depth is a common occurrence in the Equatorial and South Atlantic; however, the correlation with chlorophyll-*a* is poor (Fig. 45c).

Looking at the depths at which these Zn L3 maximum concentration points occurred (Fig. 23), it became clear that for the Southern region group (Stations Romanche, 8 and 10) the data points occurred at or immediately below depths where the phaeophytin/chlorophyll ratio surpasses a value of 1.3 or higher, which denote not initial overcoming of grazing (passing the 1 value, marked by a dashed line in Fig. 36), but a bit deeper, denoting a more intensely grazed phytoplanktonic mass; Station 6 has a point that could be also grouped with this data subset. In contrast, Stations Amazon 1 and 2 have high ligand concentrations at lower phaeophytin/chlorophyll ratios, owing to the fact these stations are dominated by net particle export in the upper section of the water column, very contrastingly to the rest of stations. These data are plotted in Fig. 45d, which seems to indicate that intensely grazed phytoplankton (to the point of phaeophytin/chlorophyll ratios higher than 1.3) may positively correlate with the Zn L3 concentration at its maximum below the MDCM. In other words, more grazing acid-squeezes more ligand out of grazed phytoplankton.

c) Non-planktonic sources:

Other potential metal and ligand sources include rain, dust, riverine organic matter and heterotrophic bacteria.

Rain has been studied from the trace metal ligand perspective only in the recent few years. Helmers and Schrems (1995) showed Zn and Cd among other metals in rain in the Equatorial and South Atlantic being more concentrated than in seawater, as they wash out effectively atmospheric metal sources coming from nearby locations of dust or anthropogenic emissions; Zn and Cd are in the range of 6 - 60 and 0.3 - 3 nM, accounting for a lot of the $M_{TD,}$ specially in the rainy ITCZ region where Station Romanche is located. Baker et al. (2007) state that the ITCZ region sees approximately equal fluxes of wet and dry deposition of Fe and Zn, while in the dry regions there is dry deposition predominance. Dry deposition in the Equatorial and North Atlantic focuses on Saharan dust bringing metals to the region. Sarthou et al. (2007) reported Fe data but there are no direct data for other metals coming from Saharan dust. From a ligand perspective, Kieber et al. (2004 and, 2008) studied the complexation and speciation of Cu and Hg in rainwater and report the presence of similarly strong ligands for Cu in rainwater as in seawater (logK' higher than 12) and methylated forms of Hg occurring in rainwater. Though there are reports that track atmospheric deposition and sustain desert dust is an important metal source to certain regions (e.g. Baker et al., 2007 and references therein), more work needs to be done on determining the complexation and speciation of metals in rainwater and in atmospheric particles in order to determine their magnitude as a source of ligands and (complexed) metals to the world's oceans.

Other source of organic metal-binding ligands is riverine organic matter. The current paradigm sustains that rivers bring weak humic-like substances to oceanic regimes and that strong ligands are produced by phytoplankton living in surface waters and hence must correlate well with chlorophyll-*a* (as discussed in the previous sections). Recently Hoffmann et al. (2007) reported ligands as strong as logK' ~ 13 for Cu and Zn in river waters; Ellwood et al. (2001) reported a strong

Zn ligand (logK' ~ 10.1) in freshwaters lakes in New Zealand; and Shank et al. (2004) found that strong ligands for Cu (logK' 13.5) can be provided to the oceans by riverine input, suggesting that their presence could have not only local, but global implications. Hoffmann et al. (2007) and Ellwood et al. (2001) would compare to Zn L1 and Zn L2, respectively. In this study, the specific influence of the Amazon River has been discussed in an earlier section of this chapter. The question is if the Amazon River evidences a source of weak or strong ligands.

The results of the upper 400m of this study (Figs. 23 and 24, Tables 10 and 11) show very high concentrations of a weak Zn ligand in excess of $Zn_{TD,}$ and a strong-ligand-dominated speciation for Cd in Station Amazon 1, the most riverine station. In contrast, Station Amazon 2 has a strong Zn ligand on top of the weak ligand and no Cd ligands. In waters below the upper 15m in both stations, the increasing presence of strong Zn and Cd ligands and the decreasing concentrations of weak ligands suggest there are biogeochemical processes that may affect the binding strength of these ligands. Besides the immediate influence of these surface waters on possibly a wide region in the Equatorial and North Atlantic Ocean, the Water Mass section of the discussion chapter suggests the influence of the Amazon River's organic matter (AEF) and also the Congo River's organic matter, sedimented to the bottom of the Congo canyon and respired at ~ 4000m depth and mobilized along a thin water mass (CSMF) on intermediate and deep waters. Separate sections discuss the influence of each of these two factors which together suggest a potential spreading of riverine organic matter sources once they fall into a water mass that could transport them; they ultimately are upwelled somewhere else or mixed with another water mass that is upwelled, spreading globally the water mass Zn and Cd complexation and speciation signature.

Another source of metals and ligands are heterotrophic bacteria (Krey, 2008). Fe ligands have been reported to be produced by heterotrophic bacteria (Krey, 2008), which accumulate metal and organic matter that could be liberated by

virtue of protozoan activity (Vogel and Fisher, 2009 and, 2010). Not much is known about heterotrophic bacteria and Zn or Cd.

5.9.5. Residence time of ligands and decay rates

In order to evaluate the residence time of these complexing ligands, their net decay rates need to be estimated. In the Water Mass section, apparent decay rates were discussed as observations of decreasing ligand concentrations in aging water masses were measured in discrete locations along their travel paths. Assuming no other processes occur than the decay discussed here, the decay rate can be estimated based on the concentration change observed in the time interval between stations, estimated from the distance between them. In the Water Mass section, it was mentioned that the stations being used for discrete points along the path of water mass are the stations near the western edge of the basins studied (Stations 6, 8 and 10) and not necessarily Station Romanche, located further east. The concentration vs. latitude plots (Figs. 25 - 31, 33, 38 and 39) show Station Romanche along the other more linearly comparable stations so that all stations could be contrasted. Figs. 25 - 29 have the data obtained in this study only, while Figs. 30, 31, 33, 38 and 39 show also points of the same parameters obtained from other studies. Given that, the decay rates estimated here were estimated with more confidence and without more analytical constraints within this dissertation's dataset only, i.e. within the Station-6-to-Station-10 north to south transect.

As mentioned in the Water Mass section, there are three methodologies commonly used to determine the water mass age; regardless of the absolute age value, Huhn et al. (2008) provided an estimate of ~ 40 years as the amount of time any of the water masses take on average to travel between Station 6 and 10 in either direction (AAIW, CPDW and AABW travel towards the north, while u- and l- NADW travel towards the south).

There is information that suggests the existence of labile and refractory metal fractions (Ellwood, 2008) which I hypothesize may extend to ligand fractions, too as complexing molecules bind each metal in each specific biocompartment difrerently (i.e. hard or soft tissues). However, when discussing the ages of a ligand whose concentration

changes in the Station-6-to-Station-10 transect, substances of similar binding strengths are counted under the same ligand label (e.g. Zn L1) and are assumed to have the same average reactivity and decay rate. At this point, this is the best that we can do, for there is no more separate ligands from either biocompartment. This is all within the realms of the discretization of ligands based simply on binding strength (logK') criterion.

Fig. 27 shows how important the three influencing factors (AEF, SWMF and CSMF) are for intermediate and deep waters (Figs. 27a and b). In deeper water masses (NADW and AABW), the lack of all four station points and the influence of possibly more than one influencing factor (Figs. 27c, d and e) makes it hard to elucidate trends in these water masses. Thus, the ligand decay study focuses on AAIW and CPDW mostly. The decay analysis will consider both concentrations and binding strengths, shown in Figs. 27 and 28, respectively.

Ignoring the effect of AEF on these two intermediate water masses (apparent at Station 6 only), Zn L3 seems to be decaying in AAIW at a slower rate than Zn_{TD}. Rephrasing that, Zn_{TD} can not decay, so the process occurring here should be either dilution of Zn-rich Southern Ocean water (implying relative apparent formation of Zn L3 and Zn L1 that comes in those waters) or Zn uptake by respiring bacteria (which would take Zn into the particulate form, implying that Zn L3 is indeed decaying). Figs. 27a and 38b suggest Zn L3 is undergoing some chemical process that might produce apparently decreasing ligand concentrations which could potentially be counterargued with the calculation of northern component dilution. What Figs. 28a and 38c doubtlessly show is a linear decrease in the logK' along the water mass path. More so, the decrease in concentration in the order of ~ 20-30 % does not have as much environmental importance as the apparent systematic decrease in ligand strength, ~ 0.8 log units within the IOC 1996 four stations in Fig. 28a (and ~ 1.2 log units in Fig. 38c, extended to this water mass's source point).

This suggests the weakening of the binding properties of the ligand is more important than the ligand concentration decrease. They may be caused by similar

chemical or biogeochemical processes; at this point there is not much that can be speculated. Mathematically speaking, there is a change of ~ 0.9 nM and ~ 0.8 log units in 40 years between Station 10 and Station 6. This means that in 50 years a concentration decrease of ~ 30 % and a binding strength decrease rate of ~ one log unit. From the concentration decrease, a presumed residence time of ~ 130 years is calculated. This does not agree with Baars et al. (2010), who suggested, based on a literature review, that the ligands they found in the Southern Ocean are porphyrins or protein complexes with residence times in the order of days to a few years.

Zn L1 does not seem to undergo the same processes, as apparently its concentrations do not change much in the same transect and its binding strength does not change much either (Figs. 27a, 28a, 38b and 38c). All this suggests L1 is more refractory than L3 to the chemical or biological processes that produced the changes to Zn L3.

The concentrations of Zn L3 in the water mass right underneath AAIW, CPDW do not seem to change much from Station 10 to Station 6, though a slight decrease is observed in Station 8 (Fig. 27b). Again, the environmentally important change is in the binding strength, which decreases ~ 1.0 log units in the Station 8 to Station 6 transect, very similarly to the decrease of logK' of Zn L3 in AAIW (Fig. 28b).

In deeper waters and waters further south, the graphs are more affected by the external influencing factors (Figs. 27c - e) and also the ligand gets saturated by increasing concentrations of metal, making it analytically difficult to obtain logK' values (Figs. 28c - e). With the ligand concentrations and the logK' remaining after the external influence factors are filtered out, not much can be elucidated, as there are not enough datapoints to concoct any hypothesis.

5.9.6. Is Zn L3 actually Zn L2 getting old ?

Focusing on the estimated binding strength decay rates for Zn L3 obtained from the plots showing log K' changing with latitude (Figs. 28a and 38c for AAIW and 28b for CPDW), it can be observed that AAIW and maybe CPDW too show changes at roughly

similar rates: the Zn ligand gets ~ one log unit weaker for every 50 years of travel along these two water masses. Similarly, Fig. 28d shows Zn L3 getting weaker in l-NADW as this water mass travels in the opposite direction.

Cd ligands show a similar decrease in the logK' between Station 8 and Romanche as AAIW and CPDW age; however, AEF influence, supposedly caused by particulate matter falling and bringing ligand with it, seems to provide for fresh strong ligand as can be implied from the increasing logK' for Cd L3 in Figs. 28a and b. In contrast, Cd L3 in u-NADW seems to be getting stronger (Fig. 28c); this could actually be the influence of SWMF as fresher ligands from near the Southern Ocean may be observed in Station 8, or the ligands from the two overlying water masses could be more particle reactive than Zn ligands and could be giving an apparent strengthening curve.

Table 8 shows a difference between the average logK's for Zn L2 and Zn L3 of 1.5 log units, and between Cd L2 and Cd L3 of 1.2 log units. This means that based on logK' values ligand nomenclature, what is called L3 at one location could have actually been called L2 in the location where it was ~ 60 - 75 years ago, presumably with a ~ one log unit stronger logK'.

In contrast, logK' for Zn L1 does not show any change (Figs. 28a and b), but maybe there is a labile pool of Zn L1 that actually degrades it to Zn L2 to Zn L3, as waters get more and more respired on top of the apparent refractory pool of Zn L1 whose logK' seems not to change within ~ 40 years of respiration in AAIW. Thus, concentrations of both Zn L1 turned into Zn L2 turned into Zn L3 should be present in deep waters in somewhat similar concentrations to Zn L1, both ligands coming from water mass formation locations. Indeed, for most of the Zn ligand profiles this can be observed (Figs. 21c, d and f), with the external influences super-imposed.

On the other hand, when the AAIW Zn L3 ligand concentration decrease data is observed, a change of 0.9 nM in ~ 40 years translates into an approximate residence time of ~ 130 years. This phenomenon would cause the labile pool of Zn ligands to decrease

and decrease, while refractory Zn L1 would accumulate in deep waters.

The common paradigm suggesting that strong ligands (L1-type) are formed in surface waters and are present only in surface waters and not in deeper ligands may be somewhat inaccurate. Locally produced surface ligands have not had time to degrade, thus causing surface and subsurface high concentrations of strong ligands. The weaker ligands in intermediate and deeper waters may be originating in strong but labile, decaying ligands from water mass formation locations. Eventually, these water masses get upwelled or mixed with other water masses, creating a consortium of organic metal binding ligands of diverse degrees of binding strength degradation.

5.9.7. Potential processes causing ligand and logK' decay

The structure of the Zn and Cd ligands is unknown. Fe ligands are suspected to belong to two chemical families, but nothing definitive is known about Zn and Cd ligands other than the fact that generally these ligands are relatively small (molecular weight less than 1000 Da, Wells et al., 1998) and that generally they are soluble. Thus, to answer the question about what chemical processes could be causing either or both ligand concentration decrease and logK' decay, all that can be done at this point is speculate about theoretical processes known to occur to other organic matter.

The Fe ligands in these very waters showed an apparent ligand strength systematic decrease which did not correlate with any ligand concentration significant changes (Powell and Donat, 2001). It is notable that Powell and Donat (2001) used mathematical methods of similar level of reliability to the methods used in this study (i.e. they used all three Ruzic, Scatchard and Gerringa mathyematical treatments) which produces comparably reliable logK' values.

As discussed before, some of the ligands are believed to originate in phytoplankton as their correlations with chlorophyll-*a* suggest. These ligands produced by phytoplankton in surface waters, when observed in water masses at depth, should reflect the level of primary productivity from the location where the water mass formed,

behaving as signature tracers of organic matter production and degradation.

There are two possible paths of degradation that could cause the ligand strength and ligand concentration to decrease: chemical and biological degradation. There is general knowledge about the chemical degradation of OM in water masses, mostly related to land vegetation signature compounds that can be traced in a water mass as it moves away from land (e.g. Hernes and Benner, 2002; Vangresheim et al., 2009). But there is no specific information about organic metal binding substances. It can be speculated that the S^{2-} based chelating center would weaken as the organic matter is oxidized, but more chemical information is needed.

Biological degradation is another factor that could be causing the chemical attack on the ligand's molecules that causes the concentration and binding strength to decrease. Powell and Donat (2001) suggested that bacteria, given their high metal requirements, may produce "acquisition" organic ligands, at least for Fe. Specifically in AAIW, it does not seem likely that bacteria produce Zn ligands, as the Zn L1 concentration and binding strength remain mostly unchanged as the water mass ages. Assuming bacteria can ingest any metal species, especially those bound to organic matter, there would be a constant source of ligand-bound Zn along this water mass due to the presence of chemical-speciation-dominant L1 (Fig. 29). The presence of viruses would enhance bacteria's role as OM oxidizers (Bonilla-Findji et al., 2008) and so will the fecal pellet dissolution caused by the acid attack that occurs during zooplankton grazing (discussed earlier).

In Powell and Donat's (2001) work, the ligand strength decrease is reported to happen in surface waters. Given the potential for OM to photo-oxidize, they relate this phenomenon to photochemical processes. Given this study's focus on intermediate and deep water masses, this factor is discarded. On the other hand, if and when these waters are upwelled (as mentioned earlier), these ligands may be very photosensitive as some of my preliminary results may indicate.

Finally, there is also adsorption/desorption onto particles, a process about which

there is little known about metal complexing ligands. It can be presumed that ligands, somewhat similar to humic substances, could adsorb readily onto clay and minerals, and that this would reduce the solubility and mobility of the ligand-metal complex (Weng et al., 2006a). This adsorption could be in steps (ligand binds to particle, then metal binds to ligand) or direct for the metal-bound ligand complex. Models have been produced for the adsorption of model molecules onto humics and fulvics (Weng et al., 2006b), yet not much is known about the organic ligands, a very small fraction of OM.

5.9.8. Specificity of Zn and Cd ligands

There are few studies that determined the complexation and speciation of more than one element simultaneously in the same location. One of such studies is presented in Bruland's (1989 and 1992) seminal papers on Zn and Cd complexation and speciation in the North Pacific. Bruland (1989) reported Zn ligands in concentrations around ~ 1.2 nM that did not change much with depth; in contrast, the Cd ligand, present in the upper, 200m of the same water column, shows maximum concentrations below 0.1 nM between 40 and 100m (1992). The same samples were analyzed for Cu speciation by Coale and Bruland (1988) and the two ligands for Cu show completely different depth profiles and concentration ranges: the stronger Cu L1 is present in the upper 150m in concentrations lower than 2.5 nM, while the weaker Cu L2 is present throughout the whole 1500m depth profile in concentrations between 5 and 10 nM with no apparent trend. The fact that all these four ligands are present in different depth distributions and concentrations suggests they are different substances, doubtlessly. Later estuarine results by Kozelka and Bruland (1998) show ligands for Cu, Pb, Zn and Cd whose concentrations do not correlate well among themselves, implying they are not the same substance.

How specific the Zn ligand is, i.e. does it bind to Zn only and not to Cd, is tested by performing one of the many controls and checks that the Bruland's papers have. By adding Zn to Cd titrations and seeing how Zn might interfere with it and *vice versa*, one can be sure that the ligands are specific for one metal. In the case of Zn and Cd ligands, they were proved to be metal specific (Bruland 1989, 1992).

In contrast to Bruland's (1989, 1992) reports, Ellwood's (2004) results show ~ 1.5 nM concentrations of a Zn ligand and the same concentration of a Cd ligand. The similar depth profiles and concentration ranges hinted towards the ligands being similar substances. In fact, once a cross metal addition experiment like that designed by Bruland was performed, it turned that the Zn ligand could bind to Cd too.

This study's results (Fig. 21) show depth profiles marked by three Zn ligands in concentrations around ~ 3 nM and approaching 10 nM in water masses influenced by AABW, in contrast to three Cd ligands with concentrations below 0.4 nM for the weaker ligands and very low maximum concentrations for Cd L1 (less than 0.010 nM). The stability constants of the Zn ligands are similar to those for Cd (Fig. 20) and in general logK's for stronger ligands (~ 11-12), intermediate (~ 10) and weaker (~ 9), irrespective of the metal. However, their concentrations, distributions and decay rates are so different they are definitely not the same substances. Alternatively, maybe the same substance could be binding to different metals and, then the metal-ligand complex could decay differently.

In some Amazon station samples, the specificity of the ligands was tested, with results indicating that the ligands were metal-specific, and that a simultaneous Zn and Cd titration could be performed. Given that all titrations were simultaneous Zn and Cd titrations, and that Zn additions are usually ~ 10 times higher than those of Cd, if there was any possibility for metal inter-replacement, the Cd ligands data would be flawed as Zn would have completely saturated the Cd ligands. Yet, the Cd titrations do not look saturated with metal, and only higher concentrations of Cd_{TD} produces that effect. Thus, I can say with certainty that these ligands are substances with high metal specificity.

5.10. SPECIATION AND BIOAVAILABILITY

In this study, processes related to metal/nutrient ratios, the apparent ligand concentration decrease and ligand binding decay and more have been discussed so far. One of the main goals of this study is to measure the concentration of metal complexing

ligands in order to calculate the chemical speciation of Zn and Cd so that the bioavailable concentrations of each metal can be determined and ultimately the bioavailable metal biological and ecological effect on phytoplankton can be predicted. That is what is discussed in this the last section of the Discussion chapter.

Figs. 23 and 24 in the Results section show the metal and ligand depth profiles contrasted with the logarithmic plot of total dissolved Zn and Cd and Zn^{2+} and Cd^{2+} for the upper 400m with pigments plotted along; Figs. 21 and 22 show the same information for the complete water column. Fig. 29 in the Discussion chapter plots the same parameters, but along the water mass path, focusing on the effect of the three influencing factors discussed (AEF, SWMF and CSMF). This discussion about speciation and bioavailability will use these five figures mostly. Fig. 29 has been extensively discussed in the Water Mass section.

5.10.1. Inorganic and organic complexation of Zn and Cd

Recapitulating briefly, the light blue and light pink bars in each of the mentioned figures depict the relative size of the inorganic side reaction coefficient for Zn and Cd (blue and pink, 0.36 and 1.57 log units), calculated from water properties (Turner et al., 1981 and van den Berg online calculating tool). These coefficients indicate the extent of inorganic ligands' complexation of the total dissolved metal in the absence of organic ligands, whatever further low the M^{n+} is taken is because of the organic ligand's presence. For Zn, the largest and most defining portion of the Zn_{TD} - Zn^{2+} gap is due to the complexation exerted by organic ligands and thus, the range in all the water column samples is very ample (~ 0.40 to ~ 3.65 log units). In contrast, for Cd, the inorganic side reaction coefficient reduces the Cd_{TD} ~ 1.57 log units to Cd^{2+}, accounting for most of the Cd_{TD} - Cd^{2+} gap; organic ligands' complexation adds up to a maximum of 0.90 log units more. Thus, the range in the Cd gap is narrow, from ~ 1.54 to ~ 2.51 log units; in the water mass analysis, by choosing the average or most representative depth, the Cd gap appears a bit narrower (~ 1.54 to ~ 1.78 log units).

The Zn- and Cd-complexing ligands in the samples discussed in this study are

related to productivity and grazing maximum depths by comparison to proxies (chlorophyll-*a* and phaeophytin/chlorophyll-*a* ratio) in surface and subsurface waters. The water masses studied in the Water Mass section form at high latitude locations (see Hydrography subsection in Results section), where the high-productivity waters impart a ligand concentration signature on each water mass. As each water mass travels first toward the Equator and then further away from their formation locations, respiration and other biogeochemical processes affect the concentrations of Zn and Cd and their ligands. The processes related to the production and apparent consumption of metal-chelating ligands in seawater were discussed in the Ligand section.

These ligands complex total dissolved Zn and Cd into their free metal concentrations. Zn_{TD} and Cd_{TD} concentrations are displayed in the left graphs of Figs. 23, 24 and 29. The free metal concentrations reflect both the organic and inorganic complexation of these metals. Adding ~ 0.36 and ~ 1.57 log units to the pZn and pCd values shown in the right graphs of Figs. 23, 24 and 29 (that is, moving these curves to the left in these figures) would produce pZn' and pCd' which would illustrate the level of organic ligand complexation only when compared with the pZn^{2+} and pCd^{2+}. Knowing that the inorganic complexation of these metals changes only slightly in seawater with similar environmental conditions (salinity, temperature and pH), the inorganic alpha coefficient bars are graphed with the purpose to visually display the cruise-average level of inorganic complexation.

The inorganic complexation of Zn and Cd are very different from each other. MineQL calculations at average seawater salinity, temperature and pH conditions show that, in the absence of organic ligands, Zn^{2+} accounts for ~ 47 % of Zn_{TD}, in contrast to the Cd^{2+} which accounts for only ~ 2.7 % of Cd_{TD}. The inorganic species of Zn are mostly chlorides (~ 35 %), followed by hydroxides (~ 12 %), carbonates (~ 4 %) and sulfates (~ 1.5 %); in contrast, for Cd, chlorides account for the 97 % of Cd, almost all of the Cd that is not free.

Organic complexation changes the chemical speciation of these two metals

drastically, depending on the ligand(s) concentration(s) and binding strength(s). Following are some examples of the speciation distribution for Zn and for Cd. A clear example of strong ligand influence is found in Station 6 at 110m where the 0.21 nM Zn_{TD} are distributed mostly (~ 98.8 %) in complexes with a very strong ligand L1 (0.46 nM, logK' 11.98), leaving less than 1% as complexes with L3, a weaker ligand present in much higher concentrations (2.34 nM, logK' 8.92) and less than 0.2 % as Zn^{2+}. Just 30m above, the Zn subsurface local maximum is located, and 0.63 nM Zn_{TD} are very differently distributed similarly among free, inorganic, L2-bound and L3-bound species (~ 21, 25, 24 and 30 %) in the absence of the strong ligand L1, with only L2 and L3 present (0.25 nM, logK' 10.01 and 1.99 nM, logK' 8.44). In contrast to Zn, Cd^{2+} varies much less among different ligand concentration cases. An example for strong ligand influence for Cd is found in Station Romanche at 60m, where a low 0.009 nM Cd_{TD} is distributed in a 1:2:2 ratio among L1-bound, L2-bound and inorganic species (~ 21, 42, 32 %) leaving very little as Cd^{2+} (less than 0.8 %) mainly because of the strength of the very scarce strong ligand L1 (0.009 nM, logK' 10.98) in comparison with the ~ 20 times more concentrated but ~ 10 times weaker L2 (0.197 nM, logK' 9.84) and the menial effect of a low-concentration of weak L3 (0.088 nM, logK' 9.14) which accounts for less than 4 % of the Cd_{TD}. An example of relatively high Cd^{2+} is found in the AEF-influenced Station 6 at 900m where 0.613 nM Cd_{TD} are distributed as inorganic complexes mostly, with a small portion as a L3 complex and a relatively high percentage as Cd^{2+} (less than 80, 18, 2.3 %) as 0.338 nM L3 (logK' 8.97) compete against the inorganic complexes for less than a fifth of the total dissolved Cd.

The Zn^{2+} percent variability range is wide (between less than 0.2 and ~ 47 % of the Zn_{TD}) because of the presence or not of complexing ligands. In contrast, Cd^{2+}'s variability is smaller (between less than 0.8 and 2.7 %) because of the inorganic complexes dominance. Because of the complexity of these calculations and the large quantity of results available, only the most important features are highlighted in Figs. 23, 24 and 29: the total dissolved Zn and Cd concentrations and the Zn^{2+} and Cd^{2+} concentrations.

The factors and processes involved in the general trends and pointed influences that are believed to cause the concentrations of total dissolved Zn and Cd and ligands are discussed earlier in this Discussion chapter. In the next paragraphs, the focus is on the pM^{n+} in the upper 400m, the whole water column and the water masses, and their relationship to potential limitation or toxicity to phytoplankton in eventual future upwelling circumstances.

5.10.2. Resulting Zn^{2+} and Cd^{2+} concentrations

The upper 400m pZn_{TD} and pZn^{2+} plots (Fig. 23) show in general low Zn^{2+} concentrations in the surface (with the Amazon Station as notable exceptions) and values increasing with depth. That is, concentrations of Zn^{2+} could limit the growth of different phytoplankton species, as they fall usually between the thresholds reported for neritic and oceanic species (Brand et a., 1983) and, in a few occasions, reach the oceanic species threshold. A notable feature present in all oceanic stations (Stations 6, Romanche, 8 and 10) is the subsurface Zn local maximum (discussed in the Metal/Nutrient Ratios section) which produces a subsurface increase in Zn^{2+} as well. In the Amazon 1 Station, which does not show this Zn subsurface increase and is dominated by particle export, the Zn^{2+} reaches the oceanic limiting threshold in subsurface waters (between ~ 80 and ~ 150m) that could be easily upwelled and could pose a potential deleterious effect to surface waters.

Below 400m, the complete water column plots (Fig. 22, left graphs) show variable Zn^{2+} increases depending on the station observed because of somewhat variable ligand concentrations that I hypothesize relates to both water mass ligand decay and pointed sources (see Water Mass and Ligand sections). Stations 6 and Romanche in deep waters have lower Zn^{2+} than Stations 8 and 10 possibly because of increased equatorial particle fall that is related in this study to the Amazon River particle export or the Equatorial increased productivity (AEF).

The water mass plot (Fig. 29) allows the complete water column profiles to be

analyzed and ligand decay trends and pointed sources to be pointed out. AEF and CSMF are important in changing the water mass trends of most water masses present in this study, in comparison to SWMF. AEF and CSMF produce the widest pZn_{TD} - pZn^{2+} gaps and thus, the lowest Zn^{2+} concentrations. These concentrations, if and when upwelled, would likely impair phytoplankton growth. On the other hand, the ligand decay may imply that these low Zn^{2+} would likely increase, ameliorating the deleterious effects, given that these intermediate and deep waters will not be upwelled immediately, but in distant locations in the North or Equatorial Atlantic.

In comparison, the pCd_{TD} and pCd^{2+} in the upper 400m (Fig. 24) show more consistent Cd^{2+} concentration profiles with inorganic complexation dominating over the relatively small effect of organic complexation. There is no Cd subsurface local maximum, so the Cd^{2+} increases more smoothly from surface and subsurface lower values to deeper values. The two Amazon Stations show slight Cd enrichment. In general, all stations' data from above ~ 250 show Cd^{2+} concentrations that are 3 to 5 log units below potentially toxic Cd^{2+} concentrations reported for neritic and oceanic phytoplankton species (Brand et al., 1986), indicating no deleterious effect to phytoplankton. Though limiting Cd^{2+} concentration ranges have not been reported yet, the low concentrations reported here would be in the very low end, close to those reported by Ellwood (2004).

Below ~ 250m, Cd^{2+} stays more than 1.5 log units below this potentially toxic threshold. The complete water column profiles (Fig. 22, right graphs) show that below the maximum respiration depth, the Cd^{2+} concentrations stays relatively uniform, regardless of the presence or not of weak ligands complexing Cd. The eventual future upwelling of waters from either water mass would probably not pose a toxicity risk to phytoplankton, as Cd^{2+} stays ~ 1.5 log units below the toxic threshold.

The water mass latitudinal profiles (Fig. 29) confirm the aforementioned low Cd_{TD} - Cd^{2+} gap variability. For example, in the locations of intense AEF and CSMF influence, the organic complexation of Cd produces the widest Cd_{TD} - Cd^{2+} gaps which produce that

less than 2.5 % of the Cd_{TD} is free. In contrast, in locations of zero organic complexation (e.g. Station 8 at 3400m) the Cd^{2+} accounts for 2.8 %. Note that a strong ligand Cd L1 is present only two times in the complete cruise dataset, in surface Station Romanche and Station 8 samples; thus, most of the Cd complexation is produced by Cd L2 and Cd L3 competing with inorganic ligands.

5.10.3. Zn, Cd and Co

Separately the lowest Zn^{2+} levels (more than 0.0001 nM Zn^{2+}) and the lowest Cd^{2+} levels (more than 0.00001 nM Cd^{2+}), located at subsurface depths for all stations, suggest there could be coastal Zn or Cd limitation if and when these waters are upwelled. Given the depths at which these minimums are located, that is possible, as there are studies that support trace metal upwelling from similar depths produced by eddies (Noble et al., 2008), a common occurrence in the Equatorial Atlantic region (Goni and Johns, 2001). Interestingly, Lohan et al. (2005) and Ellwood (2004) found similar Zn^{2+} concentrations and no evidence of Zn limitation. Ellwood (2004) found no Cd limitation, either.

Phytoplanktonic growth limitation, related to scarcity of Fe since the iron hypothesis was postulated (Martin and Fitzwater, 1988), has recently been suggested to be caused by low concentrations of a group of metals important for enzymatic functioning (Sunda and Huntsman, 1996, 1998, 2000). Among these metals, Zn, Cd, Cu and Fe share an important role. Saito and Goepfert (2008) summarized the latest development in the interrelationship between Zn, Cd and Co, reviewing the ability to interreplace these metals for their physiological requirements, primarily related to their central role in CA (Lane et al., 2005) studied in some diatoms (Price and Morel, 1990; Sunda and Huntsman, 1996) and coccolithophores (Sunda and Huntsman, 1995; Xu et al., 2007).

Given the potential enzymatic interreplacement of these three metals, Ellwood (2004) proposed a novel limitation approach based on the combined free concentrations of Zn, Cd and Co, where the sum of the free concentrations of these three metals is used as a proxy for potential CA activity and thus, a low combined free concentration could be related to CA-mediated limitation. This CA-mediated limitation is obviously more

important for phytoplankton species that use more carbonate, like for example coccolithophores that use it in their exoskeleton. Also, different phytoplankton species use different forms of carbon, e.g. CO_2 for diatoms, HCO_3^- for cyanobacteria (Tortell and Morel, 2002) and different strategies for concentrating carbon are used. Thus, phytoplankton community changes occur in case of Zn, Cd or Co, CA-mediated limitation; in contrast, direct phytoplankton growth limiting effects are expected in case of Fe limitation (Morel et al., 2003).

There are no direct Co data from this cruise. However, there are Co_{TD} data from nearby stations in the Equatorial Eastern Atlantic (stations very close to all but the westernmost Stations Amazon and 6) taken a two to four months after this study's samples (Bowie et al., 2002). There are no Co speciation data from these samples, but there are extensive Co speciation data from the Atlantic Ocean (Saito et al., 2001, 2002 and 2005) and the Southern Ocean (Bown et al., 2010) that allows for Co^{2+} to be estimated. In general, Co is strongly bound to an organic ligand that appears to correlate with chlorophyll-*a* concentrations like Zn L2 in this study and brings Co^{2+} down to a minimum value. In waters above and below the chlorophyll-*a* and ligand maximum, the Co^{2+} is not as low.

Morel et al. (2003) suggested an average $Zn^{2+} > Cd^{2+} > Co^{2+}$ where the most important effect on CA would be, simply because of higher concentration, that of Zn^{2+}. Thus, when there is high Zn^{2+}, there would be no CA-mediated limitation. Independently of the efficiency of each metal in CA, Xu et al. (2007) suggested that interreplacement of Zn, Cd, and Co should occur in regions where Zn is highly depleted. In surface waters, there usually is moderately low Zn and Co, but Cd surface depletion is a pretty common feature (Morel et al., 2003). Thus, in low Zn concentrations cases, Co could become important to avoid CA-mediated limitation.

In this study, the 400m upper water profiles for all stations except Amazon 1 show Zn^{2+} stayed mostly above or around the 10^{-12} M range in surface waters, except at two depths: a) at or around chlorophyll-*a* maximum where the Zn subsurface local maximum

increases Zn_{TD} and Zn^{2+}, and b) below chlorophyll-*a* maximum where Zn_{TD} decreased, Zn L3 increased and Zn^{2+} decreased (see Figs. 21 and 23). In contrast, Cd^{2+} was more variable from station to station and had a trend consisting of lower concentrations in the upper ~ 100m (except the Amazon Stations) ranging from 10^{-13} to 10^{-14} M and reaching a minimum at or around the chlorophyll-*a* maximum and higher concentration below that depth between 10^{-11} and 10^{-12} M (Fig. 24). The surface Co_{TD} data of Bowie et al. (2002) suggests concentrations slightly higher than those reported by Saito and Moffett (2001) in the North Atlantic. Assuming similar complexing depth profiles as those of Saito and Moffett (2001), Co^{2+} would be present in surface waters in concentrations as high as 10^{-11} M, decreasing dramatically around the chlorophyll-*a* maximum to values as low as 10^{-16} M and slightly increasing again to around 10^{-14} below ~ 200m. In contrast, Bowie et al. (2002) reported high Co_{TD} at chlorophyll maximum, which means that Co^{2+} could be not as low in this depth as Saito and Moffett (2001) suggested.

In summary, the immediately upwellable surface and subsurface waters show at chlorophyll-*a* maximum depths the most likely $Zn^{2+} > Cd^{2+} > Co^{2+}$ concentration order ($10^{-12} > 10^{-13} > 10^{-15}$) with little indication of potential CA-mediated limitation other than possibly for cyanobacteria, which have an absolute Co requirement. Below the chlorophyll-*a* maximum depth, an apparent inverse situation is observed, with lower Zn^{2+} and higher Cd^{2+} and Co^{2+}. Thus, I suggest the phytoplankton community distribution profiles are defined from a free trace metal concentration standpoint, on top of other defining biochemical parameters. In all cases, there seems to be combined free concentrations of Zn, Cd and Co higher than those reported by Ellwood (2004) for the South Pacific, above limiting ranges (more than 10^{-12} M).

There are three possible locations with a combination of measured and inferred Zn, Cd and Co speciation data that this study's final results can be compared with: the North Pacific (Bruland, 1989, 1992), the South Pacific (Ellwood, 2004) and the Southern Ocean (Baars et al., 2010; Saito and Goepfert, 2008). The North and South Pacific studies have Zn and Cd speciation and inferred Co speciation data. The Southern Ocean study has Zn speciation data and a Zn and Co co-limitation study in some phytoplankton

species; Cd speciation analyses are being performed at the moment (Croot, personal communication).

The North Pacific study, based on one station's data, shows Zn^{2+} between 10^{-12} and 10^{-13} in the upper ~ 200m, increasing gradually to $10^{-11.5}$ by 300m and $10^{-10.5}$ by 400m as Zn_{TD} increases with depth over the uniform Zn L2 concentrations. In contrast, the Cd^{2+} ranges between 10^{-13} and 10^{-14} only in the upper ~ 100m due to the presence of a Cd L2 concentration in that depth range; Cd^{2+} increases rapidly in deeper waters as Cd L2 decreases and Cd_{TD} increases, reaching 10^{-12} by 175m and 10^{-11} by 400m. There are Co^{2+} profiles from the Peru upwelling system (Saito et al., 2004) which are not representative of the North Pacific. The Co^{2+} profiles from the Atlantic (Saito and Moffett, 2001) with low Co^{2+} at chlorophyll-*a* maximum depth is assumed to be similar to what the Co^{2+} depth profile would be like in the North Pacific, showing Co^{2+} concentrations ranging between 10^{-13} and 10^{-15}.

The South Pacific study of Ellwood (2004) reports a case of an apparently non-specific ligand that binds to both Zn and Cd with comparable binding strengths to both metals, present in high and relatively uniform concentrations throughout the 60m of water column studied. The resulting free metal concentration depth distributions for the three metals are uniform, with Zn^{2+} between 10^{-12} and 10^{-13}, Cd^{2+} between $10^{-13.5}$ and $10^{-14.5}$ and, given the Co_{TD} concentration ~ 1 order of magnitude lower than the Atlantic values, inferred Co^{2+} between 10^{-14} and 10^{-16}. Despite the low combined free metal concentrations, there is no evidence for limitation and Ellwood questions if the organic ligand-bound Zn and Cd fractions are bioavailable.

The Southern Ocean study, though incomplete, shows upper 200m waters along a zero meridian transect towards Antarctica and across the Drake Passage have higher than $10^{-10.5}$ Zn^{2+} because of high Zn_{TD} concentrations that are not significantly complexed by relatively low Zn L2 concentrations. Thus, limitation by Zn in this region is very unlikely (Baars et al., 2010). Regardless of what the Cd^{2+} and Co^{2+} concentrations are, there is enough Zn^{2+} to fulfill the phytoplanktonic demand for CA. Eukaryotes (Saito and

Goepfert, 2008) and diatoms (Timmermans et al., 2001) can use either Zn or Co in these regions, which usually have elevated Zn and silicate concentrations in surface and deep waters but which can get Zn and silicate depleted in the intense bloom events. Saito and Goepfert (2008) showed eukaryotes survive *in vitro* lower concentrations of either Zn or Co (in absence of the other metal) better than diatoms, whose growth rates start to decrease below ~ $10^{-11.5}$ for Zn and Co.

Comparing this IOC 1996 study's Zn^{2+} and Cd^{2+} and inferred Co^{2+} with these three locations the following is observed: the Equatorial and South Atlantic regions seem to have combined Zn^{2+}, Cd^{2+} and Co^{2+} concentrations above those of low metal/high ligand, potentially limiting Southern Pacific regions; but below those of high metal/low ligand Southern Ocean regions. The North Pacific region studied by Bruland (1989, 1992) seems to be similarly enriched in these CA-related metals. Thus, it could be inferred that similar levels of potential limitation exist between the North Pacific and the Equatorial South Atlantic regions.

5.10.4. Fe and Cu

Zn and Fe are documented to be related to nutrient uptake (de la Rocha et al., 2000), more so in HNLC areas (Franck et al., 2003). Knowing that Fe limitation occurs in several HNLC areas of the world (e.g. Jickells et al., 2005), the next question to answer is how Fe and Zn/Cd/Co limitation compare. To elucidate that, Lohan et al. (2005) ran an experiment where Fe limitation was ameliorated by Fe additions and then Zn limitation was investigated in an area in the North Pacific. Their results show that, once Fe is added and chlorophyll-*a* increases, Zn^{2+} decreases. To avoid Zn limitation, once Fe is not the limiting factor, it was observed that "acquisition" Zn ligands are produced by phytoplankton, in order to keep Zn in solution.

Buck and Bruland (2007) suggested that Fe and a strong Fe ligand correlate above ~ 0.2nM Fe_{TD} and that the FeL1 complex could be bioavailable to phytoplankton in the Bering Sea and in other studies' locations, as it might be a siderophore "acquisition" ligand produced in excess ubiquitously through the surface waters of the world's oceans.

To understand if Fe is limiting primary productivity in this study's waters, Powell and Donat's (2001) results are discussed next. They show Fe_{TD} concentrations higher than the ~ 0.2 nM limit set up by Buck and Bruland (2007) throughout the water column and the surface waters. Organic ligands of high logK' values (12 to 14) and in excess of Fe_{TD} at all sampling points complex more than 99 % of the Fe_{TD}, leaving potentially limiting low concentrations. If the FeL1 complex is bioavailable as Buck and Bruland (2007) suggested, then Powell and Donat's (2001) data may mean there are no limiting Fe concentrations. On the contrary, if FeL1 is not bioavailable, then limiting Fe concentrations may be encountered in surface waters of this cruise, especially in Station 6 and Romanche where inorganic Fe is lower than 10^{-12} M. In these two stations, Zn^{2+} is lower than 10^{-12} M below the chlorophyll-*a* maximum, between ~ 100 and 200m, potentially setting up a case of co-limitation exerted by both Fe and Zn. The Station Amazon 1 which has the lowest subsurface Zn^{2+} concentrations of all stations, may probably not have low Fe because of the riverine influence, making up for a case where Zn limitation exits but not Fe limitation.

On the other hand, Cu has a biochemical role facilitating Fe acquisition in diatoms and transport in eukaryotes, with Cu^{2+} concentrations below 10^{-14} M being potentially limiting (Peers et al., 2005). In contrast, high concentrations of Cu antagonize the uptake sites of Mn and Zn (Sunda and Huntsman, 1998). Cu is the only element for which there is direct evidence of a complexing ligand being produced by cyanobacteria in response to high concentrations, a.k.a. "detox" ligand (Moffett and Brand, 1996); for other elements, there are some clues of such a phenomena, but no direct evidence.

In samples directly from this study, the presence of a strong Cu L1 in surface waters is related to chlorophyll-*a* (Consolvo, 2000), like previously reported in the North Pacific (Coale and Bruland, 1988 and, 1990) and the North Atlantic (Moffett, 1995). This ligand buffers the Cu_{TD} concentrations down to Cu^{2+} below 10^{-11} M in the upper 100m of Stations 10 and Romanche, while the riverine Cu at Station Amazon 1 shows three times as much Cu^{2+} in the upper ~ 5m only. Shank et al. (2004) suggested that the ubiquitous oceanic Cu ligand has riverine or estuarine origin. Moffett et al. (1990) and Moffett and

Dupont (2007) reported the presence of the Cu ligand in deeper waters in the North Atlantic and North Pacific, suggesting that the ligands are either produced in deeper waters or that they have very long residence times and are transported with water masses in similar fashion to what is reported in this study for the Zn and Cd ligands (residence time in the order of ~ 100 years). In contrast, the short residence time (~ 1yr) of the Cu ligands found in surface waters (Consolvo, 2000) counters the argument for global distribution of riverine and estuarine ligands. It needs to be pointed out that the Cu complexation in Consolvo's (2000) study is focused on the surface, subsurface and mode waters only (shallower than 600m) and no intermediate or deep water mass study was performed that could agree or disagree with more refractory ligands being transported.

In summary, the stations studied here may not undergo any Fe or Cu limitation. The Zn/Cd/Co potential to limit phytoplankton via the CA system is also unlikely. Different layers of high-Zn/low-Cd-and-Co and low-Zn/high-Cd-and-Co might produce a phytoplankton distribution that favors some species in either layer. A higher resolution study would likely produce answers to some of the questions still unanswered. But it should be a higher resolution study that includes surface, subsurface and intermediate waters at least, given the immediate potential for subsurface waters to be upwelled and the eventual and distant potential for intermediate and deep waters to be upwelled in remote locations.

CHAPTER 6

CONCLUSIONS

In this study, Zn and Cd concentrations, distributions and chemical speciation in the Equatorial and Western South Atlantic Ocean were discussed. The focus, initially on dissolved Zn and Cd and their complexing ligands, shifted from sources to processes to analysis of specific hot spots of biogeochemical importance. First, a section of this Discussion chapter analyzed the influence of the Amazon River on surface waters. Then, once the depth profiles were broken into water masses, the influence of important factors on intermediate and deep water masses were studied. Specifically, the influence of the Amazon River/Equatorial area (AEF) on intermediate water masses and the Congo River shelf matter (CSMF) on deep water masses were detailed. After that, the low oxygen depth at Station Romanche was reviewed with specific emphasis on the Zn and Cd and ligand distributions. A separate note exploring the metal/nutrients ratios followed. Then, there is a section devoted to investigating the ligands and processes that occur to them. Finally, the chemical speciation and bioavailability of Zn and Cd were discussed, in light of some inferred speciation Co data and some Cu and Fe speciation data directly measured in the same samples.

The main conclusions of this dissertation are:

1. Zn_{TD} and Cd_{TD} profiles mimic silicate and phosphate; three separate, metal-specific ligands complexing each metal are reported, thanks to the use of a novel comprehensive mathematical tool.

2. Notable features include potential regional influences on the Zn_{TD}, Cd_{TD} and L distribution exerted on surface waters near the Amazon River plume and on subsurface waters by the hypoxic region in the Equatorial Atlantic.

3. As of intermediate and deep water masses of global distribution, both the

influence of factors like the Amazon River particles/Equatorial area high productivity (AEF) on intermediate water masses and the Congo River organic-matter respired shelf matter (CSMF) on deep water masses show high Zn and Cd and even higher L signatures, in contrast to the Zn-and-silicate rich water masses originated near the Southern Ocean (SWMF).

4. The metal/nutrients ratios study shows the widespread presence of Zn_{TD} subsurface local maximums, suggesting Zn regeneration linked to grazing.

5. A study of the ligands and processes that occur to them suggests some are related to chlorophyll-*a* and some are related to grazing; some are transported in intermediate and deep water masses and both their concentrations and binding strengths (logK') decay as they age (residence times ~ 130 years), suggesting potential global distributions. Other ligands apparently do not decay away.

6. Zn and Cd chemical speciation and bioavailability are compared with some inferred Co speciation data. The studied region of the Atlantic Ocean is not prone to limitation due to the sufficient concentration of Zn^{2+} in surface waters, in contrast to regions where intermediate and deep waters are to upwell, which could show limitation due to low Zn^{2+} and Cd^{2+}.

REFERENCES

Abate, G., Masini, J.C., 2002. Complexation of Cd (II) and Pb (II) with humic acids studied by anodic stripping voltammetry using differential equilibrium functions and discrete site models. Organic Geochemistry 33, 1171-1182.

al-Farawati, R., van den Berg, C.M.G., 1999. Metal–sulfide complexation in seawater. Marine Chemistry 63, 331-352.

Alleman, L.Y., Church, T.M., Ganguli, P., Veron, A.J., Hamelin, B., Flegal, A.R., 2001. Role of oceanic circulation on contaminant lead distribution in the South Atlantic. Deep-Sea Research II 48, 2855-2876.

Andrie, C., Rhein, M., Freudenthal, S., Plahn, O., 2002. CFC time series in the deep water masses of the western tropical Atlantic, 1990–1999. Deep-Sea Research I 49, 281-304.

Baars, O., Streu, P., Croot, P.L., 2010. The distribution and speciation of dissolved zinc in the Southern Ocean. 2010 American Geophysical Union and Ocean Sciences Meeting, Portland, OR.

Baars, O., Croot, P.L., submitted. The speciation of dissolved zinc in the Southern Ocean. Deep-Sea Research II.

Badger, M.R., Price G.D., 1994. The role of carbonic anhydrase in photosynthesis. Annual Review of Plant Physiology and Plant Molecular Biology 45, 369-392.

Baker, A.R., Weston, K., Kelly, S.D., Voss, M., Streu, P., Cape, J.N., 2007. Dry and wet deposition of nutrients from the tropical Atlantic atmosphere: Links to primary productivity and nitrogen fixation. Deep-Sea Research I 54, 1704-1720.

Barbeau, K., 2006. Photochemistry of organic iron(III) complexing ligands in oceanic systems. Photochemistry and Photobiology, 82, 1505-1516.

Barbeau, K., Moffett, J.W., Caron, D.A., Croot, P.L., Erdner, D.L., 1996. Role of protozoan grazing in relieving iron limitation of phytoplankton. Nature 380, 61-64.

Benner, R., Opsahl, S., 2001. Molecular indicators of the sources and transformations of dissolved organic matter in the Mississippi river plume. Organic Geochemistry 32, 597-611.

Bergquist, B.A., Boyle, E.A., 2006. Dissolved iron in the tropical and subtropical Atlantic Ocean. Global Biogeochemical Cycles, 20, GB1015, doi:10.1029/2005GB002505.

Bischof, B., Mariano, A.J., Ryan, E.J., 2004. The North Equatorial Counter Current. Ocean Surface Currents. http://oceancurrents.rsmas.miami.edu/atlantic/north-equatorial-cc.html.

Bonhoure, D., Rowe, E., Mariano, A.J., Ryan, E.W., 2004. The South Equatorial System Current. Ocean Surface Currents. http://oceancurrents.rsmas.miami.edu/atlantic/south-equatorial.html.

Bonilla-Findji, O., Malits, A., Lefèvre, D., Rochelle-Newall, E., Lemée, R., Weinbauer, M.G., Gattuso, J.-P., 2008. Viral effects on bacterial respiration, production and growth efficiency: Consistent trends in the Southern Ocean and the Mediterranean Sea. Deep-Sea Research II 55, 790-800.

Bourles, B., Gouriou, Y., Chuchla, R., 1999. On the circulation and upper layer of the Western Equatorial Atlantic. Journal of Geophysical Research 104, 21151-21170.

Bowie, A.R., Whitworth, D.J., Achterberg, E.A., Mantoura, R.F.C., Worsfold, P.J., 2002. Biogeochemistry of Fe and other trace elements (Al, Co, Ni) in the upper Atlantic Ocean. Deep-Sea Research I 49, 605-636.

Bown, J., Boye, M., Nelson, D., Baker, A.R., 2010. The cobalt cycle in the Southern Ocean during the IPY GEOTRACES Bonus-Goodhope expedition. 2010 American Geophysical Union and Ocean Sciences Meeting, Portland, OR.

Boyd, P.W., Jickells, T., Law, C.S., Blain, S., Boyle, E.A., Buesseler, K.O., Coale, K.H., Cullen, J.J., de Baar, H.J.W., Follows, M., Marvey, M., Lancelot, C., Levasseur, M., Owens, N.P.J., Pollard, R., Rivkin, R.B., Sarmiento, J., Schoemann, V., Smetacek, V., Takeda, S., Tsuda, A., Turner, S., Watson, A.J., 2007. Mesoscale iron enrichment experiments, 1993–2005: Synthesis and future directions. Science 315, 612.

Boyle, E.A., 1988. Cadmium: Chemical tracer of deepwater paleoceanography. Paleoceanography 3, 471-489.

Boyle, E.A., Huested, S.S., Grant, B., 1982. The chemical mass balance of the Amazon plume - II. Copper, nickel, and cadmium. Deep Sea Research Part A. 29, 1355-1364.

Braga, E.C., Andrie, C., Bourles, B., Vangriesheim, A., Baurand, F., Chuchla, R., 2004. Congo River signature and deep circulation in the eastern Guinea Basin. Deep-Sea Research I 51, 1057-1073.

Brand, L.E., Sunda, W.G., Guillard, R.R.L., 1983. Limitation of marine phytoplankton reproductive rates by zinc, manganese and iron. Limnology and Oceanography 28, 1182-1195.

Brand, L.E., Sunda, W.G., Guillard, R.R.L., 1986. Reduction of marine phytoplankton reproduction rates by copper and cadmium. Journal of Experimental Marine Biology and Ecology 96, 225-250.

Broecker, W.S., Blanton, S., Smethie, W.M., Ostlund, G., 1991. Radiocarbon decay and oxygen utilization in the deep Atlantic Ocean. Global Biogeochemical Cycles 5, 87-114.

Bruland, K.W., Franks, R.P., Knauer, G.A., Martin, J.H., 1979. Sampling and analytical methods for determination of copper, cadmium, zinc and nickel at the nanogram per liter level in seawater. Analytica Chimica Acta 105, 223-245.

Bruland, K.W., 1980. Oceanographic distribution of Cd, Zn, Ni and Cu in North Pacific. Earth Planetary Science Letters 47, 176-198.

Bruland, K.W., 1989. Complexation of zinc by natural organic ligands in the central North Pacific. Limnology and Oceanography 34, 269-285.

Bruland, K.W., Donat, J.R., Hutchins, D.A., 1991. Interactive influences of bioactive trace metals on biological production in oceanic waters. Limnology and Oceanography 36, 1555-1577.

Bruland, K.W., 1992. Complexation of cadmium by natural organic ligands in the central North Pacific. Limnology and Oceanography 37, 1008-1013.

Bruland, K.W., Lohan, M., 2003. Controls of trace metals in seawater. In: Elderfield, H. (Ed.), Holland, H.D., Turekian, K.K. (Ex. Eds.), Treatise on geochemistry, Vol. 6. Elsevier-Pergamon, Oxford, pp. 23-37.

Bruland, K.W., Rue, E.L., Smith, G.J., Di Tullio, G.R., 2005. Iron, macronutrients and diatom blooms in the Peru upwelling regime: brown and blue waters of Peru. Marine Chemistry 93, 81-103.

Buck, K., Bruland, K.W., 2005. Copper speciation in San Francisco Bay: A novel approach using multiple analytical windows. Marine Chemistry 96, 185-198.

Buck, K., Bruland, K.W., 2007. The physicochemical speciation of dissolved iron in the Bering Sea, Alaska. Limnology and Oceanography 52, 1800-1808.

Buitenhuis, E.T., Timmermans, K.R., de Baar, H.J.W., 2003. Zinc-bicarbonate colimitation of *Emiliana huxleyii*. Limnology and Oceanography 48, 1575-1582.

Byrne, R.H., Kump, L.R., Cantrell, K.J., 1988. The influence of temperature and pH on trace metal speciation in seawater. Marine Chemistry 25, 163-181.

Carrasco, G.G., Duffaut, L.A., Donat, J.R., in preparation. A MatLab program that optimizes Ruzic and Scatchard results using the Levenberg-Marquardt algorithm for interpretation of metal organic complexation in seawater.

Carrasco, G.G., Donat, J.R., 2001. Concentrations, complexation and speciation of Zn and Cd in the Western South and Equatorial Atlantic Ocean. 2001 American Society of Limnology and Oceanography & Aquatic Sciences Meeting, Albuquerque, NM.

Carrasco, G.G, Donat, J.R., Burdige, D.J., 2002. Benthic fluxes of Cu, Zn and Cd and their complexing ligands in the Elizabeth River, VA and the Chesapeake Bay. Oral Presentation. 2002 American Geophysical Union & Ocean Sciences Meeting, Honolulu, HI.

Carrasco, G.G., Morton, P.L., Donat, J.R., 2008. Concentrations, complexation and chemical speciation of zinc and cadmium in the Western North Pacific Ocean: Exploring sources and transport of trace metals and their complexing ligands. 2008 American Geophysical Union Fall Meeting, San Francisco, CA.

Cenci, R.M., Martin, J.-M., 2004. Concentration and fate of trace metals in Mekong River Delta. Science of the Total Environment. 332, 167-182.

Charette, M.A., Moran, S.B., 1999. Rates of particle scavenging and particulate organic carbon export estimated using 234^{Th} as a tracer in the subtropical and equatorial Atlantic Ocean. Deep-Sea Research II, 885-906.

Christensen, J.B., Christensen, T.H., 2000. The effect of pH on the complexation of Cd, Ni and Zn by dissolved organic carbon from leachate-polluted groundwater. Water Research 34, 3743-3754.

Coale, K.H., Bruland, K.W., 1988. Copper complexation in the Northeast Pacific. Limnology and Oceanography 33, 1084-1101.

Coale, K.H., Bruland, K.W., 1990. Spatial and temporal variability in copper complexation in the North Pacific. Deep-Sea Research 37, 317-336.

Coale, K.H., Gordon, R.M., Wang, X., 2005. The distribution and behavior of dissolved and particulate iron and zinc in the Ross Sea and Antarctic circumpolar current along 170 W. Deep-Sea Research I 52, 295-318.

Coleman, J.E., 1998. Zinc enzymes. Current Opinions in Chemical Biology 2, 222-234.

Collier, R., Edmond, J., 1984. The trace element geochemistry of marine biogenic particulate matter. Progress in Oceanography 13, 113-199.

Consolvo, J.C., 2000. Copper complexation and speciation in the Western South and Equatorial Atlantic Ocean. M.Sc. Thesis, Old Dominion University, Norfolk, VA.

Corami, F., Capodaglio, G., Turetta, C., Soggia, F., Magi, E., Grotti M., 2005. Summer distribution of trace metals in the western sector of the Ross Sea, Antarctica. Journal of Environmental Monitoring 7, 1256-1264.

Crawford, D.W., Lipsen, M.S., Purdie, D.A., Lohan, M.C., Statham, P.J., Whitney, F.A., Putland, J.N., Johnson, W.K., Sutherland, N., Peterson, T.D., Harrison, P.J., Wong, P.J., 2003. Influence of zinc and iron enrichments on phytoplankton growth in the northeastern subarctic Pacific. Limnology and Oceanography 48, 1583-1600.

Croot, P.L., Baars, O., Streu, P., accepted. The distribution of dissolved zinc in the Atlantic sector of the Southern Ocean. Deep Sea Research II doi:10.1016/j.dsr2.2010.10.041.

Croot, P.L., Moffett, J.W., Brand, L.E., 2000. Production of extracellular Cu complexing ligands by eukaryotic phytoplankton in response to Cu stress. Limnology and Oceanography 45, 619-627.

Croot, P.L., Karlson, B., Wulff, A., Linares, F., Andersson, K., 2002. Trace metal/phytoplankton interactions in the Skagerrak. Journal of Marine Systems 35, 39-60.

Cullen, J.T., 2003. Effect of iron limitation on the Cd to phosphate ratio of natural phytoplankton assemblages from the Southern Ocean. Limnology and Oceanography 48, 1079-1087.

Cullen, J.T., 2006. On the nonlinear relationship between dissolved cadmium and phosphate in the modern global ocean: Could chronic iron limitation of phytoplankton growth cause the kink? Limnology and Oceanography 51, 1369-1380.

Cutter, G.A., Measures, C.I., 1999. The 1996 IOC contaminant baseline survey in the Atlantic Ocean from 33 S to 10 N: Introduction, sampling protocols and hydrographic data. Deep Sea Research II 46, 867-884.

Cutter, G.A., Cutter, L.S., 2001. Sources and cycling of selenium in the western and equatorial Atlantic Ocean. Deep-Sea Research II 48, 2917-2931.

Cutter, G.A., Cutter, L.S., Featherstone, A.M., Lohrenz, S.E., 2001. Antimony and arsenic biogeochemistry in the western Atlantic Ocean. Deep-Sea Research II 48, 2895-2915.

de Baar, H.J.W, Saager, P.M., Nolting, R.F., van der Meer, J., 1994. Cadmium versus phosphate in the world ocean. Marine Chemistry 46, 261-281.

de la Rocha, C.L., Hutchins, D.A., Brzezinski, M.A., Zhang, Y., 2000. Effects of iron and zinc deficiency on elemental composition and silica production by diatoms. Marine Ecology: Progress Series 195, 71-79.

DeMaster, D.J., Pope, R.H., 1996. Nutrient dynamics in Amazon shelf waters: results from AMASSEDS. Continental Shelf Research 16, 263-289.

DeMaster, D.J., Smith, W.O.Jr., Nelson, D.M., Aller, J.Y., 1996. Biogeochemical processes in Amazon shelf waters: chemical distributions and uptake rates of silicon, carbon and nitrogen. Continental Shelf Research 16, 617-643.

DeMaster, D.J., Aller, R.C., 2001. Biogeochemical processes on the Amazon shelf: changes in dissolved and particulate fluxes during river/ocean mixing. In:

McClain, M.E., Victoria, R.L., Richey, J.E. (Eds.), the biogeochemistry of the Amazon Basin. Oxford University Press, USA, pp. 328-357.

Dixon, J.L., Statham, P.J., Widdicombe, C.E., Jones, R.M., Barquero-Molina, S., Dickie, B., Nimmo, M., Turley, C.M., 2006. Cadmium uptake by marine micro-organisms in the English Channel and Celtic Sea. Aquatic Microbial Ecology 44, 31-43.

Donat, J.R., Bruland, K.W., 1990. A comparison of two voltammetric techniques for determining zinc speciation in Northeast Pacific Ocean waters. Marine Chemistry 28, 301-323.

Donat, J.R., Bruland, K.W., 1995. Trace Elements in the Oceans. In: Salbu, B., Steinnes, E. (Eds.), Trace elements in natural waters. CRC Press, Boca Raton, FL, pp. 247-281.

Donat, J.R., Carrasco, G.G., Consolvo, J.A., 2002. Water column trace metal concentrations and speciation in the Elizabeth River, Virginia. 2002 American Geophysical Union and Ocean Sciences Meeting, Honolulu, HI.

Donat, J.R., Lao, K.A., Bruland, K.W., 1994. Speciation of dissolved copper and nickel in South San Francisco Bay: a multimethod approach. Analytica Chimica Acta 284, 547-571.

Donat, J.R., Dryden, C.L., 2001. Transition metals and heavy metal speciation. In: Steele J. (Ed. in ch.), Encyclopedia of ocean sciences. doi:10.1016/B0-12-227430-X/00578-X, pp. 3027-3035.

Downs, J.N., Lorenzen, C.J., 1985. Carbon: Pheopigment ratios of zooplankton fecal pellets as an index of herbivorous feeding. Limnology and Oceanography 30, 1024-1036.

Dryden, C.L., Gordon, A.S., Donat, J.R., 2007. Seasonal survey of copper-complexing ligands and thiol compounds in a heavily utilized, urban estuary: Elizabeth River, Virginia. Marine Chemistry 103, 276-288.

Dupont, C.L., Ahner, B.A., 2005. Effects of copper, cadmium, and zinc on the production and exudation of thiols by *Emiliana huxleyii.* Limnology and Oceanography 50, 508-515.

Dyrham, S.T., Palenik, B., 2003. Characterization of ectoenzyme activity and phosphate-regulated proteins in the coccolithophorid *Emiliana huxleyii*. Journal of Plankton Research 25, 1215-1225.

Eglinton, T.I., Repeta, D.J., 2003. Organic matter in the contemporary ocean. In: Elderfield, H. (Ed.), Holland, H.D., Turekian, K.K. (Ex. Eds.), Treatise on geochemistry, Vol. 6. Elsevier-Pergamon, Oxford, pp. 145-180.

Eisma, D., van der Gaast, S.J., Martin, J.M., Thomas, A.J., 1978. Suspended matter and bottom deposits of the Orinoco Delta: Turbidity, mineralogy, and elementary composition. Netherland Journal of Sea Research 12, 224-251.

Elderfield, H., Rickaby, R.E.M., 2000. Oceanic Cd/phosphate ratio and nutrient utilization in the glacial Southern Ocean. Nature 405, 305-310.

Ellwood, M.J., Hunter, K.A., 1999. Determination of the Zn/silicate ratio in a diatom opal: a method for the separation, cleaning and dissolution of diatoms. Marine Chemistry 66, 149-160.

Ellwood, M.J., van den Berg, C.M.G., 2000. Zinc speciation in the Northeastern Atlantic Ocean. Marine Chemistry 68, 295-306.

Ellwood, M.J., Hunter, K.H., 2000. The incorporation of zinc and iron into the frustule of the marine diatom *Thalassiosira pseudonana*. Limnology and Oceanography 45, 1517-1524.

Ellwood, M.J., Hunter, K.A., Kim, J.P., 2001. Zinc speciation in Lakes Manapouri and Hayes, New Zealand. Marine and Freshwater Research 52, 217-222.

Ellwood, M.J., 2004. Zinc and cadmium speciation in subantarctic waters east of New Zealand. Marine Chemistry 87, 37-58.

Ellwood, M.J., 2008. Wintertime trace metal (Zn, Cu, Ni, Cd, Pb and Co) and nutrient distributions in the Subantarctic Zone between 40–52°S; 155–160°E. Marine Chemistry 112, 107-117.

Emery, W.J., 2008. Water types and water masses. In: Steele J. (Ed. in ch.), Encyclopedia of ocean sciences. doi:10.1016/B0-12-227430-X/00578-X, pp. 3179-3187.

Ferron, B., Mercier, H., Speer, K., Gargett, A., Polzin, K., 1998. Mixing in the Romanche Fracture Zone. Journal of Physical Oceanography 28, 1929-1945.

Fitzwater, S.E., Johnson, K.S., Gordon, R.M., Coale, K.H., Smith, W.O., 2000. Trace metal concentrations in the Ross Sea and their relationship with nutrients and phytoplankton growth. Deep Sea Research II 47, 3159-3179.

Ffield, A., 2005. North Brazil current rings viewed by TRMM Microwave Imager SST and the influence of the Amazon Plume. Deep-Sea Research I 52, 137-160.

Franck, V.M., Bruland, K.W., Hutchins, D.A., Brzezinski, M.A., 2003. Iron and zinc effects on silicic acid and nitrate uptake kinetics in three high-nutrient, low-chlorophyll (HNLC) regions. Marine Ecology Progress Series 252, 15-33.

Frantz, J., 2010. G3data software. www.frantz.fi/software/g3data.php

Garcia, H.E., Locarnini, R.A., Boyer, T.P., Antonov, J.I., 2006. World Ocean Atlas, 2005, Volume 3: Dissolved Oxygen, Apparent Oxygen Utilization and Oxygen Saturation. Levitus, S. (Ed.), US Government Printing Office, Washington, DC, 342 pp.

Garnier, C., Pizeta, I., Mounier, S., Benaim, J.I., Branica, M., 2004. Influence of the type of titration and of data treatment methods on metal complexing parameters determination of single and multi-ligand systems measured by stripping voltammetry. Analytica Chimica Acta 505, 263-275.

Garrigosa, A.M., Arino, C., Diaz-Cruz, J.M., Esteban, M., 2008. Alternating current anodic stripping voltammetry in the study of cadmium complexation by a reference Suwanee River fulvic acid: a model case with strong electrode adsorption and weak binding. Analytical and Bioanalytical Chemistry 390, 769-776.

Gerringa, L.J.A., Herman, P.M.J., Poortvliet, T.C.W., 1995. Comparison of the linear van den Berg/Ruzic transformation and a non-linear fit of the Langmuir isotherm applied to Cu speciation data in the estuarine environment. Marine Chemistry 48, 131-142.

Gerringa, L. J. A., de Baar, H. J. W., Nolting, R. F., Paucot, H., 2001. The influence of salinity on the solubility of Zn and Cd sulphides in the Scheldt estuary. Journal of Sea Research 46, 201-211.

Gerringa, L.J.A, Veldhuis, M.J.W., Timmermans, K.R., Sarthou, G., de Baar, H.J.W., 2006. Co-variance of dissolved Fe-binding ligands with phytoplankton

characteristics in the Canary Basin. Marine Chemistry 102, 276-290.

Gerringa, L.J.A., Thuroczy, C., Klunder, M., de Baar, H.J., Laan, P., 2010. Organic complexation of dissolved iron in the Atlantic sector of the Southern Ocean. 2010 American Geophysical Union and Ocean Sciences Meeting, Portland, OR.

Goni, G.J., Johns, W.E., 2001. A census of North Brazil Current rings observed from TOPEX/POSEIDON altimetry: 1992-1998. Geophysical Research Letters 28, 1-4.

Hedges, J.I., Mayorga, E., Tsamakis, E., McClain, M.E., Aufdenkampe, A., Quay, P., Richey, J.E., Benner, R., Opsahl, S., Black, B., Pimentel, T., Quintanilla, J., Maurice, L., 2000. Organic matter in Bolivian tributaries of the Amazon River: A comparison to the lower main stream. Limnology and Oceanography 45, 1449-1466.

Helmers, E., Schrems, O., 1995. Wet deposition of metals to the tropical north and the south Atlantic Ocean. Atmospheric Environment 29, 2475-2484.

Hendry, K.R., Rickaby, R.E.M., de Hoog, J.C.M., Weston, K., Rehkämper, M., 2008. Cadmium and phosphate in coastal Antarctic seawater: Implications for Southern Ocean nutrient cycling. Marine Chemistry 112, 149-157.

Hendry, K.H., Rickaby, R.E.M., 2008. Opal (Zn/silicate) ratios as a nearshore geochemical proxy in coastal Antarctica. Paleoceanography 23, PA2218. doi:10.1029/2007PA001576.

Henry, C.W., Donat, J.R., 1996. Zinc complexation and speciation in the Chesapeake Bay. EOS transaction AGU 77, OS72.

Hernes, P.J., Benner, R., 2002. Transport and diagenesis of dissolved and particulate terrigenous organic matter in the North Pacific Ocean. Deep Sea Research I, 49, 2119-2132.

Hirst, A.C., 1999. Determination of water component age in ocean models: application to the fate of North Atlantic Deep Water. Ocean Modelling 1, 81-94.

Ho, T.-Y., Quigg, A., Finkel, Z.V., Milligan, A.J., Wyman, K., Falkowski, P.G., Morel, F.M.M., 2003. The elemental composition of some marine phytoplankton. Journal of Phycology 39, 1145-1159.

Hoffmann, S.R., Shafer, M.M., Armstrong, D.E., 2007. Strong colloidal and dissolved organic ligands binding copper and zinc in rivers. Environmental Science and Technology 41, 6996-7002.

Hong, S., Candelone, J.P., Turetta, C., Boutron, C.F., 1996. Changes in natural Pb, Cu, Zn and Cd concentrations in central Greenland ice from 8250 to 149,100 years ago: their association with climatic changes and resultant variations of dominant source contributions. Earth and Planetary Science Letters 143, 233-244.

Hong, S., Boutron, C.F., Barbante, C., Hur, S.D., Lee, K., Gabrielli, P., Capodaglio, G., Ferrari, C.P., Turetta, C., Petit, J.R., Lipenkov, V.Y., 2005. Glacial–interglacial changes in the occurrence of Pb, Cd, Cu and Zn in Vostok Antarctic ice from 240 000 to 410 000 years BP. Journal of Environmental Monitoring 7, 1326-1331.

Hopkinson, B.A., Barbeau, K.A., 2007. Organic and redox speciation of iron in the eastern tropical North Pacific suboxic zone. Marine Chemistry 106, 2-17.

Hu, C., Montgomery, E.T., Schmitt, R.W., Muller-Karger, F.E., 2004. The dispersal of the Amazon and Orinoco River water in the tropical Atlantic and Caribbean Sea: Observation from space and S-PALACE floats. Deep-Sea Research II 51, 1151-1171.

Hudson, R.J.M., Rue, E.L., Bruland, K.W., 2003. Modeling complexometric titrations of natural water samples. Environmental Science and Technology 37, 1553-1562.

Huhn, O., Roether, W., Beining, P., Rose, H., 2001. Validity limits of carbon tetrachloride as an ocean tracer. Deep-Sea Research I, 48, 2025-2049.

Huhn, O., Roether, W., Steinfeldt, R., 2008. Age spectra in North Atlantic Deep Water along the South American continental slope, 10 N-30 S, based on tracer observations. Deep-Sea Research I 55, 1252-1276.

Huhn, O., Hellmer, H.H., Rhein, M., Rodehacke, C., Roether, W., Schodlok, M.P., Shroder, M., 2008b. Evidence of deep- and bottom-water formation in the western Weddell Sea. Deep-Sea Research II 55, 1098-1116.

Hurst, M.P., Bruland, K.W., 2007. An investigation into the exchange of iron and zinc between soluble, colloidal, and particulate size-fractions in shelf waters using

low-abundance isotopes as tracers in shipboard incubation experiments. Marine Chemistry 103, 211-226.

Jakuba, R., Moffett, J.W., Dyhrman, S.T., 2008. Evidence for the linked biogeochemical cycling of zinc, cobalt and phosphorus in the western North Atlantic Ocean. Global Biogeochemical Cycles 22, GB4012, doi:10.1029/2007GB003119.

Jakuba, R., Moffett, J.W., Saito, M.A., 2008b. Use of a modified, high-sensitivity, anodic stripping voltammetry method for determination of zinc speciation in the North Atlantic Ocean. Analytica Chimica Acta 614, 143-152.

Jickells, T.D., An, Z.S., Andersen, K.K., Baker, A.R., Bergametti, G., Brooks, N., Cao, J.J., Boyd, P.W., Duce, A., Hunter, K.A., Kawahata, H., Kubilay, N., laRoche, J., Liss, P.S., Mahowald, N., Prospero, J.M., Ridgwell, A.J., Tegen, I., Torres, R., 2005. Global iron connections between desert dust, ocean biogeochemistry, and climate. Science 308, 67-71.

Jochum, M., Malanotte-Rizzoli, P., 2003. The flow of AAIW along the equator. In: Goni, G.J., Malanotte-Rizzoli, P. (Eds.), Interhemispheric water exchange in the Atlanic Ocean. Elsevier Series, Amsterdam, pp. 193-212.

Johnson, G.C., 2008. Quantifying Antarctic Bottom Water and North Atlantic Deep Water volumes. Journal of Geophysical Research, 113, C05027, doi:10.1029/2007JC004477.

Kieber, R.J., Parler, N.E., Skrabal, S.A., Willey, J.D., 2008. Speciation and photochemistry of mercury in rainwater. Journal of Atmospheric Chemistry 60, 153-168.

Kieber, R.J., Skrabal, S.A., Smith, C., Willey, J.D., 2004. Redox speciation of copper in rainwater: Temporal variability and atmospheric deposition. Environmental Science and Technology 38, 3587-3594.

Kogut, M.B., Voelker, B.M., 2001. Strong copper-binding behavior of terrestrial humic substances in seawater. Environmental Science and Technology 35, 1149-1156.

Kozelka, P.B., Bruland, K.W., 1998. Chemical speciation of dissolved Cu, Zn, Cd, Pb in Narragansett Bay, Rhode Island. Marine Chemistry 60, 267-282.

Kremling, K., Streu, P., 2001. The behaviour of dissolved Cd, Co, Zn, and Pb in North Atlantic near-surface waters (30 N/60 W–60 N/2W). Deep-Sea Research I 48, 2541-2567.

Krey, W.B., 2008. Siderophore production by heterotrophic bacterial isolates from the Costa Rica upwelling dome. M.Sc. thesis WHOI/MIT, Woods Hole, MA.

Laes, A., Blain, S., Laan, P., Achterberg, E.P., Sarthou, G., de Baar, H.J.W., 2003. Deep dissolved iron profiles in the eastern North Atlantic in relation to water masses. Geophysical Research Letters, 30, 17, 1902, doi:10.1029/2003GL017902.

Laglera, L.M., van den Berg, C.M.G., 2006. Photochemical oxidation of thiols and copper complexing ligands in estuarine waters. Marine Chemistry 101, 130-140.

Lam, P.J., Bishop, J.K.B., Henning, C.C., Marcus, M.A., Waychunas, G.A., Fung, I.Y., 2006. Wintertime phytoplankton bloom in the subarctic Pacific supported by continental margin iron. Global Biogeochemical Cycles, 20, GB1006, doi:1029/2005GB002557.

Lam, P.J., Bishop, J.K.B., 2008. The continental margin is a key source of iron to the HNLC North Pacific Ocean. Geophysical Research Letters, 35, LO7608, doi:10.1029/2008GL033294.

Lane, T.W., Morel, F.M.M., 2000a. A biological function for Cd in marine diatoms. Proceedings of the National Academy of Sciences, USA 97, 4627-4631.

Lane, T.W., Morel, F.M.M., 2000b. Regulation of carbonic anhydrase expression by Zn, Co and CO_2 in the marine diatom *Thalassiosira weisflogii*. Plant Physiology 123, 345-352.

Lane, T.W., Saito, M.A., George, G.N., Pickering, I.J., Prince, R.C., Morel, F.F.M., 2005. A cadmium enzyme from a marine diatom. Nature 435, 42.

Lankhorst, M., Fratantoni, D., Ollitrault, M., Richardson, P., Send, U., Zenk, W., 2009. The mid-depth circulation of the northwestern tropical Atlantic observed by floats. Deep Sea Research I 56, 1615-1632.

Leal, M.F.C., Vasconcelos, M.T.S.D., van den Berg, C.M.G., 1999. Copper-induced release of complexing ligands similar to thiols by *Emiliana huxleyii* in seawater cultures. Limnology and Oceanography 44, 1750-1762.

Leblanc, K., Hare, C.E., Boyd, P.W., Bruland, K.W., Sohst, B., Pickmere, S., Lohan, M.C., Buck, K., Ellwood, M., Hutchins, D.A., 2005. Fe and Zn effects on the silicate cycle and diatom community structure in two contrasting high and low-silicate HNLC areas. Deep-Sea Research I 52, 1842-1864.

Lipscomb, W.N., Strater, N., 1996. Recent advances in zinc enzymology. Chemical Review 96, 2375-2433.

Lohan, M.C., Crawford, D.W., Purdie, D.A., Statham, P.J., 2005. Iron and zinc enrichments in the northeastern subarctic Pacific: ligand production and zinc availability in response to phytoplankton growth. Limnology and Oceanography 50, 1427-1437.

Lohan, M.C., Bruland, K.W., 2008. Elevated Fe(II) and dissolved Fe in hypoxic shelf waters off Oregon and Washington: an enhanced source of iron to coastal upwelling regimes. Environmental Science & Technology 42, 6462-6468.

Lorenzen, J., 1967. Vertical distribution of chlorophyll and phaeo-pigments: Baja California. Deep-Sea Research 14, 735-745.

Loscher, B.M., van der Meer, J., de Baar, H.J.W, Saager, P.M., de Jong, J.T.M., 1997. The global Cd/phosphate relationship in deep ocean waters and the need for accuracy. Marine Chemistry 59, 87-93.

Loscher, B.M., 1999. Relationships among Ni, Cu, Zn, and major nutrients in the Southern Ocean. Marine Chemistry 67, 67-102.

Maldonado, M. T., Price N. M., 1999. Utilization of iron bound to strong organic ligands by plankton communities in the subarctic Pacific Ocean. Deep-Sea Research II 46, 2447-2473.

Mantoura, R.F.F., Riley J.P., 1975. The use of gel filtration in the study of metal binding by humic acids and related compounds. Analytica Chimica Acta 78, 193.

Martin, J.H., Fitzwater, S.E., 1988. Iron deficiency limits phytoplankton growth in the north-east Pacific subarctic. Nature 331, 341-343.

Martin, J.M., Gordon, R.M., Fitzwater, S.E., 1990. Iron in Antarctic waters. Nature 345, 156-158.

Martin, J.M., Windom, H.L., 1991. Present and future roles of oceanic margins in regulating marine biogeochemical cycles of trace elements. In: Mantoura, R.F.C.,

Martin, J.-M., Wollast, R. (Eds.), Report of the Dahlem workshop on ocean margin processes in global change. Berlin, 1990, pp. 45-67.

Martinez, J.M., Guyot, J.L., Filizola, N., Sondag, F., 2009. Increase in suspended sediment discharge of the Amazon River assessed by monitoring network and satellite data. Catena, doi:10.1016/j.catena.2009.05.011.

Mason, R. P., Sullivan, K.A., 1999. The distribution and speciation of mercury in the South and equatorial Atlantic. Deep-Sea Research II 46, 937-956.

Mercier, H., Speer, K.G., 1998. Transport of bottom water in the Romanche Fracture Zone and the Chain Fracture Zone. Journal of Physical Oceanography 28, 779-790.

Miethke, M., Marahiel, M.A., 2007. Siderophore-based iron acquisition and pathogen control. Microbiology and Molecular Biology Reviews 71, 413-451, doi:10.1128/MMBR.00012-07.

Mikkelsen, N., 1997. Upper Quaternary diatoms in the Amazon fan of the Western Atlantic. In: Flood, R.D., Piper, D.J.W., Klaus, A., Peterson, L.C. (Eds.), Proceedings of the Ocean Drilling Program, scientific results, Vol. 155. doi:10.2973/odp.proc.sr.155.218.1997. College Station, TX, pp. 367.

Miller, L.A., Bruland, K.W., 1997. Competitive equilibration techniques for determining transition metal speciation in natural waters: Evaluation using model data. Analytica Chimica Acta 343, 161-181.

Moffett, J.W., Zika, R.G., Brand, L., 1990. Distribution and potential sources and sinks of copper chelators in the Sargasso Sea. Deep-Sea Research 37, 27-36.

Moffett, J.W., 1995. Temporal and spatial variability of strong copper complexing ligands in the Sargasso Sea. Deep Sea Research I 42, 1273-1295.

Moffett, J.W., Brand, L.E., 1996. The production of strong extracellular Cu chelators by marine cyanobacteria in response to Cu stress. Limnology and Oceanography 41, 288-293.

Moffett, J.W., Goepfert, T.J., Naqvi, S.W.A., 2007. Reduced iron associated with secondary nitrite maxima in the Arabian Sea. Deep Sea Research I 54, 1341-1349.

Moffett, J.W., Dupont, C.L., 2007. Cu complexation by organic ligands in the sub-arctic NW Pacific and Bering Sea. Deep Sea Research I 54, 586-595.

Morel, F.M.M., 1983. Principles of Aquatic Chemistry. Wiley-Interscience, New York, 446 pp.

Morel, F.M.M., Reinfelder, J.R., Roberts, S.B., Chamberlain, C.P., Lee, J.G., Yee, D., 1994. Zinc and carbon co-limitation of marine phytoplankton. Nature 369, 740-742.

Morel, F.M.M., Milligan, A.J., Saito, M.A., 2003. Marine bioinorganic chemistry: the role of trace metals in the oceanic cycles of major nutrients. In: Elderfield, H. (Ed.), Holland, H.D., Turekian, K.K. (Ex. Eds.), Treatise on geochemistry, Vol. 6. Elsevier-Pergamon, Oxford, pp. 113-143.

Morel, F.M.M., Price, N.M., 2003. The biogeochemical cycles of trace metals in the oceans. Science 300, 944-947.

Morton, P.L., Bizimis, M., Landing, W., Donat, J.R., 2008. Trace metal transport in the Western North Pacific: Relative contributions from alternative sources. 2008 American Geophysical Union Fall Meeting, San Francisco, CA.

Muller, F.L.L., 1996. Interactions of Cu, Pb and Cd with the dissolved colloidal and particulate components of estuarine and coastal waters. Marine Chemistry 52, 245-268.

Muller, F.L.L., Gulin, S.B., Kalvoy, A., 2001. Chemical speciation of copper and zinc in surface waters of the western Black Sea. Marine Chemistry 76, 233-251.

Muller, F.L.L., Jacquet, S., Wilson, W.H., 2003. Biological factors regulating the chemical speciation of Cu, Zn, and Mn under different nutrient regimes in a marine mesocosm experiment. Limnology and Oceanography 48, 2289-2302.

Muller-Karger, F.E., Richardson, P.L., McGillicuddy, D., 1995. On the offshore dispersal of the Amazon's plume in the North Atlantic: Comments on the paper by A. Longhurst, "Seasonal cooling and blooming in tropical oceans". Deep-Sea Research I 42, 2127-2137.

Muller-Karger, F.E., McClain, C.R., Richardson, P.L., 1988. The dispersal of the Amazon's water. Nature 333, 56-59.

Nielsen, A.A., 2006. Least Squares adjustment: Linear and nonlinear weighted regression analysis. http://www2.imm.dtu.dk/pubdb/p.php?2804 Technical University of Denmark and DTU Space - National Space Institute, Denmark.

Nishioka, J., Ono, T., Saito, H., Nakatsuka, T., Takeda, S., Yoshimura, T., Suzuki, K., Kuma, K., Nakabayashi, S., Tsumune, D., Mitsudera, H., Johnson, W.K., Tsuda, A., 2007. Iron supply to the western subarctic Pacific: Importance of iron export from the Sea of Okhotsk. Journal of Geophysical Research 112, C10012, doi:10.1029/2006JC004055.

Noble, A.E., Saito, M.A., Maiti, K., Benitez-Nelson, C., 2008. Cobalt, manganese, and iron near the Hawaiian Islands: A potential concentrating mechanism for cobalt within a cyclonic eddy and implications for hybrid-type trace metals. Deep Sea Research II 55, 1473-1490.

Nolting, R.F., de Baar, H.J.W., van Bennekom, A.J., Messon, A., 1991. Cadmium, copper, and iron in the Scotia Sea, Weddell Sea, and Weddell/Scotia Confluence (Antarctica). Marine Chemistry 35, 219-243.

Noriki, S., Hamahara, K., Harada, K., 1999. Particulate flux and Cd/phosphate ratio of particulate material in the Pacific Ocean. Journal of Oceanography 55, 693-703.

Nozaki, Y., 1997. A fresh look at element distribution in the North Pacific. Eos Electronic Supplement. http://www.agu.org/eos_elec/97025e.html

Orsi, A.H., Whitworth, T., Nowlin, W., 1995. On the meridional extent and fronts of the Antarctic Circumpolar Current. Deep-Sea Research I 42, 641-673.

Osterhus, S., Gammelsrod, T., 2009. Bipolar Atlantic thermohaline circulation. Climate change: global risks, challenges and decisions. IOP Conference Series: Earth and Environmental Science 6, 032023 doi:10.1088/1755-1307/6/3/032023. IOP Publishing.

Peers, G., Quesnel, S.-A., Price, N.M., 2005. Copper requirements for iron acquisition and growth of coastal and oceanic diatoms. Limnology and Oceanography 50, 1149-1158.

Pizeta, I., Branica, M., 1997. Simulation and fitting of anodic stripping voltammetry data for determination of the metal complexing capacity. Analytica Chimica Acta 35, 3-82.

Planquette, H., Fones, G.R., Statham, P.J., Morris, P.J., 2009. Origin of iron and aluminium in large particles (N53 μm) in the Crozet region, Southern Ocean. Marine Chemistry 115, 31-42.

Pointkowski, S.A., Landry, M.R., Finenko, Z.Z., Kovalev, A.V., Williams, R., Gallienne, C.P., Mishonov, A.V., Skryabin, V.A., Tokarev, Y.N., Nikolsky, V.N., 2003. Plankton communities of the South Atlantic anticyclonic gyre. Oceanologica Acta 26, 255-268.

Powell, R.T., Donat, J.R., 2001. Organic complexation and speciation of iron in the South and Equatorial Atlantic. Deep-Sea Research II 48, 2877-2893.

Price, N.M., Morel, F.M.M., 1990. Cadmium and cobalt substitution for zinc in a marine diatom. Nature 344, 658-660.

Rabouille, C., Caprais, J.-C., Lansard, B., Crassous, P., Dedieu, K., Reyss, J.L., Khripounoff, A., 2009. Organic matter budget in the Southeast Atlantic continental margin close to the Congo Canyon: *in-situ* measurements of sediment oxygen consumption. Deep Sea Research II 56, 2223-2238.

Ragueneau, O., Regaudie-de-Gioux, A., Moriceau, B., Gallinari, M., Vangriesheim, A., Baurand, F., Khripounoff, A., 2009. A benthic silicate mass balance on the Congo margin: Origin of the 4000m DSi anomaly and implications for the transfer of silicate from land to ocean. Deep-Sea Research II 56, 2197-2207.

Redfield, A.C., Ketchum, B.H., Richards, F.A., 1963. The influence of organisms on the composition of seawater. In: Hill, M.N. (Ed.), the sea., Vol. 2. Wiley-Interscience, New York, pp. 26-77.

Reuter, J.G., Morel, F.M.M., 1981. The interaction between zinc deficiency and copper toxicity as it affects the silicic acid uptake mechanism in *Thalassiosira pseudonana*. Limnology and Oceanography 26, 67-73.

Rickaby, R.E.M., Elderfield, H., 1999. Planktonic foraminiferal Cd/Ca: Paleonutrients or paleotemperature? Paleoceanography 14, 293.

Rijkenberg, M.J.A., Fischer, A.C., Kroon, J.J., Gerringa, L.J.A., Timmermans, K.R., Wolterbeek, H.Th., de Baar, H.J.W., 2005. The influence of UV irradiation on the photoreduction of iron in the Southern Ocean. Marine Chemistry 93, 119-129

Rijkenberg, M.J.A., Gerringa, L.J.A., Velzeboer, I., Timmermans, K.R., Buma, A.G.J., de Baar, H.J.W., 2006. Iron-binding ligands in Dutch estuaries are not affected by UV induced photochemical degradation. Marine Chemistry 100, 11-23.

Roether, W., Putzka, A., 1996. Transient-tracer information on ventilation and transport of South Atlantic waters. In: Wefer, G., Berger, W.H., Siedler, G., Webb, D.J. (Eds.), the South Atlantic: present and past circulation. Springer-Verlag, Berlin, pp. 45-62.

Rutgers van der Loeff, M., Helmers, E., Kattner, G., 1997. Continuous transects of Cd, Cu and al. in surface waters of the Atlantic Ocean, 50 N to 50 S: Correspondence and contrast with nutrient-like behaviour. Geochimica et Cosmochimica Acta 61, 47-61.

Ruzic, I., 1982. Theoretical aspects of the direct titration of natural waters and its information yield for trace metal speciation. Analytica Chimica Acta 140, 99-113.

Saager, P.M., de Baar, H.J.W., de Jong, J.T.M., Nolting, R.F., Schijf, J., 1997. Hydrography and local sources of dissolved trace metals Mn, Ni, Cu, and Cd in the northeast Atlantic Ocean. Marine Chemistry 57, 195-216.

Saito, M.A., Moffett, J.W., 2001. Complexation of cobalt by natural organic ligands in the Sargasso Sea as determined by a new high-sensitivity electrochemical cobalt speciation method suitable for open ocean work. Marine Chemistry 75, 49-68.

Saito, M.A., Sigman, D.M., Morel, F.M.M., 2003. The bioinorganic chemistry of the ancient ocean: the co-evolution of cyanobacterial metal requirements and biogeochemical cycles at the Archean-Proterozoic boundary? Inorganica Chimica Acta 356, 308-318.

Saito, M.A., Goepfert, T.J., 2008. Zinc-cobalt colimitation of *Phaeocystis antarctica*. Limnology and Oceanography 53, 266-275.

Saito, M.A., Moffett, J.W., DiTullio, G.R., 2004. Cobalt and nickel in the Peru upwelling region: A major flux of labile cobalt utilized as a micronutrient. Global Biogeochemical Cycles 18, GB4030, doi:10.1029/2003GB002216.

Sander, S., Kim, J.P., Anderson, B., Hunter, K.A., 2005. Effect of UVB Irradiation on Cu^{2+}-binding organic ligands and Cu^{2+} speciation in alpine lake waters of New Zealand. Environmental Chemistry 2, 56-62.

Sanudo-Wilhelmy, S.A., Olsen, K.A., Scelfo, J.M., Foster, T.D., Flegal, A.R., 2002. Trace metal distributions off the Antarctic Peninsula in the Weddell Sea. Marine Chemistry 77, 157-170.

Sarmiento, J.L., Gruber, N., 2006. Ocean biogeochemical dynamics. Princeton University Press, Princeton, NJ, 503 pp.

Sarthou, G., Baker, A.R., Kramer, J., Laan, P., Laës, A., Ussher, S., Achterberg, E.B., de Baar, H.J.W., Timmermans, K.R., Blain, S., 2007. Influence of atmospheric inputs on the iron distribution in the subtropical North-East Atlantic Ocean. Marine Chemistry 104, 186-202.

Sarthou, G., Baker, A.R., Blain, S., Achterberg, E.P., Boye, M., Bowie, A.R., Croot, P., Laan, P., de Baar, H.J.W., Jickells, T.D., Worsfold, P.J., 2003. Atmospheric iron deposition and sea-surface dissolved iron concentrations in the eastern Atlantic Ocean. Deep-Sea Research I 50, 1339-1352.

Sato, M., Takeda, S., Furuya, K., 2007. Iron regeneration and organic iron (III)-binding ligand production during in situ zooplankton grazing experiment. Marine Chemistry 106, 471-488.

Scatchard, G., 1949. The attraction of proteins for small molecules and ions. Annals of the New York Academy of Science 57, 660-672.

Schlitzer, R., 2007. Assimilation of radiocarbon and chlorofluorocarbon data to constrain deep and bottom water transports in the world ocean. Journal of Physical Oceanography, DOI: 10.1175/JPO3011.1.

Shank, G.C., Skrabal, S.A., Donat, J.R., Whitehead, R.F., Kieber, R.J., 2004. Strong copper complexation in an organic-rich estuary: The importance of allochthonous dissolved organic matter. Marine Chemistry 88, 21-39.

Shank, G.C., Whitehead, R.F., Smith, M.L., Skrabal, S.A., Kieber, R.J., 2006. Photodegradation of strong copper-complexing ligands in organic-rich estuarine waters. Limnology and Oceanography 51, 884-892.

Shaked, Y., Xu, Y., Leblanc, K., Morel, F.M.M., 2006. Zinc availability and alkaline phosphatase activity in *Emiliana huxleyii*: Implications for Zn–phosphate co-limitation in the ocean. Limnology and Oceanography 51, 299-309.

Shiller, A.M., Boyle, E., 1985. Dissolved zinc in rivers. Nature 317, 49.

Shiller, A.M., Boyle, E.A., 1991. Trace elements in the Mississippi River Delta outflow region: Behavior at high discharge. Geochimica et Cosmochimica Acta 55, 3241-3251.

Shipe, R.F., Curtaz, J., Subramaniam, A., Carpenter, E.J., Capone, D.G., 2006. Diatom biomass and productivity in oceanic and plume-influenced waters of the western tropical Atlantic ocean. Deep-Sea Research I 53, 1320-1334.

Skrabal, S.A., Donat, J.R., Burdige, D.J., 1997. Fluxes of copper-complexing ligands from estuarine sediments. Limnology and Oceanography 42, 992-996.

Skrabal, S.A., Donat, J.R., Burdige, D.J., 2000. Pore water distributions of dissolved copper and copper-complexing ligands in estuarine sediments. Geochimica Cosmochimica Acta 64, 1843-1857.

Skrabal, S.A., Lieseke, K.L., Kieber, R.J., 2006. Dissolved zinc and zinc-complexing ligands in an organic-rich estuary: Benthic fluxes and comparison with copper speciation. Marine Chemistry 100, 108-123.

Smetacek, V., 2000. The giant diatom dump. Nature 406, 574-575.

Smith, I.J., Stevens, D.P., Heywood, K.J., Meredith, M.P., 2009. The flow of the Antarctic Circumpolar Current over the North Scotia Ridge. Deep-Sea Research I 57, 14-28.

Spencer, R.G.M., Stubbins, A., Hernes, P.J., Baker, A., Mopper, K., Aufdenkampe, A.K., Dyda, R.Y., Mwamba, V.L., Mangangu, A.M., Wabakanghanzi, J.N., Six, J., 2009. Photochemical degradation of dissolved organic matter and dissolved lignin phenols from the Congo River. Journal of Geophysical Research 114, G03010, doi:10.1029/2009JG000968.

Stramma, L., England, M., 1999. On the water masses and mean circulation of the South Atlantic Ocean. Journal of Geophysical Research 104, 20863-20883.

Stramma, L., Johnson, G.C., Sprintall, J., Mohrholz, V., 2008. Expanding oxygen-minimum zones in the tropical oceans. Science 320, 655-658.

Stramma, L., Schmidtko, S., Levin, L.A., Johnson, G.C., 2010. Ocean oxygen minima expansions and their biological impacts. Deep-Sea Research I 57, 587-595.

Sunda, W.G., Guillard, R.R.L., 1976. Relationship between cupric ion activity and toxicity of copper to phytoplankton. Journal of Marine Research 34, 511-529.

Sunda, W.G., Huntsman, S.A., 1992. Feedback interactions between zinc and phytoplankton in seawater. Limnology and Oceanography 37, 25-40.

Sunda, W.G., Huntsman, S.A., 1995. Cobalt and zinc interreplacement in marine phytoplankton: biological and geochemical implications. Limnology and Oceanography 40, 1404-1417.

Sunda, W.G., Huntsman, S.A., 1996. Antagonisms between cadmium and zinc toxicity and manganese limitation in a coastal diatom. Limnology and Oceanography 41, 373-387.

Sunda, W.G., Huntsman, S.A., 1998. Interactions among Cu^{2+}, Zn^{2+}, and Mn^{2+} in controlling cellular Mn, Zn, and growth rate in the coastal alga *Chlamydomonas*. Limnology and Oceanography 43, 1055-1064.

Sunda, W.G., Huntsman, S.A., 2000. Effect of Zn, Mn and Fe on Cd accumulation in phytoplankton: implications for oceanic Cd cycling. Limnology and Oceanography 45, 1501-1516.

Sunda, W.G., Huntsman, S.A., 2005. Effect of CO_2 supply and demand on zinc uptake and growth limitation in a coastal diatom. Limnology and Oceanography 50, 1181-1192.

Talley, L.D., 1996. Antarctic Intermediate Waters in the South Atlantic. In: Wefer, G., Berger, W.H., Siedler, G., Webb, D.J. (Eds.), the South Atlantic: present and past circulation. Springer-Verlag, Berlin, pp. 45-62.

Ternon, J.F., Oudot, C., Dessier, A., Diverres, D., 2000. A seasonal tropical sink for atmospheric CO_2 in the Atlantic Ocean: the role of the Amazon River discharge. Marine Chemistry 68, 183-201.

Thor, P., Dam, H.G., Rogers, D.R., 2003. Fate of organic carbon release from decomposing copepod fecal pellets in relation to bacterial production and ectoenzymatic activity. Marine Ecology Progress Series 33, 279-288.

Tian, F., Frew, R.D., Sander, S., Hunter, K.A., Ellwood, M.J., 2006. Organic iron (III) speciation in surface transects across a frontal zone: the Chatham Rise, New Zealand. Marine and Freshwater Research 57, 533-544.

Trefry, J.H., Nelson, T.A., Trocine, R.P., Metz, S., Welter, T., 1986. Trace metal fluxes through the Mississippi River delta system. In: Kullenberg G. (Ed.), Contaminants through the coastal zone, rapports et proces-verbaux des reunions, Conseil International pour l'Exploration de la Mer (CIESM), Le Conseil, Copenhagen, pp. 277-288.

Turner, D.R., Whitfield, M., Dickson, A.G., 1981. The equilibrium speciation of dissolved components in freshwater and seawater at 25°C and 1 atm pressure. Geochimica Cosmochimica Acta 45, 855-882.

van Aken, H.M., 2000. The hydrography of the mid-latitude Northeast Atlantic Ocean II: the intermediate water masses. Deep Sea Research I 47, 789-824.

van den Berg, C.M.G., 2003. Ionic Strength Corrected Stability Constants (ISCSC) software, http://www.liv.ac.uk/~sn35/Documents/Speciation.xls

van den Berg, C.M.G., 1982. Determination of copper complexation with natural organic ligands in seawater by equilibration with MnO_2. I. Theory. Marine Chemistry 11, 307-322.

van den Berg, C.M.G., 2006. Chemical speciation of iron in seawater by cathodic stripping voltammetry with dihydroxynaphthalene. Analytical Chemistry 78, 156-163.

Vangriesheim, A., Pierre, C., Aminot, A., Metzl, N., Baurand, F., Caprais, J.C., 2009. The influence of Congo River discharges in the surface and deep layers of the Gulf of Guinea. Deep-Sea Research II, doi:10.1016/j.dsr2.2009.04.002.

Vasconcelos, M.T.S.D., Leal, M.F.C., van den Berg, C.M.G., 2002. Influence of the nature of the exudates released by different marine algae on the growth, trace metal uptake and exudation of *Emiliana huxleyii* in natural seawater. Marine Chemistry 77, 187-210.

Voelker, B.M., Kogut, M.B., 2001. Interpretation of metal speciation data in coastal waters: the effects of humic substances on copper binding as a test case. Marine Chemistry 74, 303-318.

Vogel, C., Fisher, N.S., 2010. Metal accumulation by heterotrophic marine bacterioplankton. Limnology and Oceanography 55, 519-528.

Vogel, C., Fisher, N.S., 2009. Trophic transfer of Fe, Zn and Am from marine bacteria to a planktonic ciliate. Marine Ecology Progress Series 384, 61-68.

Wei, L., Ahner, B.A., 2005. Sources and sinks of dissolved phytochelatin in natural seawater. Limnology and Oceanography 50, 13-22.

Wei, L., Donat, J.R., Fones, G., Ahner, B.A., 2003. Interactions between Cd, Cu, and Zn influence particulate phytochelatin concentrations in marine phytoplankton: Laboratory results and preliminary field data. Environmental Science and Technology 37, 3609-3618.

Well, R., Roether, W., Stevens, D.P., 2003. An additional deep-water mass in Drake Passage as revealed by ^{3}He data. Deep Sea Research I 50, 1079-1098.

Wells, M.L., Kozelka, P.B., Bruland, K.W., 1998. The complexation of "dissolved" Cu, Zn, Cd and Pb by soluble and colloidal organic matter in Narragansett Bay, RI. Marine Chemistry 62, 203-217.

Wells, M.L., Smith, G.J., Bruland, K.W., 2000. The distribution of colloidal and particulate bioactive metals in Narragansett Bay, RI. Marine Chemistry 71, 143-163.

Welschmeyer, N.A., Coping, M., Vernet, M., Lorenzen, C.J., 1984. Diel fluctuation in zooplankton grazing rate as determined from the downward vertical flux of pheopigments. Marine Biology 83, 263-270.

Weng, L., Van Riemsdijk, W.H., Koopal, L.K., Hiemstra, T., 2006a. Adsorption of humic substances on goethite: Comparison between humic acids and fulvic acids. Environmental Science and Technology 40, 7494-7500.

Weng, L., Van Riemsdijk, W.H., Koopal, L.K., Hiemstra, T., 2006b. Ligand and Charge Distribution (LCD) model for the description of fulvic acid adsorption to goethite. Journal of Colloid and Interface Science 302, 442-457.

Westerlund, S., Ohman, P., 1991. Cadmium, copper, cobalt, nickel, lead, and zinc in the water column of the Weddell Sea, Antarctica. Geochimica Cosmochimica Acta 55, 2127-2146.

Whitfield, M., 2001. Interaction between phytoplankton and trace metals in the ocean. Advances in Marine Biology 41, 1-128.

Windom, H., Byrd, J., Smith, R.Jr., Hungspreugs, M., Dharmvanij, S., Thumtrakul, W., Yeats, P., 1991. Trace metal-nutrient relationships in estuaries. Marine Chemistry 32, 177-194.

Windom, H., Smith, R.Jr., Rawlinson, C., Hungspreugs, M., Dharmvanij, S., Wattayakorn, G., 1988. Trace metal transport in a tropical estuary. Marine Chemistry 24, 293-305.

Wu, J., Jing, B., 2009. Competitive ligand exchange voltammetric determination of iron organic complexation in seawater in two-ligand case: Examination of accuracy using computer simulation and elimination of artifacts using iterative non-linear multiple regression. Marine Chemistry 114, 1-10.

Xu, Y., Wang, W.-X., 2003. Fates of diatom carbon and trace elements by the grazing of a marine copepod. Marine Ecology Progress Series 254, 225-238.

Xu, Y., Feng, L., Jeffrey, P.D., Shi, Y., Morel, F.M.M., 2008. Structure and metal exchange in the cadmium carbonic anhydrase of marine diatoms. Nature 452, 56-62.

Xu, Y., Tang, D., Shaked, Y., Morel, F.M.M., 2007. Zn, Cd and Co inter-replacement and relative use efficiencies in the coccolithophore *Emiliana huxleyii*. Limnology and Oceanography 52, 2294-2305.

Xue, H.-B., Sigg, L., 1999. Comparison of the complexation of Cu and Cd by humic and fulvic acids and by ligands observed in lake waters. Aquatic Geochemistry 5, 313-335.

Yeats, P.A., Westerlund, S., Flegal, A.R., 1995. Cd, Cu and Ni distributions at four stations on the eastern central and south Atlantic. Marine Chemistry 49, 283-293.

Yeats, P.A., 1998. An isopycnal analysis of cadmium distributions in the Atlantic Ocean. Marine Chemistry 61, 15-23.

Zhang, W., Wang, W.-X., 2004. Colloidal organic carbon and trace metal (Cd, Fe, and Zn) releases by diatom exudation and copepod grazing. Journal of Experimental Marine Biology and Ecology 307, 17-34.

VITA

Education:

2010 — Postdoctoral Research Associate,
Earth, Atmospheric and Planetary Science Department
Massachusetts Institute of Technology, Cambridge, MA, USA
Advisor: Ed Boyle

In progress — Ph.D. candidate in Chemical Oceanography,
Ocean Earth and Atmospheric Sciences Department,
Old Dominion University, Norfolk VA, USA
Advisor: John Donat

2007 — M.Sc. in Chemical Oceanography,
Ocean Earth and Atmospheric Sciences Department,
Old Dominion University, Norfolk VA, USA
Advisor: John Donat

1994 — B.Sc. in Pharmacy and Biochemistry
Universidad Católica Santa María, Arequipa, Perú

Publications in progress:

1. Carrasco, G.G., Morton, P.L., Donat, J.R. Concentrations, complexation and chemical speciation of Zn and Cd in the North West Pacific Ocean.
2. Morton, P.L., Carrasco, G.G., Donat, J.R., Landing, W.M. Atmospheric versus margin sources of trace metals to the North Pacific Ocean.
3. Carrasco, G.G., Burdige, D.J., Donat, J.R. Concentrations, complexation and chemical speciation of Cu, Zn and Cd in the Elizabeth River, VA.
4. Carrasco, G.G., Burdige, D.J., Sunda, W., Donat, J.R. Benthic fluxes of Cu, Zn and Cd and their complexing ligands in the Elizabeth River, VA: effect on the water column.
5. Carrasco, G.G., Donat, J.R. Concentrations, complexation and chemical speciation of Zn and Cd in the Western South and Equatorial Atlantic Ocean.
6. Carrasco, G.G., Duffaut, L.A., Donat, J.R. A computerized solution to determining stability constant(s) (K) and ligand concentration(s) (L) in a metal titration of organic complexes using a sequential method of linear approximation and non-linear optimization of parameters.
7. Carrasco, G.G., Donat, J.R. Notes on the simultaneous determination of chemical speciation of Zn and Cd in seawater.